

**POLITECNICO DI MILANO**  
School of Civil, Environmental and Land Management Engineering  
Master of science degree in Civil Engineering  
Structures



**POLITECNICO**  
MILANO 1863

**DYNAMIC INTERACTION BETWEEN A  
SUBMERGED FLOATING TUNNEL AND A HIGH  
SPEED TRAIN: AN UNCOUPLED APPROACH**

Supervisor: Prof.ssa Maria Gabriella Mulas

Co-supervisor: Prof. Luca Martinelli

Master thesis of

Samuele Zambon - 918222

Academic year 2019/2020



# ACKNOWLEDGMENTS

I would like to thank professor Luca Martinelli, as well as my supervisor professor Maria Gabriella Mulas, for the patience, help and encouragement they gave me in the most tiring periods of writing this thesis, when I felt disheartened and defeated. A special thanks goes to Professor Mulas who provided me the INTER code, without which I would not be able to carry out this thesis. I thank professor Andrea Collina, who kindly provided me the data of the Italian train model Frecciarossa1000, as well as providing me advice on the choice of rail irregularities. I also want to thank professor Federico Perotti who was able to give me various aids during the thesis, as well as being one of the nicest professors at the Politecnico.

I want to thank the friends of studies of these 5 years: Geremia, Giada and Mattia who have been a fundamental support. In particular Giada, without which I would have struggled much more to get to the end of my master's studies.

I also want to thank my laughter companions: Raffaele, Enrico, Tomas and Andres, who made my days happier. Together with these I also thank all the friends of Delft with whom I had an out of ordinary experience.

Last but not least, I thank my parents who have always made me have everything I needed to study, sacrificing theirs and putting their children first.



# ABSTRACT

This thesis presents the dynamic response, in terms of displacements and forces, of the submerged tunnel prototype on the Messina's strait due to travelling trains. In the dynamic analyses, both systems are modelled as mechanical systems with a finite number of DOFs. The tunnel is described with a finite element (FE) model in ANSYS, the train is modelled as a multibody system in a research code named INTER.

Based on a coupled approach for the derivation of the equation of motion, the problem is tackled making use of an uncoupled solution strategy. Train and bridge interact, through a data exchange between the two codes: the tunnel motion at contact point excites the train, the contact forces transmitted by the train wheels load the tunnel. An iterative process is set and convergence is achieved when contact forces at two subsequent iterations are within a prefixed tolerance.

In this work, an existing FE model of the tunnel is updated, to account for the mass of surrounding water and vehicles participating to tunnel vibration. Geometry, mechanical and dynamic properties, loads, static and modal solution of the prototype tunnel are thoroughly analysed. A complete coupled analysis of the system tunnel-train requires a correct description of the rails roughness and of the hunting phenomenon. Both aspects are addressed in this work. Two Italian trains are modelled, a medium speed (TMV) and a high speed (TAV) train, respectively. Their models have been implemented in the research code INTER. For each train, a complex modal analysis is performed.

This study addresses both the horizontal and vertical dynamic of the convoy. The cyclic hunting motion of a train proved not to be critical for the tunnel at study. For this effect, the train is represented through a system of moving forces. The vertical response is analysed with the complete dynamic interaction described above. Numerical results, in terms of displacements and tension in the stays show that the effects of the dynamic excitation due to travelling wagons are within the design conditions of the tunnel.



# TABLE OF CONTENTS

<b>AKNOWLEDGMENTS</b> .....	<b>III</b>
<b>ABSTRACT</b> .....	<b>V</b>
<b>TABLE OF CONTENTS</b> .....	<b>VII</b>
<b>INDEX OF FIGURES</b> .....	<b>XI</b>
<b>INDEX OF TABLES</b> .....	<b>XV</b>
<b>ABBREVIATIONS</b> .....	<b>XVII</b>
<b>1 INTRODUCTION</b> .....	<b>1</b>
1.1 LITERATURE REVIEW.....	2
1.2 OBJECTIVE OF THESIS .....	5
1.3 THESIS LAYOUT.....	6
<b>2 SUBMERGED FLOATING TUNNEL</b> .....	<b>7</b>
2.1 LAYOUT AND GEOMETRY .....	9
2.1.1 <i>Tunnel description</i> .....	9
2.1.2 <i>Anchoring systems</i> .....	12
2.1.3 <i>Connection to mainland</i> .....	14
2.2 LOAD CONFIGURATIONS.....	15
2.3 PROS AND CONS.....	16
<b>3 THE CASE STUDY: MESSINA’S STRAIT TUNNEL</b> .....	<b>17</b>
3.1 GEOMETRY.....	18
3.1.1 <i>Tunnel cross-section</i> .....	18
3.1.2 <i>Stays’ geometry and configuration</i> .....	19
3.1.3 <i>Foundations</i> .....	21
3.2 FINITE ELEMENT MODEL.....	23
3.2.1 <i>Nodes, material and elements</i> .....	23
3.2.2 <i>Damping</i> .....	24
3.2.3 <i>Constraints</i> .....	26
3.2.4 <i>Loads and masses</i> .....	27
3.3 STATIC ANALYSIS.....	30
3.3.1 <i>Empty tunnel</i> .....	31
3.3.2 <i>Tunnel in normal operation</i> .....	33
MODAL ANALYSIS.....	36
<b>4 RAILS MODELING</b> .....	<b>43</b>
4.1 CONFIGURATION AND ASSUMPTIONS.....	44
4.2 IRREGULARITIES.....	45
4.2.1 <i>Power Spectral Density (PSD)</i> .....	46
4.2.2 <i>Typical random irregularities</i> .....	46
4.2.3 <i>Typical periodic irregularities</i> .....	49
4.2.4 <i>Isolated irregularities</i> .....	49
<b>5 TRAIN MODELING</b> .....	<b>51</b>

5.1	THE MECHANICAL SYSTEM.....	52
5.2	MECHANICAL MODEL IN THE VERTICAL DIRECTION .....	53
5.2.1	<i>Contact points</i> .....	54
5.2.2	<i>Equations of motion of the train</i> .....	54
5.2.3	<i>Reduction of independent parameters</i> .....	57
5.2.4	<i>Natural frequencies</i> .....	59
5.3	MECHANICAL MODEL IN THE TRANSVERSE DIRECTION .....	62
5.3.1	<i>Hunting actions</i> .....	64
5.3.2	<i>Forces generated by irregularity</i> .....	69
5.4	TRAIN MODELS ADOPTED IN THIS STUDY .....	70
5.4.1	<i>Medium speeds train - TMV</i> .....	70
5.4.2	<i>High speed train - TAV</i> .....	74
5.5	CRITICAL SPEEDS .....	78
<b>6</b>	<b>EQUATIONS OF MOTION.....</b>	<b>81</b>
6.1	FREE COORDINATES .....	83
6.2	LAGRANGE EQUATIONS.....	86
6.2.1	<i>Kinetic energy</i> .....	87
6.2.2	<i>Potential energy</i> .....	88
6.2.3	<i>Rayleigh function</i> .....	89
6.3	COUPLED PROBLEM.....	92
6.4	UNCOUPLED SOLUTION STRATEGY.....	95
6.4.1	<i>Extension to the non-linear case</i> .....	96
6.5	EQUATION FOR THE TRANSVERSAL MOTION.....	97
<b>7</b>	<b>NUMERICAL IMPLEMENTATION.....</b>	<b>99</b>
7.1	VERTICAL INTERACTION: INTER 7.0 CODE .....	100
7.1.1	<i>WTH integration procedure</i> .....	101
7.1.2	<i>Newmark method for direct integration</i> .....	106
7.2	TRANSVERSAL INTERACTION: MATLAB CODE.....	109
7.2.1	<i>Script for two trains</i> .....	112
<b>8</b>	<b>VERTICAL INTERACTION .....</b>	<b>113</b>
8.1	MEDIUM SPEED TRAIN – TMV .....	115
8.2	HIGH SPEED TRAIN – TAV .....	124
8.3	PARTICULAR CASE: TWO TAVs 300 KM/H.....	132
8.4	SUMMARY OF RESULT .....	137
<b>9</b>	<b>TRANSVERSAL INTERACTION.....</b>	<b>139</b>
9.1	MEDIUM SPEED TRAIN – TMV .....	140
9.1.1	<i>TMV - 31,5 km/h</i> .....	140
9.1.2	<i>TMV - 160 km/h</i> .....	141
9.2	HIGH SPEED TRAIN - TAV .....	144
9.2.1	<i>TAV - 45 km/h</i> .....	144
9.2.2	<i>TAV - 300 km/h</i> .....	145
9.3	SUMMARY OF RESULTS .....	148
<b>10</b>	<b>TRAINS AND VEHICLES: STAYS' PERFORMANCE .....</b>	<b>149</b>
<b>11</b>	<b>CONCLUSIONS.....</b>	<b>151</b>
	<b>REFERENCES .....</b>	<b>155</b>
	<b>APPENDIX A .....</b>	<b>159</b>
1-	MATLAB CODE: IRREGULARITIES .....	159



2- MATLAB CODE: TRANSVERSAL FORCES.....	163
<b>APPENDIX B</b> STRUCTURAL MATRICES FOR THE TRAIN MODELS .....	172
<b>APPENDIX C</b> INPUT TEXT FILES FOR INTER VERTICAL INTERACTION .....	176



# INDEX OF FIGURES

Figure 1-1: Evolution of train-bridge interaction models [Zhai et al., 2019 ] .....	3
Figure 2-1: Crossing of a watercourse with: (1) Suspension bridge, (2) Submerged Floating tunnel, (3) Immersed tunnel and (4) Underground tunnel.....	7
Figure 2-2: Basic types of SFTs. On the left $BWR > 1$ on the right $BWR < 1$ .....	9
Figure 2-3: Twin-tunnel SFT [Perotti et al., 2018].....	10
Figure 2-4: SFT supported by pontoons .....	12
Figure 2-5: SFT supported by columns .....	13
Figure 2-6: SFT supported by cables.....	13
Figure 2-7: SFT free support .....	14
Figure 3-1: Location of tunnel ends.....	18
Figure 3-2: Tunnel section in scale - First stays in the Calabrian part .....	19
Figure 3-3: Cross sections of the anchor bars [Palamà G., 2017] .....	20
Figure 3-4: Division of the anchor sections along the tunnel [Chunxia S., 2013].....	20
Figure 3-5: Section of the 3D model of the tunnel on the Strait of Messina - Calabrian side .....	20
Figure 3-6: 3D model of the Messina tunnel with the foundations in view .....	22
Figure 3-7: Finite element model section [Palamà G., 2017].....	24
Figure 3-8: Numerical model of the tunnel on the ANSYS interface .....	24
Figure 3-9: Rayleigh damping .....	25
Figure 3-10: Volume of the additional mass in the tunnel pipes and bars.....	28
Figure 3-11: Static deformed shape of the unloaded tunnel .....	31
Figure 3-12: Static deformed shape of the anchoring bars .....	31
Figure 3-13: Static vertical deformed shape of the rods.....	32
Figure 3-14: Static deformed shape of the tunnel in operation.....	33
Figure 3-15: Static deformed shape of the anchor bars .....	34
Figure 3-16: Static vertical deformed shape of the rods.....	34
Figure 4-1: Rails anchored to a concrete slab. San Gottardo's tunnel - Switzerland	44
Figure 4-2: Profile and alignment of a rail .....	45

Figure 4-3: Power Spectral Density of profile and alignment.....	47
Figure 4-4: Realization of random profile irregularities .....	48
Figure 4-5: Realization of random alignment irregularities .....	48
Figure 5-1: Mechanical model of a train wagon with 10 DOF + 4 contact point .....	54
Figure 5-2: Vertical mechanical model of wagon with reduced parameters .....	58
Figure 5-3: Transversal mechanical model of a wagon.....	62
Figure 5-4: Impossibility of cylindrical wheels to run straight .....	64
Figure 5-5: Detail of the movement of an axle with conical wheels .....	65
Figure 5-6: Sinusoidal transversal movement of the axles.....	65
Figure 5-7: Clearance between rails and wheels .....	66
Figure 5-8: Hunting of the wagon compared to the hunting of the wheels .....	67
Figure 5-9: Forces of the cab versus the forces of the wheel .....	68
Figure 5-10: Deformation of the rails due to hunting.....	68
Figure 5-11: Passengers and motor car dimensions. TMV [Van Nguyen et al, 2009] .....	70
Figure 5-12: Hunting of the wheels for the medium speed train.....	72
Figure 5-13: Hunting forces. TMV 160 km/h .....	73
Figure 5-14: Superposition of forces due to hunting and irregularities. TMV 160 km/h.....	73
Figure 5-15: Passenger and head carriages dimensions. TAV [Canetta D., 2017] ....	74
Figure 5-16: Hunting of the wheels for the high speed train.....	76
Figure 5-17: Hunting forces. TAV 300 km/h.....	76
Figure 5-18: Superposition of forces due to hunting and irregularities. TAV 300 km/h.....	77
Figure 6-1: Relation between contact points .....	84
Figure 7-1: Vertical interaction flow chart on INTER [Palamà G., 2017] .....	105
Figure 7-2: Transformation of force into actions on the tube nodes .....	111
Figure 8-1: Position of the reference nodes.....	113
Figure 8-2: Convergence of the errors - TMV 160 km/h .....	116
Figure 8-3: 5 <sup>th</sup> wagon - TMV 160 km/h: (a) First contact point forces; (b) irregularities.....	117

Figure 8-4: Motion of DOFs - 5 <sup>th</sup> wagon - TMV 160 km/h: (a) Displacement, first axle; (b) Displacement, first bogie; (c) Displacement, second bogie; (d) Displacement, carriage; (e) First bogie pitch; (f) Second bogie pitch; (g) Carriage pitch.....	119
Figure 8-5: Carriage frequency response - 5 <sup>th</sup> wagon - TMV 160 km/h .....	119
Figure 8-6: Vertical displacement node 18133 – TMV 160 km/h.....	121
Figure 8-7: TMV 160 km/h - Axial force in stay: (a) n°16; (b) n° 22; (c) n° 27 .....	122
Figure 8-8: Convergence of the errors - TAV 300 km/h .....	124
Figure 8-9: 4 <sup>th</sup> wagon - TAV 300 km/h: (a) First contact point forces; (b) irregularities .....	125
Figure 8-10: Motion of DOFs - 4 <sup>th</sup> wagon - TAV 300 km/h: (a) Displacement, first axle; (b) Displacement, first bogie; (c) Displacement, second bogie; (d) Displacement, carriage; (e) First bogie pitch; (f) Second bogie pitch; (g) Carriage pitch.....	127
Figure 8-11: Carriage frequency response - 4 <sup>th</sup> wagon - TAV 300 km/h.....	128
Figure 8-12: Vertical displacement node 18133 – TAV 300 km/h .....	129
Figure 8-13: TAV 300 km/h - Axial force in stay: (a) n°16; (b) n° 22; (c) n° 27 ...	131
Figure 8-14: First contact point forces - 4 <sup>th</sup> wagon - TMV 160 km/h .....	133
Figure 8-15: Displacement of the carriage - 4 <sup>th</sup> wagon – Two TAV 300 km/h.....	133
Figure 8-16: Vertical displacement node 18133 – Two TAV 300 km/h .....	134
Figure 8-17: Two TAV 300 km/h - Axial force in stay: (a) n°16; (b) n° 22; (c) n° 27 .....	135
Figure 9-1: Contact force transmitted by an axle – TMV 31,5 km/h .....	140
Figure 9-2: Transversal displacements node 18133 – TMV 31,5 km/h .....	141
Figure 9-3: Contact force transmitted by an axle – TMV 160 km/h .....	142
Figure 9-4: Transversal displacements node 18133 – TMV 160 km/h .....	142
Figure 9-5: Contact force transmitted by an axle – TAV 45 km/h.....	144
Figure 9-6: Transversal displacements node 18133 – TAV 45 km/h.....	145
Figure 9-7: Contact force transmitted by an axle – TAV 300 km/h.....	146
Figure 9-8: Transversal displacements node 18133 – TAV 300 km/h.....	146



# INDEX OF TABLES

Table 3-1: Mechanical properties of the tunnel section.....	19
Table 3-2: Mechanical properties of anchoring bars .....	21
Table 3-3: Stiffness and damping values for COMBIN14 elements .....	26
Table 3-4: Stiffness and damping values for the COMBIN39 and COMBIN14 elements .....	26
Table 3-5: Archimedes thrusts and Morison masses defined in the model .....	28
Table 3-6: Balance between loads and thrusts of the system .....	30
Table 3-7: Axial forces on the stays – Static analysis unloaded tunnel.....	32
Table 3-8: Axial forces on the stays – Static analysis operational tunnel .....	35
Table 3-9: Natural modes of the Messina floating tunnel empty .....	36
Table 3-10: Natural modes of the Messina floating tunnel in operation .....	37
Table 3-11: Modal shape 1 and 2.....	38
Table 3-12: Modal shape 3 and 4.....	39
Table 3-13: Modal shape 5 and 6.....	40
Table 3-14: Modal shape 7 and 8.....	41
Table 3-15: Modal shape 9 .....	42
Table 5-1: Mechanical properties and dimensions of the medium speed train .....	71
Table 5-2: Frequencies of the medium speed train, passenger wagon .....	71
Table 5-3: Medium speed train frequencies, motor wagon .....	72
Table 5-4: Maximum transversal forces induced by a TMV .....	74
Table 5-5: Mechanical properties and dimensions for high speed train .....	75
Table 5-6: Frequencies of the high speed train.....	75
Table 5-7: Maximum transversal forces induced by a TAV .....	77
Table 5-8: Critical speeds for the vertical interaction, TMV & TAV .....	78
Table 5-9: Critical speeds for the transversal interaction, TMV & TAV .....	79
Table 5-10: Chosen speeds for the analyses .....	80
Table 8-1: Analysis data, TMV 160 km/h .....	115
Table 8-2: Errors TMV160 km/h.....	115

Table 8-3: Axial force on the anchorages – TMV 160 km/h passing on tube 1.....	121
Table 8-4: Analysis data TAV 300 km/h.....	124
Table 8-5: Errors TAV300 km/h .....	124
Table 8-6: Axial force on the anchorages – TAV 300 km/h passing in tube 1 .....	129
Table 8-7: Analysis data – Two TAVs 300 km/h.....	132
Table 8-8: Axial force on the anchorages – Two TAV 300 km/h.....	134
Table 9-1: Analysis data TMV 13,5 km/h.....	140
Table 9-2: Analysis data TMV 160 km/h.....	141
Table 9-3: Axial force on the anchorages – TMV 160 km/h.....	143
Table 9-4: Analysis data TAV 45 km/h.....	144
Table 9-5: Analysis data - TAV 300 km/h .....	145
Table 9-6: Axial force on the anchorages – TAV 300 km/h.....	147
Table 10-1: Axial force losses – [Palamà, 2017].....	149



# ABBREVIATIONS

BWR	–	Buoyancy Weight Ratio
DFT	–	Discrete Fourier Transformation
DOF	–	Degree of freedom
FEM	–	Finite Element Model
FFT	–	Fast Fourier Transformation
LHS	–	Left Hand Side
ODE	–	Ordinary Differential Equation
PSD	–	Power Spectral Density
RHS	–	Right Hand Side
SFT	–	Submerged Floating Tunnel
TAV	–	High speed train (Treno Alta Velocità)
TMV	–	Medium speed train (Treno Media Velocità)



# 1

## INTRODUCTION

The dynamic interaction that occurs between a bridge and a train involves various aspects of study related to the fields of civil, mechanical and transport engineering. In civil engineering practice, very refined models are used to simulate the behavior of the bridge and less refined models to simulate the behavior of the vehicles passing over it. On the contrary, in the practice of mechanical engineering, more attention is paid to the mechanical behavior of the vehicle. In this thesis work, there is the interest to focus on both models, structural and mechanical, in order to accurately describe all the phenomena that are triggered during their interaction.

When a train passes over a bridge, this last deforms for the weight. The wheels of each single wagon, therefore, follow the deformations of the bridge and consequently the masses constituting the wagons begin to oscillate, generating dynamic contact forces that vary around the static value. To complicate the motion there is the elastic deformation of the contact between the wheel and the rail, as well as the presence of irregularities in the rails, whose misalignment significantly affects the value of the contact forces and the motion of the vehicle.

Excessive vibrations of the structure can compromise the safety and comfort of the train's carriages.

## 1.1 Literature review

The train-bridge interaction problem can be described mathematically through a system of ordinary differential equations by coupling the single wagon and the structure, considering the wagon as a single vehicle. The equations of motion of the wagon and of the structure cannot be integrated separately, since the problem is intrinsically coupled. Numerous authors have dealt with the formulation and subsequent integration of the equations of the coupled problem. The computational burden of the problem is closely linked to the type of resolution and the complexity of the models.

In this thesis the solution to the problem developed by Mulas et al. (2008) was adopted. Mulas et al. propose two different iterative procedures for solving the dynamic vehicle-structure interaction problem. The derivation of the equations of motion is done through Lagrange's equations, obtaining a system of ordinary differential equations that take into account the physical characteristics of the structure, of the vehicle and the influence of roughness (irregularity). The system of differential equations is uncoupled thus obtaining two subsystems. The integration of the two subsystems can take place through two iterative procedures: the STS (Single Time Step) procedure or the WTH (Whole Time History) procedure. In the STS procedure the iteration is carried out at each integration step until convergence is achieved. The WTH procedure iterates over the entire domain until convergence is achieved. In both cases the convergence of the solution is imposed on the contact forces. The possibility of being able to decouple the equations of motion and entrust the structural resolution to an external calculation code (such as Ansys APDL) makes the solution of the problem more versatile, and this is the reason why this approach was adopted in this work.

In the following, a literature review of the train-bridge interaction models is presented<sup>[1]</sup>, from which follows the choice of the wagon models adopted in this study. In literature seven types of train models have been proposed in the last 2 centuries, concerning the interaction between a bridge and a train. The first attempt to analyze the interaction between train and bridge dates back to 1847, in England.

The simplest and oldest model is a moving constant force model (MCFM), widely used in the early days for research on bridge vibrations. It is attributed to Kolousek (1905), who used it for a steam locomotive to capture the vibrations of girder bridges. The accuracy of this model is evidently limited due to the excessive simplification of the train.

A subsequent development was obtained with an harmonic force in motion, the Moving Harmonic Force Model (MHFM), proposed at the beginning of the XX century by Krylov (1905) and Timoshenko (1922). These authors studied the resonance of bridges by transforming the forces of the trains into harmonic forces in motion. The interaction between the two systems is not taken into consideration also in this model, as in the previous one, leading to a valid simplification only when:

---

[1] The literature research reported and the model names are an adaptation of the literature research conducted by Zhai et al. (2019).

- The weight of the train is much smaller than that of the bridge;
- The dynamic behaviour of the train is not of interest.

In this view, this model is ideal for modelling the transverse hunting actions induced by the moving masses of the wheeled wagon. In fact, the actions induced by hunting have a very low inertia of the wagon compared to the Messina’s tunnel.

When the dynamic effect of the wagon cannot be neglected, the Moving Mass Model (MMM) must be used. This model was introduced by Willis (1849) and Stokes (1849).

On this basis, the Moving Spring-Damping-Mass Model (MSDMM) has been developed to better model the train loads, in which the suspension system is simplified as a moving mass supported by an element of damping and spring. An analytical solution was presented by Biggs and Testa (1964).

To simulate the vehicle with a rigid cab with four DOFs, the Two Axle Vehicle Bridge Model (TAVBM) was proposed, similar to the modern vehicle-bridge interaction model. In this way, vertical movements and pitching can be modelled. Solutions are provided by Wen (1960) and Fryba (1999).

Thanks to the development of the finite element method (FEM) and high performance computers, it was possible to develop the first model of dynamic interaction: Train Bridge Dynamic Interaction Model (TBDIM). In this model, the theory of multi-body system dynamics is adopted to simulate the train subsystem, while the bridge is modelled on the basis of FEM. Several authors collaborated in the development of this model, including Diana and Cheli (1989).

The trains operate on the rails, which are laid on the decks of the bridges. Therefore the train, the rail and the bridge form an integrated dynamic system for the diffusion of vibrations, an important fact with the advent of high-speed trains. Train and rails are thus coupled by the wheel-rail relationship. Based on this concept, Zhai et al. (1995) studied and developed a Train Track Bridge Dynamic Interaction Model (TTBDIM) in which the rail is modelled by a system of springs and dampers capable of simulating sleepers, ballast, fasteners, etc., as shown in Figure 1-1.

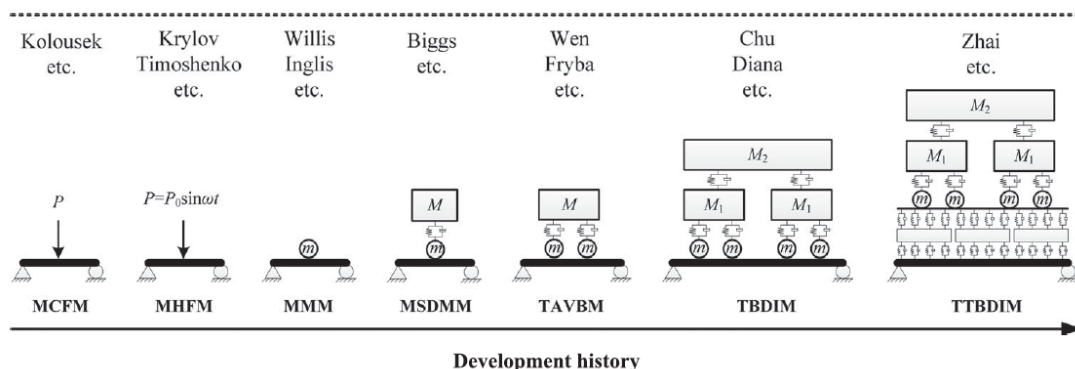


Figure 1-1: Evolution of train-bridge interaction models [Zhai et al., 2019 ]

Other authors, like Van N.D. et al. (2009), proposed 3D train-bridge interaction model, with 3D wheel-rail contact interfaces, able to represent the contact loss and possible derailments. However, the derailments are out of the objective of this thesis. In this work, for the analysis of the dynamics in the vertical direction the TBDIM model with 10 DOFs is adopted. The model of Zhai et al.(1995), being more sophisticated, requires very high computational times, and would also be of little use for the purposes of this study, since:

- The rail is anchored directly to the concrete structure, so only the elastic deformation of the fasteners must be simulated. The model of Zhai et al. results to be useful for the modelling of sleepers and ballast, that have large deformations, but in this study they are not present;
- The high number of DOFs gives back an accuracy not necessary for the purpose of this study, with computations times too long.

The transversal mechanical dynamics model is neglected in this study. However, the phenomenon of hunting is taken into account with a model similar to the MHFM, since is of considerable influence, to assess whether more refined studies are necessary.

## 1.2 Objective of thesis

The aim of this thesis is to study the dynamic response of the submerged floating tunnel prototype on the strait of Messina, under the passage of a train. The models of train will be considered to travel at low, medium and high speeds.

The floating tunnel was modelled with Ansys Mechanical APDL, using finite elements, and adapted for this case study. The interaction analysis is managed by INTER. INTER is a program written in FORTRAN language that has been carried out, and strengthened over time, by various undergraduate students of the Politecnico di Milano and by professor Mulas. It solves the coupled problem of vehicle-bridge with the approach of Mulas et al. (2008). The latest version is INTER 6.0, made by Palamà, in which strings of code were added to make the program able to exchange data with Ansys APDL. This thesis brought it to version INTER 7.0, adding to the program the ability to read and interact with train wagon models.

In order to perform the analysis of the dynamic interaction, the INTER 7.0 code will solve the equations of motion of the wagons, and the commercial software Ansys APDL will solve the structure with the loads obtained from INTER 7.0, as long as convergence is not achieved.

The models of the wagons are separate for the vertical, transversal and longitudinal motion. The INTER code it's for now designed only for the vertical dynamics of vehicles. Since a train, as it will be seen, has also a non-negligible horizontal harmonic motion, called hunting, the aim of this thesis is to conduct two dynamic analyses on the tunnel: vertical and transversal.

### **1.3 Thesis layout**

This work is divided into 11 chapters.

The first chapter introduces the nature of the problem of the dynamic interaction between the submerged floating tunnel and trains, and the objectives set for this thesis.

The second chapter analyzes all the types of floating tunnels in a synthetic, but exhaustive way, highlighting their geometric and functional differences as well as the loads acting on them.

The third chapter goes into detail of the prototype of the Messina's floating tunnel, for which the geometry, the characteristics of the materials, the description of the static and dynamic loads acting on the structure, as well as the details of the anchoring and foundation systems are depicted. The adopted finite element model is then described and the solutions of the static and modal analyzes are reported.

The fourth chapter studies the rail system, defines how it is anchored to the structure, how it is modeled into the interaction program, and describes how the irregularities of the profile and alignment are obtained.

The fifth chapter describes how the train model has been defined in the literature over time. The models implemented on INTER for vertical and transversal analysis are then described. Finally, the numerical data of the two reference trains with which the analyses are conducted are reported: a slow speed train and a Frecciarossa.

In chapter 6 the equations of motion are obtained, the decoupling of the problem is described and the fundamental hypotheses are formulated. Then the WTH integration procedure and Newmark's step-by-step integration method are presented in detail.

Chapter 7 goes into detail of the numerical implementations used. For the vertical dynamic problem INTER is described. For the transverse dynamics, the calculations contained in the MATLAB script are described.

The results of the vertical analysis, obtained from the interaction between INTER and ANSYS APDL, are reported in chapter 8. The results of the transversal analysis, obtained from the forces computed with MATLAB and inserted on ANSYS APDL, are reported in chapter 9. In those two chapters the forces exerted by the contact points, the displacements of two significant nodes of the tunnel, the axial forces of some anchors, and for the vertical analysis the displacements of the train carriage, are shown.

In chapter 10 the forces of the stays obtained from analyses of previous thesis works, concerning the vehicle loads, are superimposed with the forces obtained in this thesis, thus obtaining the maximum variation of axial action of the anchors. Chapter 11 summarizes the results obtained and highlights the aspects that emerged during this study.



## SUBMERGED FLOATING TUNNEL

In today's engineering, the crossing of a watercourse with great spans is made with suspension tunnels, immersed tunnels or underground tunnels. A fourth alternative was proposed to these three typologies in 1886 by Sir Edward James Reed: the submerged floating tunnel (SFT), also called Archimedes' bridge, see Figure 2-1. A floating tunnel is a tubular structure, travelled by vehicles, immersed at a certain depth in the water, which connects two shores of mainland. By taking advantage of Archimedes' thrust (buoyancy law) and special anchors, balance is guaranteed.

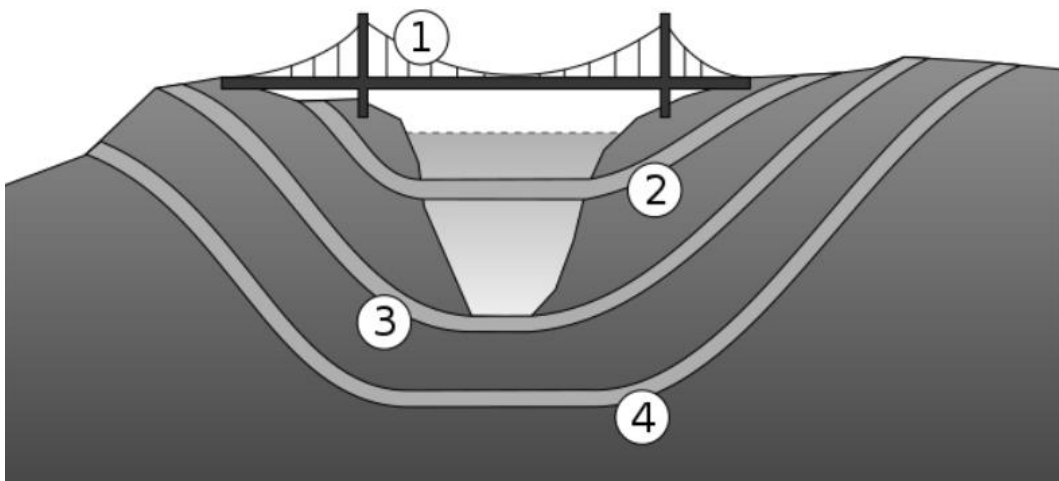


*Figure 2-1:* Crossing of a watercourse with: (1) Suspension bridge, (2) Submerged Floating tunnel, (3) Immersed tunnel and (4) Underground tunnel

Although they have never been built, the submerged floating tunnels are subject of study in several states of the world, and have to be considered as a competitive possibility to the existing ones for crossing seas, fjords, alpine lakes and water course. Indeed, the environmental and visual impact is significantly lower, if not zero, compared to traditional bridges, as well as having a reduced occupation of mainland. Furthermore, in the event of adverse weather conditions, the SFTs are those least subject to interruptions and limitations of operation, which is an aspect of no small importance when involving public transport.

Up to now, the floating tunnel has been studied with particular interest in structural dynamics, being extremely important for this type of structure. Although it has not yet materialized as a project, over the years some case studies have emerged in China and Japan, and two paradigmatic cases at European level, becoming study models and examples of analysis: the strait of Messina and the E39 motorway along the Norwegian coast, where there is the intention to cross eight fjords.

The case of Messina is of particular interest for its complex marine conditions (seaquakes, earthquakes, wind induced waves, strait currents, and ship traffic), as well as for the absolute need to support a high-speed railway that requires rather severe performance criteria.

The objective of this thesis is to study the dynamics of the tunnel prototype, designed for the Strait of Messina, under the action of travelling mechanical systems: trains.

In this chapter the generalities of the SFTs will be summarized, on which studies have been made in literature. However, this thesis is restricted to the Messina prototype, described in detail in chapter 3.

## 2.1 Layout and geometry

In floating tunnels, three structural components can be identified:

- tunnel;
- anchorages;
- connection with the mainland.

These components must provide resistance and stiffness against the various forces acting under the free surface of the water and inside the tunnel.

### 2.1.1 Tunnel description

The design aspects that must be taken into consideration are: the buoyancy weight ratio, the cross section, the longitudinal layout and the materials.

The morphology of the site and the span of the tunnel also influence the structural configuration. The length of the tunnel is clearly dependent on the distance between the shores. If the tunnel is too long, the connection systems to the mainland become a critical aspect, especially in areas where strong seismic activity is expected.

*BWR: Buoyancy weight ratio*

The floating tunnel receives a thrust from the bottom upwards, equal in intensity to the weight of the volume of the water displaced (Archimedes' thrust or Buoyancy law), which corresponds to the volume of the tunnel. Therefore, taking into consideration the serviceability and maximum acting loads to which the tunnel is subjected, we can identify the ratio between thrust and weight, also called buoyancy weight ratio. This ratio acts as a balance between the acting forces: when higher than one it indicates that the tunnel tends to emerge on surface (Resulting force upwards) when lower than one it indicates that the tunnel tends to sink (Resulting force downwards). In the first case the tunnel makes use of tensioned tethers anchored on the seabed, in the second one of floating pontoons. These are the two basic approaches for a submerged floating tunnel, as shown in Figure 2-2.

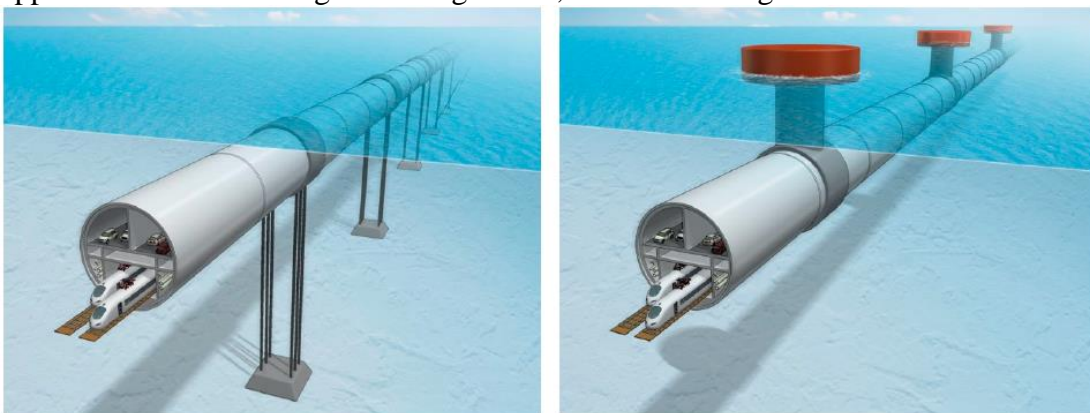


Figure 2-2: Basic types of SFTs. On the left  $BWR > 1$  on the right  $BWR < 1$

[Deokhee et al., 2019]

The BWR determines the characteristic vibrations of a tunnel, and it is of considerable importance due to the amplification of internal forces. Choosing a suitable BWR is a step to be conducted with caution in the design phase. It should be noted that too high thrust/weight ratios can be harmful to the structure, especially in case of earthquakes. The tunnel must be held by the tethers on the seabed even when it is unloaded, where the upward resulting force is maximum. On the other hand, a ratio that is too close to one, when the tunnel is loaded, would lead to tension-free cables. The same observations apply to tunnels with pontoons.

It can be assumed as reference values ratios between 1,2 and 1,5 for SFTs with tethers anchored on the seabed.

### *Cross sections*

The choice of cross-section must take into account several aspects. The first is the size of the external and internal diameters, which are the protagonists of the Archimedes' thrust. The diameters must in any case be such as to guarantee the guidelines for rail, car and motorcycle traffic. Finally, the external shape: it can be circular, elliptical or polygonal. However, a non-hydrodynamic shape has a significant effect on the behaviour of the structure. These three aspects in the design phase must be calibrated together.

The number of tubes has also become an important aspect over the course of the developments. Initially the idea was that of a single tunnel. However, the perfect tightness of the tunnel cannot be guaranteed (unless disproportionate costs). An evacuation plan was therefore envisaged by creating a two-pipe tunnel, where the second acts as a rescue. The two pipes are connected to each other at regular intervals ensuring an alternative escape route, see Figure 2-3. The possibility of partial flooding of one pipe is therefore admitted, without however compromising the second pipe or compromising the stability of the structure. What's more, it is also an escape route for any other case of fire or explosion accident. During the normal service of the work, each tube will have a direction of vehiculation, thus eliminating the risk of colliding.

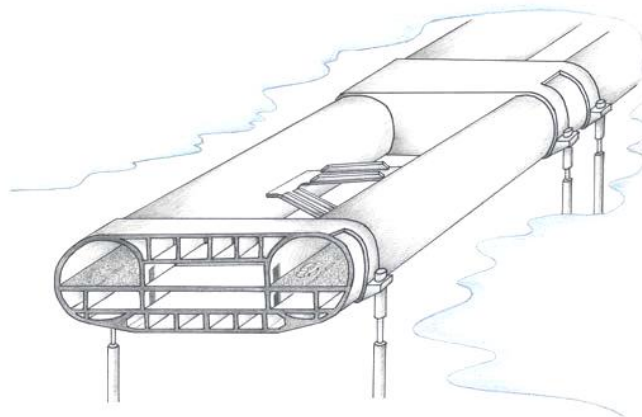


*Figura 2-3: Twin-tunnel SFT [Perotti et al., 2018]*

The decision to connect two tubes also increases their performance in terms of lateral stiffness, even if it makes the connection to the mainland more complex and articulated. Among the hypotheses studied, a possible solution is to make the two tubes approach each other as they reach the shore, which however could be a problematic solution for the train tracks.

The section of a double floating tunnel showed a more stable behaviour under the action of currents and waves, reducing the need to eliminate uncontrolled motions. Additionally, wind tunnel tests showed a preference for a double cylindrical tunnel rather than a rectangular or polygonal box [Mascella M., 2020].

The cylindrical shape minimize the vibrations induced by the waves, prevent additional torsional moments and uniform the internal and external pressure; unfortunately, however, they are more expensive.

### *Longitudinal layout*

The depth of immersion of a tunnel is decided by local regulations, by the traffic of the boats and by the depth in which there is a reduction of the forces given by the waves. A height of between 20 and 40 m from the free surface of the water can therefore be considered.

The choice of the configuration in plan can fall between a curved or straight tunnel. The curved tunnel has the benefit of the arch effect, which increases its stiffness. However, the coupling between the axial and transverse behaviour leads to a complex design for the terminal part of the curved tunnel. This planar configuration is adopted for tunnels equipped with floating pontoons with water currents directed mainly in one direction (Norwegian E39), but it is not recommended if there are strong seismic actions or movements between the two shores [Perotti et al., 2018]. In the case of straight tunnels, the transverse stiffness can be provided by bars or cables inclined in the plane orthogonal to the axis of the tunnel.

For tunnels with double cylindrical section, the connection between the two tubes is obtained with inclined bracing, to stiffen the two tubes in the plane, and with horizontal rigid connections that act also as escape routes and control areas [Perotti et al., 2018].

Lengthwise the tunnel is made up of pipes with lengths that can vary from 100 to 500 m. As regards the longitudinal stiffness, several options can be considered; the first is the adoption of double inclination tethers. The second is to rely on the constraint offered by the tube end connections: in this case the introduction of dissipation devices must be carefully evaluated, in order to mitigate the dynamic behaviour both in operation and in seismic conditions and to limit the axial forces that develop in the tunnel.

### *Materials*

The materials used for most of the projects are steel and concrete, whose quality must be such as to ensure the success of the work with high probability. In the Chinese prototype for Qindao Lake the cross section is a steel-concrete-aluminium

sandwich. The outer layer of aluminium, which is resistant to corrosion, works as an energy absorber in case of impacts from the outside, thanks to the alveolar shape [Mascella M., 2020].

Water tightness is guaranteed by concrete, not only in the ultimate limit state, but also in the serviceability limit state, for which the membrane forces in the tube must always be in compression. In this way, cracks cannot form. This criterion therefore guides the calculation of the amount of pre, or post, tensioning in the concrete section.

### 2.1.2 Anchoring systems

There are 4 types of anchorage systems: floating pontoons, support pillars or columns, cables or bars in tension and free.

#### *Floating pontoons*

Pontoons are large floating buoys that support the tunnel in such a way that it does not sink ( $BWR < 1$ ), see Figure 2-4. The unfavourable aspect of these structures is linked to the problems of surface navigation: the ships could collide with them. In addition, surface water movements directly disturb the pontoons. They are therefore recommended for use in calm and poorly surfed waters.

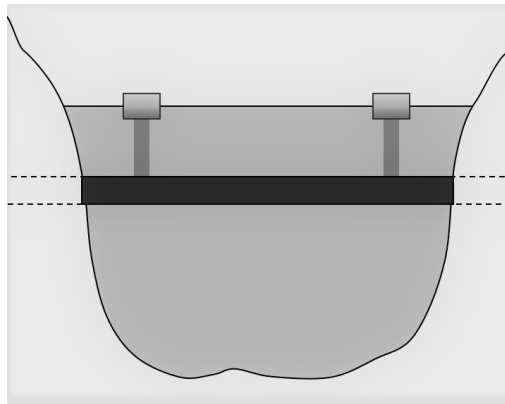


Figure 2-4: SFT supported by pontoons

#### *Support pillars or columns*

These elements can support tunnels with the resultant of forces directed both downwards and upwards. These are concrete piles, columns or towers that connect the tunnel to the seabed, as shown in Figure 2-5.

Various ideas with an anchoring system based on towers have been hypothesized, even with the aid of immersed cables or stays, so as to reduce the upward thrust of Archimedes and the deflection of the tunnel, and obtain much higher lengths between the towers. However, this solution sees as a design limit the depth of 100 m

of the seabed, beyond which building a support pylon is not economically favourable.

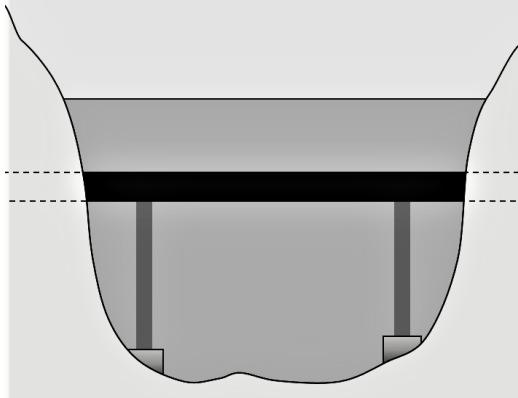


Figure 2-5: SFT supported by columns

#### *Cables or bars in tension*

There are two other types of elements that work as a link between the tunnel and the seabed: cables and bars (Figure 2-6). Both are elements that work in tension, they prevent the tunnel from emerging to the surface ( $BWR > 1$ ). The difference is that the bars are made with tubular section, and being hollow inside they receive an Archimedes thrust, which reduces their catenary shape due to their own weight when they are inclined with respect to the vertical, bringing them to a straight shape, and increasing their serviceability life. The cables, on the other hand, always show a catenary shape. The bars, compared to the cables, also have greater lateral stiffness. The layout of these anchors, as already mentioned, is inclined in the plane orthogonal to the plane of the tunnel, so as to ensure lateral stiffness.

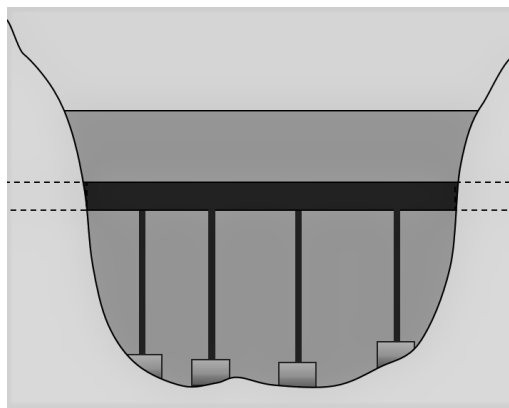
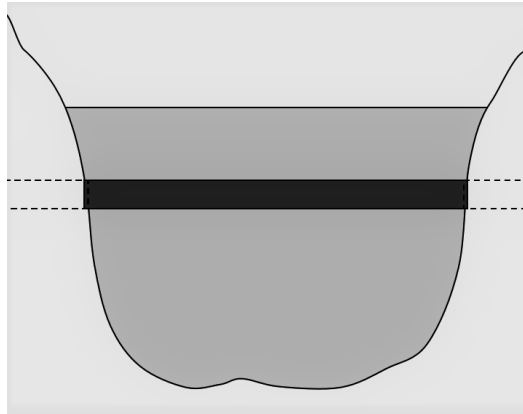


Figure 2-6: SFT supported by cables

### *Free*

In situations where there are calm waters or short distances the tunnel can be designed without anchors, using the end supports and calibrating the ratio between buoyancy and weight, as shown in Figure 2-7.

Another situation in which anchors can be avoided is using a curved profile, taking advantage of the arch effect, with reduced spans.



*Figure 2-7: SFT free support*

### **2.1.3 Connection to mainland**

The connections to the mainland must ensure water tightness in the tunnel joints. In addition, the joints must be designed to allow longitudinal expansion and contraction, as well as to be able to support the seismic action. The latter turns out to be the main problem of connections with the mainland, since if one end of the tunnel is left axially free, the other end must be constrained. This fact brings this end to be the origin of axial actions on the tunnel during an earthquake, which endanger the water tightness of the tunnel.

To overcome this problem, a device can be installed at the constrained end that is able to guarantee high plastic deformations when the axial force is greater than the limit value, and elastic behaviour below this limit force.

Alternatively, elastic-plastic devices can be adopted at both ends, connecting them in series with devices that absorb the impact, allowing slow axial movements.



## 2.2 Load configurations

A submerged tunnel, once installed and operational, is subject to static, dynamic and impact loads. Acting loads can be divided into four large groups:

Permanent loads

- Dead load
- Buoyancy
- Post-tensioning

Live loads – Environment

- Water pressure
- Currents
- Waves
- Seaquake
- Earthquake

Live loads – Serviceability

- Car traffic
- Rail traffic
- Water ballast

Accidental loads

- Explosions
- Fires
- Vehicle collisions or derailments
- Flooding
- External collisions

## 2.3 Pros and cons

The use of a floating tunnel as a solution for crossing water courses has numerous advantages. Sometimes it is even the only economic alternative, for example, when the depth of a seabed is too high for an immersed structure to sustain the pressure. Among the various advantages, the following can be identified as the most relevant:

- it can be constructed in very high seabed depth, where traditional bridges or immersed tunnels would reach excessive costs;
- any type of cross section can be made since the tubes are prefabricated and not cast in site;
- it does not create constraints or obstructions to navigation routes;
- it allows to eliminate noise pollution and the gases produced, treating them before they leave the tunnel;
- it can guarantee high speed trains;
- it keeps the landscape and environmental characteristics, having a reduced impact on the mainland;
- construction phases and activities have less impact on the aquatic marine life, and it can be removed at the end of its life;
- it is not subject to wind actions, which usually have higher effects in traditional bridges with respect to the effects of the waves on SFTs.

However, the floating tunnels also present different problems still unresolved, caused by the lack of practical applications and experimental data on the actual behaviour of the structure. Among the various unsolved problems, the following gaps can therefore be identified as the most relevant:

- scarce knowledge and experience in general due to the lack of similar work;
- connections to the mainland, with particular attention to the earthquake situation;
- effects in all the three directions of the SFT in case of a tsunami;
- optimization of the distances between tubes and connections;
- replacement of a damaged elements;
- effects of an external explosion or internal accident or internal derailment;
- doubts about the procedures of execution and construction of the work;
- dynamic interaction with a train.

This thesis work aims to solve the last of the problems, specifically for the tunnel on the Messina's strait.

## **THE CASE STUDY: MESSINA'S STRAIT TUNNEL**

The bridge over the Strait of Messina has always been a project considered crucial for the development of transport in Italy, allowing the connection between the island of Sicily and the Italian peninsula. The project proposed during the government mandates of the 2000s was that of a suspension bridge. However, a second parallel project, that of a floating submerged tunnel, took off in the same years, seeing research in constant development to be able to give a definitive answer to the feasibility of the work. This last bridge/tunnel will be the reference in this thesis work. This chapter presents its geometries and numerical modelling.

### 3.1 Geometry

The Messina's strait tunnel has the task of connecting the Calabria region and the Sicily region. The ends of the tunnel are planned near Catona, on the Calabrian coast, and near Punta San Ranieri, on the Sicilian coast, for a total length of 4680 m, see Figure 3-1. The location of the structure was subject to studies, and chosen on the basis of construction criteria and economic feasibility.

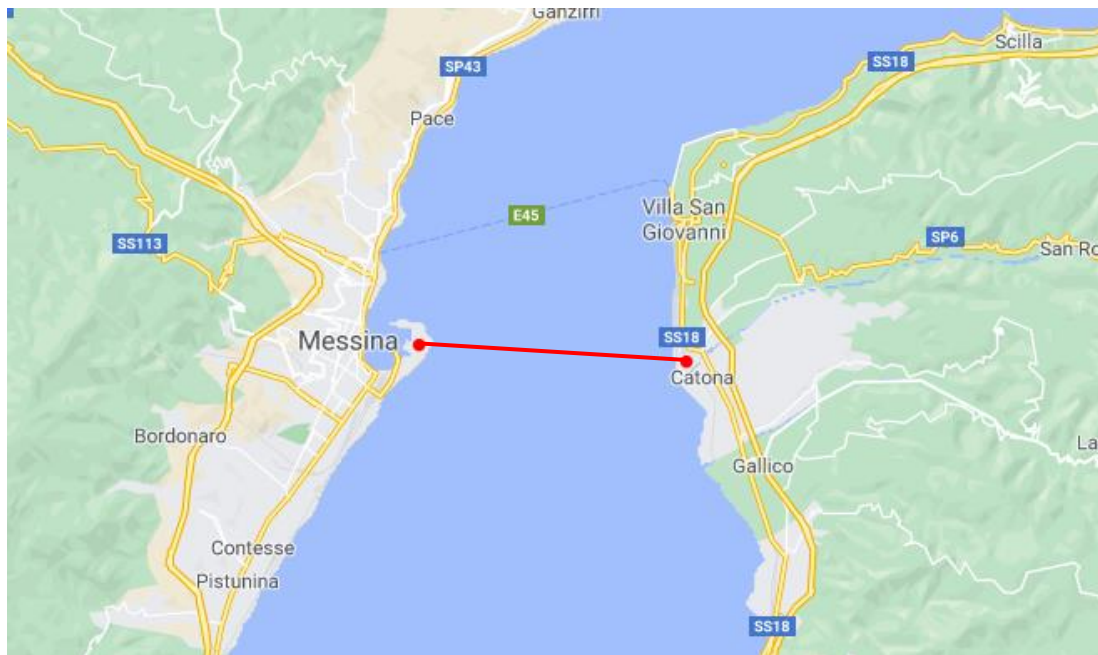


Figure 3-1: Location of tunnel ends

Since the maximum depth of the sea in the strait is equal to 350 m, the other three types of bridges presented in Figure 2-1 would be more difficult to be built than a floating tunnel. The type of floating tunnel chosen is that of a SFT with  $BWR > 1$ , therefore with emergence thrust, and anchoring cables in tension inclined and linked to the seabed, to resist forces of all kinds.

The strait is an important point for navigation, and the legislation requires that there are at least 30 m free below the free surface of water, in low tide conditions. The positioning of the tunnel is therefore foreseen at a depth of about 40 m.

#### 3.1.1 Tunnel cross-section

As anticipated in the previous chapter, the safest section of the tunnel is that of a double tube, connected together with elements that can be walked on, Figure 2-3. In compliance with Italian Legislative Decree 264/06 and the European regulation 2004/54/CE, the distance between two emergency exits inside a tunnel cannot exceed 500 m. The transverse connections between the two tunnel pipes are set every 468 m

[Palamà G., 2017]. These connections satisfy the safety requirement both in case of fire and in case of flooding, as well as making the two tubes more rigid. The shape of the tube section is circular, to ensure greater hydrodynamics (Figure 3-2). The external diameter is 15,95 m, while the internal diameter is 13,95 m.

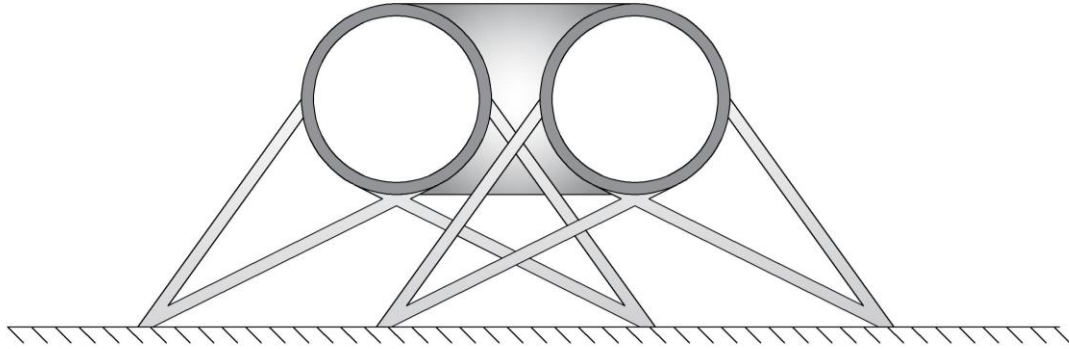


Figure 3-2: Tunnel section in scale - First stays in the Calabrian part

The tunnel thickness of 2 m is the sum of four layers: 2 steel layers have a thickness of 20 mm each and between them the third layer of concrete is placed, while the fourth is an external layer of 20 mm in stiffened steel (neglected for static purposes). The two tubes are treated as if they were made of a single material having an equivalent elastic modulus of  $E = 29430$  MPa, an equivalent shear modulus  $G = 11319$  MPa, an equivalent area of  $A = 58,24$  m<sup>2</sup> and an equivalent density of 2100 kg/m<sup>3</sup>[Chunxia S., 2013].

Given the characteristics described above, the inertia and self-weight shown in Table 3-1 are obtained. The internal partitions of the tunnel, necessary to divide the section and to allow the vehicular road above the passage of trains, were not taken into account in the calculation of inertia.

Table 3-1: Mechanical properties of the tunnel section

$D_{est}$ [m]	$D_{int}$ [m]	Area [m <sup>2</sup> ]	Equivalent Area [m <sup>2</sup> ]	I [m <sup>4</sup> ]	Weight [kN/m]	$E_x$ [GPa]	$G_{xy}$ [GPa]
15,95	13,95	46,97	58,24	1637	1200	29,430	11,319

### 3.1.2 Stays' geometry and configuration

Each tube of the tunnel is linked at its ends to the mainland, as well as to the seabed by steel stays, Figure 2-6. Stays are tubular sections that connect the sides of the rods to the foundations. These anchoring bars are placed every 72 m, with a total of 65 groups of bars over a span of 4680 m. Each tube uses 4 stays, 2 per side, for a total of 8 stays for two tubes, which become 520 anchors on the whole floating tunnel.

The length of the anchors varies according to the seabed profile, with which the section used also varies. There are three types of hollow cylindrical sections, with different geometric characteristics, shown in Figure 3-3.

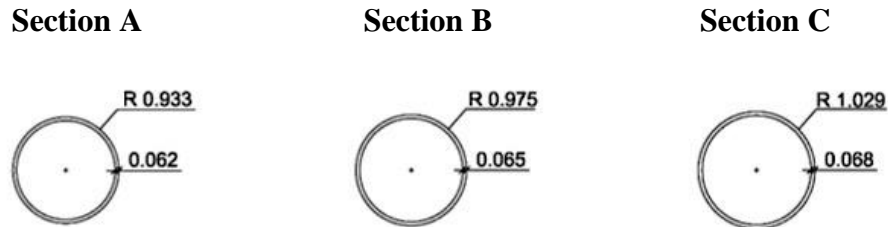


Figure 3-3: Cross sections of the anchor bars [Palamà G., 2017]

The disposition of the anchoring bars along the tunnel length is shown in Figure 3-4.

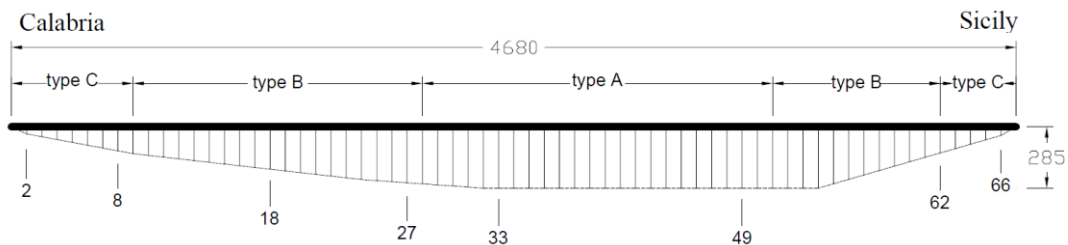


Figure 3-4: Division of the anchor sections along the tunnel [Chunxia S., 2013]

In Figure 3-5 a 3D model of the tunnel is presented

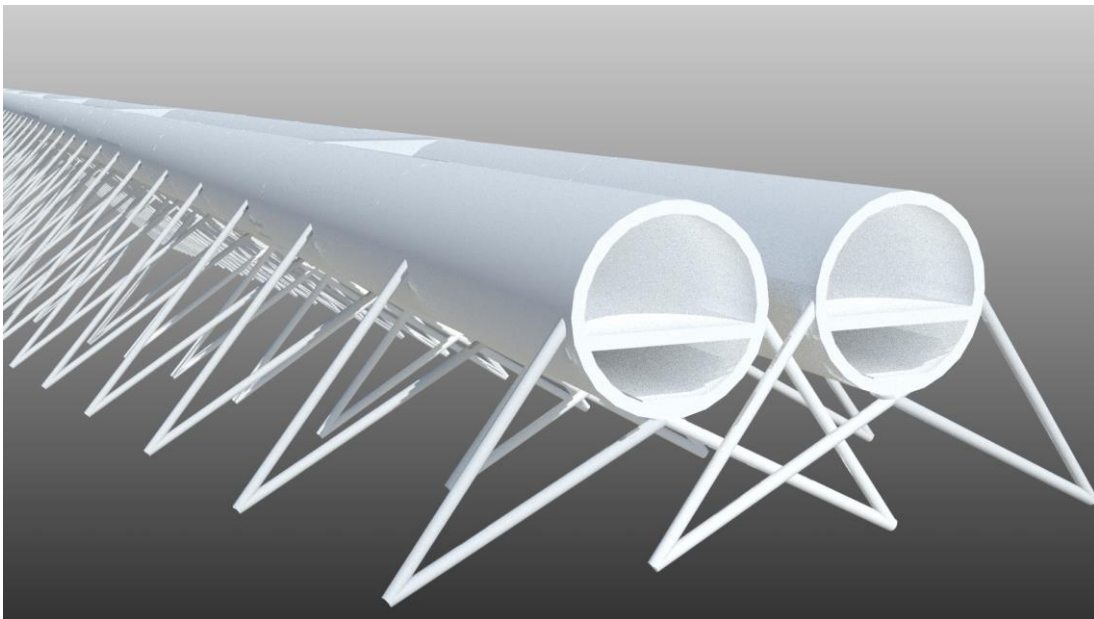


Figure 3-5: Section of the 3D model of the tunnel on the Strait of Messina - Calabrian side

Archimedes' thrust also acts on the anchors, since they are hollow and filled with air inside, thus reducing the catenary effect that would occur on longer bars.

The values and mechanical properties of the individual bars are reported in Table 3-2.

Table 3-2: Mechanical properties of anchoring bars

Section	Position	$R_{est}$ [m]	$R_{int}$ [m]	Area [m <sup>2</sup> ]	I [m <sup>4</sup> ]	Weight [kN/m]	E [GPa]	$\nu$
A-1	28 – 49	0,933	0,871	0,351	0,143	26,325	206	0,3
B-2	9–27   50– 61	0,975	0,910	0,385	0,171	28,875	206	0,3
C-3	2– 8   62– 66	1,029	0,961	0,425	0,211	31,875	206	0,3

### 3.1.3 Foundations

The type of foundation considered is that of piles that work by friction. The stays are anchored to reinforced concrete blocks, which have been sized to resist the net thrust acting on the tunnel, neglecting the weight of the anchors. The volume of a concrete block is equal to 1125 m<sup>3</sup>, with a mass of 2810 t and the shape of a parallelepiped of sides:

- L = 25 m;
- B = 15 m;
- H = 3 m.

The foundation piles are sized to resist only the traction force applied to the stays. It is assumed that the piles work for lateral friction only. Each foundation therefore consists of the foundation block, and of six piles of size:

- L = 51,5 m;
- R = 1,25 m.

This dimensioning is preliminary, useful in order to be able to determine the stiffness and damping to be attributed to the springs and dampers used in the numerical model to simulate the constraints given by the ground.

Figure 3-6 shows a second perspective of the tunnel model in 3D, with the foundations in view.

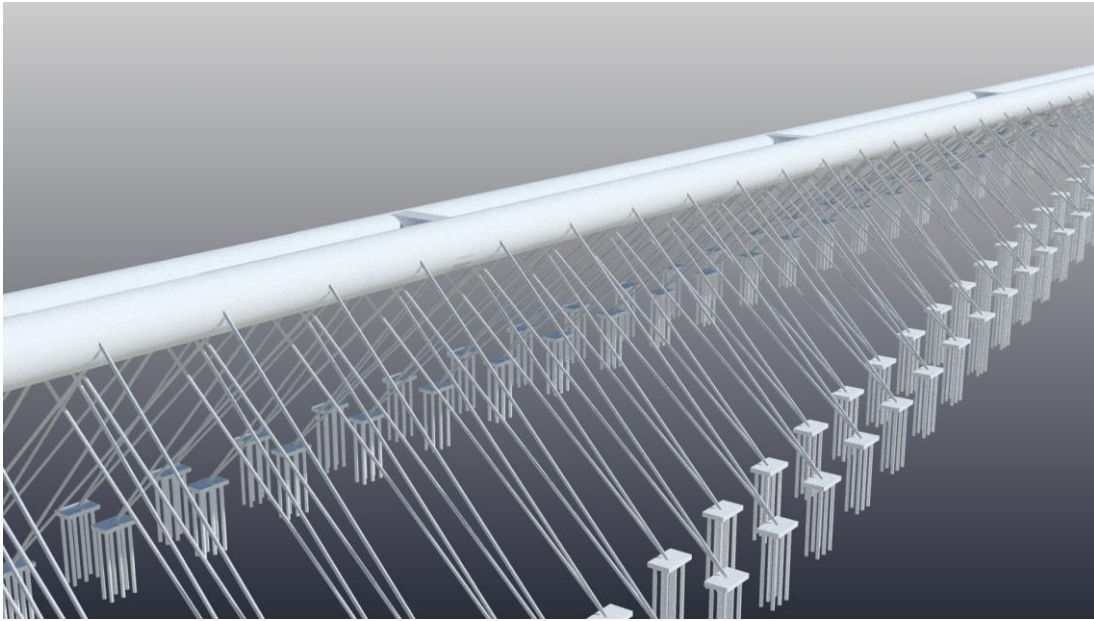


*Figure 3-6: 3D model of the Messina tunnel with the foundations in view*



## 3.2 Finite element model

The mathematical modelling of the tunnel is done with the Ansys Mechanical APDL software, which allows an easier definition of the parameters and commands through .txt files.

The finite element model used was created in a previous PhD thesis work by Chunxia (2013), subsequently refined and modified in this thesis work, adding some commands that allow it to interface with INTER and MATLAB, whose codes give the vertical and transversal loads of the train. Some of these commands were already defined by Palamà (2017), and have been upgraded in this thesis work, whereas some others are new. To the model, in this thesis, the variable masses due to the presence of vehicles in the tunnel have been added, making the tunnel in operation instead of empty, as better described at the end of paragraph 3.2.4.

In the .txt files of the finite element model, given by Chunxia (2013) and described in the following paragraphs, all the nodes are defined first, then the materials and beam elements, and finally the restraints and loads.

### 3.2.1 Nodes, material and elements

The two tubes consist of a sequential numbering of nodes from 18001 to 18265 for tube 1 and from 118001 to 118265 for tube 2, where the beginning of the numbering corresponds to the Calabrian coast. In fact, the reference system is located at the beginning of the Reggio Calabria coast, at node 18001, along tube 1, at a depth of 285 m with respect to the tunnel, which corresponds to the lowest point reached by the anchor bars. The tube's nodes have a distance equal to 18 meters (the nodes 18002, 18004, 18262, 18264 and equivalent for tube 2 must be excluded from the count).

The materials used are those defined in the previous paragraph: steel for the anchor bars and equivalent orthotropic material for the tubes. The Rayleigh damping calculated in paragraph 3.2.2, are added to the materials of the anchor bars, so as to be able to capture their non-linear behavior.

The beam elements are then defined in the finite element model. BEAM4 elements are used for the tubes. The section is not defined automatically by the program, but the individual geometric and mechanical properties are defined externally, as defined in Table 3-1. The additional mass of the outer circular crown of water, and the participating masses of the variable loads, defined in paragraph 3.2.4, are associated to this BEAM4 elements. In the center of gravity of the section, every 72 m, there is a master node. The anchor bars are connected to the section of the pipes via slave nodes to the master node. For the anchor bars, since they are long, BEAM188 elements are used, capable of capturing large displacements, for which the hollow cylindrical section is automatically defined by entering the dimensions of the internal and external radii. Each bar is modeled in the mesh with 9 elements. The connection of the bars to the ground, by means of foundation piles, as well as the connection of the pipes to the mainland at the ends, is modeled with COMBIN14 elements in each direction X, Y, Z, simulating the damper and spring system. The values used for the

stiffnesses are defined in paragraph 3.2.3. The COMBIN39 elements are also added to the ends of the tubes, to simulate the non-linear elastic behavior of the seismic dissipating devices, see paragraph 2.1.3.

Finally, the transverse connections between the two pipes are set every 468 m with the same elements defined for the pipes.

A generic section of the tunnel model is shown in Figure 3-7, while Figure 3-8 shows the geometry created on ANSYS APDL, with the reference system in view.

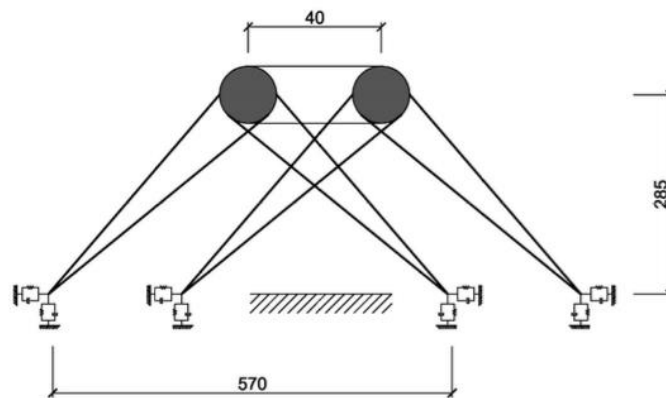


Figure 3-7: Finite element model section [Palamà G., 2017]

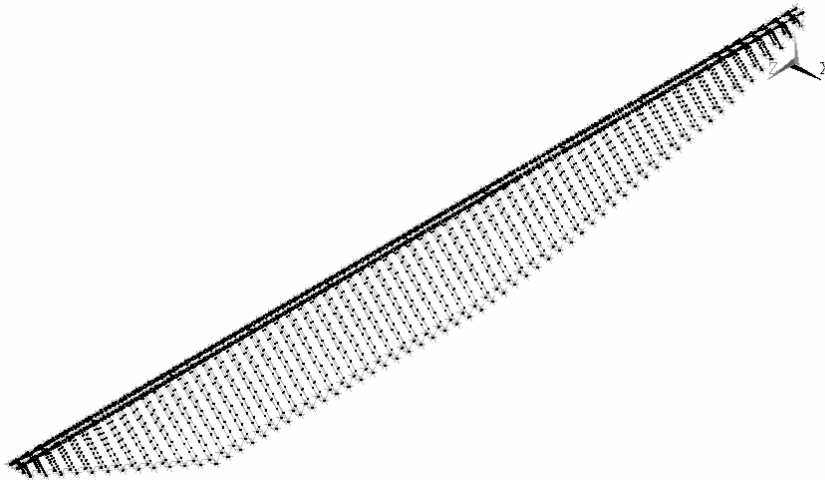


Figure 3-8: Numerical model of the tunnel on the ANSYS interface

### 3.2.2 Damping

To conduct the transverse and vertical transient analyses in this thesis it was decided to take into account the structural damping of the anchor bars, with a Rayleigh modelling. The structural damping is expressed through the damping matrix  $\underline{C}$ ,

defined at chapter 6. This matrix, according to the Rayleigh method, can be defined as a linear combination of the mass matrix  $\underline{\underline{M}}$  and the stiffness matrix  $\underline{\underline{K}}$ .

$$\underline{\underline{C}} = \alpha \underline{\underline{M}} + \beta \underline{\underline{K}} \quad (3.1)$$

These matrices, as explained in chapter 6, are known problem matrices, obtained automatically by ANSYS APDL.  $\alpha$  and  $\beta$  are real constants, chosen so as to produce a selected value of the damping ratio on two normal modes having natural frequencies equal to  $\omega_1$  and  $\omega_2$ . In Ansys what is defined is the damping ratio coefficient, equal to:

$$\zeta = \zeta_1 = \zeta_2 = 0,06 \quad (3.2)$$

Therefore, assuming, in accordance with the modal analysis,  $\omega_1 = 0,628$  rad/s and  $\omega_2 = 11,21$  rad/s, we obtain the values of  $\alpha$  and  $\beta$  reported in equations (3.3) and (3.4).

$$\alpha = \frac{2 \cdot \omega_1 \cdot \omega_2 \cdot (\omega_1 \cdot \zeta_1 - \omega_2 \cdot \zeta_2)}{\omega_1^2 - \omega_2^2} = \frac{2 \cdot \omega_1 \cdot \omega_2 \cdot \zeta}{\omega_1 + \omega_2} = 0,0714 \quad (3.3)$$

$$\beta = \frac{2 \cdot (\omega_1 \cdot \zeta_1 - \omega_2 \cdot \zeta_2)}{\omega_1^2 - \omega_2^2} = \frac{2 \cdot \zeta}{\omega_1 + \omega_2} = 0,0101 \quad (3.4)$$

This damping coefficient includes hydrodynamic damping. The effective modal damping for the modes having intermediate periods between the two chosen is lower (see Figure 3-9). For this reason, the analyses will be carried out in parallel also for a drastically reduced damping coefficient, equal to 1%, so as to report a range of solutions that will include also the real solution.

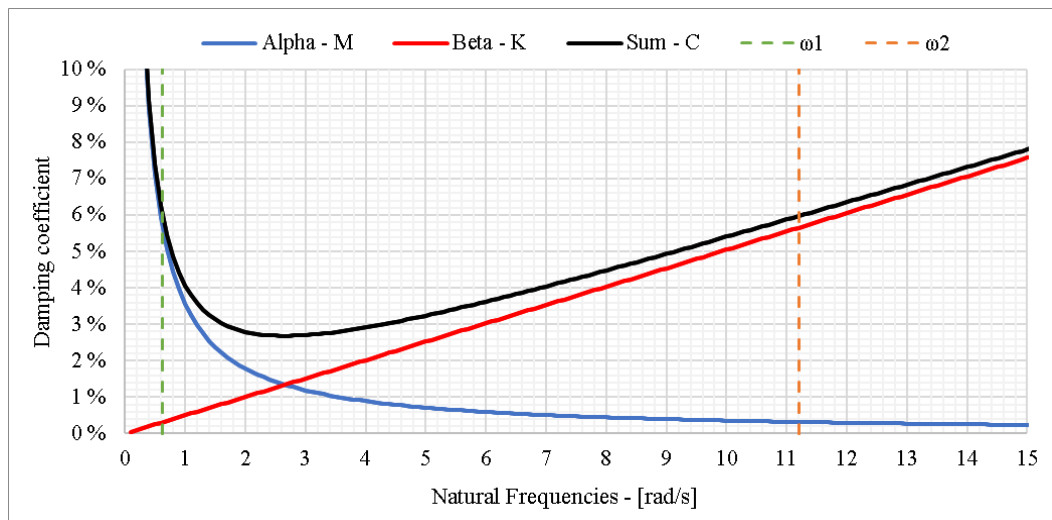


Figure 3-9: Rayleigh damping

### 3.2.3 Constraints

In the modelling of the structure a linear behaviour of the ground is assumed: the soil-structure interaction is represented by three elastic springs and three dampers positioned at the lower end of each anchor bar and at the ends of the two tunnels.

As anticipated, the constraints of the anchor bars to the ground are made with COMBIN14 elements in all three directions X, Y, Z.

Identified the maximum dimensions of the foundations, given at paragraph 3.1.3, it is possible to determine the stiffness and damping values of the three springs and the three dampers that are inserted in the model's elements. These values are reported in Table 3-3.

Table 3-3: Stiffness and damping values for COMBIN14 elements

Direction	K [kN/m]	C [kN s/m]
Transversal horizontal - X	$2,87 \cdot 10^6$	$2,66 \cdot 10^4$
Longitudinal horizontal - Z	$2,87 \cdot 10^6$	$2,66 \cdot 10^4$
Vertical - Y	$1,72 \cdot 10^7$	$1,14 \cdot 10^5$

A rigid constraint is therefore applied to the free end of the COMBIN14 elements. At the opposite end of the COMBIN14 elements, in the connection node with the anchor bars, a node containing the mass of the foundation concrete block, equal to 2810 t, is applied with the rotations constrained.

For the connections on the mainland, at the ends of the tunnel, the same COMBIN14 elements are adopted in all three directions, with the same constraints of the bars. A COMBIN14 element is added in series along the Z axis, with only damping. Also a COMBIN39 element is added in series along the Z axis, capable of simulating the non-linear elastic deformation of anti-seismic dissipating devices. In fact, as described in paragraph 2.1.3, to guarantee free deformations to the tunnel but at the same time a constraint for the earthquake, it is possible to install a device at the constrained end that is able to guarantee high plastic deformations when the axial force is higher than the limit value, and elastic behaviour below that strength. The values used in the model for the definition of the additional COMBIN39 and COMBIN14 element are described in Table 3-4.

Table 3-4: Stiffness and damping values for the COMBIN39 and COMBIN14 elements

Element	Direction	K [kN/m]	C [kN s/m]
COMBIN 14	Longitudinal horizontal – Z	0	$5,023 \cdot 10^4$
		$\epsilon$	<b>F [kN]</b>
COMBIN 39	Longitudinal horizontal – Z	0,1	$2,808 \cdot 10^5$
		4	$3,23 \cdot 10^5$

The master nodes of the tubes and the slave nodes of the bars have been constrained only for rotations, leaving X, Y and Z movements free.

### 3.2.4 Loads and masses

The complete immersion of the structure in water leads to consider very particular load conditions. The loads used for the analyses in this thesis work are:

- Dead load - Permanent;
- Archimedes' thrust - Permanent;
- Traffic load- Variable.

For the dead loads, the structure was modeled with elements with a density and an area, with which ANSYS automatically obtains its own weight per meter, once the acceleration of gravity along the Y axis has been applied. The dead loads values are those defined in the previous Tables 3-1 and 3-2.

Once that the acceleration of gravity is defined, it is applied to all the model, thus also to the additional mass defined for each element. The volume of water that surrounds the tunnel barrel, or the anchor bars, and adheres to them during motion, as defined by Morison's theory, is the additional mass. Since this volume has the same specific weight of the liquid in which it is immersed (it is always water), the Archimedes thrust that it receives is equal to its own weight. An equal and opposite force therefore must be applied, facing upwards to cancel the force of gravity of this additional mass of water. Considering the fluid-structure interaction through the Morison approach, the additional mass to be considered is calculated as:

$$m_a = \rho \cdot (C_m - 1) \cdot A = 1000 \cdot \pi \cdot R^2 \quad (3.5)$$

Where:

- $m_a$  is the additional mass per unit length;
- $\rho$  is the density of water. Since the structure is large and temperature and salinity varies, an average density of 1000 kg/m<sup>3</sup> is assumed;
- $A$  is the full section area;
- $C_m = 2$  is the mass coefficient which considers the mass adhering to the cylindrical tunnel if the immersion fluid is water.

The formula is valid for a cylindrical body immersed in a fluid. It can therefore be applied both to the tunnel tubes and to the anchor bars. The values of the additional masses are reported in Table 3-5, while in Figure 3-10 the volume of Morison water is shown in proportion to the tunnel.

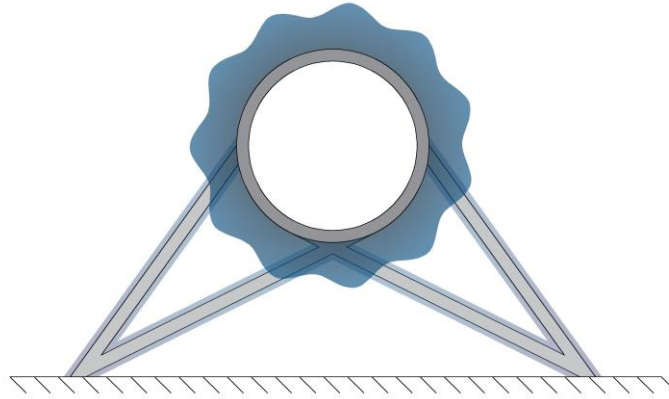


Figure 3-10: Volume of the additional mass in the tunnel pipes and bars

The second load (Archimedes' thrust) which acts on each immersed element, is equal to the volume of water displaced by the element multiplied by the density of the water and by the acceleration of gravity. Or, since  $C_m = 2$ , this thrust coincides with the additional mass multiplied by the acceleration of gravity.

Table 3-5: Archimedes thrusts and Morison masses defined in the model

Element	Archimedes' thrust [kN/m]	Morison's additional mass [kg/m]
Tube 1 and 2	1960	199807
Bars A	26,82	2733,9
Bars B	29,29	2985,6
Bars C	32,62	3325

The last type of loads, the variable one, including accessory loads, vehicle and railway loads, can reach a maximum of 50% compared to the tunnel's own weight, that is 600 kN/m [Chunxia S., 2013]. In the theses of both Chunxia (2013) and Palamà (2017), these loads were not taken into account as masses that can move together with the tunnel. They have been added in this study.

Rail traffic, as well as vehicular traffic, are dynamic variable loads, which are applied and studied together with the dynamics of the tunnel, with an iterative transient analysis. These loads have been developed in detail in the following chapters. However, when the train runs through the tunnel, also the road vehicles can be present, increasing the total mass of the tunnel excited by the transit of the train. On the basis of the variable loads, two models were created, representing two different tunnel situations.

1. Unloaded tunnel - Without vehicle masses;
2. Tunnel in operation - With vehicle masses.

The first model sees the unloaded tunnel, with a maximum net thrust of 760 kN/m, an upward maximum deformation of the tubes, and maximum tension on the anchor bars. The second model sees the tunnel in operation, with net thrust reduced to 455 kN/m, and a variable load equal to 300 kN/m, which reduces the modes of the tunnel, and increases the total inertial mass subject to displacements.

Transient analyses with trains were conducted only on the second model. To introduce the variable operating loads, the masses, corresponding to 50% of the maximum variable loads, 30581 kg/m, were added. According to Eurocode 8 (part 2 for bridges), for the earthquakes, 20% of the variable masses running in road bridges and 30% in railway bridges should be adopted. These conditions are therefore fully satisfied for our dynamic analyses, adopting 50%.

These masses are seen as vehicles that move together with the tunnel when the trains pass and excite the structure.

### 3.3 Static analysis

Given the loads shown in the previous paragraph, we can say that the permanent loads acting on the structure, per unit of length, amount to 1200 kN/m. Overall variable loads (including vehicular traffic lines) can result in an increase of up to a maximum of 50% compared to permanent loads. The net load acting on the tunnel can be calculated by subtracting the buoyancy force per unit length, equal to 1960 kN/m, from the structure's own weight per unit length. The resulting action on the tunnel is 160 kN/m upwards. This means that the tunnel will be pushed upwards even in the most unfavorable case: there is always a residual Archimedes' thrust. Otherwise, the diameter of the tunnel would have had to be increased to increase the BWR. When the tunnel is unloaded from vehicular loads, the residual Archimedes' thrust will be equal to 760 kN/m. Therefore, the tunnel in operation has a residual thrust varying between  $160 \div 760$  kN/m, corresponding to 13% and 63% of its own weight.

It must be observed that this residual thrust acts only on the two tubes. The anchor bars have been sized to balance their weight with the Archimedes' thrust. The foundation blocks and piles, on the other hand, have been sized to ensure a negative downward action. The balance of forces of the whole system is negative, so that even in the case with zero loads, with the maximum residual thrust on the tunnels, they do not come to the water surface. The system balance is shown in Table 3-6 in MN for the case of an unloaded tunnel. The elements therefore respond in this way in static conditions: the tubes tend to emerge, pulling the anchor bars in tension, which in turn will pull the foundation blocks upwards, however too heavy for the strength received, and therefore they will result in compression on the ground and constrained in their position by the friction of the piles.

Table 3-6: Balance between loads and thrusts of the system

Element	Weight	Archimedes' thrust	Net thrust	Number of components	Total [MN]	Progressive balance [MN]
<b>Tube</b>	-5616	+9173	+3557	2	+7114	+7114
<b>Links</b>	- 48	+78	+30	9	+274	+7388
<b>Bars – A</b>	-26,33	+26,82	+0,49	24x8x402m	+38	+7426
<b>Bars – B</b>	-28,88	+29,29	+0,41	28x8x281m	+26	+7452
<b>Bars – C</b>	-31,88	+32,62	+0,74	13x8x229m	+18	+7470
<b>Foundation blocks</b>	-28,1	+11	-17,07	65 x 4	-4437	+3033
<b>Piles</b>	-5,456	+2,479	-2,977	6 x 65 x 4	-4644	-1611

To obtain the static solution of the ANSYS model, a non-linear analysis is performed that takes into account the large displacements of the structure and the non-linear behaviour of the elements.



Two static analyses were carried out, representing the two situations of empty tunnel and tunnel in operation.

### 3.3.1 Empty tunnel

Figure 3-11 shows the static deformation of the tunnel in the three-dimensions, while Figure 3-12 shows the static deformations of the middle anchor bars, in a view on the XY plane.

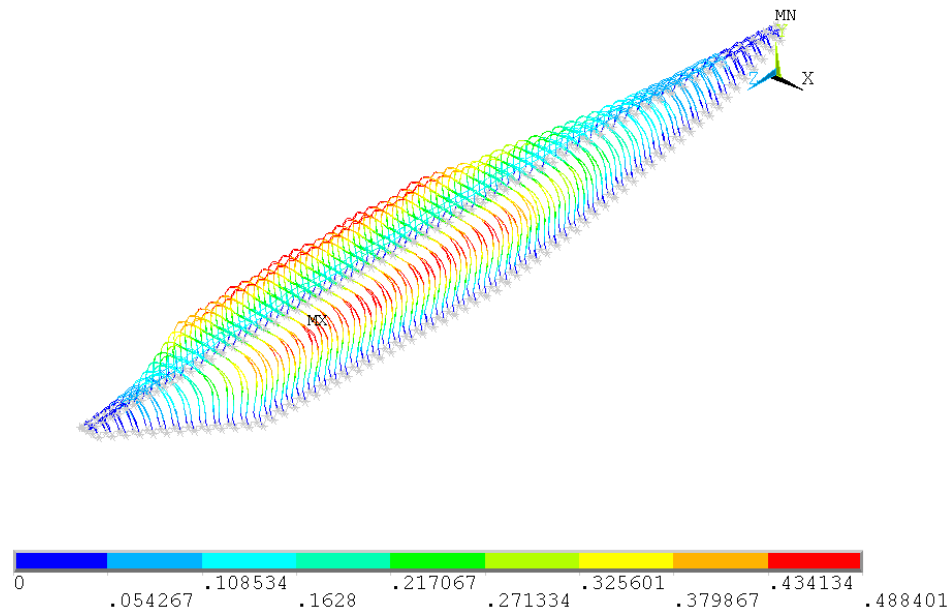


Figure 3-11: Static deformed shape of the unloaded tunnel

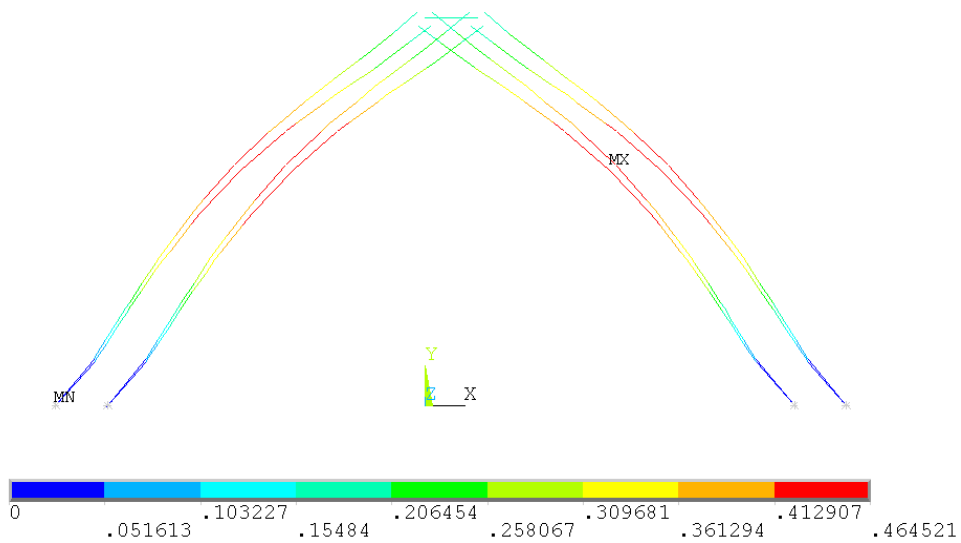


Figure 3-12: Static deformed shape of the anchoring bars

It is apparent that the displacements of the anchoring systems are larger than the displacements of the tunnel. To better represent the deformation of the tunnel, the vertical displacement of the nodes of the two pipes has been reported in the graph of Figure 3-13.

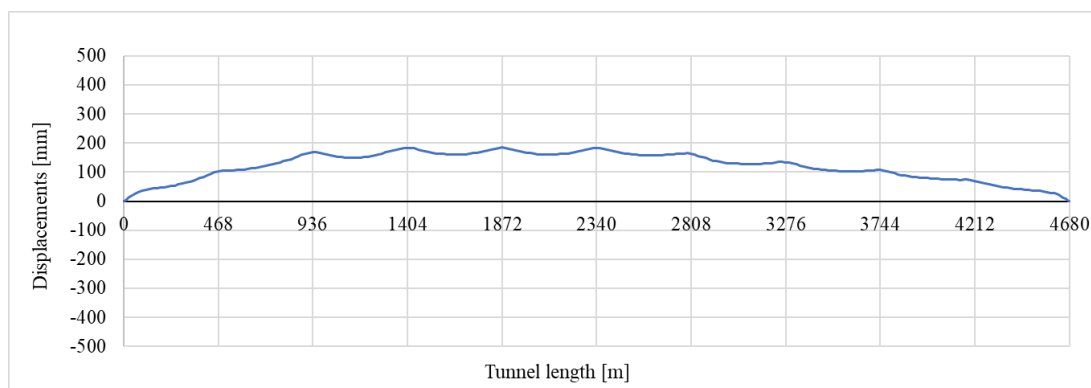


Figure 3-13: Static vertical deformed shape of the rods

Also in the transverse direction the tunnel sees a negligible deformation of 0,03 mm, halfway between two subsequent connections, where the pipes have fewer transverse constraints.

Some stays are taken from the model, shown in Table 3-7. The values of the axial actions and the related stresses are reported. The bending moments are omitted, not because they are absent, but for simplicity of presentation. The stays referred to are positioned on the high outer sides of the two tubes, sampled in a regular and non-regular way. Inner stays have identical or very similar actions, while those positioned at a low level have lower actions. For this reason it is considered sufficient to report only the present 28 stays between all 520.

Table 3-7: Axial forces on the stays – Static analysis unloaded tunnel

Anchor bar	Position from reference system [m]	Model element	Length [m]	Section	Axial force [kN]	Stress [MPa]
<b>Tube 2</b>						
1	36	3163	46,24	C	+17247	40,58
2	396	3343	138,65	C	+22657	53,31
3	756	3523	209,65	B	+20722	53,82
4	1116	3703	266,19	B	+20677	53,71
5	1476	3883	322,74	B	+22255	57,80
6	1836	4063	366,57	B	+23631	61,38
7	2196	4243	401,92	A	+21127	60,19
8	2556	4423	401,92	A	+20757	59,14
9	2916	4603	401,92	A	+21676	61,75

<b>10</b>	3276	4783	401,92	B	+23427	60,85
<b>11</b>	3636	4963	401,92	B	+21750	56,49
<b>12</b>	3996	5143	315,48	B	+20671	53,69
<b>13</b>	4356	5323	171,38	C	+21599	50,82
<b>14</b>	4644	5467	56,39	C	+16418	38,63
<b>Tube 1</b>						
<b>15</b>	36	9	46,24	C	+17247	40,58
<b>16</b>	468	225	157,20	B	+24743	64,27
<b>17</b>	756	369	209,65	B	+20722	53,82
<b>18</b>	1188	585	277,50	B	+20604	53,52
<b>19</b>	1476	729	322,74	B	+22255	57,80
<b>20</b>	1908	945	373,64	A	+22507	64,12
<b>21</b>	2196	1089	401,92	A	+21127	60,19
<b>22</b>	2628	1305	401,92	A	+20893	59,52
<b>23</b>	2916	1449	401,92	A	+21676	61,75
<b>24</b>	3348	1665	401,92	A	+22293	63,51
<b>25</b>	3636	1809	401,92	B	+21750	56,49
<b>26</b>	4068	2025	286,63	B	+20937	54,38
<b>27</b>	4356	2169	171,38	C	+21599	50,82
<b>28</b>	4644	2313	56,39	C	+16418	38,63

### 3.3.2 Tunnel in normal operation

Figure 3-14 shows the three-dimensional static deformation of the tunnel with 50% of the vehicular loads, while Figure 3-15 shows the static deformations of the anchor bars in the middle, in a view on the XY plane.

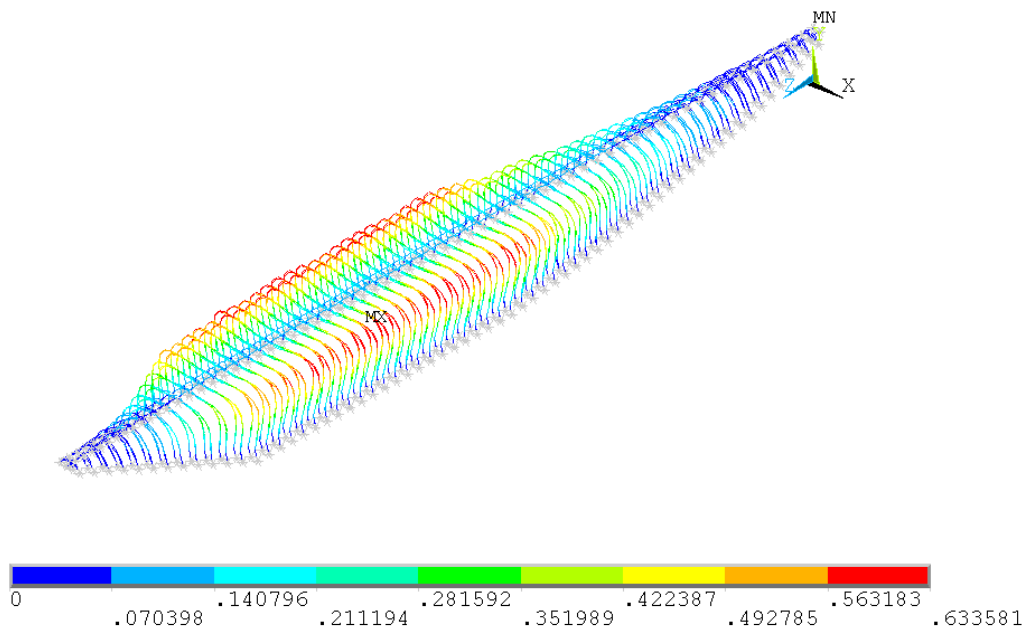


Figure 3-14: Static deformed shape of the tunnel in operation

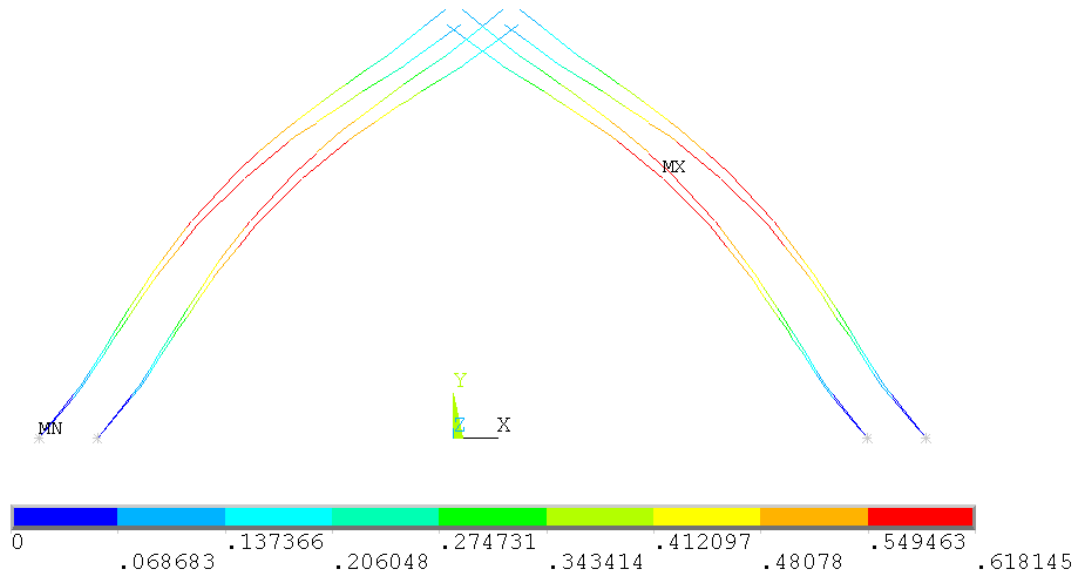


Figure 3-15: Static deformed shape of the anchor bars

Also in this situation the displacements of the anchoring systems are greater than the displacements of the tunnel. It is also possible to observe that the deformation of the bars is greater in this situation than in the previous one. In fact, the tubes with less net thrust give less tension to the anchors.

In order to better represent the deformation of the tunnel, the vertical displacement of the nodes of the two tubes has been reported in the graph of Figure 3-16.

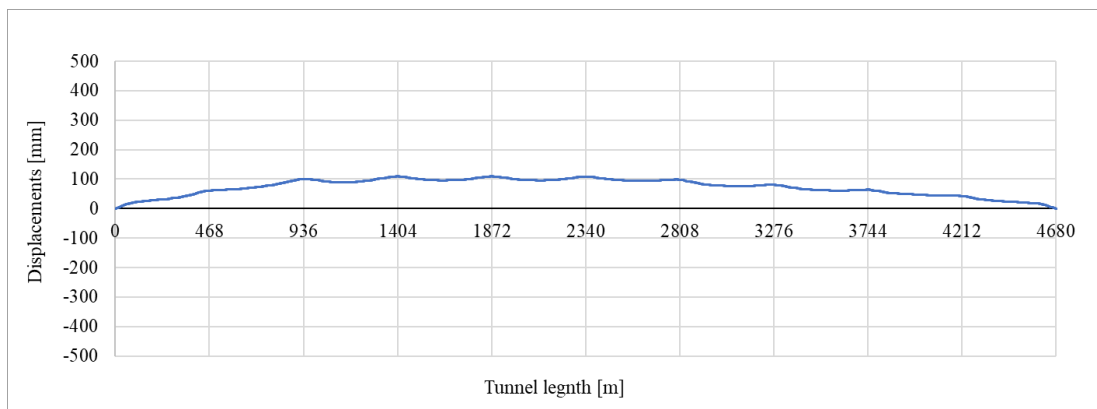


Figure 3-16: Static vertical deformed shape of the rods

The same stays as before are taken from the model, shown in Table 3-8, as a reference for evaluating the variation in the axial forces with the masses of the vehicles.

Table 3-8: Axial forces on the stays – Static analysis operational tunnel

Anchor bar	Position from reference system [m]	Model element	Length [m]	Section	Axial force [kN]	Stress [MPa]
<b>Tube 2</b>						
1	36	3163	46,24	C	+10521	24,76
2	396	3343	138,65	C	+13944	32,81
3	756	3523	209,65	B	+12824	33,31
4	1116	3703	266,19	B	+12866	33,42
5	1476	3883	322,74	B	+13890	36,08
6	1836	4063	366,57	B	+14765	38,35
7	2196	4243	401,92	A	+13279	37,83
8	2556	4423	401,92	A	+13050	37,18
9	2916	4603	401,92	A	+13606	38,76
10	3276	4783	401,92	B	+14656	38,07
11	3636	4963	401,92	B	+13680	35,53
12	3996	5143	315,48	B	+12921	33,56
13	4356	5323	171,38	C	+13350	31,41
14	4644	5467	56,39	C	+10035	23,61
<b>Tube 1</b>						
15	36	9	46,24	C	+10521	24,76
16	468	225	157,20	B	+15232	39,56
17	756	369	209,65	B	+12824	33,31
18	1188	585	277,50	B	+12837	33,34
19	1476	729	322,74	B	+13890	36,08
20	1908	945	373,64	A	+14078	40,11
21	2196	1089	401,92	A	+13279	37,83
22	2628	1305	401,92	A	+13132	37,41
23	2916	1449	401,92	A	+13606	38,76
24	3348	1665	401,92	A	+13978	39,82
25	3636	1809	401,92	B	+13680	35,53
26	4068	2025	286,63	B	+13049	33,89
27	4356	2169	171,38	C	+13350	31,41
28	4644	2313	56,39	C	+10035	23,61

## Modal analysis

The modal analysis of the entire structure is based on the equilibrium configuration obtained from the non-linear static analysis of the previous paragraph. The results of the modal analysis show many local modes of the bars, leading to a very complex representation in which the behavior of the tunnel is partially hidden. To solve this problem and obtain a more representative image of the modal shapes of the two tubes, anchoring bars consisting of a single element and having inertia concentrated only at the ends were used [Chunxia S., 2013]. The modal shapes of the first 9 modes are shown in Tables 3-11 – 3-15.

Since in the case of tunnel in operation some masses distributed on the pipes are added, this mass increment implies a variation of the period equal to:

$$\frac{T_2 - T_1}{T_1} = \frac{\sqrt{\frac{m_2}{k}} - \sqrt{\frac{m_1}{k}}}{\sqrt{\frac{m_1}{k}}} = \frac{\sqrt{m_2} - \sqrt{m_1}}{\sqrt{m_1}} = \sqrt{1,095} - \sqrt{1} = 4,6 \% \quad (3.6)$$

Where  $m_1$  is the mass of the unloaded tunnel, and  $m_2$  is the mass of the tunnel in operation, which corresponds to 9,5% greater than  $m_1$ . If the periods then increase by 4,6%, the frequencies will decrease by 4,6%. The modal shapes do not change, only the periods are shifted. Table 3-9 shows the natural frequencies of the unloaded tunnel, while Table 3-10 shows the natural frequencies of the tunnel in operation. Transient analyses with trains have been carried out only with the latter.

Table 3-9: Natural modes of the Messina floating tunnel empty

Mode	Direction	Natural frequency [Hz]	Period [s]
1	Longitudinal – 1	0,157	6,369
2	Longitudinal – 2	0,337	2,967
3	Torsional – 1	0,443	2,257
4	Torsional – 2	0,517	1,934
5	Longitudinal – 3	0,534	1,873
6	Transversal – 1	0,559	1,789
7	Vertical – 1	0,561	1,782
8	Vertical – 2	0,565	1,769
9	Transversal – 2	0,565	1,769

*Table 3-10: Natural modes of the Messina floating tunnel in operation*

<b>Mode</b>	<b>Direction</b>	<b>Natural frequency [Hz]</b>	<b>Period [s]</b>
1	Longitudinal – 1	0,150	6,662
2	Longitudinal – 2	0,322	3,103
3	Torsional – 1	0,424	2,361
4	Torsional – 2	0,494	2,023
5	Longitudinal – 3	0,510	1,959
6	Transversal – 1	0,534	1,871
7	Vertical – 1	0,536	1,864
8	Vertical – 2	0,540	1,850
9	Transversal – 2	0,540	1,850

Observing the first nine natural modes we can say that the SFT can respond to the travelling of the trains for vertical dynamics with the torsional modes (third and fourth) and with the vertical modes (seventh and eighth). As for the transverse dynamic analysis, on the other hand, the SFT can respond to the passage of the train with transversal modes (sixth and ninth).

The easiest way to vibrate is the longitudinal one associated with a translation of the SFT. This result is due to the presence of dampers and anchoring springs to the mainland which allow a relative displacement of the structure as described in the previous paragraphs.

Table 3-11: Modal shape 1 and 2

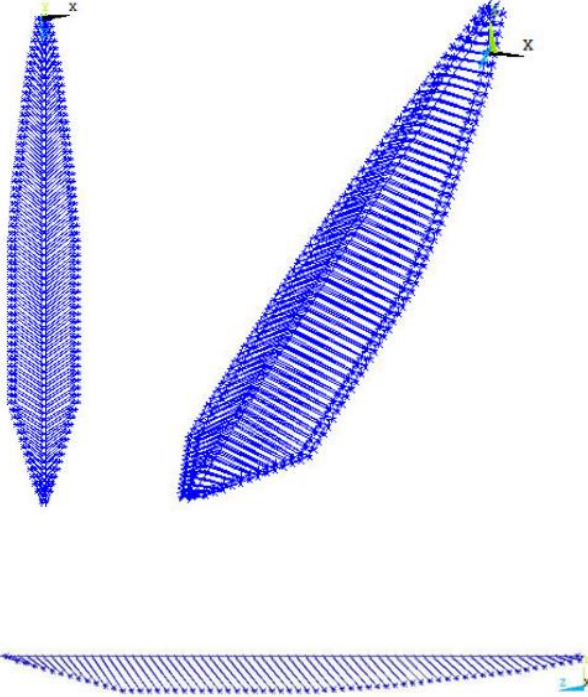
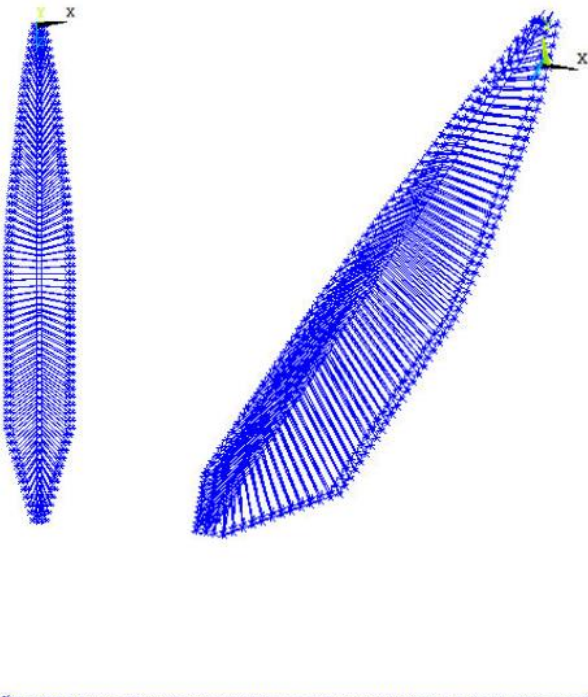
	<p style="text-align: center;"><b>Mode 1</b></p> <p style="text-align: center;"><i>First longitudinal mode</i></p> <p style="text-align: center;"><math>T_1</math> - Empty = 6,369 s</p> <p style="text-align: center;"><math>T_1</math> - Operation = 6,662 s</p>
	<p style="text-align: center;"><b>Mode 2</b></p> <p style="text-align: center;"><i>Second longitudinal mode</i></p> <p style="text-align: center;"><math>T_2</math> - Empty = 2,967 s</p> <p style="text-align: center;"><math>T_2</math> - Operation = 3,103 s</p>



Table 3-12: Modal shape 3 and 4

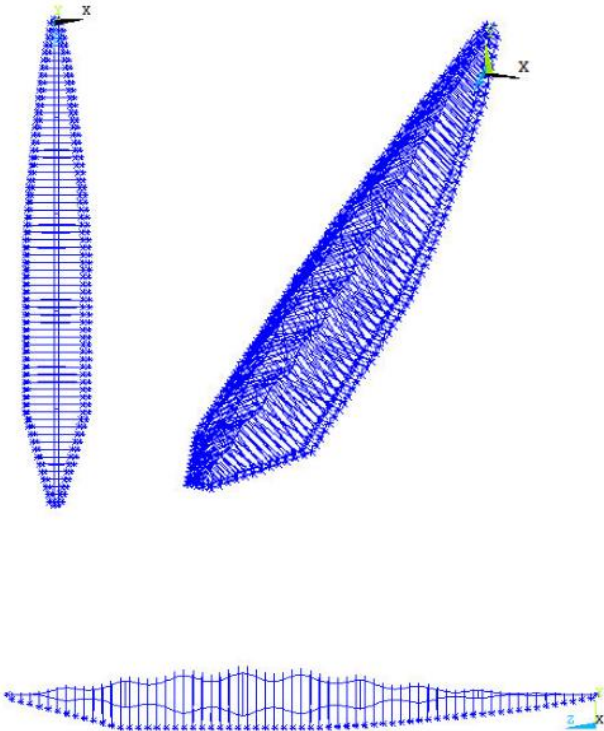
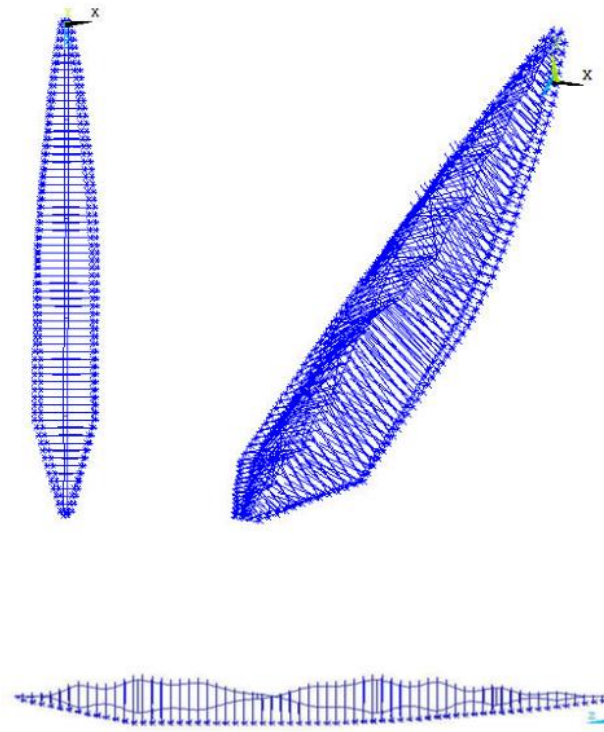
	<p style="text-align: center;"><b>Mode 3</b></p> <p style="text-align: center;"><i>First torsional mode</i></p> <p style="text-align: center;"><math>T_3</math> - Empty = 2,257 s</p> <p style="text-align: center;"><math>T_3</math> - Operation = 2,361 s</p>
	<p style="text-align: center;"><b>Mode 4</b></p> <p style="text-align: center;"><i>Second torsional mode</i></p> <p style="text-align: center;"><math>T_4</math> - Empty = 1,934 s</p> <p style="text-align: center;"><math>T_4</math> - Operation = 2,023 s</p>

Table 3-13: Modal shape 5 and 6

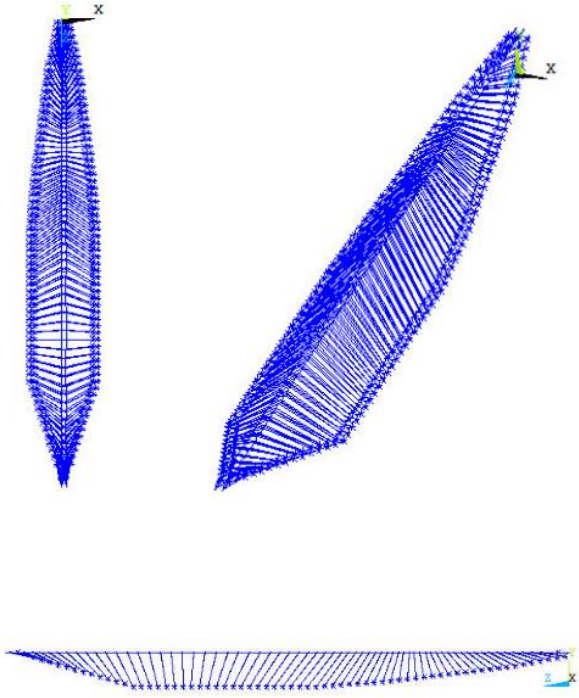
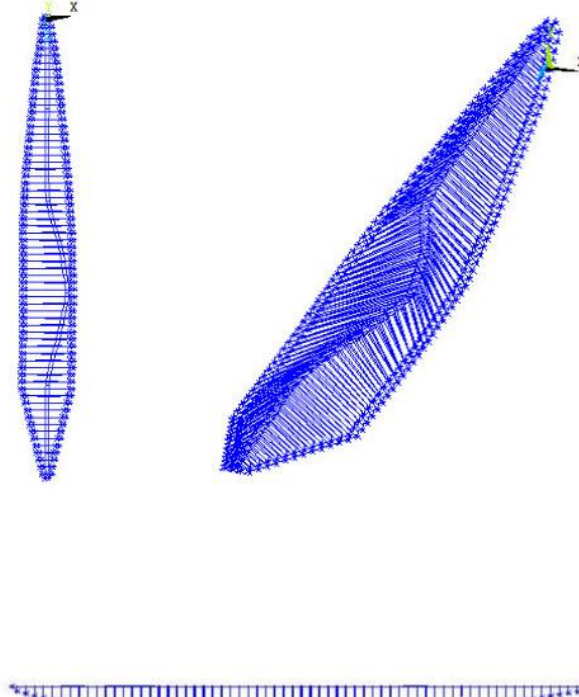
	<p style="text-align: center;"><b>Mode 5</b></p> <p style="text-align: center;"><i>Third longitudinal mode</i></p> <p style="text-align: center;">T<sub>5</sub> - Empty = 1,873 s</p> <p style="text-align: center;">T<sub>5</sub> - Operation = 1,959 s</p>
	<p style="text-align: center;"><b>Mode 6</b></p> <p style="text-align: center;"><i>First transversal mode</i></p> <p style="text-align: center;">T<sub>6</sub> - Empty = 1,789 s</p> <p style="text-align: center;">T<sub>6</sub> - Operation = 1,871 s</p>

Table 3-14: Modal shape 7 and 8

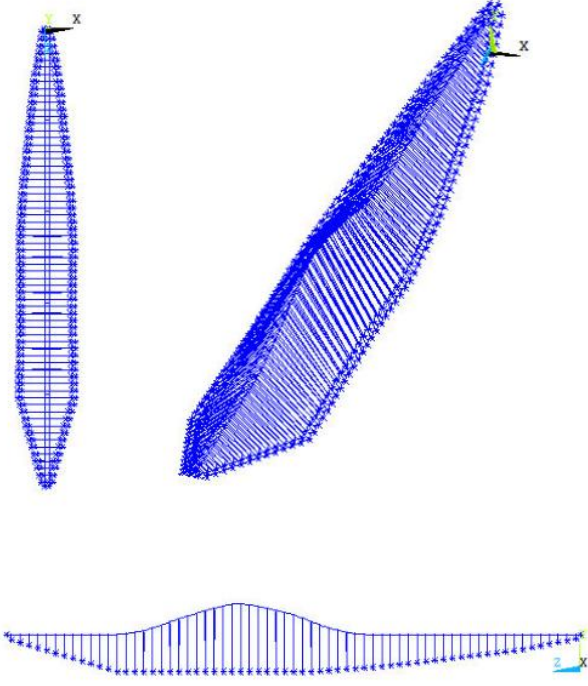
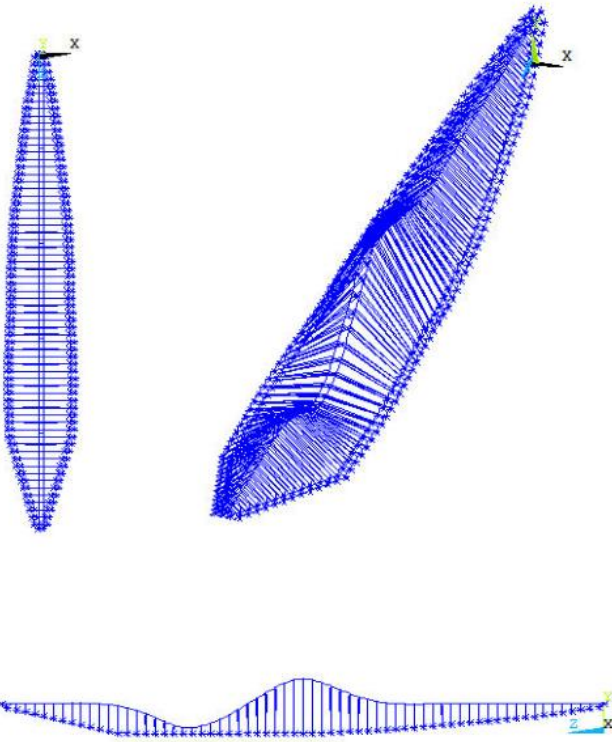
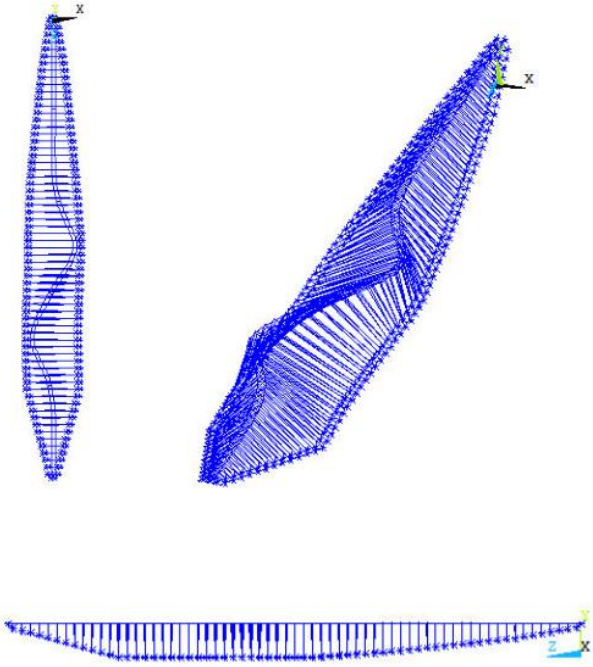
	<p style="text-align: center;"><b>Mode 7</b></p> <p style="text-align: center;"><i>First vertical mode</i></p> <p style="text-align: center;"><math>T_7</math> - Empty = 1,782 s</p> <p style="text-align: center;"><math>T_7</math> - Operation = 1,864 s</p>
	<p style="text-align: center;"><b>Mode 8</b></p> <p style="text-align: center;"><i>Second vertical mode</i></p> <p style="text-align: center;"><math>T_8</math> - Empty = 1,769 s</p> <p style="text-align: center;"><math>T_8</math> - Operation = 1,850 s</p>

Table 3-15: Modal shape 9

	<b>Mode 9</b>
	<p data-bbox="979 707 1302 741"><i>Second transversal mode</i></p> <p data-bbox="1007 781 1275 815">T<sub>9</sub> - Empty = 1,769 s</p> <p data-bbox="984 855 1297 889">T<sub>9</sub> - Operation = 1,850 s</p>

# 4

## **RAILS MODELING**

This chapter describes the way in which rails are considered and introduced within the model. First, the type of rail on which the analyses are performed is defined. Subsequently, the irregularities of the tracks are calculated, to be inserted in the coupled equation of motion.

## 4.1 Configuration and assumptions

Since the structure on which the train has to travel is a concrete tunnel, the rail will be anchored directly on the concrete plates, with fastenings and concrete alignment flanges. In this way, the tracks (superstructure) are fixed directly to the tunnel (substructure), avoiding elastic deformations caused by sleepers, ballast or subsoil. However, the deformations due to the fastenings (anchoring hooks and rail pad between the rail and the tunnel), are not null. These deformations are considered in the model.

This rail construction technique is already widely adopted in underground tunnels; see the Figure 4-1, representing a section of the San Gottardo's tunnel in Switzerland.

During the motion, the generic wheel oscillates vertically due to the deformation of both the substructure (tunnel) and the superstructure (irregularities present in the rail system). The rail profile is thus inserted as a function that defines the coordinate of the contact point between the wheel and the rail with respect to the axis of the tunnel, as the length of the tunnel varies. This function is hereinafter referred to as roughness or irregularity.



*Figure 4-1: Rails anchored to a concrete slab. San Gottardo's tunnel - Switzerland*

## 4.2 Irregularities

Today's rail track construction techniques tend to be increasingly accurate and precise, making horizontal and vertical misalignments practically imperceptible. However human errors, wear, thermal effects and time degradation are unavoidable factors that cause variations of the rails. Irregularities are small imperfections compared to the idealized geometry of the track. Such discrepancies are a major source of excitation when a train passes over a tunnel, and certainly cannot be overlooked for a floating tunnel.

Two types of irregularities can be distinguished:

- Typical irregularities: are divided in random and periodic;
- Isolated irregularities: represented by specific functions, eight types exists.

The sources of typical random irregularities, which characterize a track, are wear, the clearance between the wheels, settlements, insufficient maintenance or the presence of areas with different stiffness. Their nature is therefore completely random and for this reason they are represented by PSD (Power Spectral Density). The typical periodic irregularities are caused by the joints at the ends of the rail. Finally, isolated irregularities are consequences of specific problems in the track of interest.

These misalignments can be expressed in several forms, depending on the reference system considered. In this work only the vertical profile and the horizontal alignments are considered. Both correspond to the average function between the two rails taken individually. Thus obtained the vertical profiles ( $Z_R$ ,  $Z_L$ ) and the horizontal alignments ( $Y_R$ ,  $Y_L$ ), of the right and left rail, of a certain population of tracks, the profile and the alignment to refer to are obtained as:

$$I_P(x) = [Z_R(x) + Z_L(x)]/2 \quad (4.1)$$

$$I_A(x) = [Y_R(x) + Y_L(x)]/2 \quad (4.2)$$

Where  $I_P$  indicates the vertical irregularity of the profile, and  $I_A$  indicates the horizontal irregularity of the alignments, as function of the longitudinal coordinate  $x$ . Figure 4-2 shows the difference between the irregularities of the single rail and the average ones.

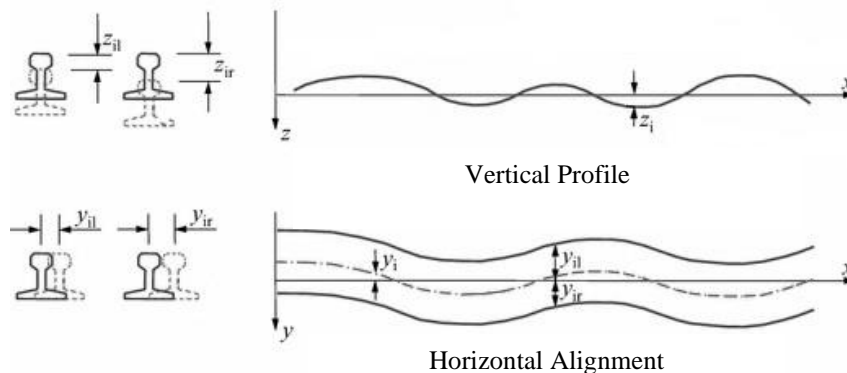


Figure 4-2: Profile and alignment of a rail

Each of the previous functions is obtained from accurate measurements on the single rail, both horizontally and vertically, usually conducted by the national institutes.

In this thesis work, reference is made to a rail for high-speed trains resting on concrete slabs. It follows that there are neither isolated nor periodic irregularities, but only random irregularities, as illustrated in the next paragraphs.

### 4.2.1 Power Spectral Density (PSD)

Several measurements have shown that typical random irregularities represent a stochastic stationary process and can be described by a power spectral density function (PSD). Each of the random horizontal and vertical irregularity profiles  $I_{P,A}$ , in an arbitrary position  $x$ , is described by its spatial mean value and its autocorrelation function  $R_I$ . Applying the Fourier transform we obtain the power spectral density function  $S(\Omega)$ .  $\Omega$  is the angular frequency, measured in [rad/m], and obtained from the ratio  $2\pi/\lambda$ , where  $\lambda$  represents the wavelength measured in meters. To classify the quality of the rails, national authorities such as Germany, China and America presented PSD functions in closed analytical form. For this work the Power Spectral Densities defined in Germany by Claus & Schiehlen (1998) and adapted by Salcher et al. (2019) have been used:

$$S_{P,A}(\Omega) = Q_{P,A} \frac{\Omega_c^2}{2(\Omega_r^2 + \Omega^2)(\Omega_c^2 + \Omega^2)} \quad (4.3)$$

$S_P$  refers to the profile, while  $S_A$  refers to the alignment of the rail. The values of the constants are  $\Omega_C = 0,8246$  rad/m and  $\Omega_R = 0,0206$  rad/m. The spectral amplitude is defined by  $Q$ , which represents the roughness of the rail (both for the profile and for the alignment), and it is dependent on the rail class. The higher the class, the better the quality and the lower the roughness, so the smaller the width of irregularities. This constant varies within the range  $Q_{High} = 5,923 \cdot 10^{-7}$  m rad and  $Q_{Low} = 15,861 \cdot 10^{-7}$  m rad, where "High" indicates a high class of rail and "Low" a low class.

This report considers for the profile  $Q_P = 7,51308 \cdot 10^{-7}$  m rad and for the alignment  $Q_A = 5,923 \cdot 10^{-7}$  m rad, corresponding to high roughness classes, i.e. the equivalent class 6 in subdivisions of American classes. The graphs obtained, in logarithmic scale, of the PSD are shown in Figure 4-3.

### 4.2.2 Typical random irregularities

The realization of the irregularities is obtained with equation (4.4), taking into account equation (4.3) in a certain finite range of frequencies, provided by Salcher et al. (2019).

$$I_{P,A}(x) = \sqrt{\frac{2}{\pi}} \sum_{j=1}^J \sqrt{S(\Omega_j) \Delta\Omega} \cos(\Omega_j x + \varphi_j) \quad (4.4)$$



In equation (4.4)  $J$  is the total number of discrete angular frequencies  $\Omega_j$ , considered within the frequency window;  $\varphi_j$  is the independent random phase, uniformly distributed in the interval  $[0, 2\pi]$  with  $j=1, \dots, J$ ;  $\Delta\Omega = (\Omega_{\text{Max}} - \Omega_{\text{Min}})/J$  is the frequency increment with which it can be defined  $\Omega_{j+1} = \Omega_j + \Delta\Omega$ ;  $\Omega_{\text{Max}}$  is the maximum frequency considered in the range and  $\Omega_{\text{Min}}$  the minimum. The variable  $x$  can vary between 0 and infinite. In this case study  $0 \leq x \leq 5680$  m, i.e. the length of the tunnel of 4680 m plus an additional initial and final track of 500 m.

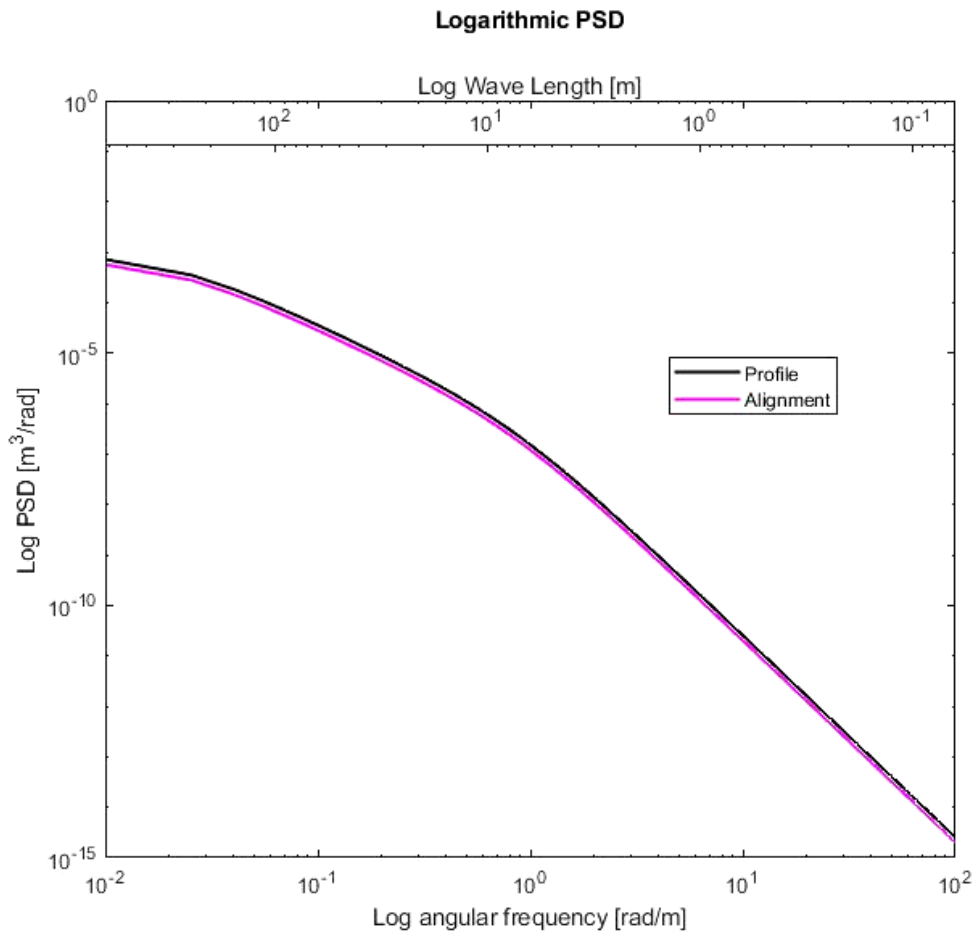


Figure 4-3: Power Spectral Density of profile and alignment

For the choice of the frequency window, Claus & Schiehlen (1998) take into account wavelengths up to 0,48 m (13 rad/m).

Other authors in the literature adopt wavelengths between 150 m and 0,5 m, making use of American and German PSDs. However, the FRA (Federal Railroad Administration) defines that wavelengths that are too long, over 100 m (frequencies that are too low) are caused by settlements either of the sleepers or of the ballast. These causes cannot be present in this case study since the rail is anchored to concrete slabs.

The following frequency window is therefore considered:

$$\begin{cases} \Omega_{\text{Max}} = 4\pi \left[ \frac{\text{rad}}{\text{m}} \right] \rightarrow \lambda_{\text{Min}} = 0,50 \text{ m} \\ \Omega_{\text{Min}} = \frac{\pi}{50} \left[ \frac{\text{rad}}{\text{m}} \right] \rightarrow \lambda_{\text{Max}} = 100 \text{ m} \end{cases} \quad (4.5)$$

The number of realizations that can be obtain is infinite. Those adopted in the following analyses are described in Figures 4-4 and 4-5.

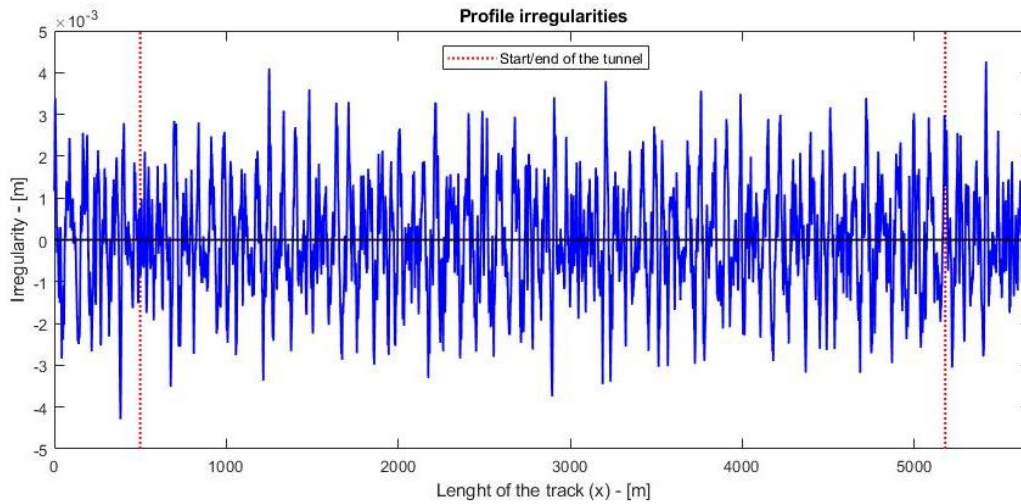


Figure 4-4: Realization of random profile irregularities

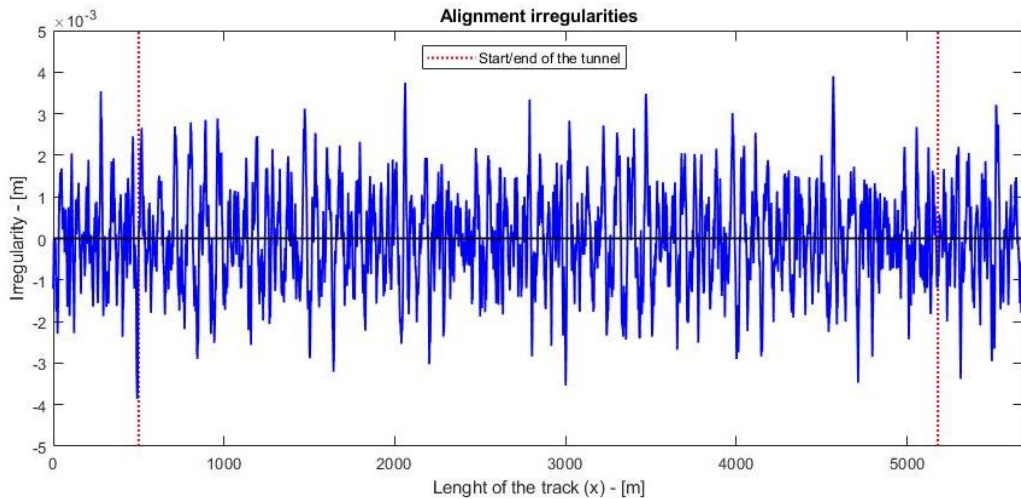


Figure 4-5: Realization of random alignment irregularities

### 4.2.3 Typical periodic irregularities

The production of the rails in the workshop takes place by rolling, the maximum length of which varies from the country of production. In Italy, the UNI standard lengths are adopted, for which there are rails long 12, 18 and 36 m, which can be electrically welded together to reach higher lengths.

For rails used for high-speed trains, electric welding can prevent the presence of bolted joints, avoiding periodic irregularities. Thus, no periodic irregularities will be considered in this work.

### 4.2.4 Isolated irregularities

The power spectral density function cannot take into account the presence of isolated irregularities with large amplitudes, since these irregularities are obscured by the stochastic process [FRA, 1983]. Isolated variations represent occasional irregularities with shapes that can be defined by mathematical functions. These variations can produce great dynamic responses in the vehicle and in the structure.

According to FRA (1983), 8 kind of isolated irregularities can be identified in the rails. However, most of these, such as sinusoids and trough, develop due to ballast settlements, and have no reason to exist for a rail resting on concrete slabs. Other irregularities, such as jogs and bumps occur in situations of curves or spirals, which are not present inside the tunnel.

Therefore, also these irregularities are not taken into account in this thesis work.



# 5

## TRAIN MODELING

In the design of a bridge the most important class of dynamic loads acting in operation is represented by the loads from traffic. The vehicles that will transit on the SFT are motorbikes, road vehicles and trains.

This work focuses on railway vehicles. The problem of the train-structure dynamic interaction arises from the need to study the coupled response of the two systems. The floating tunnel deforms under the action of the contact forces transmitted by the traveling bodies. The wheels of the wagons, following the deformed bridge profile, undergo displacements. The inertial effects of the masses constituting the wagons generates dynamic contact forces and the two systems start to oscillate. The variability of the irregularities of the rails, which significantly affects the motion of the wagons, is added to the deformation of the floating tunnel.

This chapter describes the train models adopted in the dynamic analysis of train-SFT in vertical and transversal direction.

## 5.1 The mechanical system

A train is a multi-degree of freedom system (MDOF), and is intrinsically coupled to the rail and structure system. However, to conduct a numerical dynamic analysis, the number of DOFs must be limited, to reduce the computation times. Several models, described in paragraph 1.1, were introduced in the literature with the development of increasingly powerful computers.

For the dynamic analysis, in this work a mechanical model decoupled among the three axes of direction is used. In the vertical direction, a plane model with 10 DOF is adopted, while for the transverse dynamic analysis the model is simplified into a convoy of traveling forces with varying direction and amplitude.

The wagons are not connected through transverse or vertical constraints, but are joined in the longitudinal direction only, since each wagon is linked to the other and pulled by the motor wagon to ensure the same constant speed. The displacements of the masses and the induced dynamics response have to be attributed to the single wagon, isolated, and not influenced by the previous or following wagons. Thus, the train result in a convoy of vehicles. The motor cars have different properties and masses than the passenger cars. The number of wagons and their arrangement varies according to the type of convoy considered. Two convoys will be used:

- Convoy for low and medium speeds;
- Convoy for high speeds.

Although freight trains are those with greater mass, compared to passenger trains, the former can only travel up to 100/120 km/h, resulting in lower dynamic actions than a medium or high speed train.

## 5.2 Mechanical model in the vertical direction

The behaviour of the wagon is analysed separately in vertical, transversal and longitudinal direction. In this thesis, the vertical behaviour of the single wagon is schematized as a plane mechanical system (two-dimensional - without depth) consisting of rigid bodies, with mass and inertia, connected to each other through springs and viscous dampers. The TBDIM model is used in this study within the INTER 7.0 code. The model has 10 DOFs, to which 4 DOFs must be added for the contact points between the wheel and the rail.

The basic assumptions for the definition of the train model, according to the approach of Mulas et al. (2008 and 2010), are:

- The vertical, horizontal and longitudinal motions of the single wagon are uncoupled;
- The convoy travels at a constant speed and equal for each wagon, along a straight track parallel to the axis of the tunnel;
- The contact point between the wheel and rail is reduced to a point without mass, and the transmitted force in this point is orthogonal to the plane of the tunnel;
- The contact between wheel and rail is perfect;
- The internal and external constraints are smooth, bilateral, and holonomic.

With these hypotheses, it is possible to describe the motion of the wagon masses through a set of Lagrangian vertical coordinates and rotations, as shown in Figure 5-1.

Figure 5-1 represents a classic four-axle wagon, whose depth is neglected, and having seven masses. The cab has a mass  $M$  and inertia  $I_0$ , the bogies have a mass  $m_i$  and inertia  $I_i$ , while all the wheels have a mass  $m_w$ . The index  $i$  varies between 1 and 2 and indicates the properties of the right (front) or left (rear) bogie, respectively. The body cab, like the bogie bodies, have two DOFs: vertical displacement ( $q_5, q_6, q_7$ ) and rotation around the centre of mass ( $q_8, q_9, q_{10}$ ). The wheels have only one DOF: vertical translation ( $q_1, q_2, q_3, q_4$ ). The position of the cab's centre of mass is identified by the distances  $a_i$ , which in the case of the centre of mass coincident with the centre of gravity is reduced to  $a_1 = a_2 = a$ . The position of the centre of mass of the bogies is considered to coincide with the geometric centre, and is therefore positioned at the distance  $b_i$  with respect to the axis of the wheels.

The four wheels of the wagon are connected to the bogies by means of elastic primary springs  $K_{Pn}$  and viscous primary dampers  $C_{Pn}$  where  $n$  varies between 1 and 4. The two bogies are in turn connected to the carriage by means of elastic secondary springs  $K_{Si}$  and viscous secondary dampers  $C_{Si}$ , where  $i$  varies between 1 and 2.

The connection between wheel and rail is made with a linear damped spring model, whose parameters are  $K_{Tm}$  and  $C_{Tm}$ .

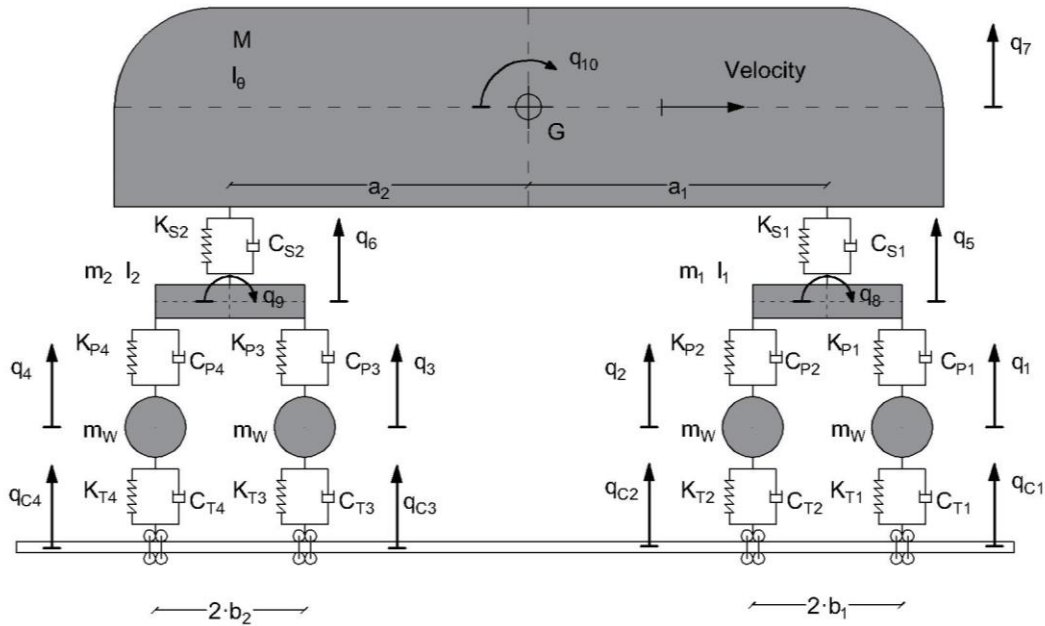


Figure 5-1: Mechanical model of a train wagon with 10 DOF + 4 contact point

### 5.2.1 Contact points

The values of the stiffness  $K_{Tm}$  of the spring and  $C_{Tm}$  of the dampers are chosen to simulate the deformability of the fastenings rail system. In a railway superstructure as the one at study (Rail-fasteners-slab track), without ballast, the rails are anchored on concrete slabs, with rail-pad set between the rail and the concrete to capture vibration induced by the passage of the train. The values of the dynamic parameters of the fastening system are constant along the entire rail and have been set equal to:  $K_{Tm} = 12 \text{ MN/m}$  and  $C_{Tm} = 50 \text{ kN s/m}$ , according to Ling et al. (2020).

### 5.2.2 Equations of motion of the train

The equations of motion for conservative discrete systems and with holonomic smooth constraints can be obtained directly through the Lagrange equations<sup>[2]</sup>.

In compact form, the motion of the convoy can be described as follows:

$$\underline{\underline{M}}_j \cdot \underline{\underline{\ddot{q}}} + \underline{\underline{C}}_j \cdot \underline{\underline{\dot{q}}} + \underline{\underline{K}}_j \cdot \underline{\underline{q}} = \underline{\underline{Q}} \quad (5.1)$$

- The matrices  $\underline{\underline{M}}_j$ ,  $\underline{\underline{C}}_j$  and  $\underline{\underline{K}}_j$  represent respectively the mass, damping and stiffness matrices of the system. The subscript  $j$  indicates the wagon considered. The matrices assume different values for motor wagons ( $j = 1$ ) and passenger wagons ( $j = 2$ );

<sup>[2]</sup>More details on the derivation of the equations of motion are given in chapter 6. These derivations, as well as the one presented in these paragraphs follow the works of Mulas et al. (2008 and 2010).



- The vector  $\underline{Q}$  is the vector of the generalized components of the forces;
- The vector  $\underline{q}$  contains the Lagrangian coordinates of the system.

The vector  $\underline{q}$  of the coordinates of the generic wagon, is partitioned into  $\underline{q}_{cv}$ , relative to the coordinates of the contact points, and  $\underline{q}_v$ , relative to the coordinates of the rigid bodies of the wagon:

$$\underline{q} = [q_{c1} \ q_{c2} \ q_{c3} \ q_{c4} \ | \ q_1 \ q_2 \ q_3 \ q_4 \ q_5 \ q_6 \ q_7 \ q_8 \ q_9 \ q_{10}]^T = [\underline{q}_{cv} \ | \ \underline{q}_v]^T \quad (5.2)$$

The same partition applies to the vector of external forces, which is partitioned as follows:

$$\underline{Q} = [F_1 \ F_2 \ F_3 \ F_4 \ | \ 0 \ 0 \ 0 \ 0 \ 0 \ 0 \ 0 \ 0 \ 0 \ 0]^T = [\underline{Q}_{cv} \ | \ \underline{Q}_v]^T \quad (5.3)$$

The contact points are points in which forces and displacements are exchanged between the train system and the tunnel system. Since the train and the tunnel are solved separately, but physically coupled, the information at the contact points, processed by the single systems, goes back and forth between two solvers (Ansys APDL for the tunnel and INTER for the train) until convergence is reached.

The same partition can be applied to the matrices of the train system:

$$\underline{\underline{M}}_j = \begin{bmatrix} \underline{\underline{m}}_{cv,cv} & \underline{\underline{m}}_{cv,v} \\ \underline{\underline{m}}_{v,cv} & \underline{\underline{m}}_{v,v} \end{bmatrix} \quad (5.4)$$

$$\underline{\underline{C}}_j = \begin{bmatrix} \underline{\underline{c}}_{cv,cv} & \underline{\underline{c}}_{cv,v} \\ \underline{\underline{c}}_{v,cv} & \underline{\underline{c}}_{v,v} \end{bmatrix} \quad (5.5)$$

$$\underline{\underline{K}}_j = \begin{bmatrix} \underline{\underline{k}}_{cv,cv} & \underline{\underline{k}}_{cv,v} \\ \underline{\underline{k}}_{v,cv} & \underline{\underline{k}}_{v,v} \end{bmatrix} \quad (5.6)$$

The submatrices  $\underline{\underline{m}}_{cv,cv}$ ,  $\underline{\underline{c}}_{cv,cv}$ ,  $\underline{\underline{k}}_{cv,cv}$  are associated with the coordinates of the contact points, while  $\underline{\underline{m}}_{v,v}$ ,  $\underline{\underline{c}}_{v,v}$ ,  $\underline{\underline{k}}_{v,v}$  are the submatrices associated with the remaining free coordinates of the wagon. The mixed submatrices  $\underline{\underline{m}}_{cv,v}$  and  $\underline{\underline{m}}_{v,cv}$  are null, as well as  $\underline{\underline{m}}_{cv,cv}$ .

By replacing the vectors and matrices in (5.1) we obtain the equation of motion (5.7) in matrix form.

$$\begin{bmatrix} \underline{\underline{0}} & \underline{\underline{0}} \\ \underline{\underline{0}} & \underline{\underline{m}}_{v,v} \end{bmatrix} \cdot \begin{bmatrix} \underline{\underline{\ddot{q}}}_{cv} \\ \underline{\underline{\ddot{q}}}_v \end{bmatrix} + \begin{bmatrix} \underline{\underline{c}}_{cv,cv} & \underline{\underline{c}}_{cv,v} \\ \underline{\underline{c}}_{v,cv} & \underline{\underline{c}}_{v,v} \end{bmatrix} \cdot \begin{bmatrix} \underline{\underline{\dot{q}}}_{cv} \\ \underline{\underline{\dot{q}}}_v \end{bmatrix} + \begin{bmatrix} \underline{\underline{k}}_{cv,cv} & \underline{\underline{k}}_{cv,v} \\ \underline{\underline{k}}_{v,cv} & \underline{\underline{k}}_{v,v} \end{bmatrix} \cdot \begin{bmatrix} \underline{\underline{q}}_{cv} \\ \underline{\underline{q}}_v \end{bmatrix} = \begin{bmatrix} \underline{\underline{Q}}_{cv} \\ \underline{\underline{0}} \end{bmatrix} \quad (5.7)$$

From (5.7) it is apparent the presence of two subsystems:

$$\underline{\underline{c}}_{cv,v} \cdot \dot{\underline{q}}_v + \underline{\underline{k}}_{cv,v} \cdot \underline{q}_v = \underline{Q}_{cv} - \underline{\underline{c}}_{cv,cv} \cdot \dot{\underline{q}}_{cv} - \underline{\underline{k}}_{cv,cv} \cdot \underline{q}_{cv} \quad (5.8a)$$

$$\underline{\underline{m}}_{v,v} \cdot \ddot{\underline{q}}_v + \underline{\underline{c}}_{v,v} \cdot \dot{\underline{q}}_v + \underline{\underline{k}}_{v,v} \cdot \underline{q}_v = \underline{0} - \underline{\underline{c}}_{cv,v} \cdot \dot{\underline{q}}_{cv} - \underline{\underline{k}}_{cv,v} \cdot \underline{q}_{cv} \quad (5.8b)$$

The resolution of the problem in this form sees integration in two steps. In (5.8b) the RHS is composed only of the variables at contact points. These displacements depends only on the motion of the structure, solved separately by Ansys, and are the same as those of the rail since we have assumed the hypothesis of perfect contact. Solving then (5.8b) the values of the free coordinates of the bodies of the vehicle  $\underline{q}_v$  can be obtained. By inserting now the displacements of the masses and the displacements of the contact points, in the LHS of (5.8a), the forces applied at the contact points can be obtained. These forces are then transmitted to the structure and therefore reworked by Ansys, for each time step, until convergence is reached. The convergence criterion and the details of the calculation codes used are described in chapter 7.

The system matrices, and the related submatrices, are defined independently on the wagon; however the associated values vary according to the j-th wagon.

For the stiffness and damping matrices, only the submatrices are shown for the sake of brevity. The complete matrices are shown in appendix B.

$$\underline{\underline{M}}_j = \begin{bmatrix} 0 & 0 & 0 & 0 & | & 0 & 0 & 0 & 0 & 0 & 0 & 0 & 0 & 0 & 0 \\ 0 & 0 & 0 & 0 & | & 0 & 0 & 0 & 0 & 0 & 0 & 0 & 0 & 0 & 0 \\ 0 & 0 & 0 & 0 & | & 0 & 0 & 0 & 0 & 0 & 0 & 0 & 0 & 0 & 0 \\ 0 & 0 & 0 & 0 & | & 0 & 0 & 0 & 0 & 0 & 0 & 0 & 0 & 0 & 0 \\ - & - & - & - & + & - & - & - & - & - & - & - & - & - & - \\ 0 & 0 & 0 & 0 & | & m_w & 0 & 0 & 0 & 0 & 0 & 0 & 0 & 0 & 0 \\ 0 & 0 & 0 & 0 & | & 0 & m_w & 0 & 0 & 0 & 0 & 0 & 0 & 0 & 0 \\ 0 & 0 & 0 & 0 & | & 0 & 0 & m_w & 0 & 0 & 0 & 0 & 0 & 0 & 0 \\ 0 & 0 & 0 & 0 & | & 0 & 0 & 0 & m_w & 0 & 0 & 0 & 0 & 0 & 0 \\ 0 & 0 & 0 & 0 & | & 0 & 0 & 0 & 0 & m_1 & 0 & 0 & 0 & 0 & 0 \\ 0 & 0 & 0 & 0 & | & 0 & 0 & 0 & 0 & 0 & m_2 & 0 & 0 & 0 & 0 \\ 0 & 0 & 0 & 0 & | & 0 & 0 & 0 & 0 & 0 & 0 & M & 0 & 0 & 0 \\ 0 & 0 & 0 & 0 & | & 0 & 0 & 0 & 0 & 0 & 0 & 0 & I_1 & 0 & 0 \\ 0 & 0 & 0 & 0 & | & 0 & 0 & 0 & 0 & 0 & 0 & 0 & 0 & I_2 & 0 \\ 0 & 0 & 0 & 0 & | & 0 & 0 & 0 & 0 & 0 & 0 & 0 & 0 & 0 & I_\theta \end{bmatrix} \quad (5.9)$$

$$\underline{\underline{C}}_{cv,cv} = \begin{bmatrix} C_{T1} & 0 & 0 & 0 \\ 0 & C_{T2} & 0 & 0 \\ 0 & 0 & C_{T3} & 0 \\ 0 & 0 & 0 & C_{T4} \end{bmatrix} \quad (5.10a)$$

$$\underline{\underline{C_{cv,v}}} = \underline{\underline{C_{v,cv}^T}} = \begin{bmatrix} -C_{T1} & 0 & 0 & 0 & 0 & 0 & 0 & 0 & 0 & 0 \\ 0 & -C_{T2} & 0 & 0 & 0 & 0 & 0 & 0 & 0 & 0 \\ 0 & 0 & -C_{T3} & 0 & 0 & 0 & 0 & 0 & 0 & 0 \\ 0 & 0 & 0 & -C_{T4} & 0 & 0 & 0 & 0 & 0 & 0 \end{bmatrix} \quad (5.10b)$$

$$\underline{\underline{K_{cv,cv}}} = \begin{bmatrix} K_{T1} & 0 & 0 & 0 \\ 0 & K_{T2} & 0 & 0 \\ 0 & 0 & K_{T3} & 0 \\ 0 & 0 & 0 & K_{T4} \end{bmatrix} \quad (5.11a)$$

$$\underline{\underline{K_{cv,v}}} = \underline{\underline{K_{v,cv}^T}} = \begin{bmatrix} -K_{T1} & 0 & 0 & 0 & 0 & 0 & 0 & 0 & 0 & 0 \\ 0 & -K_{T2} & 0 & 0 & 0 & 0 & 0 & 0 & 0 & 0 \\ 0 & 0 & -K_{T3} & 0 & 0 & 0 & 0 & 0 & 0 & 0 \\ 0 & 0 & 0 & -K_{T4} & 0 & 0 & 0 & 0 & 0 & 0 \end{bmatrix} \quad (5.11b)$$

### 5.2.3 Reduction of independent parameters

Trains of the modern times are made with high performance to avoid eccentricity and to achieve ever higher levels of comfort. For these reasons, in today's train models the constants introduced in the generic model of Figure 5-1, as well as the distances, are reduced to those of Figure 5-2. In detail, we assume that  $a_1 = a_2 = a$ ,  $b_1 = b_2 = b$ ,  $m_1 = m_2 = m$ ,  $e_1 = e_2 = e$ ,  $I_1 = I_2 = I$ . Introducing the following hypotheses:

- The geometric centre of the cab and bogies corresponds to the centre of mass;
- The bogies are placed at the same distance,  $a$ , from the cab's centre of mass;
- The two bogies have the same wheel spacing,  $b$ ;
- The two bogies are identical in mass and inertia.

Moreover, it is also assumed that  $K_{T1} = K_{T2} = K_{T3} = K_{T4} = K_T$ ,  $C_{T1} = C_{T2} = C_{T3} = C_{T4} = C_T$ ,  $K_{P1} = K_{P2} = K_{P3} = K_{P4} = K_P$ ,  $C_{P1} = C_{P2} = C_{P3} = C_{P4} = C_P$ ,  $K_{S1} = K_{S2} = K_S$ ,  $C_{S1} = C_{S2} = C_S$ , by adopting these last hypotheses:

- The four primary elastic springs between wheels and bogies, as well as the four primary dampers between wheels and bogies, assume the same constant value identified as  $K_P$  and  $C_P$ , respectively;
- The two secondary elastic springs and the two secondary viscous dampers placed between the bogies and the carriage assume the same value, identified as  $K_S$  and  $C_S$  respectively.

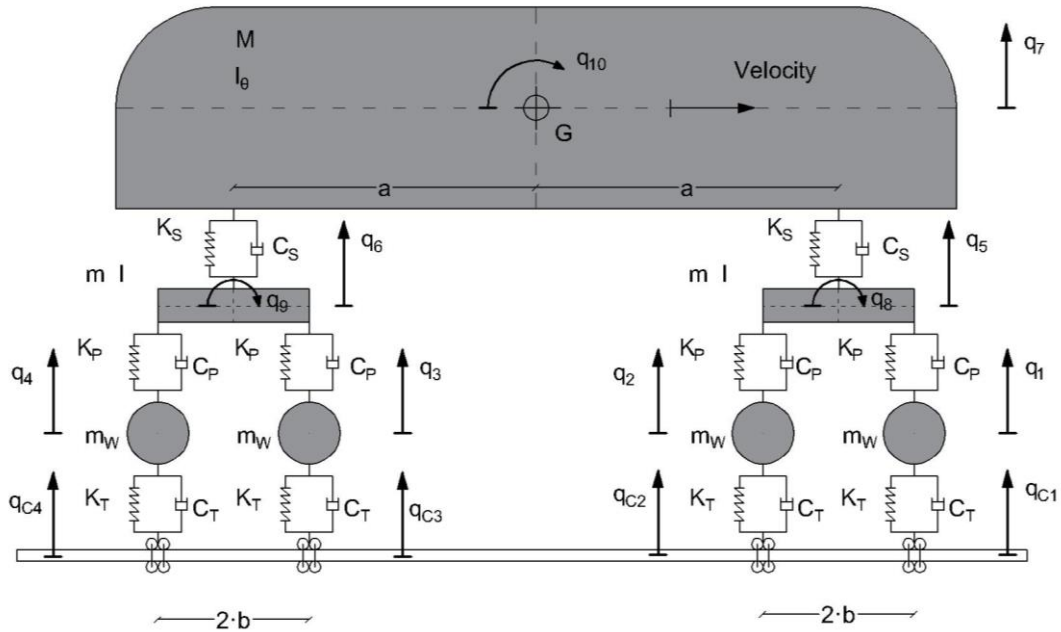


Figure 5-2: Vertical mechanical model of wagon with reduced parameters

These hypotheses simplify the calculation of the matrices  $\underline{\underline{M}}$ ,  $\underline{\underline{K}}$  and  $\underline{\underline{C}}$ , and make some terms null in the submatrices  $\underline{\underline{K}}_{v,v}$  and  $\underline{\underline{C}}_{v,v}$ . The new system matrices are defined in 5.12 - 5.14.

$$\underline{\underline{M}}_j = \begin{pmatrix} 0 & 0 & 0 & 0 & | & 0 & 0 & 0 & 0 & 0 & 0 & 0 & 0 & 0 & 0 \\ 0 & 0 & 0 & 0 & | & 0 & 0 & 0 & 0 & 0 & 0 & 0 & 0 & 0 & 0 \\ 0 & 0 & 0 & 0 & | & 0 & 0 & 0 & 0 & 0 & 0 & 0 & 0 & 0 & 0 \\ 0 & 0 & 0 & 0 & | & 0 & 0 & 0 & 0 & 0 & 0 & 0 & 0 & 0 & 0 \\ - & - & - & - & + & - & - & - & - & - & - & - & - & - & - \\ 0 & 0 & 0 & 0 & | & m_w & 0 & 0 & 0 & 0 & 0 & 0 & 0 & 0 & 0 \\ 0 & 0 & 0 & 0 & | & 0 & m_w & 0 & 0 & 0 & 0 & 0 & 0 & 0 & 0 \\ 0 & 0 & 0 & 0 & | & 0 & 0 & m_w & 0 & 0 & 0 & 0 & 0 & 0 & 0 \\ 0 & 0 & 0 & 0 & | & 0 & 0 & 0 & m_w & 0 & 0 & 0 & 0 & 0 & 0 \\ 0 & 0 & 0 & 0 & | & 0 & 0 & 0 & 0 & m & 0 & 0 & 0 & 0 & 0 \\ 0 & 0 & 0 & 0 & | & 0 & 0 & 0 & 0 & 0 & m & 0 & 0 & 0 & 0 \\ 0 & 0 & 0 & 0 & | & 0 & 0 & 0 & 0 & 0 & 0 & M & 0 & 0 & 0 \\ 0 & 0 & 0 & 0 & | & 0 & 0 & 0 & 0 & 0 & 0 & 0 & I & 0 & 0 \\ 0 & 0 & 0 & 0 & | & 0 & 0 & 0 & 0 & 0 & 0 & 0 & 0 & I & 0 \\ 0 & 0 & 0 & 0 & | & 0 & 0 & 0 & 0 & 0 & 0 & 0 & 0 & 0 & I_\theta \end{pmatrix} \quad (5.12)$$

$$\underline{\underline{C}}_j = \left[ \begin{array}{cccc|cccccccc} C_T & 0 & 0 & 0 & -C_T & 0 & 0 & 0 & 0 & 0 & 0 & 0 & 0 & 0 \\ 0 & C_T & 0 & 0 & 0 & -C_T & 0 & 0 & 0 & 0 & 0 & 0 & 0 & 0 \\ 0 & 0 & C_T & 0 & 0 & 0 & -C_T & 0 & 0 & 0 & 0 & 0 & 0 & 0 \\ 0 & 0 & 0 & C_T & 0 & 0 & 0 & -C_T & 0 & 0 & 0 & 0 & 0 & 0 \\ - & - & - & - & + & - & - & - & - & - & - & - & - & - \\ -C_T & 0 & 0 & 0 & C_T + C_P & 0 & 0 & 0 & -C_P & 0 & 0 & C_P \cdot b & 0 & 0 \\ 0 & -C_T & 0 & 0 & 0 & C_T + C_P & 0 & 0 & -C_P & 0 & 0 & -C_P \cdot b & 0 & 0 \\ 0 & 0 & -C_T & 0 & 0 & 0 & C_T + C_P & 0 & 0 & -C_P & 0 & 0 & C_P \cdot b & 0 \\ 0 & 0 & 0 & -C_T & 0 & 0 & 0 & C_T + C_P & 0 & -C_P & 0 & 0 & -C_P \cdot b & 0 \\ 0 & 0 & 0 & 0 & -C_P & -C_P & 0 & 0 & 2 \cdot C_P + C_S & 0 & -C_S & 0 & 0 & C_S \cdot a \\ 0 & 0 & 0 & 0 & 0 & 0 & -C_P & -C_P & 0 & 2 \cdot C_P + C_S & -C_S & 0 & 0 & -C_S \cdot a \\ 0 & 0 & 0 & 0 & 0 & 0 & 0 & 0 & -C_S & 2 \cdot C_S & 0 & 0 & 0 & 0 \\ 0 & 0 & 0 & 0 & C_P \cdot b & -C_P \cdot b & 0 & 0 & 0 & 0 & 0 & C_P \cdot b^2 + C_P \cdot b^2 & 0 & 0 \\ 0 & 0 & 0 & 0 & 0 & 0 & C_P \cdot b & -C_P \cdot b & 0 & 0 & 0 & 0 & C_P \cdot b^2 + C_P \cdot b^2 & 0 \\ 0 & 0 & 0 & 0 & 0 & 0 & 0 & 0 & C_S \cdot a & -C_S \cdot a & 0 & 0 & 0 & C_S \cdot a^2 + C_S \cdot a^2 \end{array} \right] \quad (5.13)$$

$$\underline{\underline{K}}_j = \left[ \begin{array}{cccc|cccccccc} K_T & 0 & 0 & 0 & -K_T & 0 & 0 & 0 & 0 & 0 & 0 & 0 & 0 & 0 \\ 0 & K_T & 0 & 0 & 0 & -K_T & 0 & 0 & 0 & 0 & 0 & 0 & 0 & 0 \\ 0 & 0 & K_T & 0 & 0 & 0 & -K_T & 0 & 0 & 0 & 0 & 0 & 0 & 0 \\ 0 & 0 & 0 & K_T & 0 & 0 & 0 & -K_T & 0 & 0 & 0 & 0 & 0 & 0 \\ - & - & - & - & + & - & - & - & - & - & - & - & - & - \\ -K_T & 0 & 0 & 0 & K_T + K_P & 0 & 0 & 0 & -K_P & 0 & 0 & K_P \cdot b & 0 & 0 \\ 0 & -K_T & 0 & 0 & 0 & K_T + K_P & 0 & 0 & -K_P & 0 & 0 & -K_P \cdot b & 0 & 0 \\ 0 & 0 & -K_T & 0 & 0 & 0 & K_T + K_P & 0 & 0 & -K_P & 0 & 0 & K_P \cdot b & 0 \\ 0 & 0 & 0 & -K_T & 0 & 0 & 0 & K_T + K_P & 0 & -K_P & 0 & 0 & -K_P \cdot b & 0 \\ 0 & 0 & 0 & 0 & -K_P & -K_P & 0 & 0 & 2 \cdot K_P + K_S & 0 & -K_S & 0 & 0 & K_S \cdot a \\ 0 & 0 & 0 & 0 & 0 & 0 & -K_P & -K_P & 0 & 2 \cdot K_P + K_S & -K_S & 0 & 0 & -K_S \cdot a \\ 0 & 0 & 0 & 0 & 0 & 0 & 0 & 0 & -K_S & 2 \cdot K_S & 0 & 0 & 0 & 0 \\ 0 & 0 & 0 & 0 & K_P \cdot b & -K_P \cdot b & 0 & 0 & 0 & 0 & 0 & K_P \cdot b^2 + K_P \cdot b^2 & 0 & 0 \\ 0 & 0 & 0 & 0 & 0 & 0 & K_P \cdot b & -K_P \cdot b & 0 & 0 & 0 & 0 & K_P \cdot b^2 + K_P \cdot b^2 & 0 \\ 0 & 0 & 0 & 0 & 0 & 0 & 0 & 0 & K_S \cdot a & -K_S \cdot a & 0 & 0 & 0 & K_S \cdot a^2 + K_S \cdot a^2 \end{array} \right] \quad (5.14)$$

## 5.2.4 Natural frequencies

Once the parameters of the model are known, a modal analysis can be performed to determine the system's natural frequencies. The analysis is conducted with the subsystem (5.8b), considering a null RHS: or, only the free vibration is studied, neglecting the motion of the contact points.

The damping matrix,  $\underline{\underline{C}}$ , is a non-classical matrix, since it does not satisfy the following condition:

$$\underline{\underline{C}}_j \underline{\underline{M}}_j^{-1} \underline{\underline{K}}_j = \underline{\underline{K}}_j \underline{\underline{M}}_j^{-1} \underline{\underline{C}}_j \quad (5.15)$$

For this reason the eigenvalues and eigenvectors of the problem will be complex and conjugated. It is necessary to solve the following problem with complex eigenvalues:

$$\left( \lambda^2 \underline{\underline{M}} + \lambda \underline{\underline{C}} + \underline{\underline{K}} \right) \underline{\underline{\psi}} = 0 \quad (5.16)$$

Where  $\lambda$  indicates the generic eigenvalue while  $\underline{\underline{\psi}}$  indicates the corresponding eigenvector. The problem admits non-trivial solutions if and only if:

$$\det \left( \lambda^2 \underline{\underline{M}} + \lambda \underline{\underline{C}} + \underline{\underline{K}} \right) = 0 \quad (5.17)$$

Developing the determinant, we obtain a polynomial of degree  $2N$ , where  $N$  is the number of DOFs of the wagon (10 DOF), known as the characteristic equation. The equation therefore admits, as solutions,  $N$  pairs of complex and conjugated eigenvalues and  $N$  pairs of complex and conjugated eigenvectors, of dimension  $N$ . The eigenvalues can be written as:

$$\lambda_n, \bar{\lambda}_n = -\zeta_n \omega_n \pm i \omega_{nD} \quad (5.18)$$

Where  $n = 1, 2, \dots, N$  are the number of natural modes,  $\omega_n$  represents the  $n$ -th undamped pulsation (circular frequency),  $\omega_{nD}$  is the corresponding damped pulsation and  $\zeta_n$  is the modal damping.

The terms listed above can be mathematically expressed as:

$$\omega_n = |\lambda_n| = \sqrt[2]{\text{Re}(\lambda_n)^2 + \text{Imm}(\lambda_n)^2} \quad (5.19)$$

$$\zeta_n = -\frac{\text{Re}(\lambda_n)}{|\lambda_n|} \quad (5.20)$$

$$\omega_{nD} = \text{Imm}(\lambda_n) = \omega_n \sqrt{1 - \zeta_n^2} \quad (5.21)$$

Once the damped pulsation is known, the natural frequencies of the system can be obtained with the following formula:

$$f_{nD} = \frac{\omega_{nD}}{2\pi} \quad (5.22)$$

Once the eigenvalues are known, it is possible to solve the problem (5.16) to obtain the corresponding eigenvectors. The  $N$  pairs of complex and conjugated eigenvectors are defined as:

$$\underline{\psi}_n, \bar{\underline{\psi}}_n = \underline{\phi}_n \pm i \underline{\chi}_n \quad (5.23)$$

The eigenvectors can be assembled into an  $N \times N$  matrix known as a modal matrix, in which each column represents a natural mode of the system:

$$\underline{\underline{\Psi}} = \begin{bmatrix} \psi_{11} & \psi_{12} & \cdots & \psi_{1N} \\ \psi_{21} & \psi_{22} & \cdots & \psi_{2N} \\ \cdots & \cdots & \cdots & \cdots \\ \psi_{N1} & \psi_{N2} & \cdots & \psi_{NN} \end{bmatrix} \quad (5.24)$$

The  $N$  eigenvalues  $\omega_n^2$  can be ordered in the diagonal matrix  $\underline{\underline{\Omega}}^2$ , known as the spectral matrix of the eigenvalue problem:

$$\underline{\underline{\Omega^2}} = \begin{bmatrix} \omega_1^2 & & & \\ & \omega_2^2 & & \\ & & \ddots & \\ & & & \omega_n^2 \end{bmatrix} \quad (5.25)$$

In this study 10 modes of vibration are found. The natural frequencies for the systems at study are reported in chapter 5.4.

### 5.3 Mechanical model in the transverse direction

The mechanical model to be referred for the study of the transverse actions of the train takes into consideration the MHFM. The harmonic forcing is ideal to simulate the actions due to hunting of the train.

However, the model here adopted is not exactly identical to the MHFM, since includes also alignment irregularities, which, being more sudden than the hunting motion, cause higher accelerations, that lead to higher actions.

The computation of the forces acting on the tunnel takes place by considering the displacements of the wheels, and deriving them twice over time, to obtain the accelerations, linked to the speed of the train. By means of Newton's law,  $F = m a$ , the forces at each time instant are obtained.

For the choice of the masses to apply, the wheel displacements is analysed in detail. The hunting is a cause of the self-alignment of the wheels, so it is induced from the wagon to the rails and then to the tunnel. The irregularities, on the other hand, are displacements imposed by the rails on the wheels, which are then transmitted on the bogies and on the carriage. In the first case, the hunting of the wheels is damped even before reaching the carriage, to the point of being imperceptible for a passenger. Therefore only the masses of the wheels are considered, neglecting the movement of the carriage and the bogies. In the second case, the irregularities of the rail are so small and sudden that the inertia of the carriage cannot even follow them. Therefore, also here, only the masses of the wheels and bogies are considered.

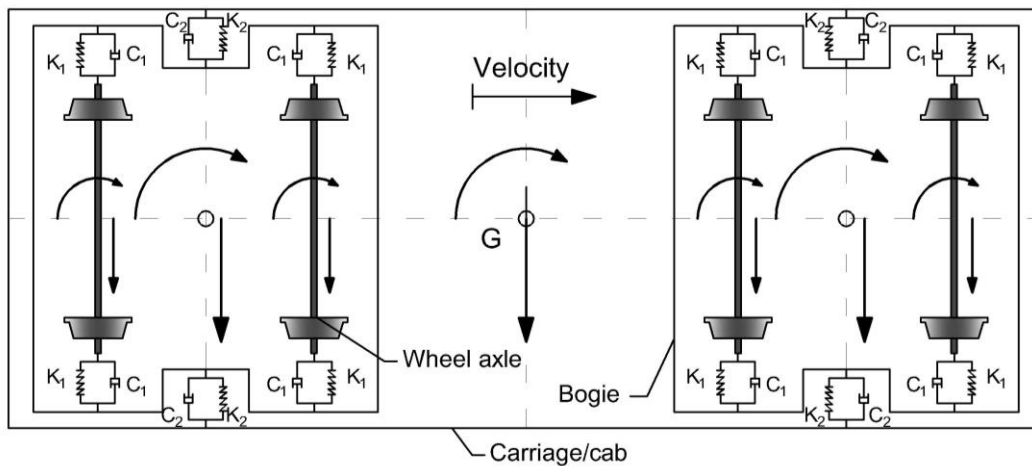


Figure 5-3: Transversal mechanical model of a wagon

From a theoretical point of view, a transverse dynamic analysis coupled between the tunnel and the train should be conducted (as done for the vertical analysis), in which the wheels follow the motion of the hunting, combined with the alignments, and transfer the forces to the tunnel, elaborated from the dynamic problem of the convoy, as described in Figure 5-3. However, the interest is to analyse if the transverse motion of the train is critical for the transversal motion of the tunnel. In fact, the aim



is to define whether these actions are important and whether a solution with a more accurate model is needed or not.

In any case the choice of the model have been weighted considering the model of figure 5-3, in order to obtain forces that simulate the dynamics.

The transverse model of the wagon of Figure 5-3 has two primary springs between the axle and the bogie and two secondary springs between the bogie and the carriage. Typically, the primary springs have much higher stiffness than the secondary ones. This difference serves to ensure that, when a sudden motion of the wheels occurs, the bogie will follow it partially, with a slight time delay and a damped motion. The carriage is not affected by this motion due to the low stiffness of the secondary springs, damping any velocity, and maintaining its inertial position, so as to ensure high comfort for passengers.

Therefore, if the carriage is weakly affected by the wheel motion, and also the bogies slightly dampens the initial motion, multiplying the accelerations of the wheels by the masses of the axles, without considering the damping of is in favour of safety. To support this observation, a comparison is reported, applied to the case of hunting, in Figures 5-8 and 5-9.

It is important to note that the displacement of an axle is different from the next or previous wheel axle, thus introducing a rotation of the bogies and on the carriage. However, rotational inertias (yaws inertias) have been neglected, including those of the axles. Only the transverse displacement of an axle is considered.

The hypotheses that are therefore being introduced with this model are:

- The transverse behaviour of the train is not influenced by the displacements of the tunnel, and its dynamic is neglected (negligible displacements of the SFT);
- The inertia of the train is small compared to that of the tunnel;
- The yaws of carriages, bogies and axles are neglected;
- The movements and forces induced by the cab are negligible compared to those of the axles.

The forces have been computed with a code in MatLab, reported in appendix A-2, as a function of the train used and the speed. The forces are then applied with a time shift that simulated the distances of the train axles, based on the train speed. Furthermore, the values of the forces differ between motor wagons and passenger wagons, depending on the masses and distances of the wheels of each wagon.

The equations and procedures at the base of the calculation of the forces, used in the MatLab code, are presented in the next paragraphs.

### 5.3.1 Hunting actions

The wheels of a wagon do not have the ability to steer. To ensure the ability to tackle curves, rails are placed at different heights, and wheels are made conical, to be able to negotiate the differences.

In straight tracks, wheels could be cylindrical, ideally. However, the imperfections of rails and wheels make it impossible for two cylinders to run straight for long times. The conical wheels instead make possible to bring the train back into alignment - see Figures 5-4 and 5-5.

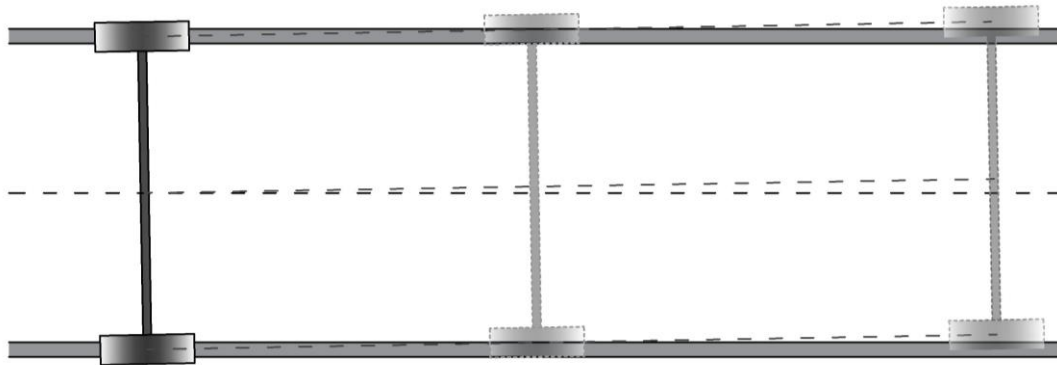


Figure 5-4: Impossibility of cylindrical wheels to run straight

The conicity of the wheels is therefore necessary, and required, to ensure:

- Negotiations on the curve;
- Self-alignment.

However, the need for conical wheels imposes a number of other problems caused by hunting, such as deformation of the rails, comfort and derailments. Anyway, there is no interest in evaluating the possible derailment, but only in obtaining the forces induced by the horizontal motion.

Conical wheels advance unevenly. Since there is a conicity  $\gamma$  (see Figure 5-5), first a wheel advances – the left for instance – until it reaches a radius of the cone –  $R_l = R_0 - \gamma y$  – less than the radius of the cone of the wheel at the other end of the axle – the right:  $R_r = R_0 + \gamma y$  – being  $y$  the horizontal displacement of the axle. Then the second wheel starts to move, until it reaches a smaller radius in turn, at which time the previous wheel starts moving again, thus triggering a cyclic motion - see Figure 5-6. To prevent the possible occurrence that the wheel rolls diagonally off the rail, i.e. derailment problems, flanges are inserted on the wheels.

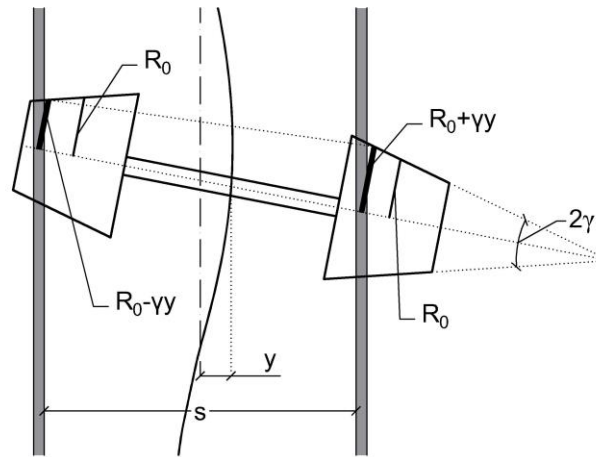


Figure 5-5: Detail of the movement of an axle with conical wheels

When the convoy reaches a constant speed, the wheels reach a constant cyclic motion, called hunting. This simple harmonic motion has a wavelength  $L$ .

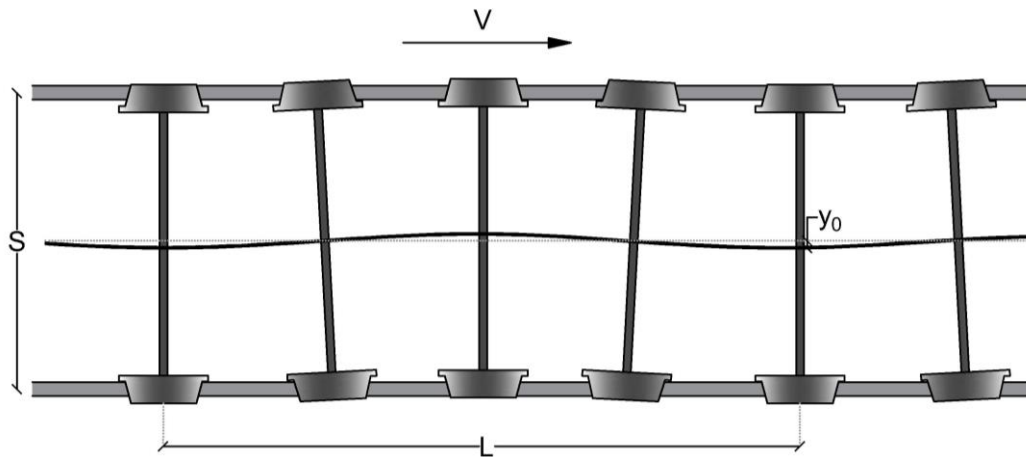


Figure 5-6: Sinusoidal transversal movement of the axles

Once the wagon is fully operational, the motion of the wheels is given by a sinusoid of constant amplitude, which describes the trajectory of the motion of the wheel-rail's contact point:

$$y(x) = y_0 \text{sen} \left( \frac{2\pi x}{L} \right) \tag{5.26}$$

In (5.26)  $y_0$  is the maximum amplitude of the sinusoid. To define this value, reference can be made to the maximum clearance between the edge of the flange and the rail, Figure 5-7. This clearance has a value between 2,0 and 10,0 mm for high and low quality rails, respectively. As already mentioned, the value is valid for the axle only. If we consider the actual displacement of the cab, it turns out to be less than about a decimal, 0,2 ÷ 1,0 mm or lower, due to the presence of springs and dampers that reduce motion, as well as due to the large inertia;

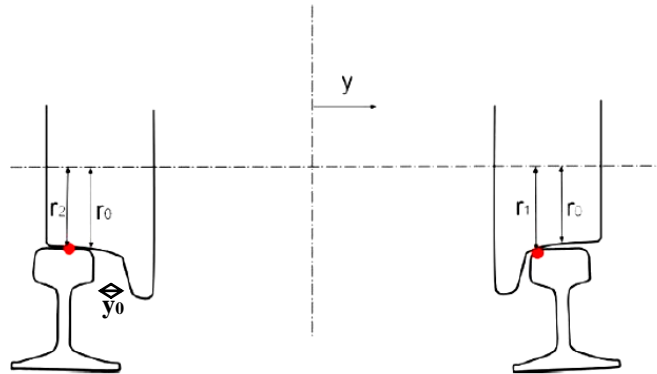


Figure 5-7: Clearance between rails and wheels

$L$  is the Klingel wavelength, measured in meters, well known also as the Klingel's formula (derived in 1883):

$$L = 2\pi \sqrt{\frac{R_0 \cdot s}{2 \cdot \gamma}} \quad (5.27)$$

$R_0$  is the average rolling radius of the two wheels, depending on the type of train, between approximately 0,45 ÷ 0,46 m;

$s$  is approximately the distance between the two rails, assumed to be 1,5 m;

$\gamma$  is the conicity of the wheel: tangent of the inclination angle of the truncated cone, approximately equal to the angle itself. It can be assumed as a conicity a value of 1/10 ÷ 1/20 for low and medium speed trains (used in Italy, France, Belgium and Spain), while a conicity of 1/40 ÷ 1/50 for high speed trains.

Also the wavelengths differ between those of the wheels and those of the cab. The dampers bring the wavelength of the cab to be about 4 times longer than that of an axle. The comparison of Figure 5-8 on the displacements of a generic train, shows wavelengths equal to 16 m and 64 m for the axles and the cab, respectively.

It should be noted that the sinusoid and its wavelength are independent of the speed of the convoy. Therefore, the number of waves that a train causes along the tunnel remains constant, independently of its speed, being an effect caused by the geometry of the wheels. However the speed determines the time in which these waves are

travelled. The higher the speed, the greater the force that these waves cause, since the transverse acceleration will be higher.

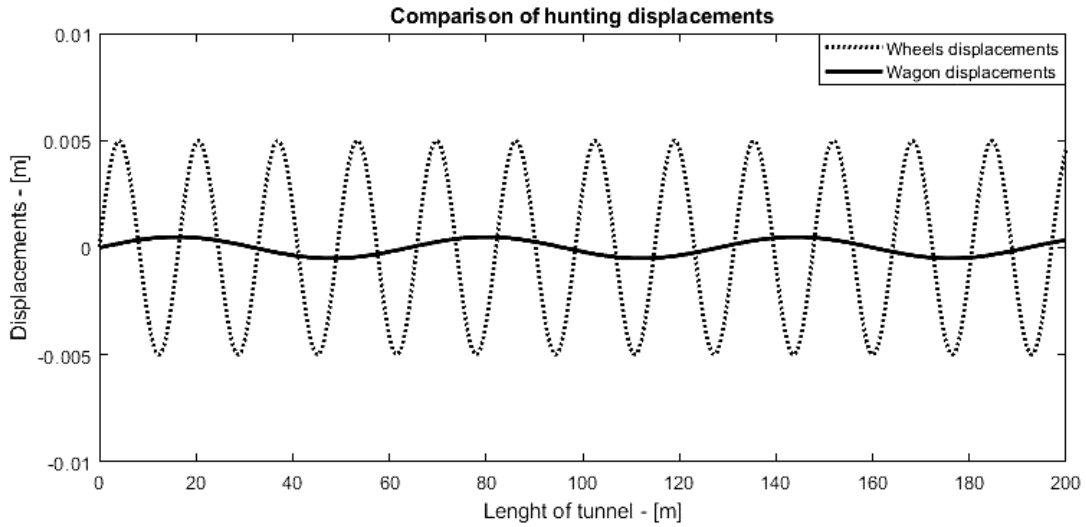


Figure 5-8: Hunting of the wagon compared to the hunting of the wheels

The transverse acceleration of the wheels is obtained as the double derivative over time of equation (5.26).

Given the speed,  $v$ , and assuming that it is constant, the  $x$  position of the train can be defined as:

$$x = v \cdot t \quad (5.28)$$

Accounting for (5.28), (5.26) becomes:

$$y(x) = y(vt) = y(t) = y_0 \sin\left(\frac{2\pi vt}{L}\right) \quad (5.29)$$

Its first derivative gives the transversal velocity, and it is equal to:

$$v(t) = \frac{dy(t)}{dt} = y_0 \cdot \frac{2v\pi}{L} \cdot \cos\left(\frac{2\pi vt}{L}\right) \quad (5.30)$$

The second derivative gives the transversal acceleration of the axles, defined as:

$$a(t) = \frac{dv(t)}{dt} = -y_0 \cdot \frac{4v^2\pi^2}{L^2} \cdot \sin\left(\frac{2\pi vt}{L}\right) \quad (5.31)$$

The forces are then obtained with Newton's law:

$$F(t) = m \cdot a(t) \quad (5.32)$$

Where  $m$  is equal to the mass of an axle.

For a comparison between the forces acting on the axle and those of the cab, for the example of Figure 5-8, Figure 5-9 shows the values of the forces obtained with a generic train speed of 100 km/h, considering the masses of the axles on the movement of the wheels (1,7 ton) and the masses of the whole wagon on the movement of the cab (54,9 ton/4).

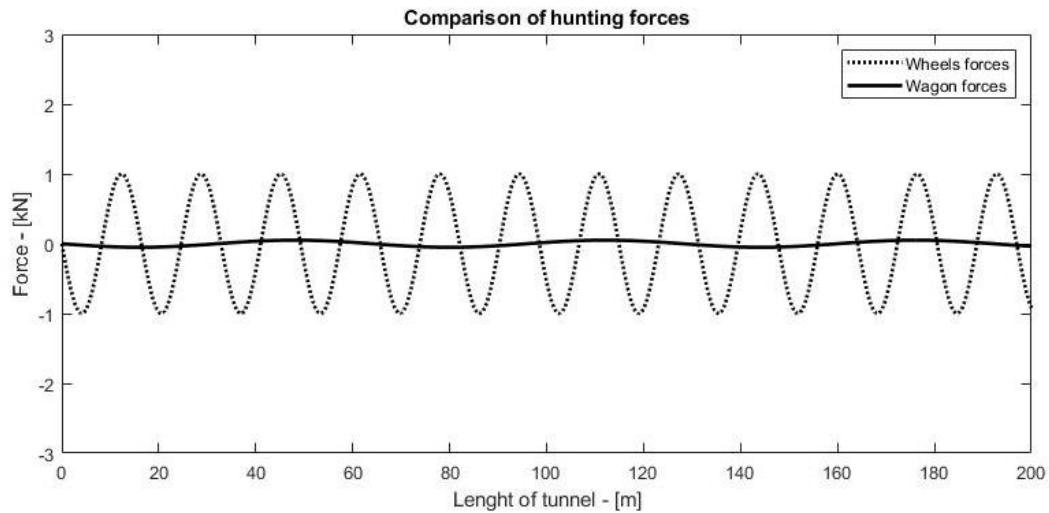


Figure 5-9: Forces of the cab versus the forces of the wheel

It is now clear and justified to have neglected the forces induced by the wagons. Figure 5-10 highlights the importance of evaluating the hunting motion and its impact on the rails.



Figure 5-10: Deformation of the rails due to hunting

### 5.3.2 Forces generated by irregularity

With more and more performing convoys, over the years irregularities have become the dominant actions compared to hunting actions, while in the past the reverse was true.

As already mentioned, irregularities are more sudden than hunting, and are displacements and velocities imposed by the alignments of the rail on the wheels. Alignments were defined in paragraph 4.2.2.

As for hunting, considering the coordinate  $x=v \cdot t$  with constant speed, the double derivative over the time of the displacements provides the transverse accelerations to be multiplied by the masses of the axles.

The alignments are typical random irregularities, herein derived from an internal MatLab code. Forces are obtained in the same way as for hunting, applying (5.32) to the final accelerations, with the masses of the wheels. The final forces generated by the irregularities, comparing various speeds of the convoy, are always higher than those due to hunting.

## 5.4 Train models adopted in this study

For the study of the tunnel dynamics, the convoy is simulated using two types of trains:

- Medium-low speeds train – TMV (Treno Media Velocità);
- High speeds train – TAV (Treno Alta Velocità).

The two trains differ in terms of mass values, properties of the springs and dampers, geometry of wagons, position of the motor wagons, number of wagons, admissible speeds and conicity of the wheels.

The first train is a generic train obtained from the model of Van Nguyen et al. (2009), designed to simulate generic regional trains, which make the same journeys several times a day, in short and constant tracks.

The second train is a Frecciarossa 1000, also called ETR1000 - V300ZEFIRO, designed by Bombardier and built by AnsaldoBreda (Hitachi Rail Italy), used to simulate the high-speed train that run throughout the Italian territory.

### 5.4.1 Medium speeds train - TMV

The convoy for low-medium speeds, in Figure 5-11, does not refer to a particular train, but to a generic train, with medium properties, such as an Italian regional or fast regional train. The maximum admissible speed of an Italian regional train is 160 km/h. Over this speed, no analyses are carried out for this train.

The train under analysis is equipped with 10 wagons, including the leading wagons which are also motor wagons, with higher masses and different geometries. The total length is approximately 240 m, for a total of 40 axles and 20 bogies.

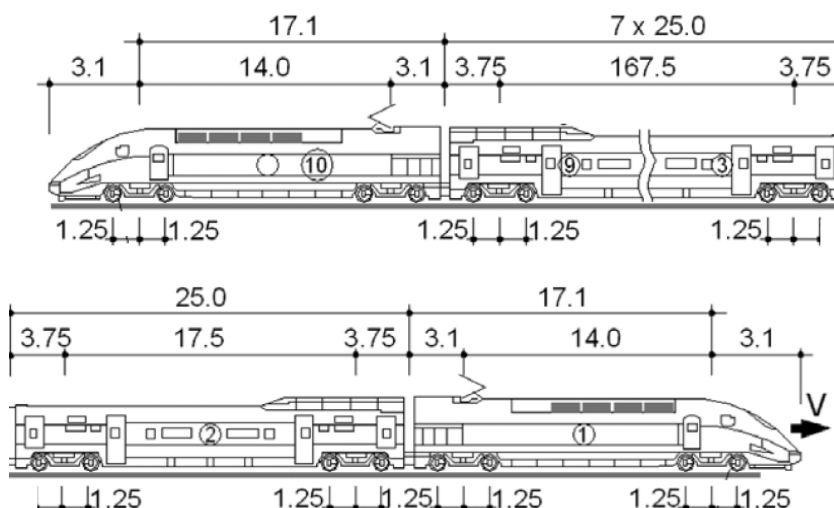


Figure 5-11: Passengers and motor car dimensions. TMV [Van Nguyen et al, 2009]



The values of the parameters (described in Figure 5-2) necessary for the vertical and transversal models are listed in Table 5-1.

Table 5-1: Mechanical properties and dimensions of the medium speed train

Description	Name	Unit	Motor car	Passenger car
Number of wagons	-	-	2	8
Wagon position	j	-	1 e 10	2,3,4,5,6,7,8,9
Cab length	l	m	20.2	25
Bogie's distance	2a	m	14	17.5
Wheel's distance	2b	m	2.5	2.5
Cab mass	M	ton	54.92	41.75
Cab inertia	$I_{\theta}$	ton·m <sup>2</sup>	2485.4	2080
Bogie mass	m	ton	3.434	3.040
Bogie inertia	I	ton·m <sup>2</sup>	4.905	3.934
Wheel mass	$m_w$	ton	1.776	1.776
Wheel medium radius	$R_0$	m	0.455	0.455
Primary suspension stiffness	$K_P$	kN/m	1226.250	590
Primary suspension damping	$C_P$	kN·s/m	29.430	19.620
Secondary suspension stiffness	$K_S$	kN/m	1245.870	265.000
Secondary suspension damping	$C_S$	kN·s/m	98.100	45.120
Contact point stiffness	$K_T$	MN/m	12	12
Contact point damping	$C_T$	kN·s/m	50	50
Wheel-Rail clearance	$y_0$	m	0,005	0,005
Wheel's conicity	$\gamma$	-	1/20	1/20

### Free vibrations

The free vibrations for the medium speed train differ between the passenger cars and the motor cars.

For the passenger wagon, the frequencies relative to the first ten modes are reported in Table 5-2, with the type of motion that prevails for that mode.

Table 5-2: Frequencies of the medium speed train, passenger wagon

Mode	Frequency [Hz]	Period [s]
1 – Carriage vertical translation and pitch	0,50877	1,965
2 – Rear bogie and third axle vertical translation	0,50884	1,965
3 – Carriage pitch	0,62972	1,588
4 – Front bogie vertical translation	3,3583	0,298
5 – Carriage vertical translation and rear bogie pitch	3,3609	0,298
6 – Front bogie and fourth axle vertical translation	3,4077	0,293
7 – Rear bogie pitch and carriage vertical translation	3,4095	0,293
8 – First axle vertical translation and front bogie pitch	13,419	0,075
9 – Third axle and rear bogie vertical translation	13,420	0,075
10 – Second axle vertical translation	13,422	0,075

For the motor wagon, the frequencies relative to the first ten modes are reported in Table 5-3, with the type of motion that prevails for that mode.

Table 5-3: Medium speed train frequencies, motor wagon

Mode	Frequency [Hz]	Period [s]
1 – Carriage and rear bogie pitch	0,85149	1,174
2 – Carriage and bogies pitch	0,88486	1,130
3 – Front bogie and fourth axle vertical translation	4,2147	0,237
4 – Carriage vertical translation t and pitch	4,2149	0,237
5 – Fourth axle and front bogie vertical translation	5,0761	0,197
6 – Carriage vertical translation and pitch	5,0793	0,197
7 – First axle vertical translation	13,805	0,072
8 – Third axle vertical translation	13,805	0,072
9 – Third axle and rear bogie vertical translation	13,808	0,072
10 – Second axle vertical translation	13,808	0,072

In both the wagons the lower frequencies are mainly associated to the motion of the carriage, whereas the higher frequencies are associated to the vertical translation of the wheels. Moreover, having the motor wagon higher values of the suspensions than the passenger wagon, its periods are lower.

#### Maximum displacements and transversal forces

As described in paragraph 5.3.1., the hunting of the wheel axles is not affected by the speed or the masses. The hunting of the axles for a portion of the tunnel is shown in Figure 5-12. The wavelength is equal to  $L = 16,41$  m, according to equation (5.27) with the values of Table 5-1, and the amplitude is fixed at  $y_0 = 5$  mm.

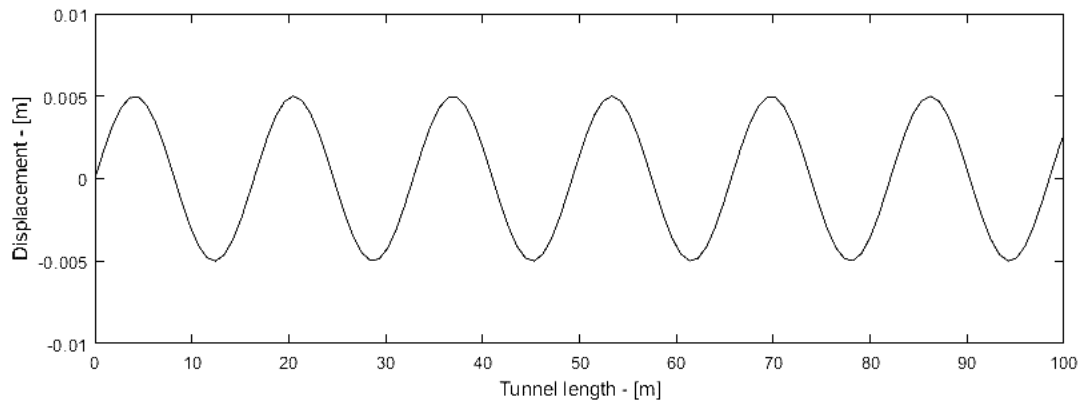


Figure 5-12: Hunting of the wheels for the medium speed train

Forces transmitted by the wheels to the rail, due to the hunting motion, are obtained by deriving these displacements over time and multiplying them by the quantity of mass participating to this motion, assumed equal to  $m_w$ . Using the values of Table 5-1, a mass of 1,776 tons is obtained for both the motor wagons and the passenger wagons. Each speed will correspond to a different force, which can be more or less critical for the tunnel. The maximum force that can be obtained corresponds to the maximum speed of 160 km/h, and is equal to 2,5 kN, as shown in Figure 5-13.

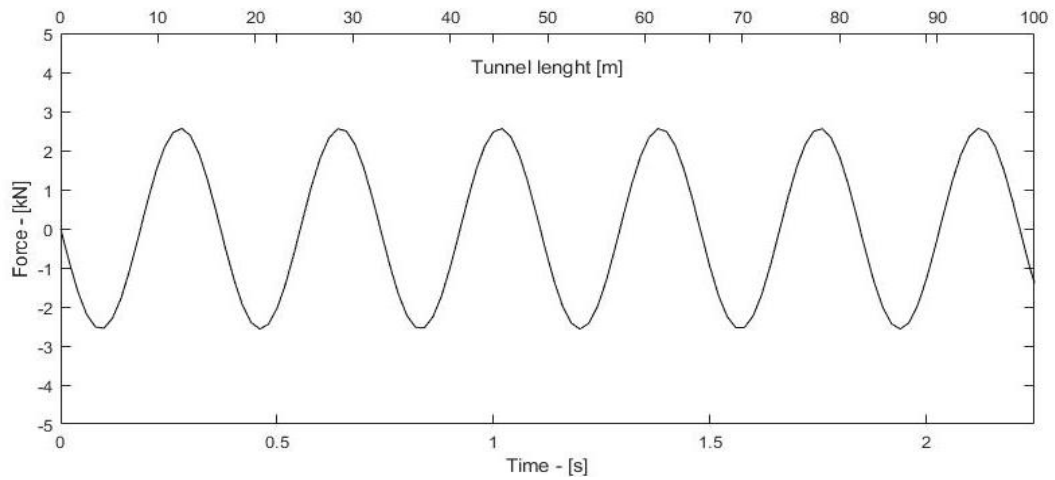


Figure 5-13: Hunting forces. TMV 160 km/h

Applying the same procedure to the irregularities, defined by equation (4.4), and joining the related forces to the hunting forces, we obtain the final maximum forces of Figure 5-14.

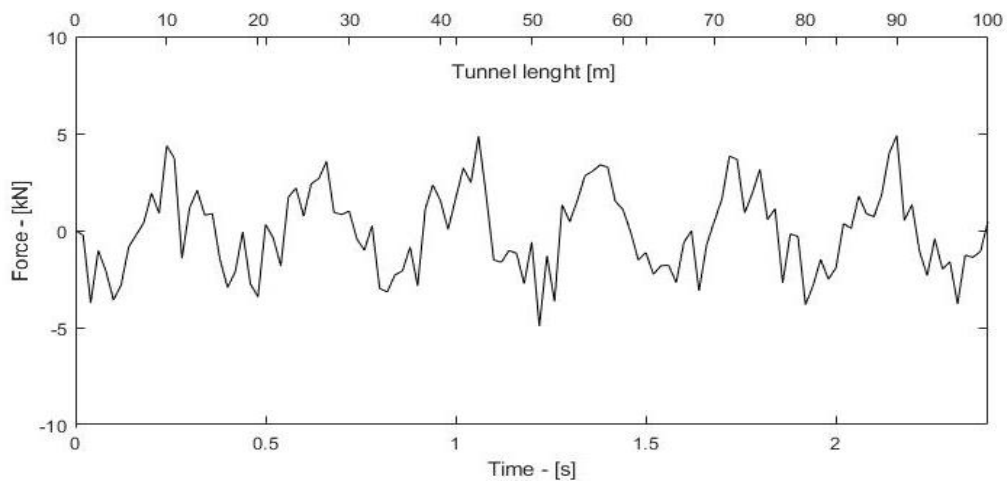


Figure 5-14: Superposition of forces due to hunting and irregularities. TMV 160 km/h

The complete forces time histories used for the analyses are reported for each transversal analyses of chapter 9. In Table 5-4 the extreme values of the hunting and total force are reported as a function of the speed.

Table 5-4: Maximum transversal forces induced by a TMV

Speed [km/h]	Maximum axle forces [kN]	
	Hunting	Total
20	$\pm 0,04$	$\pm 0,1$
40	$\pm 0,15$	$\pm 0,3$
60	$\pm 0,36$	$\pm 0,8$
80	$\pm 0,65$	$\pm 1,5$
100	$\pm 1,0$	$\pm 2,0$
120	$\pm 1,5$	$\pm 3,0$
140	$\pm 2,0$	$\pm 4,0$
160	$\pm 2,5$	$\pm 5,0$

### 5.4.2 High speed train - TAV

The ETR1000 is composed of 8 wagons, with no differences between motor wagons and passengers, since the engines are distributed throughout the train. The length of the train is 202 m with 16 supporting axles and 16 driving axles, for a total of 32 axles and 16 bogies.

The maximum speed that can be reached is 400 km/h. The commercial speed is 360 km/h. However, it can reach a maximum speed of 300 km/h on Italian lines, as the railway network does not allow higher speeds.

The details of the head and passenger carriages are shown in Figure 5-15, together with the whole extension of the train.

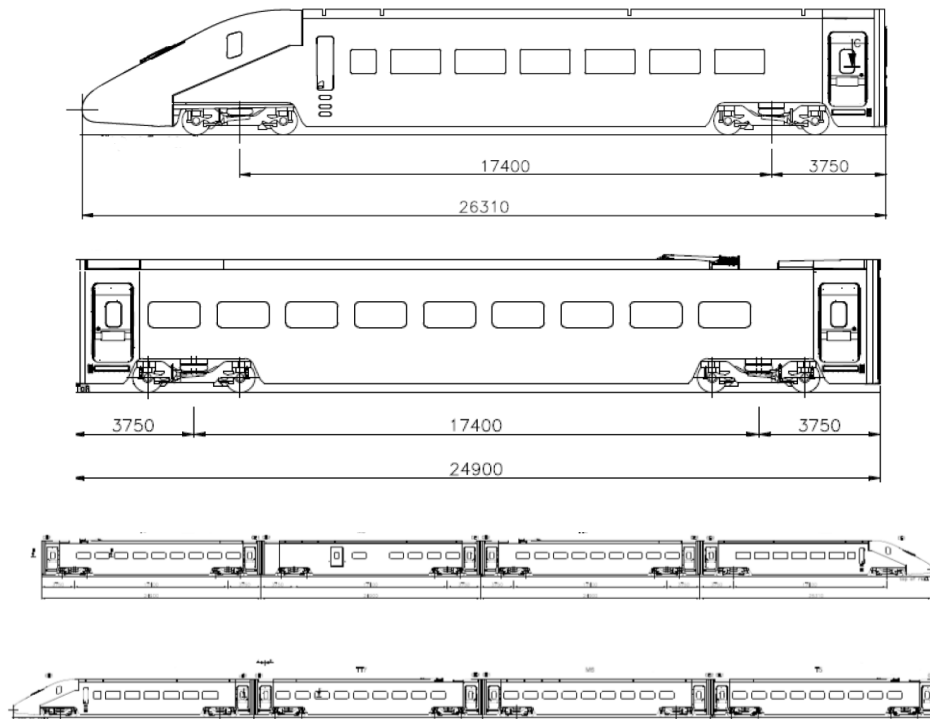


Figure 5-15: Passenger and head carriage dimensions. TAV [Canetta D., 2017]

The parameter values (described in Figure 5-2), required for the vertical and transversal models, are listed in Table 5-5.

Table 5-5: Mechanical properties and dimensions for high speed train

Description	Name	Unit	Head car	Passenger car
Number of wagons	-	-	2	6
Wagon position	j	-	1 e 8	2,3,4,5,6,7
Cab length	l	m	26.31	24.90
Bogie's distance	2a	m	17.4	17.4
Wheel's distance	2b	m	2.85	2.85
Cab mass	M	ton	36.498	36.498
Cab inertia	$I_0$	ton·m <sup>2</sup>	1710	1710
Bogie mass	m	ton	2.775	2.775
Bogie inertia	I	ton·m <sup>2</sup>	1.664	1.664
Wheel mass	$m_w$	ton	1.873	1.873
Wheel medium radius	$R_0$	m	0.46	0.46
Primary suspension stiffness	$K_T$	kN/m	3880	3880
Primary suspension damping	$C_T$	kN·s/m	32	32
Secondary suspension stiffness	$K_S$	kN/m	682	682
Secondary suspension damping	$C_S$	kN·s/m	60	60
Contact point stiffness	$K_T$	MN/m	12	12
Contact point damping	$C_T$	kN·s/m	50	50
Wheel-Rail clearance	$y_0$	m	0,002	0,002
Wheel's conicity	$\gamma$	-	1/40	1/40

### Free vibrations

The natural frequencies for the high-speed train do not differ between passenger cars and head cars. The frequencies related to the first ten modes are reported in Table 5-6, with the type of motion that prevails for that mode

Table 5-6: Frequencies of the high speed train

Mode	Frequency [Hz]	Period [s]
1 – Carriage and bogies (in phase) vertical translation	0,92006	1,087
2 – Vertical translation second axle	0,92009	1,087
3 – Carriage and bogies (out of phase) vertical translation	1,1687	0,856
4 – Rear and front bogie vertical translation (in phase)	7,3526	0,136
5 – Rear and front bogie vertical translation (in counterphase)	7,3544	0,136
6 – Third axle vertical translation	10,697	0,093
7 – Carriage pitch and first axle vertical translation	10,697	0,093
8 – Fourth axle and rear bogie vertical translation	15,423	0,065
9 – Front bogie pitch and vertical translation and carriage vertical translation	15,423	0,065
10 – Front bogie pitch and vertical translation and carriage vertical translation (in phase)	18,444	0,054

The frequencies of the TAV are higher than those of the passenger and motor wagons of the TMV, having the primary suspension higher values. Moreover, it can

be notice that the firsts modes represent also for this train the vertical translation of the carriage.

#### Maximum displacements and transversal forces

As described in paragraph 5.3.1., the hunting of the wheel axles is not affected by the speed or the masses. The hunting of the axles, for a section of the tunnel, is shown in Figure 5-16. It should be noted that the wavelength is equal to  $L = 23,34$  m, according to equation (5.27) with the values of Table 5-5, and the amplitude is fixed at  $y_0 = 2$  mm.

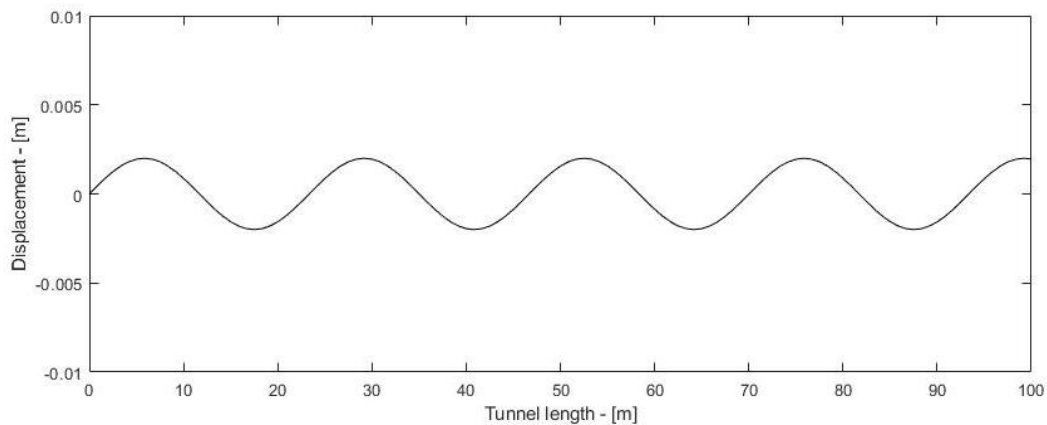


Figure 5-16: Hunting of the wheels for the high speed train

Forces transmitted by the wheels to the rail, due to the hunting motion, are obtained by deriving these displacements over time and multiplying them by the quantity of mass participating to this motion, assumed equal to  $m_w$ . Using the values of Table 5-5, a mass of 1,873 tons is obtained for all the wagons. Each speed will give a different force, which can be more or less critical for the tunnel. The maximum force that can be obtained corresponds to the maximum speed of 300 km/h, and is equal to 2 kN, as shown in Figure 5-17.

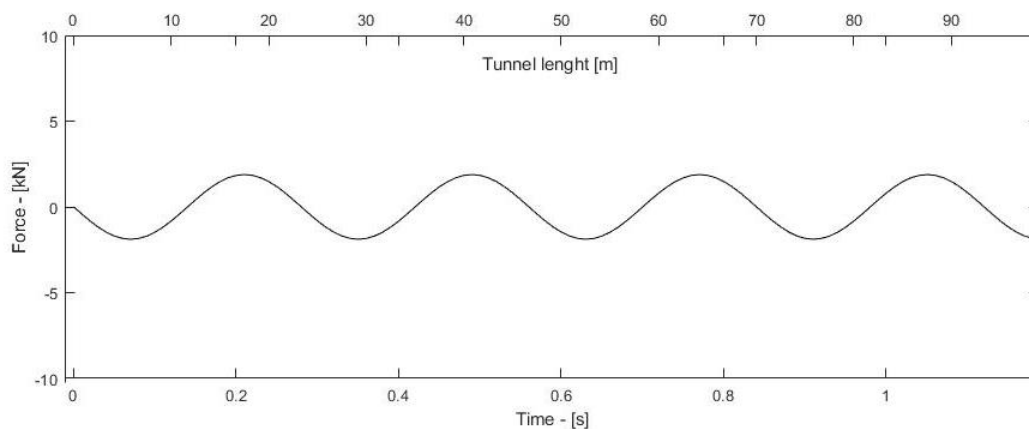


Figure 5-17: Hunting forces. TAV 300 km/h

By applying the same procedure to the irregularities, defined by equation (4.4), and joining the related forces to the hunting forces, the final maximum forces of Figure 5-18 are obtained. It can be observed how the motion of Figure 5-17 is faintly perceptible in the superposition. It is more hidden by the irregularities than in the case of the medium speeds train. This is because the hunting forces are smaller, attributable to a lower conicity and clearance, with a longer wavelength and lower amplitude.

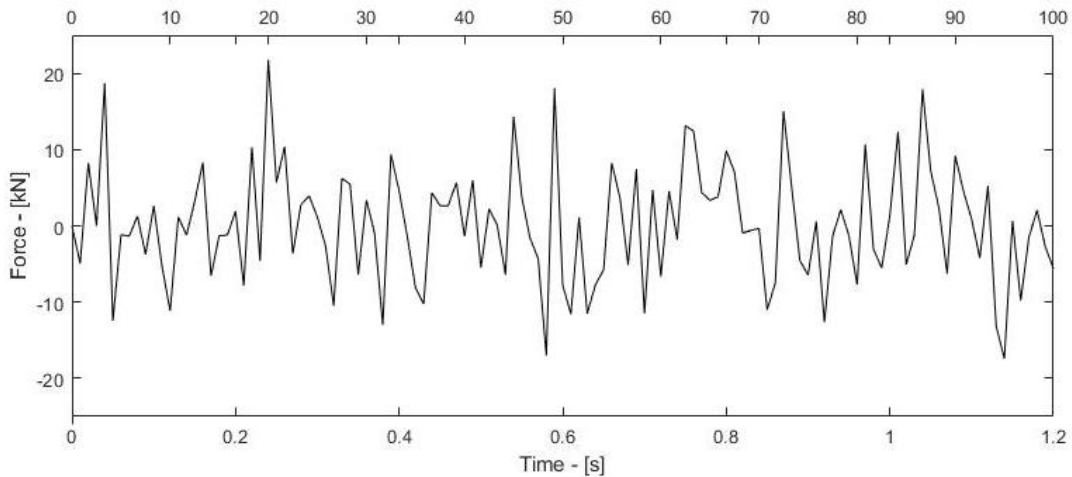


Figure 5-18: Superposition of forces due to hunting and irregularities. TAV 300 km/h

In Table 5-7 the extreme values of the hunting and total force are reported as a function of the speed.. The values are listed also for a hypothetical speed of 400 km/h.

Table 5-7: Maximum transversal forces induced by a TAV

Speed [km/h]	Maximum axle forces [kN]	
	Hunting	Total
20	± 0,008	± 0,1
40	± 0,03	± 0,4
60	± 0,08	± 0,8
80	± 0,13	± 1,5
100	± 0,2	± 2
120	± 0,3	± 3
140	± 0,4	± 4
160	± 0,5	± 6
180	± 0,7	± 8
200	± 0,85	± 10
220	± 1	± 12
240	± 1,2	± 15
260	± 1,5	± 16
280	± 1,7	± 18
300	± 2	± 20
400	± 3,4	± 35

## 5.5 Critical speeds

The speeds of the convoys to be adopted in the vertical and transverse dynamic analyses of the tunnel are chosen based on the admissible speed range and on the basis of critical speeds.

A speed is called critical when the train induces oscillations that lead the tunnel to resonance. To determine the critical speeds values, for both vertical and transverse motion, use of equation (5.33) is done, which relates the frequencies induced by the train to its speed and to the wavelengths of the irregularities. This equation can also be extended to the motion of the hunting of the wheels.

$$f = \frac{V}{\lambda} \text{ [Hz]} \quad (5.33)$$

It therefore follows that, by setting as frequencies those of the tunnel's natural modes, presented in chapter 3, and by entering the ranges of wavelengths used for alignment and profile irregularities, the respective critical speed ranges are obtained. Furthermore, for hunting, having a specific wavelength for each individual train, the speed will be unique, and not an interval. The values of the critical speeds are shown in the following Tables 5-8 and 5-9.

Table 5-8: Critical speeds for the vertical interaction, TMV & TAV

Irregularities of the profile			
Wave length : 0,5 ÷ 100 [m]			
Tunnel mode	Natural frequency [Hz]	Velocity TMV [km/h]	Velocity TAV [km/h]
1 – Longitudinal	0,150	0,3 ÷ 54	0,3 ÷ 54
2 – Longitudinal	0,322	0,6 ÷ 115,9	0,6 ÷ 115,9
<b>3 – Torsional</b>	<b>0,424</b>	<b>0,8 ÷ 152,6</b>	<b>0,8 ÷ 152,6</b>
<b>4 – Torsional</b>	<b>0,494</b>	<b>0,9 ÷ 160</b>	<b>0,9 ÷ 177,8</b>
5 – Longitudinal	0,510	0,9 ÷ 160	0,9 ÷ 183,6
6 – Trasversal	0,534	–	–
<b>7 – Vertical</b>	<b>0,536</b>	<b>1 ÷ 160</b>	<b>1 ÷ 193</b>
<b>8 – Vertical</b>	<b>0,540</b>	<b>1 ÷ 160</b>	<b>1 ÷ 194,4</b>
9 – Trasversal	0,540	–	–

The natural frequencies of the tunnel have prevalent modal shapes. If these involve displacements mainly in one direction, it makes no sense to define a critical speed of a model that induces actions in another direction. For this reason, vertical and torsional modes have been associated to the vertical wagon model, and transverse modes to the transverse wagon model. The critical speeds for the longitudinal modes have been computed for both models.



Table 5-9: Critical speeds for the transversal interaction, TMV &amp; TAV

Irregularities of the alignments			
Wave length : 0,5 ÷ 100 [m]			
Tunnel mode	Natural frequency [Hz]	Velocity TMV [km/h]	Velocity TAV [km/h]
1 – Longitudinal	0,150	0,3 ÷ 54	0,3 ÷ 54
2 – Longitudinal	0,322	0,6 ÷ 115,9	0,6 ÷ 115,9
3 – Torsional	0,424	–	–
4 – Torsional	0,494	–	–
5 – Longitudinal	0,510	0,9 ÷ 160	0,9 ÷ 183,6
<b>6 – Trasversal</b>	<b>0,534</b>	<b>1 ÷ 160</b>	<b>1 ÷ 192,2</b>
7 – Vertical	0,536	–	–
8 – Vertical	0,540	–	–
<b>9 – Trasversal</b>	<b>0,540</b>	<b>1 ÷ 160</b>	<b>1 ÷ 194,4</b>
Hunting			
Tunnel mode	Natural frequency [Hz]	Wave length 16,41 m Velocity TMV [km/h]	Wave length 23,34 m Velocity TAV [km/h]
1 – Longitudinal	0,150	8,9	12,6
2 – Longitudinal	0,322	19	27,1
3 – Torsional	0,424	–	–
4 – Torsional	0,494	–	–
5 – Longitudinal	0,510	30,1	42,9
<b>6 – Trasversal</b>	<b>0,534</b>	<b>31,5</b>	<b>44,9</b>
7 – Vertical	0,536	–	–
8 – Vertical	0,540	–	–
<b>9 – Trasversal</b>	<b>0,540</b>	<b>31,9</b>	<b>45,4</b>

It can therefore be concluded that speeds in the range of 0 and 200 km/h can all be critical for the floating tunnel at study, with particular attention to the 30 ÷ 45 km/h interval for hunting. These outcomes are based on the frequency window chosen for the response spectrum, see equation (4.5).

Therefore, contrary to what could be expected, a train traveling at high speed, with speeds above 200 km/h, induces less risk of resonance in the floating tunnel than a low-speed train. However, for high speeds, the variation of acting force will be greater, and therefore greater displacements will occur compared to lower speeds.

The speeds for which the solutions of the vertical and transverse interactions of the tunnel will be analysed are indicated in Table 5-10. For vertical interaction, an analysis is performed with the maximum speed of the two trains, at 160 km/h for the TMV and 300 km/h for the TAV. For the other speeds (inside the critical ranges) many analyses have been conducted, not reported here, that highlighted the capacity of the tunnel to withstand these forces without undergoing critical displacements or resonance. With higher speeds, the forces applied are larger as the displacements induced in the tunnel. Therefore, considering the maximum speed of the trains is equivalent to consider the worst case scenario for that train. Only for the transversal

interaction the analyses with the critical speeds of the hunting motion are listed (being a single value) emphasizing that the tunnel can withstand critical loads.

*Table 5-10: Chosen speeds for the analyses*

<b>Interaction</b>	<b>Train</b>	<b>Speed [km/h]</b>	<b>Interest of the analysis</b>
Vertical	TMV	160	Maximum admissible speed for TMV in Italy
	TAV	300	Maximum admissible speed for TAV in Italy
Trasversal	TMV	31,5	Critical speed for hunting
		160	Maximum admissible speed for TMV in Italy
	TAV	45	Critical speed for hunting
		300	Maximum admissible speed for TAV in Italy

# 6

## EQUATIONS OF MOTION

The study of the dynamic interaction between an Archimedes' floating submerged tunnel and a convoy of wagons requires that the two dynamic systems are analysed simultaneously. The motion of the first system depends on the motion of the second, and vice versa. The need to define the irregularities of the rail is added to this problem. Contact points, which change at every instant in time with a constant speed, must be traced.

The mechanical behaviour of the two systems is described through the coupled equation of motion, following the works by Mulas et al. (2008 and 2010) and the thesis of Palamà (2017), under the following assumptions:

- The analysis of the structure is based on the static equilibrium configuration reached at the end of the non-linear analysis;
- The wagons travel at a constant speed and in a straight line parallel to the axis of the tunnel;
- The vertical and transverse motions of the wagons are uncoupled;
- The contact between the wheel and the rail is perfect and is reduced to a single point without mass;
- The internal and external constraints are smooth, bilateral and holonomic.

These hypotheses allow us to describe the interaction between wagons and structure with a system of concentrated forces and the motion of the tunnel. These forces, unlike the vertical interaction, in the transverse interaction do not take into account of the dynamic response of the wagon, as already illustrated, simplifying the final equations.

Therefore, the equations of motion with specific validity for vertical analysis are shown below, following the derivation of Mulas et al. (2008 and 2010). These equations will still have general validity for the transversal analysis, which is described in detail in paragraph 6.5, where the effect of the wagons is reduced to forces without accounting the dynamic properties of the wagon.

## 6.1 Free coordinates

The submerged tunnel is modeled through the ANSYS Mechanical APDL finite element program, while the generic wagon is described by a system of rigid bodies, with mass and rotational inertia, connected to each other through springs and viscous dampers in the INTER code. To describe the dynamic response of the coupled tunnel and convoy system, it was decided to discretize the tunnel by means of finite elements and to use a finite number of Lagrangian coordinates contained in the vector  $\underline{q}$ :

$$\underline{q} = \begin{bmatrix} \underline{q}_{sft} \\ \underline{q}_{trains} \end{bmatrix} \quad (6.1)$$

The vector  $\underline{q}$  can be partitioned into  $\underline{q}_{sft}$  and  $\underline{q}_{trains}$  which represent the vectors containing the Lagrangian coordinates of the tunnel and of the train's wagons, respectively.

Having assumed that the constraints are bilateral (perfect adherence) and that the contact between the wheel and the rail is reduced to a massless point, it is possible to express the displacements and velocities of the contact points of the wagons, through displacements, velocities and roughness of the corresponding contact points of the bridge. In this view it is necessary to divide the vector  $\underline{q}_{sft}$  containing the Lagrangian coordinates of the bridge as follows:

$$\underline{q}_{sft} = \begin{bmatrix} \underline{q}_t \\ \underline{q}_c \end{bmatrix} \quad (6.2)$$

The vector  $\underline{q}_c$  contains the coordinates of the points of the bridge directly loaded by the contact forces transmitted by the wagons. The vector  $\underline{q}_t$  contains all the remaining coordinates of the tunnel.

When the generic wagon travels in the tunnel, at the time instant  $t$ , the contact points in most cases are not in correspondence with the nodes of the finite element model. Since it is not possible to update the bridge mesh at each integration step to make these points coincide with the nodes, the solution is interpolated within the finite element model using appropriate shape functions. A new set of coordinates  $\underline{q}_{ct}$  is then defined, which allows to describe the vertical positions of the contact points relative to the bridge in the deformed configuration, as:

$$\underline{q}_{ct} = \underline{N} \cdot \underline{q}_c \quad (6.3)$$

The matrix  $\underline{N}$  contains a set of shape functions. Not all the  $\underline{q}_c$  become  $\underline{q}_{ct}$ , but only those of the nodes around the contact point. This matrix varies for each position that the generic contact point assumes within the finite element and therefore represents a time-varying matrix. If the point is the same as the tunnel node,  $\underline{q}_{ct} = \underline{q}_c$ .

In an analogous way, it is possible to partition the free coordinates of the trains as follows:

$$\underline{q}_{trains} = \begin{bmatrix} \underline{q}_{w,1} \\ \underline{q}_{w,2} \\ \underline{q}_{w,j} \\ \vdots \\ \underline{q}_{w,n} \end{bmatrix} = \begin{bmatrix} \underline{q}_{cv} \\ \underline{q}_v \end{bmatrix} \quad (6.4)$$

Where  $\underline{q}_{w,j}$  is the vector of the coordinates of the  $j$ -th wagon, as previously identified in (5.2):

$$\underline{q}_{w,j} = [\underline{q}_{cv,j} \mid \underline{q}_{v,j}]^T = [q_{c1} \ q_{c2} \ q_{c3} \ q_{c4} \mid q_1 \ q_2 \ q_3 \ q_4 \ q_5 \ q_6 \ q_7 \ q_8 \ q_9 \ q_{10}]_j^T \quad (6.5)$$

The coordinates  $\underline{q}_{cv}$  are therefore the set of all the contact points, of all the wagons, of all the trains. The coordinates  $\underline{q}_v$  are the set of the remaining coordinates of the wagons, necessary to describe the configuration of the rigid bodies of the train models.

Between  $\underline{q}_{cv}$  and  $\underline{q}_c$  there is a relationship, due to the hypothesis of perfect contact. At the generic time instant  $t$ , the longitudinal position of a contact point can be described by the function  $z(t)$ . At this position the roughness of the rail assumes the value  $r(z(t))$ . The displacement of the generic contact point of the train, contained in  $\underline{q}_{cv}$ , must be equal to the sum between the corresponding displacement of the contact point of the tunnel, contained in  $\underline{q}_{ct}$ , and the roughness of the rail  $r(z(t))$  – see Figure 6-1.

$$\underline{q}_{cv}(t) = \underline{r}(z(t)) + \underline{q}_{ct}(t) = \underline{r}(z(t)) + \underline{N}(z(t)) \cdot \underline{q}_c(t) \quad (6.6)$$

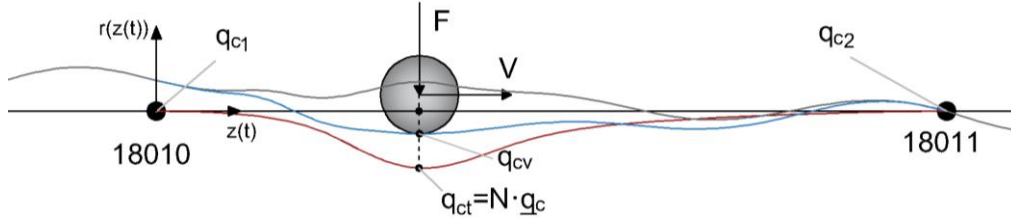


Figure 6-1: Relation between contact points

The black line in Figure 6-1 represents the beam element (BEAM4) of the model in ANSYS, to which are associated the displacements  $\underline{q}_c$ . The red line represents the deformation of the tunnel beam under the contact load, given by the shape functions ( $\underline{q}_{ct}$ ). The final displacement  $\underline{q}_{cv}$  is represented by the blue line, which takes into account the roughness (grey line).

By deriving equation (6.6) the velocity of the contact points can be expressed:

$$\dot{\underline{q}}_{cv}(t) = \dot{\underline{r}}(z(t)) + \underline{\dot{N}}(z(t)) \cdot \underline{q}_c(t) + \underline{N}(z(t)) \cdot \dot{\underline{q}}_c(t) \quad (6.7)$$

Setting  $c$  as the train speed, it can be defined:

$$\underline{\dot{r}} = c \cdot \underline{r}' \quad \text{and} \quad \underline{\dot{N}} = c \cdot \underline{N}' \quad (6.8)$$

The vertical velocities of the contact points can be expressed as:

$$\underline{\dot{q}}_{cv}(t) = c \cdot \underline{r}' + \underline{N}(z(t)) \cdot \underline{\dot{q}}_c(t) + c \cdot \underline{N}' \cdot \underline{q}_c \quad (6.9)$$

Thanks to equations (6.6) and (6.9), the coupled system (tunnel + trains) can be completely described by the following Lagrangian coordinates vector (Mulas et al., 2010).

$$\underline{q} = \begin{bmatrix} \underline{q}_t \\ \underline{q}_c \\ \underline{q}_v \end{bmatrix} \quad (6.10)$$

## 6.2 Lagrange equations

The equation of motion for discrete systems (with a finite number of degrees of freedom), conservative and with smooth and holonomic constraints (which can be described through mathematical equations), can be obtained through the Lagrange equations.

Let  $q_k$  be the free coordinates that describe the configuration of the system starting from that of static equilibrium  $C_0$ , and consider only the small oscillations around  $C_0$ . The  $k$ -th equation of motion becomes:

$$\frac{d}{dt} \left( \frac{\partial L}{\partial \dot{q}_k} \right) - \frac{\partial L}{\partial q_k} = Q_k + Q_{D,k} \quad k = 1, 2, \dots, n_{dof} \quad (6.11)$$

Where:

- $L$  represents the Lagrangian function, given by the difference between the kinetic energy and the potential energy of the system:  $L = T(\underline{\dot{q}}) - V(\underline{q}, t)$
- $Q_k$  is the generalized component of the external forces;
- $Q_{D,k}$  is the generalized component of the dissipative forces.

In the case at study, the external force is given by the weight of the structure and train, and the buoyancy force acting on the tunnel. The generalized component of the dissipation force, can be expressed through the Lord Rayleigh function, called the dissipation function and indicated by  $D$ . For the fundamental property of the Lord Rayleigh function we can express  $Q_{D,k}$  as:

$$Q_{D,k} = - \frac{\partial D}{\partial \dot{q}_k} \quad k = 1, 2, \dots, n_{dof} \quad (6.12)$$

The Lagrangian equation can be rewritten as:

$$\frac{d}{dt} \left( \frac{\partial L}{\partial \dot{q}_k} \right) - \frac{\partial L}{\partial q_k} + \frac{\partial D}{\partial \dot{q}_k} = Q_k \quad k = 1, 2, \dots, n_{dof} \quad (6.13)$$

To define the equations of motion of the coupled system it is therefore necessary to determine the kinetic energy  $T$ , the potential energy  $V$  and the dissipation function  $D$ , which are given by the sum of the contributions of the two subsystems: tunnel and wagons.

$$\begin{aligned} T &= T_{tunnel} + T_{wagons} \\ V &= V_{tunnel} + V_{wagons} \\ D &= D_{tunnel} + D_{wagons} \end{aligned} \quad (6.14)$$



### 6.2.1 Kinetic energy

The kinetic energy  $T$  is represented by the following quadratic form:

$$T = \frac{1}{2} \underline{\dot{q}}^T \underline{M} \underline{\dot{q}} \quad (6.15)$$

In the hypothesis of small oscillations, the mass matrix  $\underline{M}$  is symmetric, positive definite with constant coefficients equal to the values assumed in the equilibrium configuration  $C_0$ .

For wagons, remembering that the contact points are massless and in perfect contact to the rail, the kinetic energy is:

$$T_{wagons} = \frac{1}{2} \left( \underline{\dot{q}}_v^T \underline{m}_{v,v} \underline{\dot{q}}_v \right) + \frac{1}{2} c^2 \sum_{j=1}^{n_v} M_j \quad (6.16)$$

Where:

- $\underline{\dot{q}}_v$  represents the velocity vector associated to the masses of the wagons;
- $\underline{m}_{v,v}$  is the wagon mass matrix, symmetrical and with constant coefficients by definition, defined in chapter 5 for a wagon, equation (5.9);
- $M_j$  is the total mass of the single wagon;
- $c$  is the horizontal speed of the wagons, assumed constant;
- $n_v$  is the total wagons number.

In equation (6.16), the first term represents the kinetic energy associated to the motion of the masses of the wagons (vertical translation), while the second term represents the kinetic energy associated to the translation along the direction of travel. Based on the train used and on the number of wagons and axles present, the size of the matrices and vectors will change accordingly.

For the tunnel, the kinetic energy can be written as:

$$T_{tunnel} = \frac{1}{2} \begin{bmatrix} \underline{\dot{q}}_t^T & \underline{\dot{q}}_c^T \end{bmatrix} \begin{bmatrix} \underline{m}_{t,t} & \underline{m}_{t,c} \\ \underline{m}_{c,t} & \underline{m}_{c,c} \end{bmatrix} \begin{bmatrix} \underline{\dot{q}}_t \\ \underline{\dot{q}}_c \end{bmatrix} \quad (6.17)$$

Where:

- $\underline{\dot{q}}_c$  represent the vector of the velocities of the nodes of the tunnel loaded by the contact forces;
- $\underline{\dot{q}}_t$  represent the vector of the velocities associated to the remaining points;
- The mass matrix of the tunnel is divided in four submatrices according with the partitioning of the free coordinates. For the case study discussed in this thesis work, the mass matrix include the contributions of the mass of the

structure, the mass of the water that surround the tunnel and the mass of the vehicle, which oscillates together with the bridge.

Therefore the total kinetic energy is:

$$\begin{aligned} T &= T_{tunnel} + T_{wagons} \\ &= \frac{1}{2} \begin{bmatrix} \dot{q}_t^T & \dot{q}_c^T \end{bmatrix} \begin{bmatrix} \underline{\underline{m}}_{t,t} & \underline{\underline{m}}_{t,c} \\ \underline{\underline{m}}_{c,t} & \underline{\underline{m}}_{c,c} \end{bmatrix} \begin{bmatrix} \dot{q}_t \\ \dot{q}_c \end{bmatrix} + \frac{1}{2} \left( \dot{q}_v^T \underline{\underline{m}}_{v,v} \dot{q}_v \right) + \frac{1}{2} c^2 \sum_{j=1}^{n_v} M_j \end{aligned} \quad (6.18)$$

## 6.2.2 Potential energy

The potential energy can be obtained from the series development of the elastic potential  $V$  around the equilibrium configuration  $C_0$ :

$$V(\underline{q}) = V_0 + \left. \frac{\partial V}{\partial \underline{q}} \right|_0 + \frac{1}{2} \left. \frac{\partial^2 V}{\partial \underline{q}^2} \right|_0 + \dots = \frac{1}{2} \underline{q}^T \underline{\underline{K}} \underline{q} \quad (6.19)$$

The constant term  $V_0$  does not affect the motion as the potential is placed under a derivate. The linear term it is null as well, since  $C_0$  is the equilibrium configuration for the system. The potential  $V(q)$  represents a positive definite quadratic form since  $C_0$  is a stable equilibrium configuration; therefore the stiffness matrix  $K$  is positive definite and symmetrical and its terms are calculated as:

$$k_{ij} = \left. \frac{\partial^2 V}{\partial q_i \partial q_j} \right|_{q=0} \quad (6.20)$$

In the case under study it is also necessary to consider the contribution offered by the conservative forces represented by the static and variable loads and by the buoyancy forces applied to the system. The potential energy of these loads is calculated, except the sign, as the work done by these forces for the associated displacements:

$$V^G = -W = -\underline{Q} \underline{q} \quad (6.21)$$

For the trains, indicating with  $\underline{Q}^T_0 = [0 \ \underline{Q}^T_{0,v}]$  the vector containing all the gravitational loads of all wagons, and remembering that according to equation (6.6) the coordinates of the wagon's contact points can be written as a function of corresponding coordinates of the tunnel, the potential energy is:

$$V_{wagons} = \frac{1}{2} \left[ \left( \underline{r}^T + \underline{q}_c^T \underline{\underline{N}}^T \right) \underline{q}_v^T \right] \begin{bmatrix} \underline{\underline{k}}_{cv,cv} & \underline{\underline{k}}_{cv,v} \\ \underline{\underline{k}}_{v,cv} & \underline{\underline{k}}_{v,v} \end{bmatrix} \begin{bmatrix} \underline{r} + \underline{\underline{N}} \underline{q}_c \\ \underline{q}_v \end{bmatrix} - [0 \ \underline{Q}^T_{0,v}] \begin{bmatrix} \underline{r} + \underline{\underline{N}} \underline{q}_c \\ \underline{q}_v \end{bmatrix} \quad (6.22)$$

Where:

- The coordinate vector has been partitioned according to (6.4);
- The stiffness matrix  $\underline{K}$  is divided into 4 submatrices in accordance with the partitioning of the coordinates. This matrix is time independent and positive semidefinite. This partitioning was detailed in chapter 5.2 for a single wagon;
- The second term takes into account the contribute of gravitational loads.

For the structural system, the static loads are grouped in the vector  $\underline{Q}^T_0 = [\underline{Q}^T_{0,t} \quad \underline{Q}^T_{0,v}]$  and the potential energy can be expressed as:

$$V_{tunnel} = \frac{1}{2} \begin{bmatrix} \underline{q}_t^T & \underline{q}_c^T \end{bmatrix} \begin{bmatrix} \underline{k}_{t,t} & \underline{k}_{t,c} \\ \underline{k}_{c,t} & \underline{k}_{c,c} \end{bmatrix} \begin{bmatrix} \underline{q}_t \\ \underline{q}_c \end{bmatrix} - \begin{bmatrix} \underline{Q}_{0,t}^T & \underline{Q}_{0,c}^T \end{bmatrix} \begin{bmatrix} \underline{q}_t \\ \underline{q}_c \end{bmatrix} \quad (6.23)$$

Where:

- The vector of the coordinates has been partitioned according with (6.2);
- The stiffness matrix  $\underline{K}$  is divided into four submatrices in accordance with the partitioning of the free coordinates;
- The second term takes into account the contribution due to the gravitational loads of the tunnel and the applied buoyancy force.

Therefore the total potential energy is:

$$\begin{aligned} V &= V_{tunnel} + V_{wagons} \\ &= \frac{1}{2} \begin{bmatrix} \underline{q}_t^T & \underline{q}_c^T \end{bmatrix} \begin{bmatrix} \underline{k}_{t,t} & \underline{k}_{t,c} \\ \underline{k}_{c,t} & \underline{k}_{c,c} \end{bmatrix} \begin{bmatrix} \underline{q}_t \\ \underline{q}_c \end{bmatrix} - \begin{bmatrix} \underline{Q}_{0,t}^T & \underline{Q}_{0,c}^T \end{bmatrix} \begin{bmatrix} \underline{q}_t \\ \underline{q}_c \end{bmatrix} \\ &\quad + \frac{1}{2} \left[ \left( \underline{r}^T + \underline{q}_c^T \underline{N}^T \right) \underline{q}_v^T \right] \begin{bmatrix} \underline{k}_{cv,cv} & \underline{k}_{cv,v} \\ \underline{k}_{v,cv} & \underline{k}_{v,v} \end{bmatrix} \begin{bmatrix} \underline{r} + \underline{N} \underline{q}_c \\ \underline{q}_v \end{bmatrix} - \begin{bmatrix} 0 & \underline{Q}_{0,v}^T \end{bmatrix} \begin{bmatrix} \underline{r} + \underline{N} \underline{q}_c \\ \underline{q}_v \end{bmatrix} \end{aligned} \quad (6.24)$$

### 6.2.3 Rayleigh function

The Rayleigh function or dissipation function is defined as half the power dissipated by the  $s$  dampers present in the system:

$$D = \frac{1}{2} \sum_{r=1}^s c_r \cdot \dot{z}_r^2 \quad (6.25)$$

Where:

- $c_r$  represent the damping constant;
- $z_r$  is the relative elongation of the dampers.

Indicating with  $n$  the number of the free coordinates, for the linearity of the problem, it is possible to express  $\dot{z}_r$  as:

$$\dot{z}_r = \sum_{i=1}^n \frac{\partial z_r}{\partial q_i} \dot{q}_i \quad (6.26)$$

Substituting (6.26) in (6.25), we obtain:

$$D = \frac{1}{2} \sum_{r=1}^s c_r \cdot \sum_{i=1}^n \frac{\partial z_r}{\partial q_i} \dot{q}_i \cdot \sum_{j=1}^n \frac{\partial z_r}{\partial q_j} \dot{q}_j \quad (6.27)$$

The damping matrix  $\underline{\underline{C}}$  is composed of the terms:

$$c_{ij} = \sum_{r=1}^s c_r \frac{\partial z_r}{\partial q_i} \frac{\partial z_r}{\partial q_j} \quad (6.28)$$

Therefore, the dissipating function can be rewritten as:

$$D = \frac{1}{2} \underline{\underline{\dot{q}}}^T \underline{\underline{C}} \underline{\underline{\dot{q}}} \quad (6.29)$$

For the wagons, the function (6.27) becomes:

$$D_{wagons} = \frac{1}{2} \begin{bmatrix} \underline{\underline{\dot{q}}}_{cv}^T & \underline{\underline{\dot{q}}}_v^T \end{bmatrix} \begin{bmatrix} \underline{\underline{c}}_{cv,cv} & \underline{\underline{c}}_{cv,v} \\ \underline{\underline{c}}_{v,cv} & \underline{\underline{c}}_{v,v} \end{bmatrix} \begin{bmatrix} \underline{\underline{\dot{q}}}_{cv} \\ \underline{\underline{\dot{q}}}_v \end{bmatrix} \quad (6.30)$$

Considering the definition of  $\underline{\underline{q}}_{cv}$  expressed in (6.7), the function of dissipation of the wagons in its final form is written as:

$$D_{wagons} = \frac{1}{2} \left[ \left( \underline{\underline{\dot{r}}}^T + \underline{\underline{\dot{q}}}_c^T \underline{\underline{N}}^T + \underline{\underline{q}}_c^T \underline{\underline{\dot{N}}}^T \right) \underline{\underline{\dot{q}}}_v^T \right] \begin{bmatrix} \underline{\underline{c}}_{cv,cv} & \underline{\underline{c}}_{cv,v} \\ \underline{\underline{c}}_{v,cv} & \underline{\underline{c}}_{v,v} \end{bmatrix} \begin{bmatrix} \underline{\underline{\dot{r}}} + \underline{\underline{N}} \underline{\underline{\dot{q}}}_c + \underline{\underline{\dot{N}}} \underline{\underline{q}}_c \\ \underline{\underline{\dot{q}}}_v \end{bmatrix} \quad (6.31)$$

For what concern the tunnel, the dissipating function is:

$$D_{tunnel} = \frac{1}{2} \begin{bmatrix} \underline{\underline{\dot{q}}}_t^T & \underline{\underline{\dot{q}}}_c^T \end{bmatrix} \begin{bmatrix} \underline{\underline{c}}_{t,t} & \underline{\underline{c}}_{t,c} \\ \underline{\underline{c}}_{c,t} & \underline{\underline{c}}_{c,c} \end{bmatrix} \begin{bmatrix} \underline{\underline{\dot{q}}}_t \\ \underline{\underline{\dot{q}}}_c \end{bmatrix} \quad (6.32)$$

The final Rayleigh function therefore is:

$$\begin{aligned}
D &= D_{tunnel} + D_{wagons} \\
&= \frac{1}{2} [\underline{\dot{q}}_t^T \quad \underline{\dot{q}}_c^T] \begin{bmatrix} \underline{c}_{t,t} & \underline{c}_{t,c} \\ \underline{c}_{c,t} & \underline{c}_{c,c} \end{bmatrix} \begin{bmatrix} \underline{\dot{q}}_t \\ \underline{\dot{q}}_c \end{bmatrix} \\
&+ \frac{1}{2} \left[ (\underline{\dot{r}}^T + \underline{\dot{q}}_c^T \underline{N}^T + \underline{q}_c^T \underline{\dot{N}}^T) \quad \underline{\dot{q}}_v^T \right] \begin{bmatrix} \underline{c}_{cv,cv} & \underline{c}_{cv,v} \\ \underline{c}_{v,cv} & \underline{c}_{v,v} \end{bmatrix} \begin{bmatrix} \underline{\dot{r}} + \underline{N} \underline{\dot{q}}_c + \underline{\dot{N}} \underline{q}_c \\ \underline{\dot{q}}_v \end{bmatrix}
\end{aligned} \tag{6.33}$$

### 6.3 Coupled problem

The equations of the coupled problem are obtained from the Lagrange equation (6.13), deriving the functions obtained in the previous paragraphs. Considering  $Q_k$  equal to zero, each term at RHS can be derived separately.

The first term is the derivative of kinetic and potential energy with respect to velocities. Since the potential energy depends only on the displacements, and therefore is independent of velocity, its derivative in the velocities domain is zero. It is therefore:

$$\frac{d}{dt} \left( \frac{\partial L}{\partial \dot{q}_k} \right) = \frac{d}{dt} \left( \frac{\partial T}{\partial \dot{q}_k} - \frac{\partial V}{\partial \dot{q}_k} \right) = \frac{d}{dt} \left( \frac{\partial T}{\partial \dot{q}_k} \right) \quad (6.34)$$

The second term is the derivative of kinetic and potential energy by displacements. The opposite happens here, since the kinetic energy is independent of displacements. It turns out therefore:

$$\frac{\partial L}{\partial q_k} = \frac{\partial T}{\partial q_k} - \frac{\partial V}{\partial q_k} = - \frac{\partial V}{\partial q_k} \quad (6.35)$$

The third term is not null. Taking into account (6.34) and (6.35), the Lagrange equation is rewritten in the form (6.36).

$$\frac{d}{dt} \left( \frac{\partial T}{\partial \dot{q}_k} \right) + \frac{\partial D}{\partial \dot{q}_k} + \frac{\partial V}{\partial q_k} = 0 \quad k = 1, \dots, n_{dof} \quad (6.36)$$

The derivatives of each term are computed to obtain (6.36) in an extended form. By deriving the kinetic and potential energy and the dissipation function with respect to the vector  $\underline{q}$ , partitioned as in the previous paragraphs, the derivatives (6.37), (6.38) and (6.39) are obtained.

$$\frac{d}{dt} \left( \frac{\partial T}{\partial \underline{\dot{q}}} \right) = \begin{bmatrix} \underline{m}_{t,t} & \underline{m}_{t,c} & 0 \\ \underline{m}_{c,t} & \underline{m}_{c,c} & 0 \\ 0 & 0 & \underline{m}_{v,v} \end{bmatrix} \begin{bmatrix} \underline{\ddot{q}}_t \\ \underline{\ddot{q}}_c \\ \underline{\ddot{q}}_v \end{bmatrix} \quad (6.37)$$

$$\begin{aligned} \frac{\partial D}{\partial \underline{\dot{q}}} &= \begin{bmatrix} \underline{c}_{t,t} & \underline{c}_{t,c} & 0 \\ \underline{c}_{c,t} & \underline{c}_{c,c} + \underline{N}^T \underline{c}_{cv,cv} \underline{N} & \underline{N}^T \underline{c}_{cv,cv} \\ 0 & \underline{N}^T \underline{c}_{cv,cv} & \underline{c}_{v,v} \end{bmatrix} \begin{bmatrix} \underline{\dot{q}}_t \\ \underline{\dot{q}}_c \\ \underline{\dot{q}}_v \end{bmatrix} \\ &+ \begin{bmatrix} 0 & 0 & 0 \\ 0 & \underline{\dot{N}}^T \underline{c}_{cv,cv} \underline{\dot{N}} & 0 \\ 0 & \underline{c}_{cv,v}^T \underline{\dot{N}} & 0 \end{bmatrix} \begin{bmatrix} \underline{q}_t \\ \underline{q}_c \\ \underline{q}_v \end{bmatrix} + \begin{bmatrix} 0 & & \\ \underline{N}^T \underline{c}_{cv,cv} \underline{\dot{r}} & & \\ \underline{c}_{cv,v}^T \underline{\dot{r}} & & \end{bmatrix} \end{aligned} \quad (6.38)$$

$$\frac{\partial V}{\partial \underline{q}} = \begin{bmatrix} \underline{k}_{t,t} & \underline{k}_{t,c} & 0 \\ \underline{k}_{c,t} & \underline{k}_{c,c} + \underline{N}^T \underline{k}_{cv,cv} \underline{N} & \underline{N}^T \underline{k}_{cv,cv} \\ 0 & \underline{N}^T \underline{k}_{cv,cv} & \underline{k}_{v,v} \end{bmatrix} \begin{bmatrix} \underline{q}_t \\ \underline{q}_c \\ \underline{q}_v \end{bmatrix} + \begin{bmatrix} 0 \\ \underline{N}^T \underline{k}_{cv,cv} \underline{r} \\ \underline{k}_{cv,v}^T \underline{r} \end{bmatrix} - \begin{bmatrix} \underline{Q}_{0,t} \\ \underline{Q}_{0,c} \\ 0 \end{bmatrix} - \begin{bmatrix} 0 \\ 0 \\ \underline{Q}_{0,v} \end{bmatrix} \quad (6.39)$$

Substituting these last three derivatives in (6.36) the equations of motion are obtained:

$$\begin{bmatrix} \underline{m}_{t,t} & \underline{m}_{t,c} & 0 \\ \underline{m}_{c,t} & \underline{m}_{c,c} & 0 \\ 0 & 0 & \underline{m}_{v,v} \end{bmatrix} \begin{bmatrix} \underline{\ddot{q}}_t \\ \underline{\ddot{q}}_c \\ \underline{\ddot{q}}_v \end{bmatrix} + \begin{bmatrix} \underline{c}_{t,t} & \underline{c}_{t,c} & 0 \\ \underline{c}_{c,t} & \underline{c}_{c,c} + \underline{N}^T \underline{c}_{cv,cv} \underline{N} & \underline{N}^T \underline{c}_{cv,cv} \\ 0 & \underline{N}^T \underline{c}_{cv,cv} & \underline{c}_{v,v} \end{bmatrix} \begin{bmatrix} \underline{\dot{q}}_t \\ \underline{\dot{q}}_c \\ \underline{\dot{q}}_v \end{bmatrix} + \begin{pmatrix} \begin{bmatrix} 0 & 0 & 0 \\ 0 & \underline{N}^T \underline{c}_{cv,cv} \underline{\dot{N}} & 0 \\ 0 & \underline{c}_{cv,v}^T \underline{\dot{N}} & 0 \end{bmatrix} + \begin{bmatrix} \underline{k}_{t,t} & \underline{k}_{t,c} & 0 \\ \underline{k}_{c,t} & \underline{k}_{c,c} + \underline{N}^T \underline{k}_{cv,cv} \underline{N} & \underline{N}^T \underline{k}_{cv,cv} \\ 0 & \underline{N}^T \underline{k}_{cv,cv} & \underline{k}_{v,v} \end{bmatrix} \begin{bmatrix} \underline{q}_t \\ \underline{q}_c \\ \underline{q}_v \end{bmatrix} \\ = \begin{bmatrix} \underline{Q}_{0,t} \\ \underline{Q}_{0,c} \\ 0 \end{bmatrix} + \begin{bmatrix} 0 \\ 0 \\ \underline{Q}_{0,v} \end{bmatrix} - \begin{bmatrix} 0 \\ \underline{N}^T \underline{k}_{cv,cv} \underline{r} \\ \underline{k}_{cv,v}^T \underline{r} \end{bmatrix} - \begin{bmatrix} 0 \\ \underline{N}^T \underline{c}_{cv,cv} \underline{\dot{r}} \\ \underline{c}_{cv,v}^T \underline{\dot{r}} \end{bmatrix} \end{pmatrix} \quad (6.40)$$

The equations of motion can be written in compact form in the following way:

$$\underline{M} \cdot \underline{\ddot{q}} + \underline{C} \cdot \underline{\dot{q}} + (\underline{K}_c + \underline{K}_k) \cdot \underline{q} = \underline{Q}_0 + \underline{Q}_w(t) - \underline{Q}_r(t) - \underline{Q}_{\dot{r}}(t) \quad (6.41)$$

The matrices  $\underline{M}$ ,  $\underline{C}$  and  $\underline{K}$  of the system are all symmetrical. The mass matrix has constant coefficients, the stiffness and damping matrixes are time dependent as they contain the matrix of the shape functions  $\underline{N}(z(t))$ . The stiffness is given by the sum of two contributions: the first derives from the dissipation function and is indicated with  $\underline{K}_c$ , the second derives from the potential energy and is indicated with  $\underline{K}_k$ . The first contribution is not symmetrical and is time dependent, but can be neglected if the convective term  $\underline{\dot{N}}$  is negligible. In this case the problem becomes symmetrical again.

The vector  $\underline{Q}_0$  contains the static forces of the bridge and the buoyancy forces, while the term  $\underline{Q}_w$  contains the static forces associated with the weight of the wagons. The last two vectors  $\underline{Q}$  contain the forces deriving from the roughness profile and its variation along the tunnel and are related respectively to the potential energy and the dissipation force.

It should be noted that since the stiffness and damping matrixes are time dependent, due to the matrix of the shape functions, this system of equations is not easy to integrate even in the case of a symmetrical problem. The difficulty lies in the need to compute and assemble the matrixes at each step; this requires a high computational

burden. To avoid this problem, it is possible to adopt an uncoupled solution strategy, that will be presented in the following - see next paragraph.



## 6.4 Uncoupled solution strategy

The above system of equations (6.40) makes it impossible to study the response of either subsystem unless both are solved simultaneously. The coupling of the equations depends on the mixed terms that appear in the stiffness and damping matrices, and relate the coordinates of the two subsystems. However, a strategy can be devised, that allows the separate integration of the two subsystems.

Uncoupling can be done simply by transporting the mixed coupling terms and the time dependent terms to the RHS, thus considering them as forcing terms:

$$\begin{aligned}
 & \begin{bmatrix} \underline{m}_{t,t} & \underline{m}_{t,c} & 0 \\ \underline{m}_{c,t} & \underline{m}_{c,c} & 0 \\ 0 & 0 & \underline{m}_{v,v} \end{bmatrix} \begin{bmatrix} \underline{\ddot{q}}_t \\ \underline{\ddot{q}}_c \\ \underline{\ddot{q}}_v \end{bmatrix} + \begin{bmatrix} \underline{c}_{t,t} & \underline{c}_{t,c} & 0 \\ \underline{c}_{c,t} & \underline{c}_{c,c} & 0 \\ 0 & 0 & \underline{c}_{v,v} \end{bmatrix} \begin{bmatrix} \underline{\dot{q}}_t \\ \underline{\dot{q}}_c \\ \underline{\dot{q}}_v \end{bmatrix} + \begin{bmatrix} \underline{k}_{t,t} & \underline{k}_{t,c} & 0 \\ \underline{k}_{c,t} & \underline{k}_{c,c} & 0 \\ 0 & 0 & \underline{k}_{v,v} \end{bmatrix} \begin{bmatrix} \underline{q}_t \\ \underline{q}_c \\ \underline{q}_v \end{bmatrix} \\
 & = \begin{bmatrix} \underline{Q}_{0,t} \\ \underline{Q}_{0,c} \\ 0 \end{bmatrix} + \begin{bmatrix} 0 \\ 0 \\ \underline{Q}_{0,v} \end{bmatrix} - \begin{bmatrix} 0 \\ \underline{N}^T \underline{k}_{cv,cv} \underline{r} \\ \underline{k}_{cv,v}^T \underline{r} \end{bmatrix} - \begin{bmatrix} 0 \\ \underline{N}^T \underline{c}_{cv,cv} \underline{\dot{r}} \\ \underline{c}_{cv,v}^T \underline{\dot{r}} \end{bmatrix} - \begin{bmatrix} 0 \\ \underline{N}^T (\underline{c}_{cv,cv} \underline{N} \underline{\dot{q}}_c + \underline{c}_{cv,cv} \underline{\dot{q}}_v) \\ \underline{c}_{cv,v}^T \underline{N} \underline{\dot{q}}_c \end{bmatrix} \\
 & - \begin{bmatrix} 0 \\ \underline{N}^T (\underline{k}_{cv,cv} \underline{N} \underline{q}_c + \underline{k}_{cv,cv} \underline{q}_v) \\ \underline{k}_{cv,v}^T \underline{N} \underline{q}_c \end{bmatrix} - \begin{bmatrix} 0 \\ \underline{N}^T \underline{c}_{cv,cv} \underline{\dot{N}} \underline{q}_c \\ \underline{c}_{cv,v}^T \underline{\dot{N}} \underline{q}_c \end{bmatrix} \quad (6.42)
 \end{aligned}$$

The previous matrices can be rewritten in the following way:

$$\begin{bmatrix} \underline{m}_{t,t} & \underline{m}_{t,c} \\ \underline{m}_{c,t} & \underline{m}_{c,c} \end{bmatrix} \begin{bmatrix} \underline{\dot{q}}_t \\ \underline{\dot{q}}_c \end{bmatrix} + \begin{bmatrix} \underline{c}_{t,t} & \underline{c}_{t,c} \\ \underline{c}_{c,t} & \underline{c}_{c,c} \end{bmatrix} \begin{bmatrix} \underline{\dot{q}}_t \\ \underline{\dot{q}}_c \end{bmatrix} + \begin{bmatrix} \underline{k}_{t,t} & \underline{k}_{t,c} \\ \underline{k}_{c,t} & \underline{k}_{c,c} \end{bmatrix} \begin{bmatrix} \underline{q}_t \\ \underline{q}_c \end{bmatrix} = \begin{bmatrix} \underline{Q}_{0,t} \\ \underline{Q}_{0,c} - \underline{N}^T \underline{f} \end{bmatrix} \quad (6.43a)$$

$$\underline{m}_{v,v} \underline{\ddot{q}}_v + \underline{c}_{v,v} \underline{\dot{q}}_v + \underline{k}_{v,v} \underline{q}_v = \underline{Q}_{0,v} - \underline{f}_v \quad (6.43b)$$

The vector  $\underline{f}$  contains the wagon forces acting on the structure, and it is equal to:

$$\underline{f} = \underline{k}_{cv,cv} (\underline{r} + \underline{N} \underline{q}_c) + \underline{c}_{cv,cv} (\underline{\dot{r}} + \underline{N} \underline{\dot{q}}_c + \underline{\dot{N}} \underline{q}_c) + \underline{c}_{cv,v} \underline{\dot{q}}_v + \underline{k}_{cv,v} \underline{q}_v \quad (6.44)$$

This force vector, that acts on the structure due to the wagons, is a function of three physically different terms: the first is given by the displacements and velocities of the irregularities,  $\underline{r}$  and  $\underline{\dot{r}}$ ; the second depends on the displacements and velocities of the contact points  $\underline{q}_c$ ; the third is due to the motion  $\underline{q}_v$  and  $\underline{\dot{q}}_v$  of the wagons.

The vector  $\underline{f}_v$  contains the forces that excites the wagons and is equal to:

$$\underline{f}_v = \underline{k}_{cv,cv}^T (\underline{r} + \underline{N} \underline{q}_c) + \underline{c}_{cv,cv}^T (\underline{\dot{r}} + \underline{N} \underline{\dot{q}}_c + \underline{\dot{N}} \underline{q}_c) \quad (6.45)$$

This forcing term, which acts on the contact points of the wagons, depends on the roughness of the rails as well as on the displacements and velocities of the contact points.

With this transformation the matrices of the two systems are symmetrical. However, the two subsystems cannot be solved independently since the displacements of the structure excite the wagons and vice versa for the contact forces that the wagons transmit to the structure. The two systems are intrinsically coupled. Nevertheless, in this configuration of equations the two systems can be solved separately, with an iterative procedure, that will be described in chapter 7.

#### **6.4.1 Extension to the non-linear case**

The equations of motion of the coupled problem have been written considering a linear behavior of the structure and wagons. Thanks to the uncoupled approach, the analysis can also be extended to structures with non-linear behavior. In fact, the resolution of the equations of motion of the wagon depends on the variation of displacement and velocity of the contact points and not on the type of structural analysis performed [Palamà G., 2017].

## 6.5 Equation for the transversal motion

For the case of transversal motion the same equations hold, which however are reduced since the dynamics of the train is omitted and only known actions (forces and moments) are applied at the tunnel nodes.

Considering the uncoupled equations of motion (6.42), for the transverse interaction they reduce to:

$$\begin{bmatrix} \underline{m}_{t,t} & \underline{m}_{t,c} \\ \underline{m}_{c,t} & \underline{m}_{c,c} \end{bmatrix} \begin{bmatrix} \underline{\ddot{q}}_t \\ \underline{\ddot{q}}_c \end{bmatrix} + \begin{bmatrix} \underline{c}_{t,t} & \underline{c}_{t,c} \\ \underline{c}_{c,t} & \underline{c}_{c,c} \end{bmatrix} \begin{bmatrix} \underline{\dot{q}}_t \\ \underline{\dot{q}}_c \end{bmatrix} + \begin{bmatrix} \underline{k}_{t,t} & \underline{k}_{t,c} \\ \underline{k}_{c,t} & \underline{k}_{c,c} \end{bmatrix} \begin{bmatrix} \underline{q}_t \\ \underline{q}_c \end{bmatrix} = \begin{bmatrix} Q_{0,t} \\ Q_{0,c} - \underline{f} \end{bmatrix} \quad (6.46)$$

These equations coincide with (6.43a). Only the tunnel response is computed. Reducing all the motion of the wagon to a convoy of actions it turns out that (6.43b) is null.

The component of external forces  $\underline{f}$  is now a vector of forces acting on the tunnel nodes, variable in time, obtained as function of the irregularities of the rail and of the hunting of the wheels, transformed in a proper way with the shape functions.

Neglecting the motion of the wagon, with the consequent simplification of the equations, is possible thanks to the hypothesis of small transverse displacements of the tunnel as the train passes, which, as will be seen later, is confirmed, making the motion of the train independent on the deformations of the bridge.



# 7

## NUMERICAL IMPLEMENTATION

A numerical uncoupled solution strategy has been adopted for the mathematical solution of the equations of motion. In this work, the tunnel, loaded by wagons contact forces, is modeled and solved on ANSYS Mechanical APDL. At each time instant, displacements and velocities at contact points are computed and stored. The loads of the wagons are computed by:

- INTER 7.0: if the interaction is vertical and include the train dynamics;
- MATLAB script: if the interaction is transversal and does not include the train dynamics.

This chapter illustrates in detail how the computation of the loads of the wagons takes place and how the different codes interact.

## 7.1 Vertical interaction: INTER 7.0 code

INTER 7.0 is a program written in FORTRAN language and created specifically to solve the problem of dynamic vehicle-structure interaction. The code is versatile and able to solve the dynamic interaction problem in different ways. The code, receiving information regarding the tunnel and vehicle models, use to return displacements, velocities and accelerations of the coordinates of both systems. It was then modified, maintaining the initial functionalities, to rely on external finite element programs, such as ANSYS, for the solution of more complex structures. The two functionalities have been kept separately in the same code thanks to the thesis work of Maneco (2015), who added to the initial functionality (STS) that of WTH, and to the thesis work of Palamà (2017), which made possible to use WTH with ANSYS APDL.

A number of vehicle models can be used, being defined within the code. There are models of concentrated forces and forces with damped springs, cars with two or four wheels and models of 6-wheel trucks. In this thesis work, the wagon model has been implemented for the trains. A train now can transit in both the directions of a bridge and at different speeds with several wagons in a row, simulating a train in its completeness.

Within the INTER code, the equations of motion can be written and solved in incremental form with the Newmark method, by adopting one of the following procedures: STS (Single Time Step) and WTH (Whole Time History). The difference lies in the domain of integration. The first integrates over a single time step, the second over the entire time domain. So in total there are three ways of solving the problem: STS internal to INTER, WTH internal to INTER, WTH external with Ansys. The third approach is the one adopted for the vertical interaction in this thesis.

The complete description of the Fortran code is not reported in this work, since it is beyond its scope. However, comprehensive presentation of the code can be found in previous thesis works conducted by Palamà (2017) and Maneco (2015). Only the processes and methods adopted for the development of vertical interactions with the external WTH analysis are reported below.

The interaction, from the point of view of the convoy, can be divided into three time segments:

- I. *Rigid section before the tunnel*: the wagons travel on a rigid profile with rail irregularities, so as to cancel the initial conditions of the motion, and enter in the tunnel with a steady motion. This process is calculated internally in INTER. It's done only on the first iteration.
- II. *Dynamic wagon-tunnel interaction*: the values of the forces on the wagon are calculated by INTER. The contact forces are applied to the tunnel in ANSYS at each time instant and the solution of the dynamic deformations are obtained. Then the forces of the wagons on INTER are recalculated, on the basis of these latter deformations provided by ANSYS, and the process is repeated until convergence is obtained.

- III. *Free oscillations (rigid section after the tunnel)*: it is the imaginary section that follows the previous temporal section, when the train runs out of the tunnel and the bridge oscillates freely. It differs from the previous section being the tunnel in these time instants without forces. At each iteration, therefore, INTER prints, in the dynamic analysis files, time instants subsequent to those with the forces in which no force is applied, to obtain the displacement motion of the tunnel when the train has left.

From the point of view of the external WTH numerical procedure, on the other hand, three integration blocks are distinguished in the algorithm:

- I. *Rigid profile before the tunnel*: the static analysis of the tunnel is carried out and the displacements of the tunnel nodes are obtained. The vehicles travel on a rigid profile that takes into account only the roughness, and the motion of the wagons is obtained for the first time. The acting forces of the first iteration are calculated by INTER considering the motion of the vehicles and the structure at rest. From these, the contact forces to be applied to the tunnel are obtained and they are written on the files “time.csv” and “load\_treno.csv”.
- II. *Tunnel integration*: the forces obtained for each instant of the time domain are applied to the tunnel in ANSYS (including the null forces during the final moments of free vibration of the tunnel), the dynamic analysis is conducted obtaining the displacements and velocities of the nodes.
- III. *Vehicle integration*: once the motion of the tunnel is known, the displacements and velocities of the contact points of the wagons are calculated with INTER. The new contact forces to apply to the tunnel are obtained and their convergence is checked, verifying that the difference between the contact forces of two subsequent iterations is lower than the tolerance. If the criterion is not respected, the code returns to the previous block with the new contact forces just calculated, extracted in the files "time.csv" and "carichi\_treno.csv".

The external WTH procedure just illustrated is described in detail in the next two paragraphs. The first paragraph defines the code iteration processes, the second goes into detail about the method used to integrate the motion of the wagons.

### 7.1.1 WTH integration procedure

The WTH (Whole Time History) procedure iterates along the entire time history. At each cycle the wagons are positioned at the beginning of the tunnel and the integration is repeated.

The procedure can be described in 10 phases, which include the determination of the forces and the separate integration of the two systems. Indicating the iteration with  $j$  and the integration steps with  $k$ , the procedure can be drawn as follows:

1. At the first iteration –  $j=1$  – the structure, that is at rest, is considered rigid, and the wagons are subject only to the roughness of the rails. For each step  $k$ , the action that moves the wagons masses is:

$$\underline{f}_v^{1,k} = - \left[ \underline{k}_{cv,v}^T \underline{r}^k + \underline{c}_{cv,v}^T \underline{\dot{r}}^k \right] \quad (7.1)$$

To this term the contribute due to initial conditions of the wagons must be added:

$$\underline{f}_v^{1,k,i.c.} = \underline{m}_{v,v} \left[ \frac{1}{\beta \Delta t} \underline{\dot{q}}_v^{1,k-1} + \frac{1}{2\beta} \underline{\ddot{q}}_v^{1,k-1} \right] + \underline{c}_{v,v} \left[ \Delta t \left( \frac{\gamma}{2\beta} - 1 \right) \underline{\ddot{q}}_v^{1,k-1} + \frac{\gamma}{\beta} \underline{\dot{q}}_v^{1,k-1} \right] \quad (7.2)$$

Where:

- $\underline{m}_{v,v}$  mass matrix of all the wagons;
- $\underline{c}_{v,v}$  is the damping matrix of all the wagons;
- $\beta$  and  $\gamma$  are the Newmark parameters, defined in the next paragraph.

The vector in incremental form of effective force for each step  $k$ , of the first iteration, is defined as:

$$\Delta \underline{f}_v^{*1,k} = \Delta \underline{f}_v^{1,k} + \underline{f}_v^{1,k,i.c.} = \underline{f}_v^{1,k} - \underline{f}_v^{1,k-1} + \underline{f}_v^{1,k,i.c.} \quad (7.3)$$

2. The equation of motion of the wagons is solved with the Newmark method to derive the increment in the displacements of the masses.

$$\underline{\hat{K}}_{v,v} \Delta \underline{q}_v^{1,k} = \Delta \underline{f}_v^{*1,k} \quad (7.4)$$

Where:

- The effective stiffness matrix is calculated as:

$$\underline{\hat{K}}_{v,v} = \underline{m}_{v,v} \frac{1}{\beta \Delta t^2} + \underline{c}_{v,v} \frac{\gamma}{\beta \Delta t} + \underline{k}_{v,v} \quad (7.5)$$

- $\Delta \underline{q}_v^{1,k}$  is the increment of the total displacements with respect to the previous step of the coordinates of the wagons, having considered a rigid tunnel profile;
  - $\Delta \underline{f}_v^{*1,k}$  is the effective load increment calculated as indicated at point 1 in (7.1).
3. The contact forces transmitted to the tunnel for each step are calculated starting from the displacements and velocities of the wagons and considering the structure at rest and infinitely rigid:

$$\underline{f}_{ct}^{1,k} = - \left[ \underline{k}_{cv,cv} \underline{r}^k + \underline{c}_{cv,cv} \underline{\dot{r}}^k + \underline{k}_{cv,v} \underline{q}_v^{1,k} + \underline{c}_{cv,cv} \underline{\dot{q}}_v^{1,k} \right] \quad (7.6)$$



Points 1, 2 and 3 are performed only at the first iteration, for all time steps  $k$ . Once this first phase is completed, we return to the beginning of the tunnel and proceed with point 4, which is the starting point for each new iteration, where the iterative cycle begins.

4. The contact forces are transformed into equivalent nodal forces of the tunnel by using the shape functions matrix, which is assembled at each step, as it depends on the position:

$$\underline{p}_c^{j,k} = (\underline{N}^k)^T \underline{f}_{ct}^{j,k} \quad (7.7)$$

5. The vector of equivalent nodal loads, is applied to the finite element model in ANSYS APDL and the solution in terms of nodal displacements and velocities is obtained.

To transform the velocities and displacements of the nodes in the corresponding values at the contact points, the shape functions calculated in the final position of the current step are used:

$$\underline{q}_{ct}^{j,k} = \underline{N}^k \underline{q}_c^{j,k} \quad (7.8)$$

$$\underline{\dot{q}}_{ct}^{j,k} = \underline{N}^k \underline{\dot{q}}_c^{j,k} \quad (7.9)$$

6. Once the displacements and velocities of the structure acting at the contact points on the wheels are known, the load vector of the wagons is determined in accordance with the equation (6.45):

$$\underline{f}_v^{j,k} = - \left[ \underline{k}_{cv,v}^T (\underline{r}^k + \underline{N} \underline{q}_c^{j,k}) + \underline{c}_{cv,v}^T (\underline{\dot{r}}^k + \underline{N} \underline{\dot{q}}_c^{j,k} + \underline{\dot{N}} \underline{q}_c^{j,k}) \right] \quad (7.10)$$

To this term it is necessary to add that due to initial conditions, obtained from displacements and velocities at the previous step:

$$\underline{f}_v^{j,k,i.c.} = \underline{m}_{v,v} \left[ \frac{1}{\beta \Delta t} \underline{\dot{q}}_v^{j,k-1} + \frac{1}{2\beta} \underline{\ddot{q}}_v^{j,k-1} \right] + \underline{c}_{v,v} \left[ \Delta t \left( \frac{\gamma}{2\beta} - 1 \right) \underline{\dot{q}}_v^{j,k-1} + \frac{\gamma}{\beta} \underline{q}_v^{j,k-1} \right] \quad (7.11)$$

7. The vector of the effective loads increments  $\Delta \underline{f}_v^{*j,k}$  is calculated summing the increments of the loads  $\Delta \underline{f}_v^{j,k}$  to the term due to initial conditions  $\underline{f}_v^{*j,k,i.c.}$ :

$$\Delta \underline{f}_v^{*j,k} = \Delta \underline{f}_v^{j,k} + \underline{f}_v^{j,k,i.c.} = \underline{f}_v^{j,k} - \underline{f}_v^{j,k-1} + \underline{f}_v^{j,k,i.c.} \quad (7.12)$$

8. The equation of motion of the wagons is integrated over time using the Newmark procedure, illustrated in paragraph 7.1.2.

$$\underline{\hat{K}}_{v,v} \Delta \underline{q}_v^{j,k} = \Delta \underline{f}_v^{*j,k} \quad (7.13)$$

Where:

- The effective stiffness matrix is calculated according (7.5);
  - $\Delta q_v^{j,k}$  is the total displacement increment of the coordinates of the wagons with respect to the previous time step;
  - $\Delta f_v^{*,j,k}$  is the total effective increment calculated as indicated at point 7 in (7.12).
9. The contact forces transmitted by the wagons to the tunnel are recalculated considering the displacements and velocities of the systems at the current iteration:

$$\begin{aligned} \underline{f}_{ct}^{j,k} = & -\underline{k}_{cv,cv} \left( \underline{r}^k + \underline{N} \underline{q}_c^{j,k} \right) - \underline{c}_{cv,cv} \left( \dot{\underline{r}}^k + \underline{N} \dot{\underline{q}}_c^{j,k} + \dot{\underline{N}} \underline{q}_c^{j,k} \right) \\ & - \underline{k}_{cv,v} \underline{q}_v^{j-1,k} - \underline{c}_{cv,v} \dot{\underline{q}}_v^{j-1,k} \end{aligned} \quad (7.14)$$

10. At this point the convergence check is carried out. At the end of each step, the difference between the contact force of the  $i$ -th wheel in the current iteration and that in the previous iteration is calculated and a vector  $\underline{R}_i^j$  is assembled, having the dimensions of the number of integration steps  $N_t$ :

$$\underline{R}_i^j = \underline{f}_i^j - \underline{f}_i^{j-1} \quad (7.15)$$

The convergence criterion is expressed in terms of  $\underline{R}_i^j$  by calculating the standardized mean square value on the total vehicle weight. By indicating with  $W_i$  the static contact force of the  $i$ -th wheel, with  $N_t$  the number of steps and with  $n_w$  the total number of wheels, the error is computed as:

$$err_i = \frac{1}{W_i} \sqrt{\frac{\sum_{k=1}^{N_t} (R_{i,k}^j)^2}{N_t}} \leq \lambda \quad i = 1, \dots, n_w \quad (7.16)$$

The iteration stops when for each wheel the error  $err_i$  is lower than the predetermined tolerance value  $\lambda$ . When convergence is achieved, a warning is given on the command prompt that the analysis was conducted correctly. Conversely, if convergence is not achieved, the program goes back to point 4.

Figure 7-1 shows the flow chart of the procedure just illustrated.

Within the INTER code, processes are managed by several subroutines and functions. One of these subroutines is the “Newmark\_WTH.for” that contains all the previous steps. This part of the code is subordinate to the “Main.for” which manages the whole program, as well as introducing other parallel subroutines for reading the initial data, provided by the “ndati” and “nveic” text files (see appendix C). The “Newmark\_WTH.for” subroutine calls other subroutines, to manage all the steps of Figure 7-1. Among these there is the “car” subroutine which calls the “newmark\_ve”

subroutine. “newmark\_ve” is the subroutine that solves the equation of motion of the wagons, according to the Newmark method, which will be described in paragraph 7.1.2.

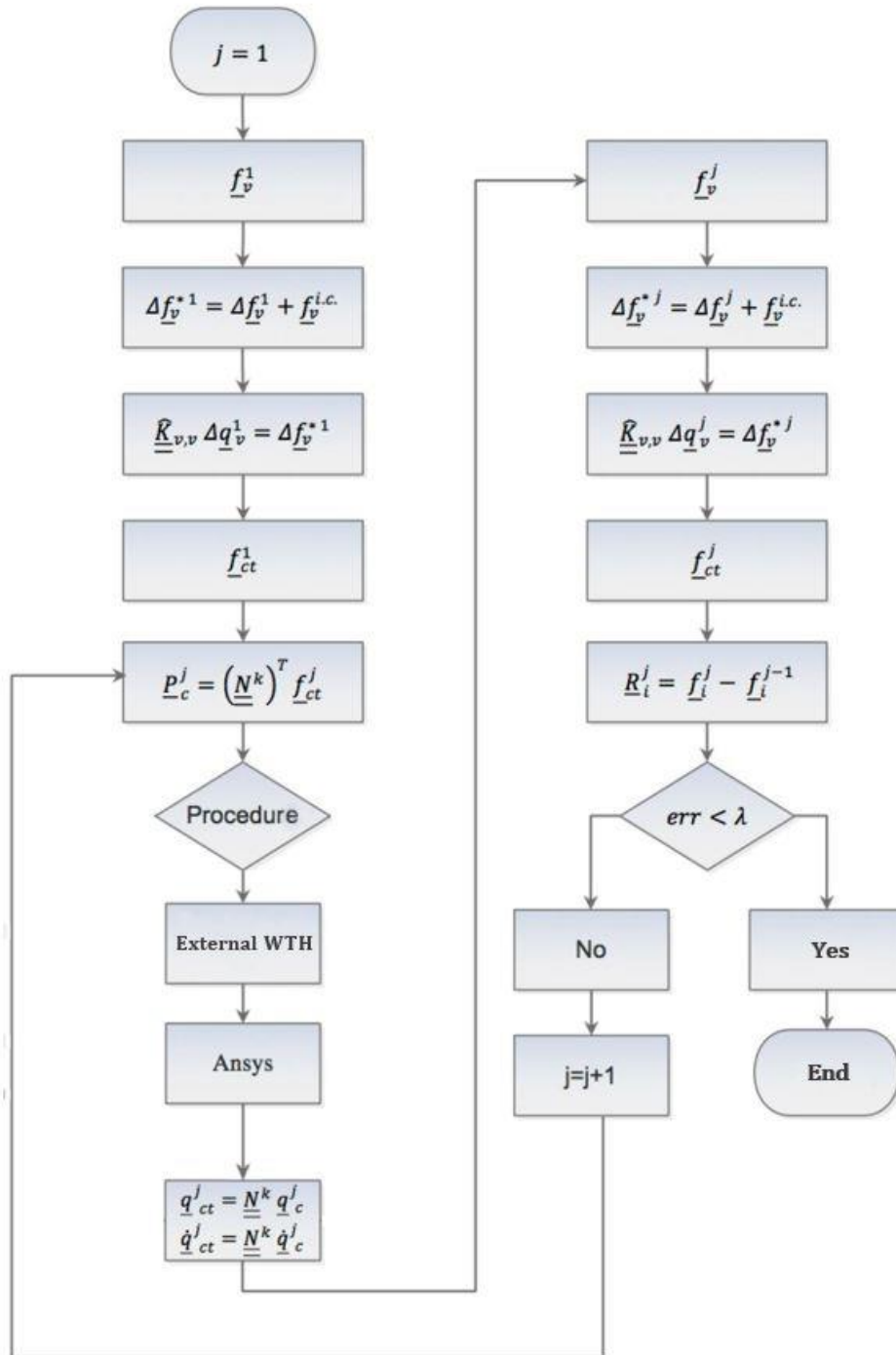


Figure 7-1: Vertical interaction flow chart on INTER [Palamà G., 2017]

## 7.1.2 Newmark method for direct integration

In steps 2 and 8 of the previous solution algorithm, the integration of the motion of the wagon is performed through the Newmark method. Below it is described how the direct integration takes place within the code.

The equation of motion of a system is obtained by imposing the dynamic equilibrium of the forces acting on this system, i.e. by imposing that the sum of the generalized components of inertia, restoring and perturbation forces are zero. This balance is formally expressed as:

$$\underline{Q}_I(t) + \underline{Q}_D(t) + \underline{Q}_E(t) = \underline{Q}(t) \quad (7.17)$$

The terms of the previous equation are written in the following way:

$$\underline{Q}_I(t) = \underline{m} \ddot{\underline{q}} \quad (7.18a)$$

$$\underline{Q}_D(t) = \underline{c} \dot{\underline{q}} \quad (7.18b)$$

$$\underline{Q}_E(t) = \underline{k} \underline{q} \quad (7.18c)$$

The first identifies the inertia term, the second the damping term and the third the elastic term.

Equation (7.17) represents a system of ordinary differential equations (ODE) whose integration allows to calculate the displacement of the system and, for subsequent derivations, also the velocities and acceleration and finally the acting forces.

However, it is not always possible to solve the problem by integrating the equations of motion or by carrying out modal analysis. In some circumstances, such as when the system matrices are time dependent, the only way to solve the system is to adopt a step-by-step method of numerical integration. These methods have a certain similarity to the finite element methods in the sense that the search for the continuous response in time is not performed, but the unknowns of motion, i.e. displacements, velocities and accelerations, are determined at discrete and constant time intervals.

The dynamic equilibrium equation is certainly valid for two successive instants of time and therefore can be written in incremental form as follows:

$$\Delta \underline{Q}_I(t) + \Delta \underline{Q}_D(t) + \Delta \underline{Q}_E(t) = \Delta \underline{Q}(t) \quad (7.19)$$

As for (7.17), the terms of relation (7.19) are written in the following way:

$$\Delta \underline{Q}_I(t) = \underline{m}_t \Delta \ddot{\underline{q}} \quad (7.20a)$$

$$\Delta \underline{Q}_D(t) = \underline{c}_t \Delta \dot{\underline{q}} \quad (7.20b)$$

$$\Delta \underline{Q}_E(t) = \underline{k}_t \Delta \underline{q} \quad (7.20c)$$

Therefore, the equation of motion written in incremental form assumes the following form:

$$\underline{\underline{m}}_t \Delta \underline{\underline{\ddot{q}}} + \underline{\underline{c}}_t \Delta \underline{\underline{\dot{q}}} + \underline{\underline{k}}_t \Delta \underline{\underline{q}} = \Delta \underline{\underline{Q}}(t_k) \quad (7.21)$$

The (7.21) represents a system of  $N$  equations in the  $3N$  unknowns, since, having imposed the equilibrium only at a certain number of time instants, velocities and accelerations can no longer be derived but represent independent unknowns. In order to solve this system, it is necessary to write  $2N$  additional equations in the same unknowns of the problem. Such equations can be written as:

$$\Delta \underline{\underline{q}} = \underline{\underline{\dot{q}}}_k \Delta t + \frac{1}{2} \Delta t^2 \underline{\underline{\ddot{q}}}_k + \beta \Delta t^2 \Delta \underline{\underline{\ddot{q}}} \quad (7.22)$$

$$\Delta \underline{\underline{\dot{q}}} = \underline{\underline{\dot{q}}}_k \Delta t + \gamma \Delta t \Delta \underline{\underline{\ddot{q}}} \quad (7.23)$$

The increment (7.22) and (7.23) are written as a function of  $\Delta \underline{\underline{\dot{q}}}$ , making use of the parameters  $\beta$  and  $\gamma$ . Equation (7.21) completes the system of equations, which can be solved at this point.

The solution in this thesis work is obtained with the constant acceleration Newmark algorithm. This name derives from the fact that a constant acceleration is assumed during the integration step and equal to the average between the values it assumes at the beginning and at the end of the step. This assumption implies that the Newmark parameters assume the following values:  $\gamma = 1/2$  e  $\beta = 1/4$ .

The equation of motion is rewritten in such way that the only unknown is the increment in displacement. To this purpose (7.22) is rewritten by explicating  $\Delta \underline{\underline{\dot{q}}}$ :

$$\Delta \underline{\underline{\ddot{q}}} = \frac{1}{\beta \Delta t^2} \Delta \underline{\underline{q}} - \frac{1}{\beta \Delta t} \underline{\underline{\dot{q}}}_k - \frac{1}{2\beta} \underline{\underline{\ddot{q}}}_k \quad (7.24)$$

Substituting the equation just obtained in (7.23) the velocity increment can be expressed as a function of  $\Delta \underline{\underline{q}}$ :

$$\Delta \underline{\underline{\dot{q}}} = \underline{\underline{\ddot{q}}}_k \Delta t + \frac{\gamma}{\beta \Delta t} \Delta \underline{\underline{q}} - \frac{\gamma}{\beta} \underline{\underline{\dot{q}}}_k - \frac{\gamma}{2\beta} \Delta t \underline{\underline{\ddot{q}}}_k \quad (7.25)$$

At this point the two relations (7.24) and (7.25) which express the increment in velocity and acceleration as a function of the increment in displacement, velocity and acceleration at the beginning of the step, can be replaced in the equation of dynamic equilibrium in the incremental form:

$$\underline{\underline{m}}_t \left[ \frac{1}{\beta \Delta t^2} \Delta \underline{\underline{q}} - \frac{1}{\beta \Delta t} \underline{\underline{\dot{q}}}_k - \frac{1}{2\beta} \underline{\underline{\ddot{q}}}_k \right] + \underline{\underline{c}}_t \left[ \underline{\underline{\ddot{q}}}_k \Delta t + \frac{\gamma}{\beta \Delta t} \Delta \underline{\underline{q}} - \frac{\gamma}{\beta} \underline{\underline{\dot{q}}}_k - \frac{\gamma}{2\beta} \Delta t \underline{\underline{\ddot{q}}}_k \right] + \underline{\underline{k}}_t \Delta \underline{\underline{q}} = \Delta \underline{\underline{Q}}(t_k) \quad (7.26)$$

As it can be observed, the equation (7.26) depends uniquely on the displacement increment  $\Delta \underline{\underline{q}}$ , whereas the velocity and the acceleration at the beginning of the step are known quantity. Reordering this equation, bringing the unknown terms to the LHS and the known ones to the RHS, it can be obtained:

$$\left[ \underline{\underline{m}}_t \frac{1}{\beta \Delta t^2} + \underline{\underline{c}}_t \frac{\gamma}{\beta \Delta t} + \underline{\underline{k}}_t \right] \Delta \underline{q} = \Delta \underline{Q}(t_k) + \underline{\underline{m}}_t \left[ \frac{1}{\beta \Delta t} \dot{\underline{q}}_k + \frac{1}{2\beta} \ddot{\underline{q}}_k \right] + \underline{\underline{c}}_t \left[ -\dot{\underline{q}}_k \Delta t + \frac{\gamma}{\beta} \dot{\underline{q}}_k + \frac{\gamma}{2\beta} \Delta t \ddot{\underline{q}}_k \right] \quad (7.27)$$

The same expression can be expressed in compact form:

$$\underline{\underline{k}}^* \Delta \underline{q} = \Delta \underline{Q}^* \quad (7.28)$$

with:

$$\underline{\underline{k}}^* = \underline{\underline{m}}_t \frac{1}{\beta \Delta t^2} + \underline{\underline{c}}_t \frac{\gamma}{\beta \Delta t} + \underline{\underline{k}}_t \quad (7.29)$$

$$\Delta \underline{Q}^* = \Delta \underline{Q}(t_k) + \underline{\underline{m}}_t \left[ \frac{1}{\beta \Delta t} \dot{\underline{q}}_k + \frac{1}{2\beta} \ddot{\underline{q}}_k \right] + \underline{\underline{c}}_t \left[ -\dot{\underline{q}}_k \Delta t + \frac{\gamma}{\beta} \dot{\underline{q}}_k + \frac{\gamma}{2\beta} \Delta t \ddot{\underline{q}}_k \right] \quad (7.30)$$

It is to be noticed that (7.28) is formally analogous to the equilibrium condition for linear systems in which, however, the coefficient matrix is a modified form of the stiffness matrix and takes into account the mass and damping contributions.

Thanks to (7.28) it is possible to calculate the displacement increments  $\Delta \underline{q}$  which will be added to the displacements obtained at the previous step to obtain the configuration at the current step of the system. Once the displacements are known, it is possible to calculate velocity and acceleration increments using equations (7.24) and (7.25).

## 7.2 Transversal interaction: Matlab code

The transversal interaction in this thesis does not take into account the dynamics of the train. On the structure, forces are applied to the nodes of the tubes, at each time instant, exactly as for the vertical analysis. Unlike the latter, however, the forces are calculated with a MATLAB script, reported in Appendix A-2, built on the models and formulas illustrated in paragraph 5.3, which does not interact with the ANSYS solver. The forces acting are therefore calculated considering the displacements of the masses of the axles, due to hunting and irregularities, and neglecting the tunnel motion. The code parts are illustrated in the following steps.

### *Data entry*

The MATLAB script requires as input data the speed and type of train, to choose between the two defined in chapter 5 (TMV or TAV). The code also automatically collects data on irregularities, by calling the external script "Roughness\_Alignment.m", which generates different irregularities each time an analysis is carried out, guaranteeing their randomness. This script contains the definition of the irregularities only of the alignments of the rail, as explained in chapter 4. It is an extract from the script in Appendix A-1.

### *Property and geometry of the trains*

The code analyses the two trains. By entering the input "1", all the properties of the train at medium speed will be chosen, while with "2" all the properties of the high-speed train will be chosen. The properties that have been inserted are the masses of the axles, the position of the motor wagons and of the passenger wagons, the length of the head wagons and that of the passenger wagons, the distance between the axles and between the bogies, so as to be able to distribute the forces on the axles as close as possible to reality. The radius of the wheels and the conicity are also defined, for the calculation of the wavelengths of the hunting. Finally, the distance of the rails and the maximum rail-wheel clearance are provided for the definition of the hunting amplitude.

### *Hunting*

The wavelength is calculated and the time and space vectors are defined, based on the speed of the train. At this point the hunting accelerations are calculated with the equation (5.31) and multiplied by the mass.

### *Irregularity*

The random irregularities given by "Roughness\_Alignment.m" are derived over time, obtaining the accelerations. Here too, the final accelerations' irregularity are multiplied by the masses, obtaining the time varying forces of each axle.

### *Final forces*

The hunting and irregular forces are superimposed. Then, proceeding with reference to the time and space vectors of the hunting, the irregularities are interpolated in the same points.

At this point the values of the final forces for an axle of a motor wagon and for an axle of a passenger wagon are known. However, on our tunnel there are 40 axles in the case of TMV and 32 axles in the case of TAV. Thus two matrices are created, with a number of rows equal to the number of total axles. In the first matrix all the forces are collected in order of axle. In the other matrix, the times related to each axle are collected, and for each time step. Time 0 will be that in which the first axle gets on the tunnel, while the final time will be that in which the last axle gets off the tunnel. The total travel time therefore depend on the total length of the train and on its speed.

### *Sampling and transformation of the forces*

First of all, the total number of time instants and the time step to be integrated are defined (for this thesis work a constant spatial step of 2 meter has been used). The total number of steps have been chosen so as to capture at least 5 points on a sinusoid of the hunting and avoid aliasing phenomena<sup>[3]</sup>. The minimum number of instants is therefore fixed at 837 instants for a TAV and 1199 instants for a TMV. The time step is obtained by dividing the sinusoid fraction chosen (2 meter) by the train speed.

At this point the forces are sampled. Since the time instants of the analyses do not match the steps with which the force of the axle is defined, the forces are interpolated.

The third and final phase is the transformation of the acting forces. In fact, as for the vertical interaction, also in the transversal one the position of the axle of the wagon can be found in any point of a finite element, and more rarely in its node. To overcome this problem, the loads on the finite element are transformed into actions (forces and moments) on its nodes, using the equations (7.31a ÷ 7.31d) - see Figure 7-2. This operation has the computational cost to consider 2 nodes instead of 1, and 4 actions instead of one force. However, the result is the exact one, and the additional analysis times are marginal.

---

[3] Aliasing: It is the phenomenon for which two different analogic signals can become indistinguishable once sampled. The cause of the phenomenon is the sampling times (or spaces) and it is a serious problem that is reflected directly on the output of the system under examination, altering its truthfulness.



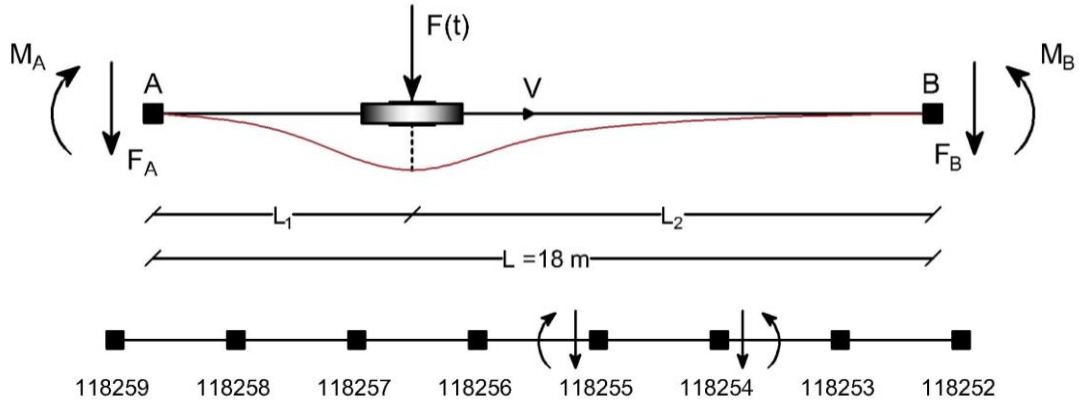


Figure 7-2: Transformation of force into actions on the tube nodes

In Figure 7-2, the actions on the nodes are defined by the equations (7.31a-d), whatever the force  $F(t)$  is, considering the beam clamped:

$$F_A = \frac{F \cdot L_2^2}{L^3} \cdot (3 \cdot L - 2 \cdot L_2) \tag{7.31a}$$

$$F_B = \frac{F \cdot L_1^2}{L^3} \cdot (3 \cdot L - 2 \cdot L_1) \tag{7.31b}$$

$$M_A = \frac{F \cdot L_1 \cdot L_2^2}{L^2} \tag{7.31c}$$

$$M_B = \frac{F \cdot L_1^2 \cdot L_2}{L^2} \tag{7.31d}$$

Therefore, two output matrices are created, namely "carichi\_treno" and "time" respectively. The first contains the actions to be applied to the tunnel and the related node, the second contains the time instant and the number of nodes involved. A series of FOR cycles are carried out to calculate the number of axles present on the tube for each time instant, based on time, and transform the acting forces into actions on the relative nodes of that element. These nodes are stored in each cycle in the matrices mentioned above.

Since not all beams are equally spaced, some IF conditions have been imposed to help with the node count. The default tube to which these actions are applied is the first, with the nodes ranging from 18001 to 18265. If the right tube, 2, were chosen, the nodes would go from 118265 to 118001. The direction of these nodes is decreasing because being the tube on the right, the train travels in the opposite direction.

It must be observed that a beam finite element is 18 meters long, and there can be from one to more axles on the same beam and at the same instant in time. Such overlapping of actions is allowed and always gives exact solutions.

Actions are computed in Newtons and meters.

### *Analysis*

As output, the Matlab script returns two .csv files: "carichi\_treno.csv" and "time.csv". These scripts are saved inside the "Input\Transversal" folder in the Ansys model folders. When the "Train\_Interaction\_Transversal.txt" text file on Ansys is started, the two .csv files are read from the "time\_history\_transversal.txt" text file and their forces are attributed to the nodes for each time step, which is solved with a nonlinear dynamic analysis by the solver.

The results of the displacements of the nodes, as well as the axial forces of the anchor bars, for each time instant, are automatically saved in the "Output\Transversal" folder and subsequently processed. The data obtained from the transversal analyses are reported in chapter 9.

#### **7.2.1 Script for two trains**

To conduct analysis with two trains, which run through the two tubes and with different speeds, the previous script is no longer sufficient. The output .csv files remains with the same setting, the number of forces, the nodes involved and possibly, if deemed necessary, the integration steps increase. To obtain the actions for this case, a script identical and parallel to the previous one is started: "Hunting\_Twotrains.m" (Appendix A-2). This recalls the previous script which defines the vectors of forces and times for the train running in tunnel 1 and then creates new vectors for the train running in tunnel 2. The reorganization and transformation of all the forces in the various nodes of the tubes takes place simultaneously and for sequential time instants, until the last force of the last train has been associated with a node and a time step.

The analysis is then conducted in the same way as in the case with a single train.

## VERTICAL INTERACTION

This chapter describes the time histories of the forces induced by trains, calculated in the analyses, and the related responses of the tunnel in terms of displacements and actions, with graphs representing the histories of nodes and anchor bars, as well as the displacements of the carriages of the wagons.

Two nodes are used for the evaluation of the displacements of the tunnel: node 18133 and 18120. The first node represents the exact half of the tunnel, 2340 m from the origin, and coincides with a transverse connection (higher stiffness), representing in this way the response of the whole tunnel system. The second node is 234 m offset from the centerline towards the Calabrian coast: 2106 m from the system origin. This node represents the midpoint of a 468 m long tube element, between two transversal connection, near the center of the tunnel. See Figure 8-1 for the location of the two nodes.

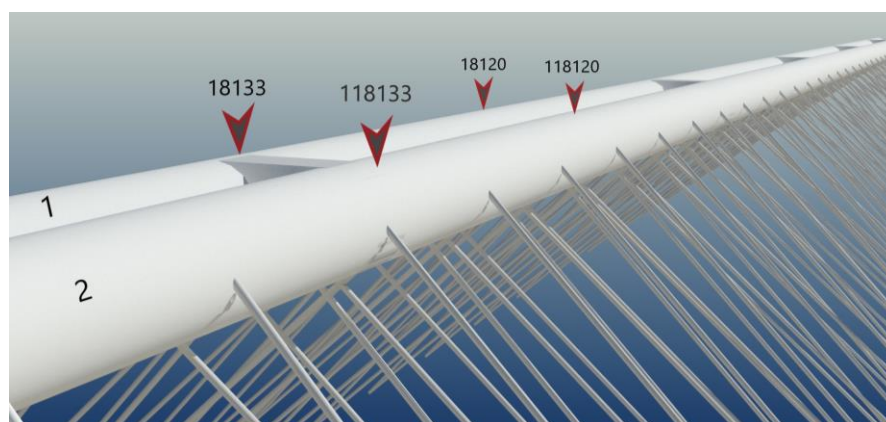


*Figure 8-1: Position of the reference nodes*

The axial forces of the anchors are taken at the base of the anchor bars, near the foundations, in correspondence with the elements defined in Table 3-8.

The analyses in total are 3, of which 2 with single trains running only in tube 1 (direction from Calabria to Sicily).

Each wagon has its own movements and forces. Since representing the displacements and the forces exchanged between all the DOF of all the wagons is time-consuming and unnecessary, the forces and displacements of the carriage placed halfway of the trains are reported: coach 5 and 4 for medium and high speed trains, respectively. The choice focuses on these carriages because the deformation of the tunnel is maximum in the middle of the train, thus inducing greater oscillations and forces on the wagon.

Each analysis has an additional 10 s to the tunnel crossing time, illustrating the free oscillations of the structure when the train has exited the tube. The total travel times of the train are not complete because the INTER 7.0 code needs to start all the wagons already in a row on the tunnel, occupying a length of 220 meters for the TMV and 174 meters for the TAV. The time that the train would need to reach this configuration is absent in the analyses reported, but is used by the code, together with the first 500 meters of roughness, to delete the initial condition of the train. The amount of time instants less depend on the speed at which the train runs (this time is equal to the time lag between the first axle and the last axle). All the times and data relating to the analysis are reported for each interaction.

For each analysis two interactions were run, the first with structural damping of the tunnel at 1% and the second with damping at 6%. The difference in terms of displacements and acting forces is irrelevant. The recorded displacements have a difference between the two cases of the order of one centesimal of a millimetre, completely negligible for this type of bridge. Therefore, only the analyses with damping at 6% have been illustrated here.

As already explained in the last paragraph of chapter 5, the analyses with the possible critical speeds induced by roughness were conducted but not reported here. In fact, no particular increment in the displacements of the tunnel was detected for any speed. What was observed instead is a predominant deformation caused by the weight of the train, and negligible undulations, which increase their amplitude and wavelength in proportion with the speed and mass of the train. Two analyses are therefore reported, one per convoy, with the maximum permissible speeds, being the most critical scenarios for the train in use.

The third analysis is conducted to evaluate the actions induced in case that two high-speed trains run in the two opposite directions of the tunnels.

All the analyses were carried out with a constant spatial step, equal to 2 meters, which implies different time steps for each analysis depending on the speed of the train. The tolerance for the convergence was set at 0,01 for all the analyses. The error reached lower values in all analyses with a single iteration.

## 8.1 Medium Speed Train – TMV

The maximum speed of the TMV is 160 km/h, that correspond to 44,44 m/s. The total number of time steps used for the analysis is 2563, with a time step of 0,045 s, of which 214 final steps represent 10 s of free oscillations of the tunnel. The train would take a total of 110,62 s to cross the tunnel. However, in INTER 7.0 the actual travel time of the train is 105,70 s, being the first axle displaced of 220,2 m from the first point of the tunnel. 5,33 s are the offset between the first and last axle. The data of the analysis are shown in Table 8-1.

Table 8-1: Analysis data, TMV 160 km/h

Spatial step [m]	Time step [s]	N° steps	Train Speed [m/s]
2	0,045	2563	44,44

The total analysis time is 8 hours, with convergence achieved in one iteration. The convergence it is not equal for all the wagons and all the contact points. The error tends to diminish a little faster for the first and last contact points of the train. Thus, the extremities of the train tends to have an higher accuracy in less time. This is most likely due to the fact that the maximum displacement of the tunnel, i.e. the maximum dynamic forces in the wagons, are always in the middle of the train, being the weight of the train a distributed load. With respect to the middle coach the error difference has however just an order of difference, as reported in Table 8-2.

Table 8-2: Errors TMV160 km/h

Iteration	Wagon	Contact point			
		First	Second	Third	Fourth
0	1	0,97006	0,97008	0,97005	0,97007
	5	0,97013	0,97014	0,97014	0,97013
	10	0,97005	0,97005	0,97009	0,97009
1	1	8,79E-06	9,48E-06	1,11E-05	1,10E-05
	5	1,79E-05	1,87E-05	1,63E-05	1,70E-05
	10	2,05E-06	1,71E-06	3,04E-06	3,36E-06

Representing all the errors of all the wagons in a graph, Figure 8-2, the difference among the errors is imperceptible, as shown in figure below.

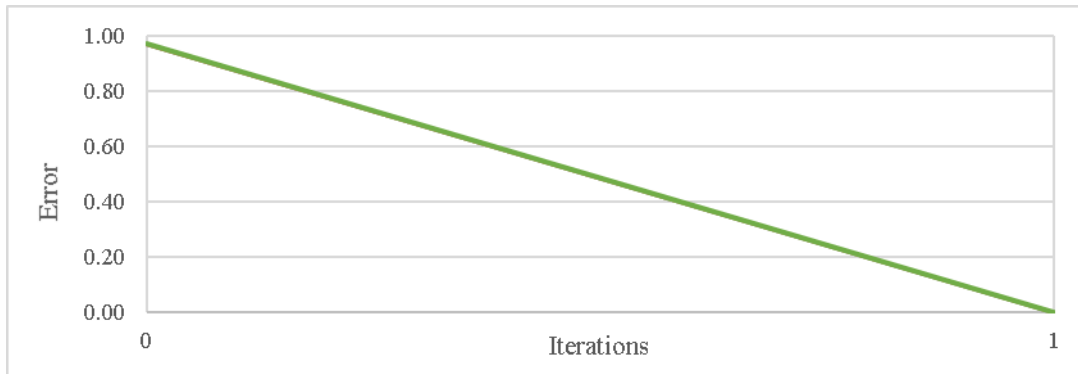


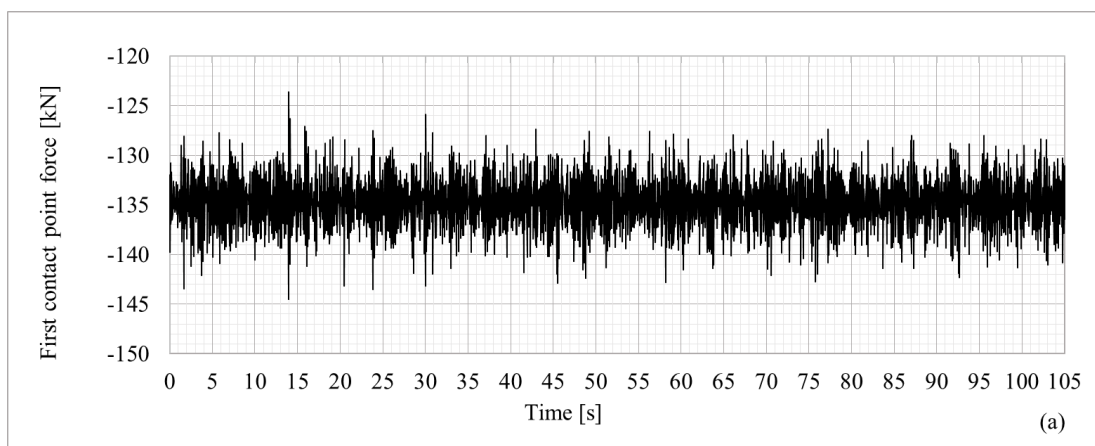
Figure 8-2: Convergence of the errors - TMV 160 km/h

### Train response

The train does not present appreciable differences in the wagons responses. Hence, only the results of the fifth coach, the most excited, are reported.

In Figure 8-3a the forces of the first contact point (front wheel of the 5<sup>th</sup> coach) shared between the train and the tunnel are shown. They represent the static force caused by the weight of the wagon on an axle, plus and minus the dynamic forces caused by the motion of the wagon, the irregularities and the motion of the tunnel. The static load applied on an axle for a passenger wagon is equal to - 134,725 kN, and it corresponds to the mean value of the graph. Only the forces of the first contact point are reported, being almost equal to the others three contact points.

Together with these, the roughness profile actually sampled with a spatial pitch of two meters is reported in Figure 8-3b. It is observed that the roughness profile is the main source of excitation for the train, with respect to the displacements of the tunnel.



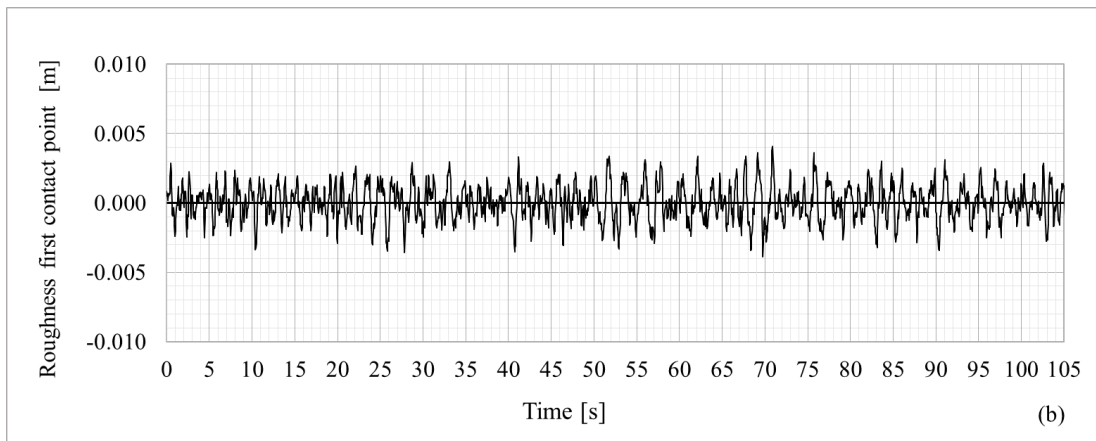
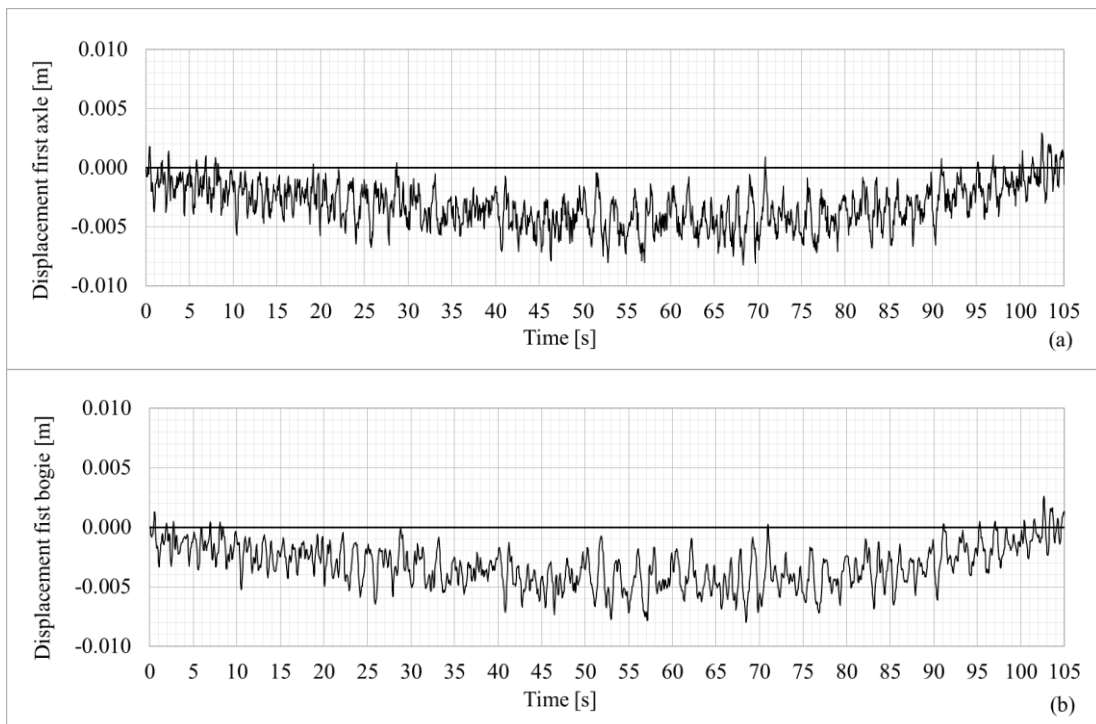
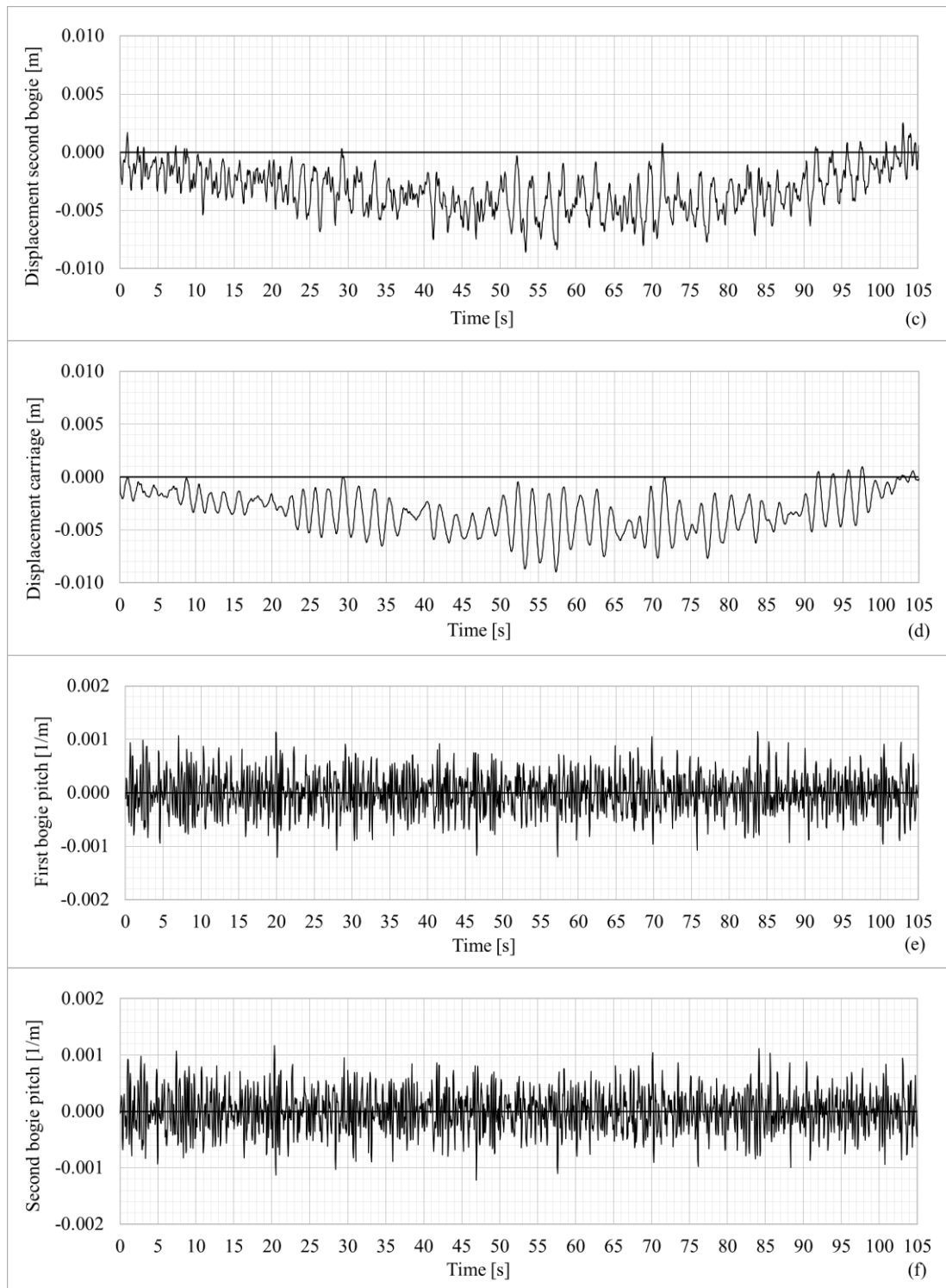


Figure 8-3: 5<sup>th</sup> wagon - TMV 160 km/h: (a) First contact point forces; (b) irregularities

These forces are the final ones, at the last iteration, and correspond to the forces induced by the train to the tunnel. Therefore, associated to these forces there is the motion of the ten DOFs of the wagon. In Figures 8-4 (a to g) are shown the vertical displacements of the first wheel, of the two bogies, of the carriage, and the pitch movements of the bogies and the carriage, respectively.







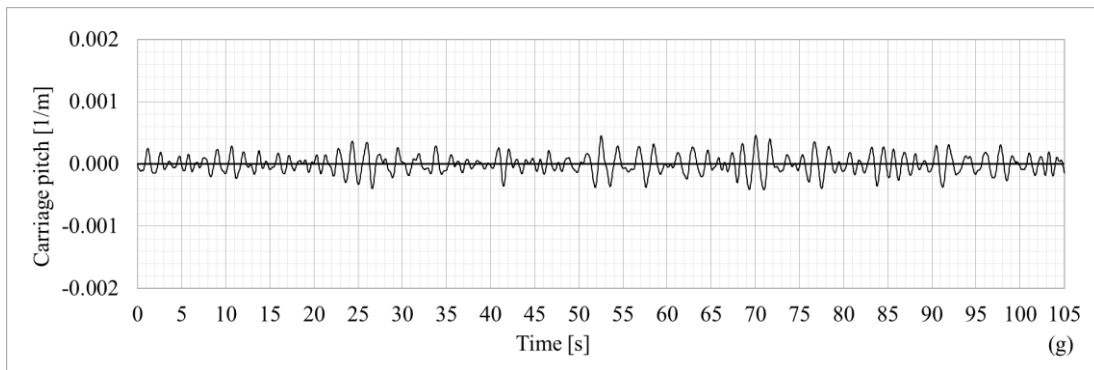


Figure 8-4: Motion of DOFs - 5<sup>th</sup> wagon - TMV 160 km/h: (a) Displacement, first axle; (b) Displacement, first bogie; (c) Displacement, second bogie; (d) Displacement, carriage; (e) First bogie pitch; (f) Second bogie pitch; (g) Carriage pitch

In all the vertical displacement (DOFs from 1 to 7) the mean value it is not completely around zero. This is caused by the tunnel vertical downward deformation, as a consequence of the train load. In fact as the train approaches to the midpoint of the SFT the displacements increases, decreasing as the train approaches to the coast. The displacements of the bogies, as well as its rotations, are almost comparable between the two. Their amplitude are also comparable to those of the wheelset, but it can be noticed that are damped. In fact the lower and faster oscillations disappear for the bogies. The same can be noticed with more evidence for the carriage. This was expected and desired, and demonstrate the reliability of the code; in fact, the development of the connections between carriages and the rest of the bodies in a train is such to have this response, to keep an high comfort for the passengers. To validate the code results, the graph of the displacements of the seventh DOF has been converted from time domain to frequency domain, through a Fourier transform in Matlab.

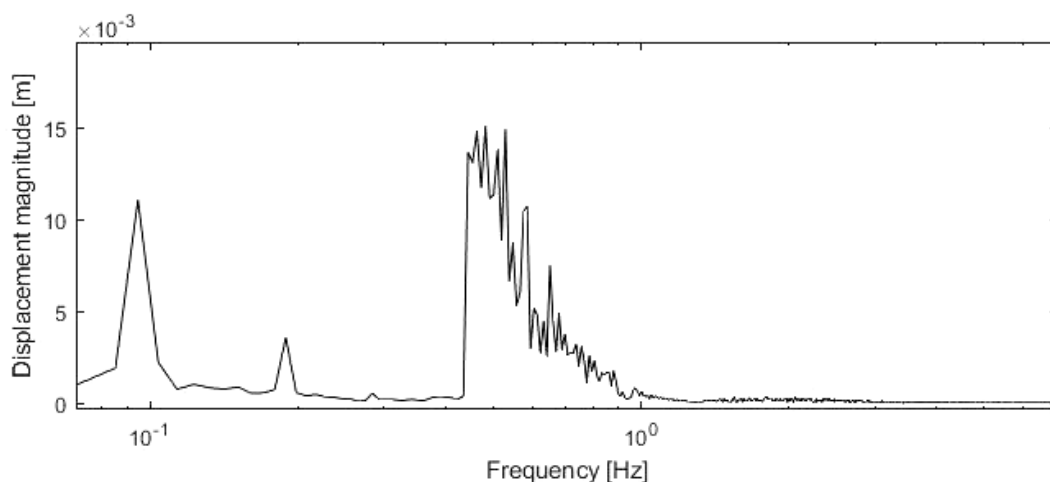


Figure 8-5: Carriage frequency response - 5<sup>th</sup> wagon - TMV 160 km/h

The graph, in Figure 8-5, is clearly showing that the vertical motion of the carriage of the fifth coach (passenger wagon) is exciting the first and third natural frequencies of Table 5-2, in which the prevailing movement of the mode is that of the carriage. The higher frequencies are always frequencies corresponding to the wagon, but that does not involve predominantly the carriage.

An investigation is performed on the first peak of the graph, with a very low frequency. In the tunnel, every 468 m there's a rigid connection between the two tubes, that increase the stiffness of the tunnel. Considering all the 11 connections, at the speed of 44,444 m/s, the train sees every 10,53 s a rigid connection, that is 0,095 Hz, the same frequency of the graph. Thus what is happening is that the train, running in the rail, feels a lower deformation of the tunnel every 10 s and this influence his motion. Also this detail was expected and confirms the reliability of the results.

### *Structural response*

The structural response is represented in terms of deformation of the central nodes of the tunnel and of forces applied in the stays.

The deformation of the tunnel is characterized, for each node of the tube on which the train runs, by two types of displacement. The first one is the deformation caused by the distributed dead load of the train. The second one, on the other hand, is due to the oscillations induced by the motion and speed of the train.

The first displacement is larger at the centre of the train, so it moves as the train moves, and increases its amplitude as it approaches the tunnel midpoint. At node 18133, this displacement is equal to  $-3,86$  mm. Its maximum amplitude, however, is reached at the nodes in the middle between two connections, and close to the halfway of the tunnel. Thus, in the node 18120 the deformation is of  $-5$  mm.

The second type of deformation are the oscillations induced by the passage of the train, and they begin to be visually present in the instant the train leaves the node. These oscillations for the medium-speed train running at 160 km/h are equal to  $\pm 0,14$  mm for node 18133 and  $\pm 0,15$  mm for node 18120. The order of magnitude of a decimal of a millimetre for the transit of vehicles or wagons is completely negligible. Even for the tunnel, an oscillation of this magnitude is of little importance.

Figure 8-6 shows the displacements of node 18133 (the tunnel midpoint), in which these two types of displacements can be seen.

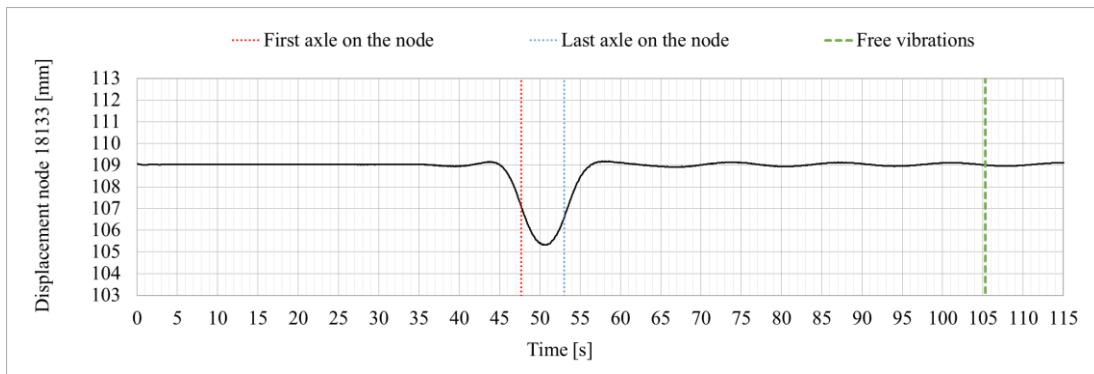


Figure 8-6: Vertical displacement node 18133 – TMV 160 km/h

28 stays are selected along the entire tunnel, in accordance with those selected by Palamà (2017). The variations of the forces in the stays are shown in the next Table 8-3. The train runs in tube 1, reducing the tension of the stays. Therefore, the forces variations between tube 1 and 2 differ since there are only small variations in the second tube, induced by the vibrations of the train passing through tube 1.

Table 8-3: Axial force on the anchorages – TMV 160 km/h passing on tube 1

Anchor bar	Static axial force [kN]	Static stress [MPa]	Damping 6 %
			Load variation [kN]
Tube 2			
1	+10521	24,76	± 9
2	+13944	32,81	± 22
3	+12824	33,31	± 23
4	+12866	33,42	± 19
5	+13890	36,08	± 24
6	+14765	38,35	± 34
7	+13279	37,83	± 17
8	+13050	37,18	± 21
9	+13606	38,76	± 20
10	+14656	38,07	± 41
11	+13680	35,53	± 18
12	+12921	33,56	± 20
13	+13350	31,41	± 28
14	+10035	23,61	± 12
Tube 1			
15	+10521	24,76	– 591
16	+15232	39,56	– 640
17	+12824	33,31	– 629
18	+12837	33,34	– 609
19	+13890	36,08	– 591
20	+14078	40,11	– 541
21	+13279	37,83	– 593

<b>22</b>	+13132	37,41	- 593
<b>23</b>	+13606	38,76	- 587
<b>24</b>	+13978	39,82	- 568
<b>25</b>	+13680	35,53	- 589
<b>26</b>	+13049	33,89	- 616
<b>27</b>	+13350	31,41	- 683
<b>28</b>	+10035	23,61	- 540

In tube 2 the drop in tension is not evident as for tube 1 because the two tubes are anchored separately. The passage of the train, with its own weight, loads only the beam on which it runs, and only in the instant in which the train is above the stay of interest. This last aspect can be observed by looking the time histories of stays in Figure 8-7 (a to c).

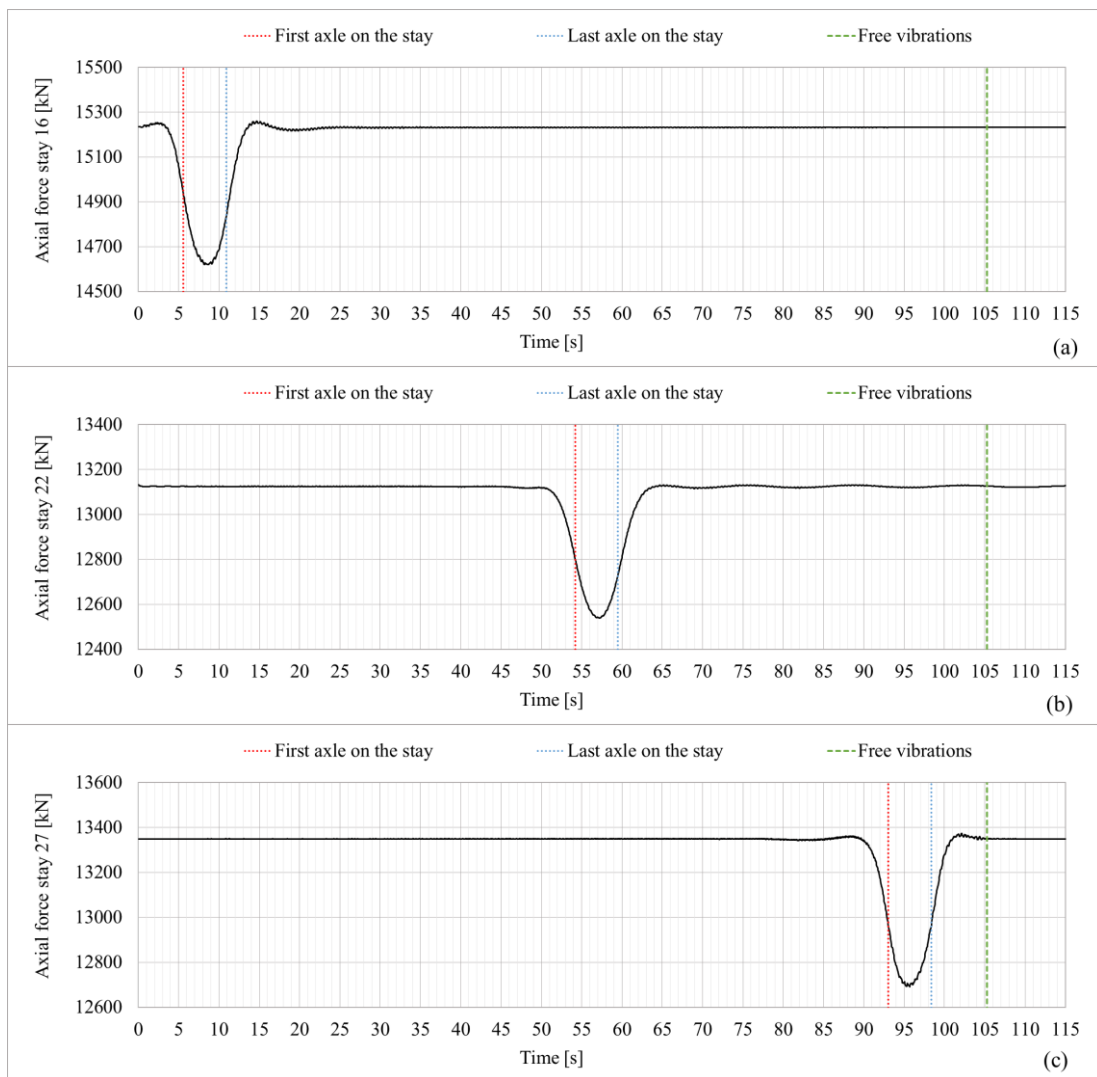


Figure 8-7: TMV 160 km/h - Axial force in stay: (a) n°16; (b) n° 22; (c) n° 27

It can be seen from the stories of the three previous stays that the free oscillations for the stays at the beginning and end of the tunnel quickly fade away. On the contrary, the oscillations in the centre continue, showing that the tunnel in the centre continues to oscillate for a few more seconds.

In any case, the results obtained do not significantly affect the tunnel or the medium-speed train that travels at its maximum speed of 160 km/h.

## 8.2 High Speed Train – TAV

The maximum speed of the TAV is 300 km/h, which corresponds to 83,33 m/s. The total number of time steps used for the analysis is 2757, with a time step of 0,024 s, of which 406 final steps are devoted to represent 10 s of free vibrations. The train would take a total of 58,51 s to cross the tunnel. However, in INTER 7.0 the actual travel time of the train is 56,42 s, being the first axis set at 174,3 m from the first point of the tunnel. 2,33 s is the offset between the first and last axle. The data of the analysis are shown in Table 8-4.

Table 8-4: Analysis data TAV 300 km/h

Spatial step [m]	Time step [s]	N° steps	Train Speed [m/s]
2	0,024	2757	83,3333

The total analysis time is 8 hours, with convergence achieved in one iteration. As for the TMV, the convergence is not equal for all the wagons and all the contact points. The error (Table 8-5) tends to diminish a little faster for the lasts contact points of the train. Thus, the extremities of the train tends to have a higher accuracy in less time.

Table 8-5: Errors TAV300 km/h

Iteration	Wagon	Contact point			
		First	Second	Third	Fourth
0	1	0,97098	0,97132	0,97092	0,97130
	4	0,97088	0,97121	0,97095	0,97128
	8	0,97097	0,97118	0,97098	0,97128
1	1	2,37E-05	2,51E-05	3,08E-05	3,06E-05
	4	3,76E-05	3,74E-05	3,64E-05	3,62E-05
	8	7,71E-06	6,54E-06	6,08E-06	5,36E-06

However, representing all the errors of all the wagons in a graph, the difference among the errors is imperceptible, as shown in Figure 8-8.

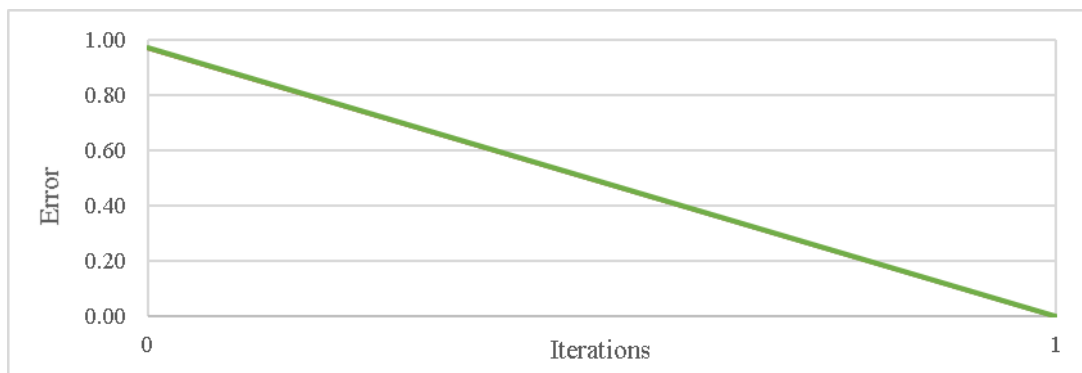


Figure 8-8: Convergence of the errors - TAV 300 km/h

### Train response

The train does not present appreciable differences between the wagons responses; only the results of the fourth coach, the most excited, are reported.

In Figure 8-9a the forces of the first contact point (front wheel of the 4<sup>th</sup> coach) shared between the train and the tunnel are shown. They represent the static force caused by the weight of the wagon on an axle, plus and minus the dynamic forces caused by the motion of the wagon, the irregularities and the motion of the tunnel. The static load applied on an axle for a passenger wagon is equal to - 121,497 kN, and it corresponds to the mean value of the graph. Only the forces of the first contact point are reported, being almost equal to those of the others three contact points.

Together with these, the roughness profile (Figure 8-9b) sampled with a spatial pitch of two meters is shown. It is observed that the roughness profile is the main source of excitation for the train, with respect to the tunnel displacements.

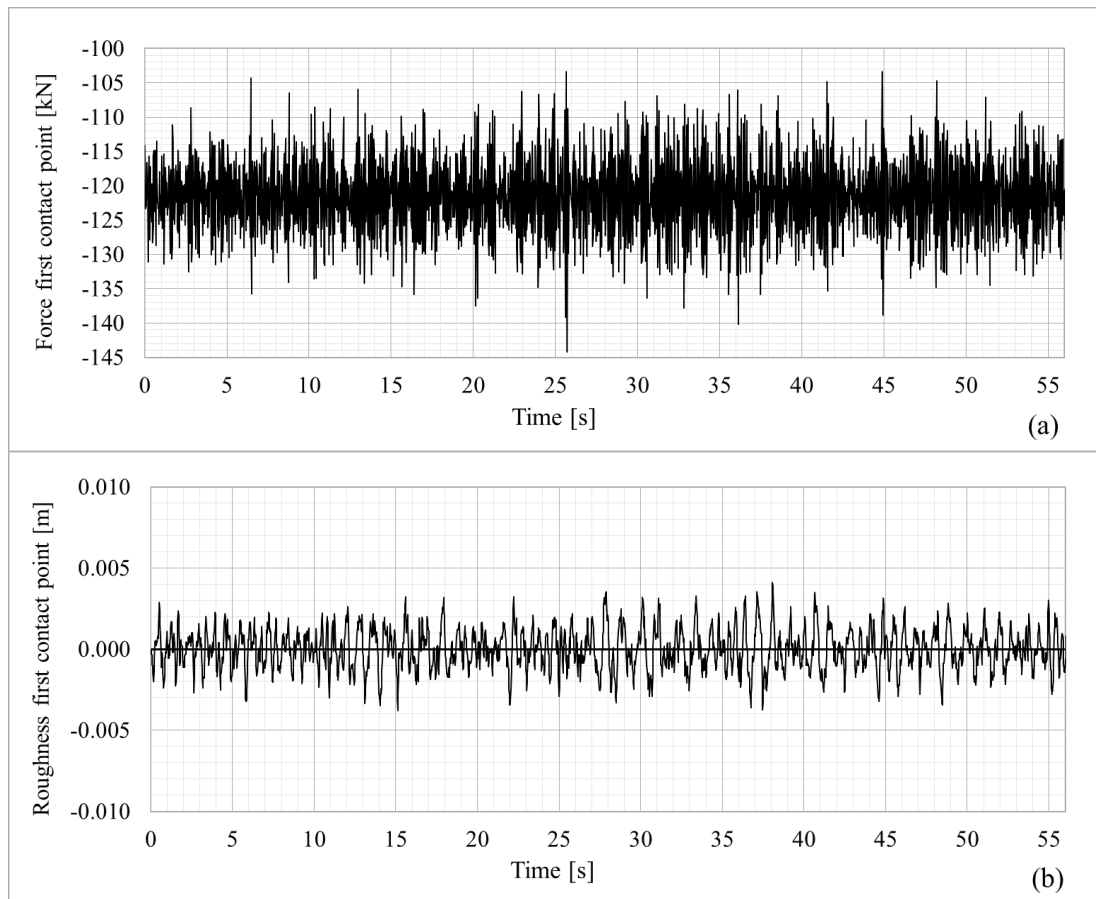
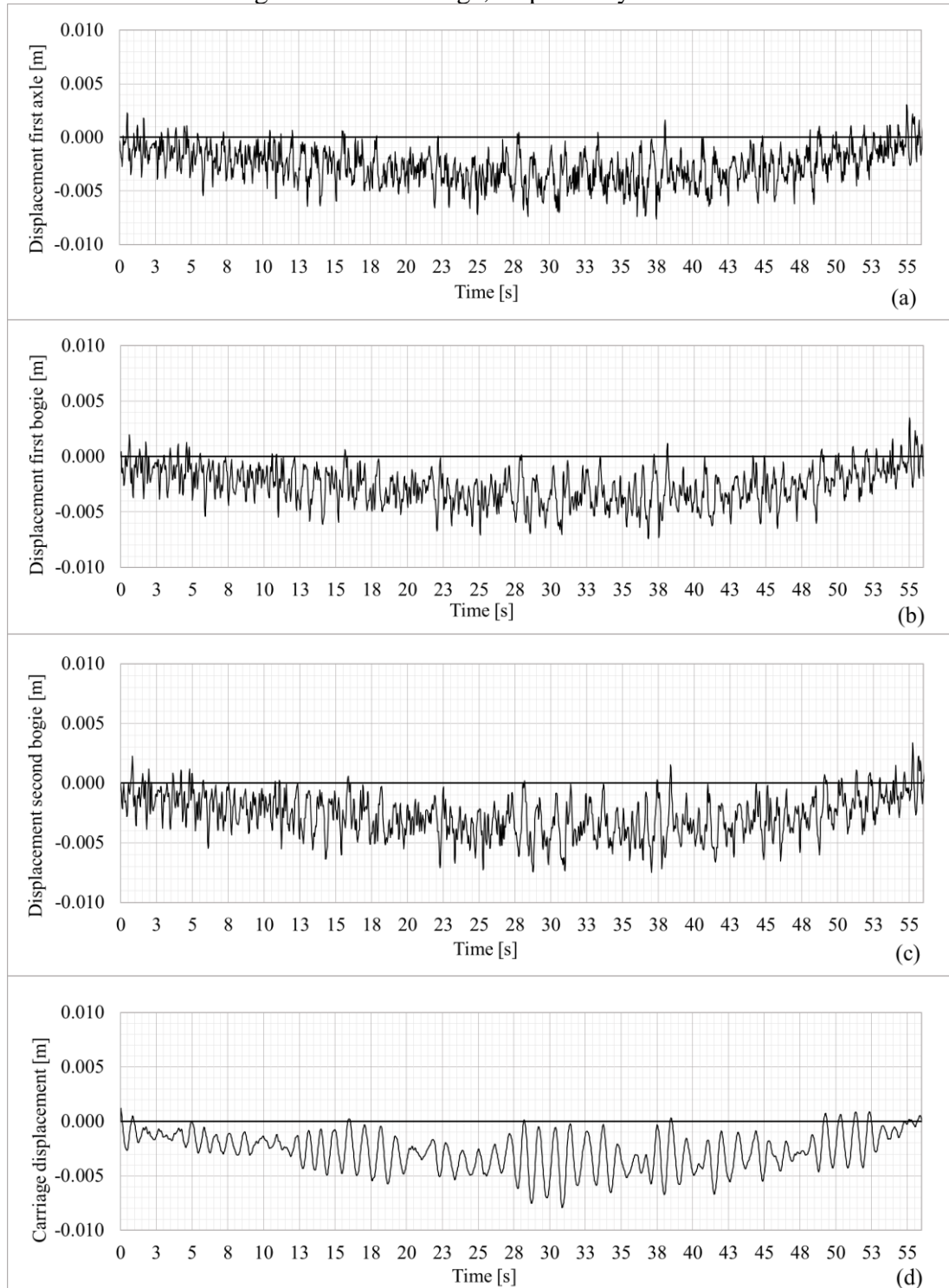


Figure 8-9: 4<sup>th</sup> wagon - TAV 300 km/h: (a) First contact point forces; (b) irregularities

As expected, with the increment of the speed the dynamic forces of the contact points increase, even though the roughness is the same. These forces are associated to the motion of the ten DOFs of the wagon. Figure 8-10 (a to g) shows the vertical

displacements of the first wheel, of the two bogies, of the carriage, and the pitch movements of the bogies and the carriage, respectively.





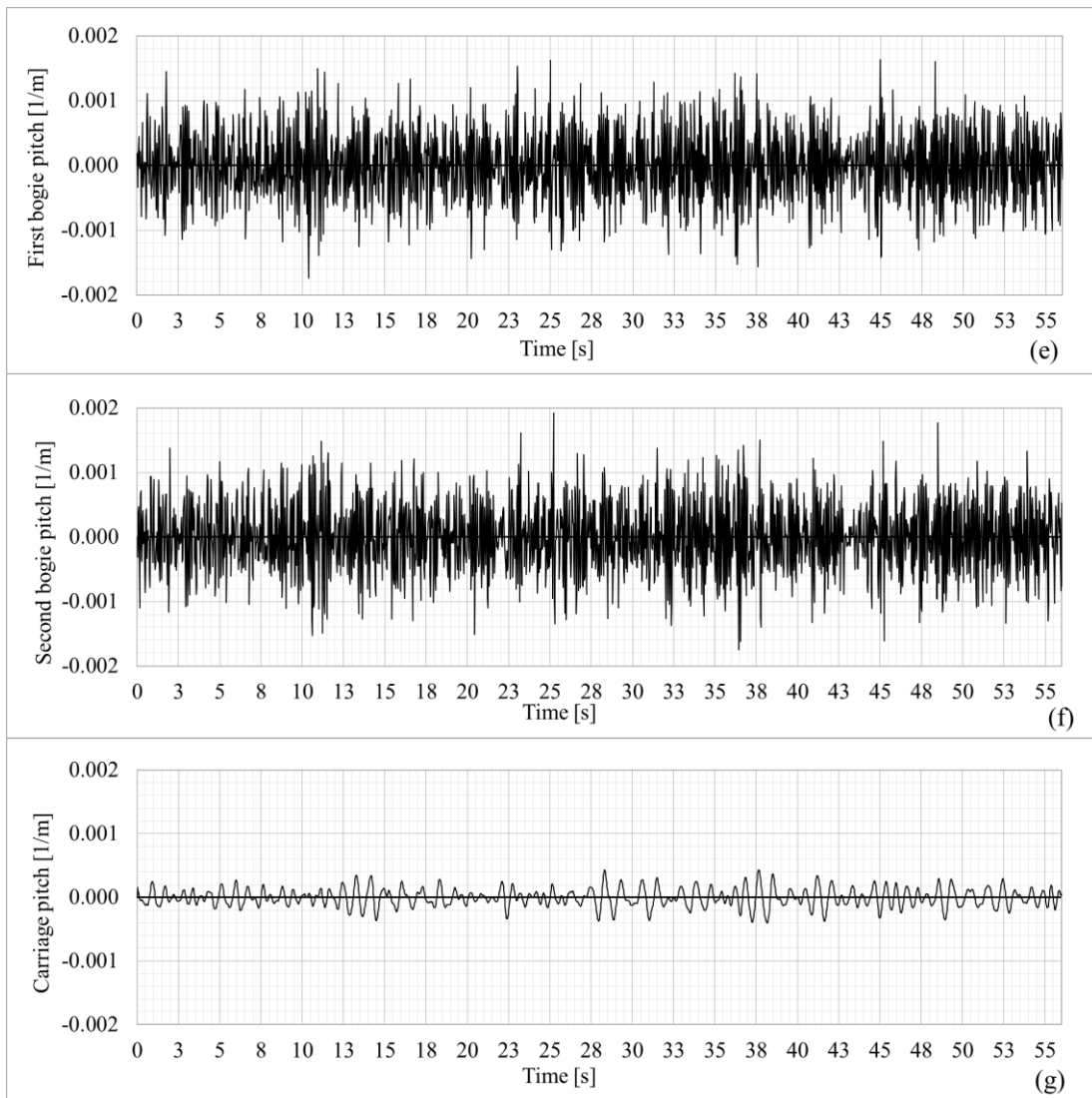


Figure 8-10: Motion of DOFs - 4<sup>th</sup> wagon - TAV 300 km/h: (a) Displacement, first axle; (b) Displacement, first bogie; (c) Displacement, second bogie; (d) Displacement, carriage; (e) First bogie pitch; (f) Second bogie pitch; (g) Carriage pitch

The displacements of the bogies, as well as their rotations, are almost comparable between the two. Their amplitude are also comparable to those of the wheelset, but it can be noticed that are damped. As for the TMV, the lower and faster oscillations disappear for the bogies. The same it can be noticed with more evidence for the carriage. This demonstrates the reliability of the code.

To validate the code results also for the TAV, the graph of the displacements of the seventh DOF has been converted from time domain to frequency domain, through a Fourier transform in Matlab.

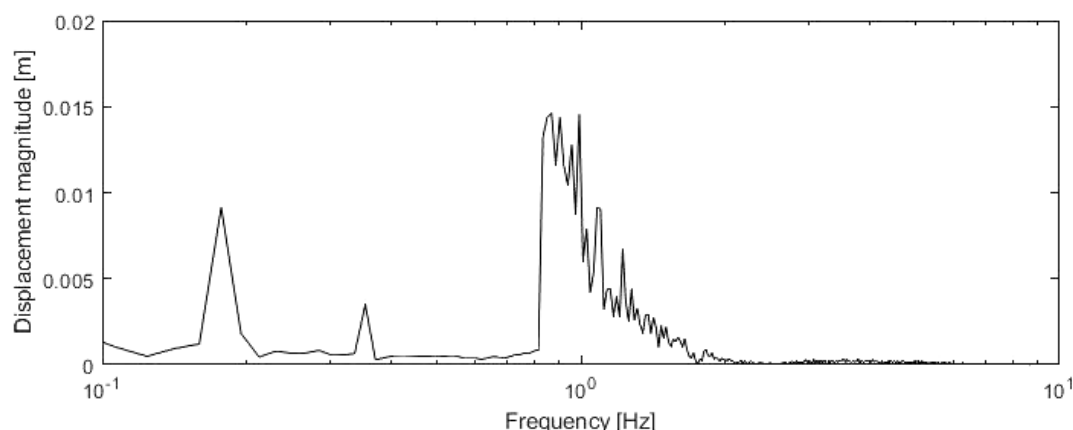


Figure 8-11: Carriage frequency response - 4<sup>th</sup> wagon - TAV 300 km/h

The graph, in Figure 8-11, is clearly showing that the vertical motion of the carriage of the fourth coach (passenger wagon) is exciting the first and third natural frequencies of Table 5-6, in which the prevailing motion of the mode is that of the carriage. The same first and third modes were excited in the TMV. The higher frequencies are frequencies corresponding to the wagon, but that does not involve predominantly the carriage.

As for the TMV, the lower frequencies are associated to displacements of the tunnel. At the speed of 83,333 m/s, the train sees every 5,616 s a rigid connection, that is 0,178 Hz, the same frequency of the graph.

These aspects confirm the reliability of the results also for the TAV.

### Structural response

The response of the tunnel changes with the change of train or speed only in terms of maximum amplitudes of displacements and of the minimum axial forces. In fact, the high-speed train is composed of 8 coaches, each of which weighs 13,228 kN less than the TMV wagons, per axle, for a total of 423,296 kN on eight wagons. Moreover the TAV has other 1077,8 kN less than the TMV for the two absent wagons. There is therefore a total decrement of 1,5 MN, which inevitably leads to a decrement in the actions acting on the structure with respect to the TMV, even though the dynamic actions are increased of 10 kN per axle with the increase in speed.

In the node 18133 the vertical displacement is equal to  $-3,18$  mm. The maximum displacement, however, is still present in the nodes placed in the middle between two rigid links, and close to the midpoint of the tunnel. Node 18120 has a vertical displacement of  $-4,13$  mm. About a millimeter less than the TMV.

The oscillations induced by the passage of the high-speed train running at 300 km/h are equal to  $\pm 0,09$  mm for node 18133 and  $\pm 0,10$  mm for node 18120, a bit lower than those of the TMV at 160 km/h. The order of magnitude of a decimal of a millimeter for the transit of vehicles or wagons is completely negligible. Also for the tunnel, an oscillation of this magnitude is of little influence.

It is therefore apparent that both the increment in mass and speed of the train have a direct proportionality with the increment in vertical displacement and oscillations of the tunnel. In particular, the mass has a significant influence, whereas speed has a lower influence.

The Figure 8-12 shows the displacements of node 18133.

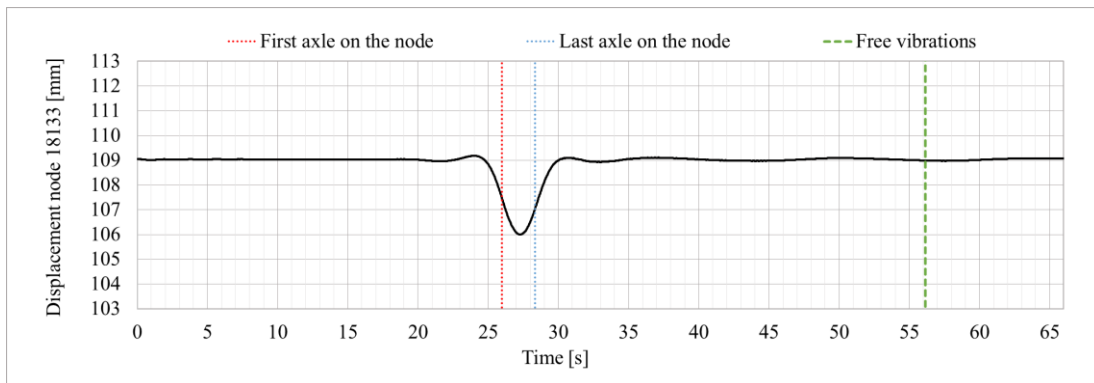


Figure 8-12: Vertical displacement node 18133 – TAV 300 km/h

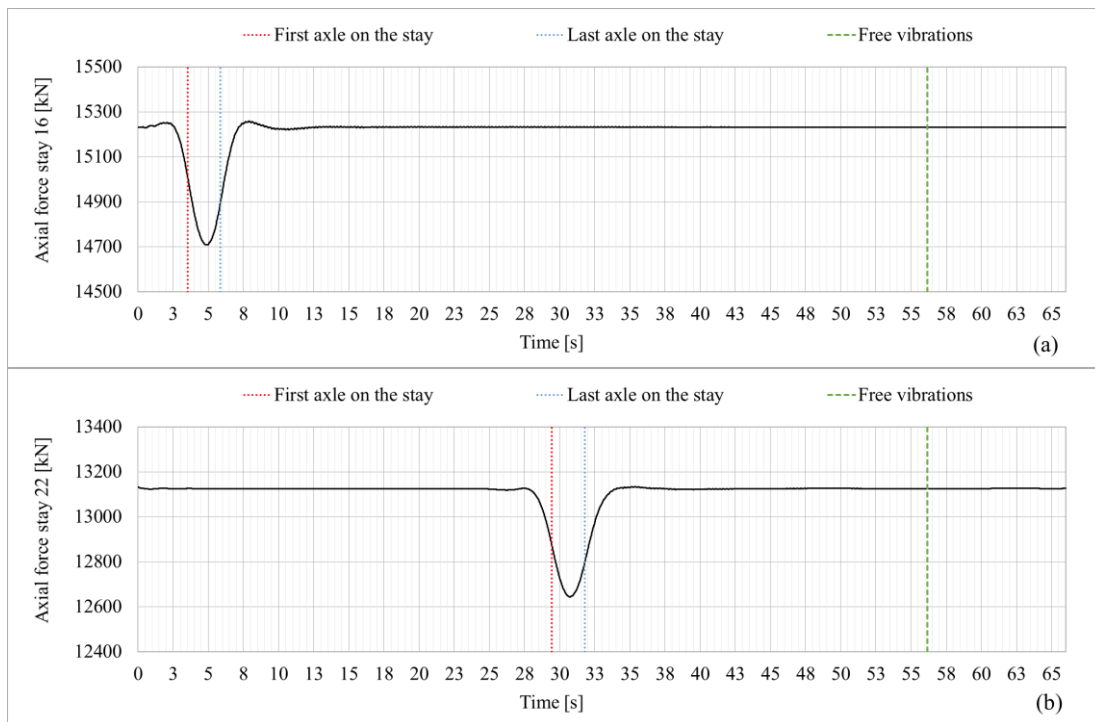
The variations of the forces in the stays are shown in the next Table 8-6. Also in this analysis the force variations between tube 1 and 2 differ since there are only small variations in the second tube, induced by the vibrations of the train passing through tube 1.

Table 8-6: Axial force on the anchorages – TAV 300 km/h passing in tube 1

Anchor bar	Static axial force [kN]	Static stress [MPa]	Damping 6 %
			Load variation [kN]
Tube 2			
1	+10521	24,76	± 7
2	+13944	32,81	± 19
3	+12824	33,31	± 20
4	+12866	33,42	± 17
5	+13890	36,08	± 22
6	+14765	38,35	± 31
7	+13279	37,83	± 14
8	+13050	37,18	± 17
9	+13606	38,76	± 19
10	+14656	38,07	± 35
11	+13680	35,53	± 15
12	+12921	33,56	± 17
13	+13350	31,41	± 23
14	+10035	23,61	± 9

Tube 1			
15	+10521	24,76	– 532
16	+15232	39,56	– 550
17	+12824	33,31	– 531
18	+12837	33,34	– 505
19	+13890	36,08	– 490
20	+14078	40,11	– 452
21	+13279	37,83	– 492
22	+13132	37,41	– 490
23	+13606	38,76	– 484
24	+13978	39,82	– 469
25	+13680	35,53	– 492
26	+13049	33,89	– 513
27	+13350	31,41	– 568
28	+10035	23,61	– 472

In tube 2 the drop in tension is not evident as for tube 1 because the two tubes are anchored separately. The passage of the train stresses, with its own weight, only the beam on which it runs, and only in the instant in which the train is above the stay of interest. This last aspect can be observed by looking the time histories of stays in Figure 8-13 (a to c).



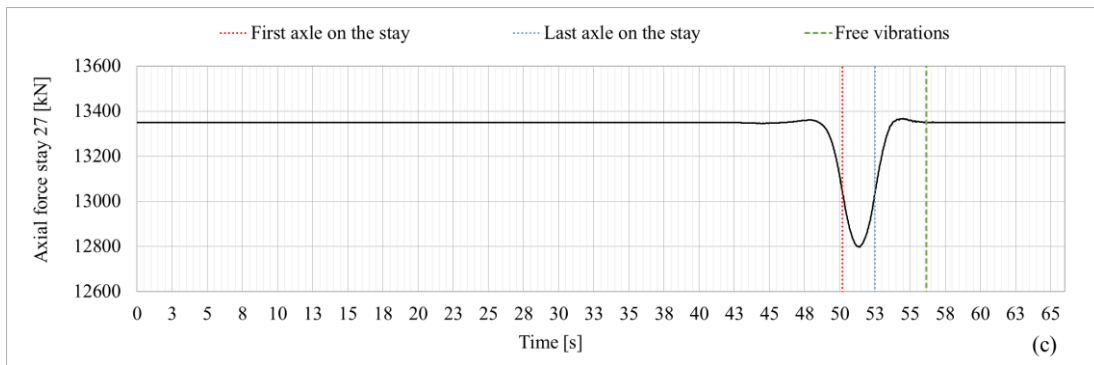


Figure 8-13: TAV 300 km/h - Axial force in stay: (a) n°16; (b) n° 22; (c) n° 27

It can be seen from the stories of the three previous stays that the free oscillations quickly fade away.

Anyway, also in the case of TAV, all the results obtained do not significantly affect the tunnel or the high-speed train that travels at its maximum speed of 300 km/h.

### 8.3 Particular case: Two TAVs 300 km/h

The question arises whether the results change, if instead of just one train crossing the tunnel, there were two high-speed trains traveling in opposite directions through the tunnel at maximum speed, thus doubling the mass. On the Italian territory the railways allow a maximum speed of 300 km/h. This speed is therefore applied to the case study of the submerged tunnel of Messina.

Since the tunnel has the tubes anchored individually to the seabed, it is expected that adding a second train, on the tube so far left empty, will not have a significant effect on the results of the first tube. To demonstrate this, the axial forces of the stays in tube 2 in all the previous cases can be analyzed.

Not all the displacements of the DOFs of the convoy are reported in this interaction, since they are comparable to those of the single TAV at 300 km/h, having maintained the same roughness.

The total number of time instants used for the analysis remained 2757, with a time step of 0,024 s, of which 406 final steps were devoted to represent 10 s of free oscillation of the tunnel. The train would take a total of 58,51 s to travel through the tunnel. However, in INTER 7.0 the actual travel time of the train is 56,42 s, of which 2,33 s are offset between the first and last axle. The two trains start together from their respective positions at the beginning of the two pipes, so the total time remains unchanged. The data of the analysis are shown in Table 8-7.

Table 8-7: Analysis data – Two TAVs 300 km/h

Spatial step [m]	Time step [s]	N° steps	Train Speed [m/s]
2	0,024	2757	83,3333

The total analysis time is 8 hours, with convergence achieved in one iteration and errors with the same order of the single TAV at 300 km/h.

#### *Train response*

In order to evaluate the effects of an additional train on the second tube, the responses of the same wagon of the previous interaction, i.e. the fourth wagon of the train running on tube 1, are analysed, to compare the differences.

Figure 8-14 shows the forces of the first contact point (of the 4th coach) shared between the train and the, which also for this case are similar to those of the other three contact points.

As expected, the dynamic forces of the contact points did not increase with respect to the case of a single TAV that travels at the same speed. Having maintained the same roughness profile, the history of forces is practically identical to that of the previous case, highlighting that each tube responds individually, without significantly affecting the adjacent tube.

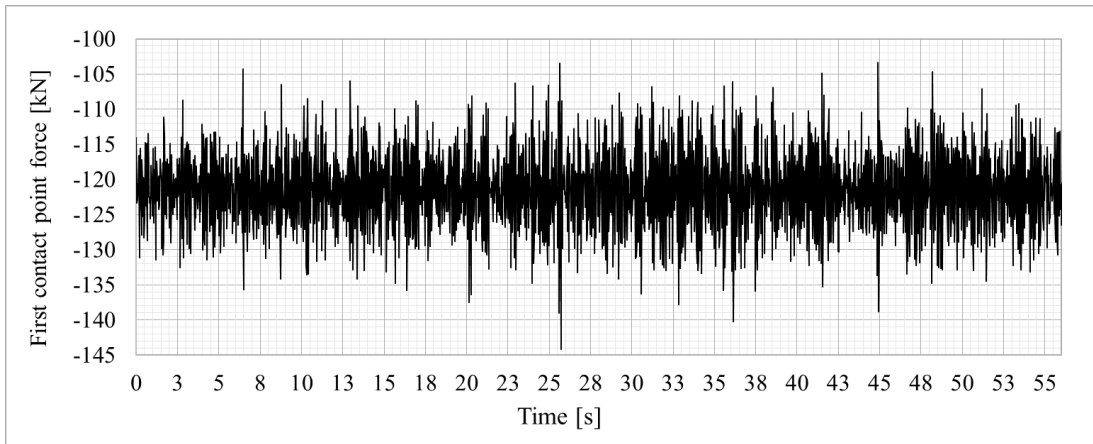


Figure 8-14: First contact point forces - 4<sup>th</sup> wagon - TMV 160 km/h

These forces are associated with the motion of the ten DOFs of the wagon. These movements are not reported since they are identical to those of the previous case. As an example, the vertical displacements of the carriage (7th DOF), are shown in Figure 8-15.

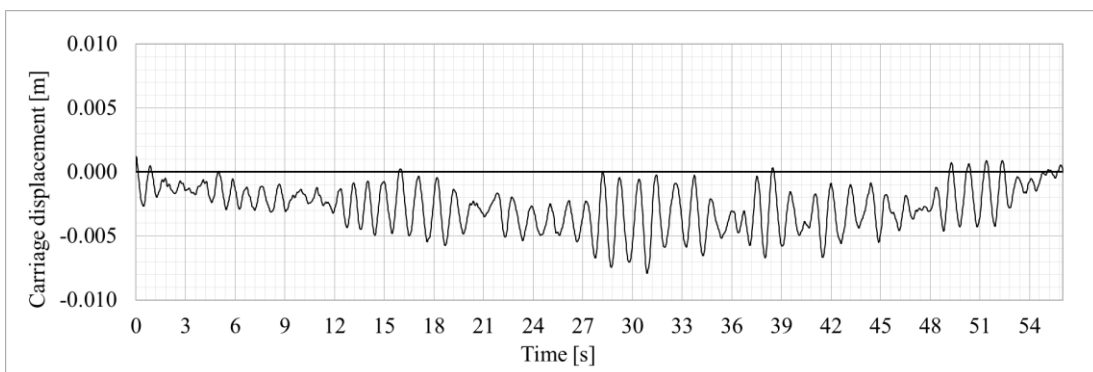


Figure 8-15: Displacement of the carriage - 4<sup>th</sup> wagon – Two TAV 300 km/h

### Structural response

The structural response has undergone differences. The introduction of a traveling mechanical system inside the second tube led to displacements like those of the first tube. However, since the two pipes are rigidly connected every 468 meters, as the trains pass in correspondence of these connections, the lowering occurs not only for the tube on which the train passes, but also for the opposite tube. It is therefore evident that the maximum displacement for this case occurs when both trains are present on a connection. In this analysis, the trains meet at node 18133, where there is a displacement equal to  $-4,26$  mm. The amplitude of the displacement in the nodes in the middle between two rigid connections is no longer the maximum, having no rigid links. In fact, node 18120 has a displacement of  $-4,13$  mm, identical to the case of a single train. The node 18133 instead recorded an increment of more than 1 mm.

The oscillations induced by the passage of the high-speed train running at 300 km/h are equal to  $\pm 0,09$  mm for node 18133 and  $\pm 0,10$  mm for node 18120, identical to those of the previous iteration. Figure 8-16 shows the displacements of node 18133.

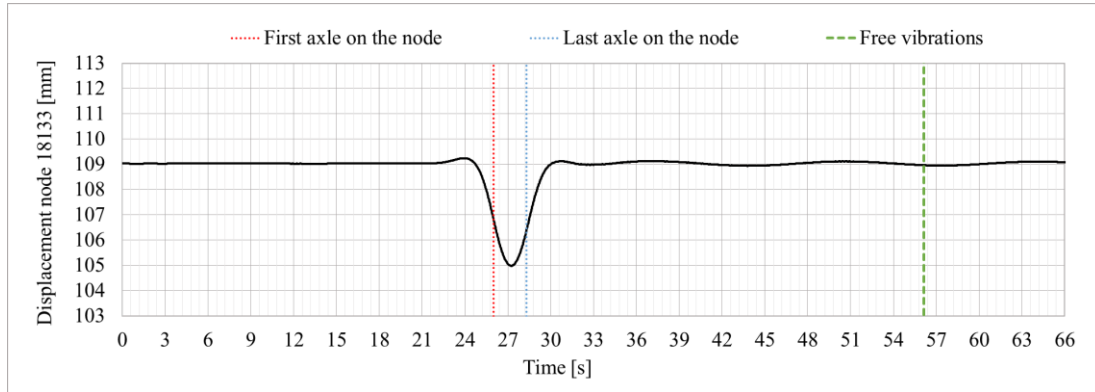


Figure 8-16: Vertical displacement node 18133 – Two TAV 300 km/h

The variations of the forces in the stays are shown in Table 8-8.

Table 8-8: Axial force on the anchorages – Two TAV 300 km/h

Anchor bar	Static axial force [kN]	Static stress [MPa]	Damping 6 %
			Load variation [kN]
Tube 2			
1	+10521	24,76	– 525
2	+13944	32,81	– 572
3	+12824	33,31	– 558
4	+12866	33,42	– 537
5	+13890	36,08	– 489
6	+14765	38,35	– 480
7	+13279	37,83	– 469
8	+13050	37,18	– 508
9	+13606	38,76	– 492
10	+14656	38,07	– 452
11	+13680	35,53	– 492
12	+12921	33,56	– 524
13	+13350	31,41	– 595
14	+10035	23,61	– 471
Tube 1			
15	+10521	24,76	– 532
16	+15232	39,56	– 550
17	+12824	33,31	– 558
18	+12837	33,34	– 536
19	+13890	36,08	– 490



<b>20</b>	+14078	40,11	– 454
<b>21</b>	+13279	37,83	– 474
<b>22</b>	+13132	37,41	– 512
<b>23</b>	+13606	38,76	– 487
<b>24</b>	+13978	39,82	– 471
<b>25</b>	+13680	35,53	– 498
<b>26</b>	+13049	33,89	– 531
<b>27</b>	+13350	31,41	– 594
<b>28</b>	+10035	23,61	– 472

In tube 2 the drop in tension is the same of tube 1, because the two tubes are anchored separately.

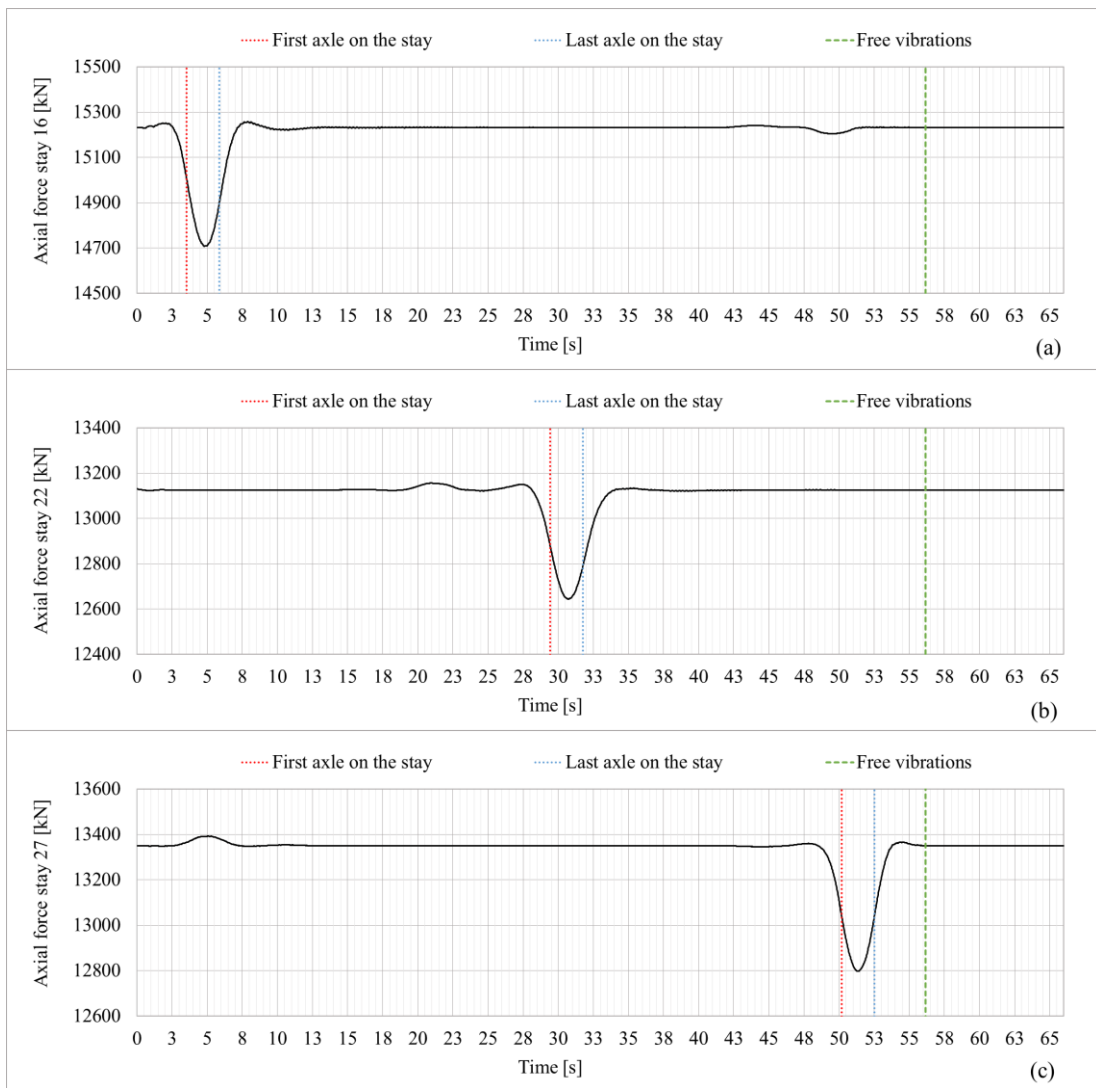


Figure 8-17: Two TAV 300 km/h - Axial force in stay: (a) n°16; (b) n° 22; (c) n° 27

It can be seen from the time histories of the three stays in Figure 8-17 that the free oscillations quickly fade away. Furthermore, since the rigid connections influence the two tubes mutually, sudden increase of forces are observed in the stays in the time instants in which the train passes over the rigid links close to the stay analysed. Also for these interactions the results obtained do not significantly affect the tunnel, which remains weakly stressed by trains both in the case of a single train and in the case of a double train.

## 8.4 Summary of result

The vertical dynamic of train-SFT interaction highlighted the following relevant results:

- The traveling mass is the most important data, which directly affects the deformation of the tunnel;
- The increase in speed causes an increase in dynamic forces and therefore in the forces exchanged between train and tunnel. However, the differences in terms of tunnel response, as the speed varies, are negligible;
- The use of different mechanical parameters in the wagon models (TMV and TAV) did not cause differences in the movement of the tunnel, but only in the motion of the wagon.

Thus, the tunnel responds more critically to the weight of the mass of the train rather than to the speed at which it travels. A train at 300 km/h, with a lower mass, is less demanding for the tunnel than a train traveling at 160 km/h with 180 tons more. The train is subjected to displacements and velocities from the tunnel lower than those caused by the roughness of the rail, which therefore are not such as to amplify its motion, but allow the train to run as if it was in a normal high speed rail.



## TRANSVERSAL INTERACTION

The purpose of this interaction analysis is to establish whether the transverse actions induced by trains are a crucial aspect for the SFT and if the need exist to study the problem more thoroughly or whether they can be neglected. To this aim, the tunnel response is analysed for various train speeds, defined in Table 5-10.

The time histories of the forces, used in the transversal interaction, and the related responses of the tunnel in terms of displacements and forces on the stays, with graphs representing the time histories, are illustrated in this chapter.

The total number of cases is 5, of which 4 with a single train running in tube 1. Two of the single train analyses are conducted with a TMV and other two with a TAV. For both trains the analysis with the critical hunting speeds for the tunnel are reported first, then the analysis with the maximum speeds (hence maximum actions) are shown.

All the cases have been analysed with both 1% and 6% damping, showing that there is a negligible difference in the displacements, lower than a centesimal of millimetre for all the cases. Therefore, the analyses shown are only those with 6% damping. Hence, the damping parameter is not considered a critical aspect.

In these analyses, the displacements of the tunnel are very low, validating the first hypothesis of this interaction. The node for which the displacement are reported is just the 18133, corresponding to the midpoint of the SFT (see Figure 8-1 for the node position).

The axial forces of the anchorages are taken in the same position of the stays of the vertical interaction, corresponding to the elements defined in Table 3-8.

The step with which the analyses have been conducted is constant and equal to 2 m, for which the relative time step as a function of the speed of the train are obtained in each analysis.

## 9.1 Medium Speed Train – TMV

For this train the results of the transversal interaction with the critical speed of 31,5 km/h due to hunting and the maximum critical speed of 160 km/h are reported, to evaluate the maximum forces and displacements.

### 9.1.1 TMV - 31,5 km/h

The total number of time steps used for the analysis is 2504, of which 45 represent 10 s of free vibrations, with a time step of 0,22857 s. The train takes a total of 562 s to travel through the tunnel, that is 535 s for the first axle to cross the tunnel, plus 27 s offset between the first axle and the last one. The total analysis therefore last 572 s, considering the 10 s of free vibration. The solution required 4h with an high performance calculator. The data of the analysis are shown in Table 9-1.

Table 9-1: Analysis data TMV 13,5 km/h

Spatial step [m]	Time step [s]	N° steps	Train Speed [m/s]
2	0,22857	2504	8,75

#### Train loads

Train contact force computation differ between passenger wagons and motor wagons. However, the masses of the wheels are the same. The final time histories (containing hunting + irregularity) of the loads applied by each axle of the wagons are reported. The average value of the forces is zero.

The time histories of the contact forces are calculated for a single axle, for each type of wagon. For TMV these loads are equal for both the passenger and motor wagon, and shown in Figure 9-1. Thus, all the contact forces transmit the same time history load, shifted in space of the distance between the wheels.

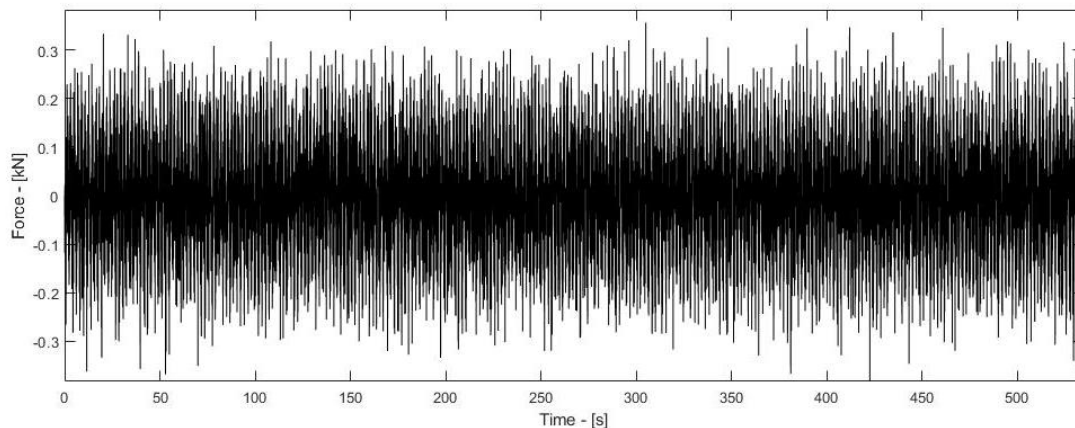


Figure 9-1: Contact force transmitted by an axle – TMV 31,5 km/h

### Structural response

The maximum amplitude obtained for the horizontal displacements of node 18133 is  $\pm 0,0014$  mm (Figure 9-2). To be able to see such displacements we should use a microscope in real life.

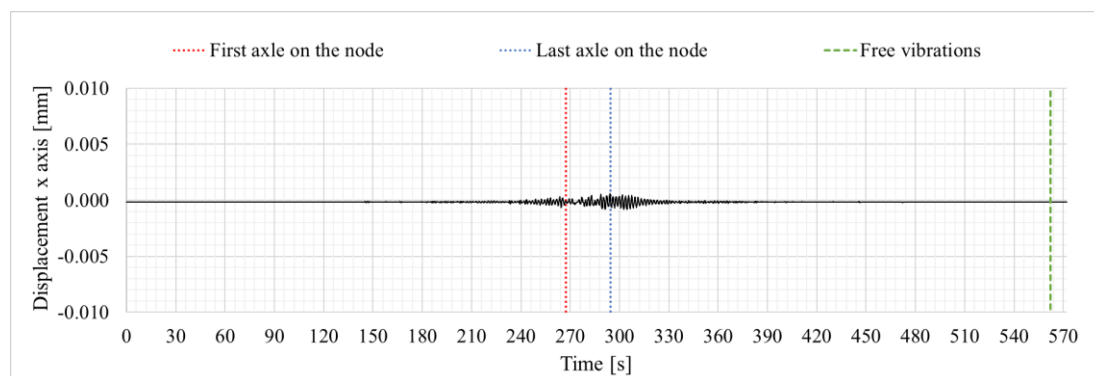


Figure 9-2: Transversal displacements node 18133 – TMV 31,5 km/h

The loads introduced by this train, with the critical speed given by the hunting, are not critical for the tunnel. In fact, both the displacements of the nodes and the axial forces have variations that are too small to be effectively felt by the system. The maximum axial force variation in the stays is about equal to 5 kN corresponding to a stress variation of 0,012 MPa. The maximum recorded displacement is of the order of one millesimal of a millimetre.

### 9.1.2 TMV - 160 km/h

In this analysis, the medium-speed train runs at the maximum speed allowed by the Italian state railways.

The total number of time instants used for the analysis is 2682, of which 222 steps for 10 s of free oscillations, with a time step of 0,045 s. The train takes a total of 110,62 s to travel through the tunnel, or 105,3 s for the first axle to cross the tunnel, plus 5,33 s of displacement between the first axle and the last. The total analysis duration is therefore 120 s, considering 10 s of free oscillations. The solution required 4 hours with a high-performance computer. The data of the analysis are shown in Table 9-2.

Table 9-2: Analysis data TMV 160 km/h

Spatial step [m]	Time step [s]	N° steps	Train Speed [m/s]
2	0,045	2682	44,4444

### Train loads

The final time histories (hunting + irregularities) of the loads applied by one axle of one wagon are reported in Figure 9-3.

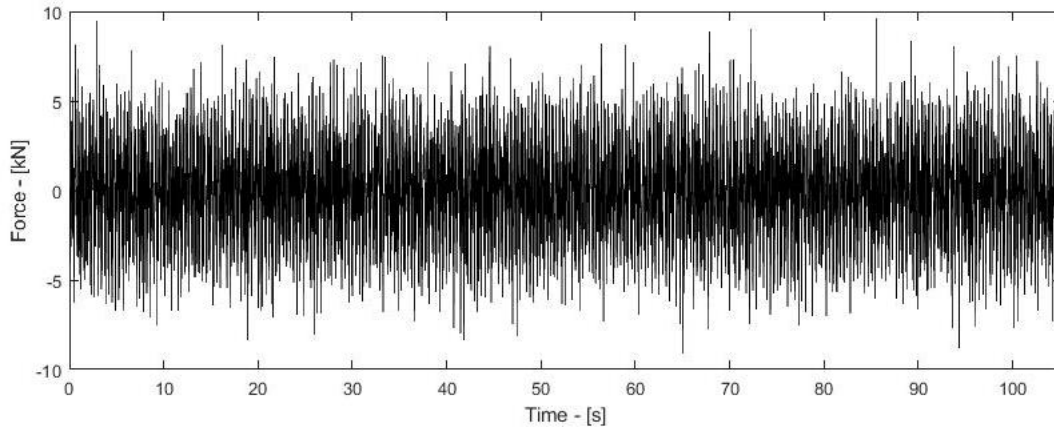


Figure 9-3: Contact force transmitted by an axle – TMV 160 km/h

The increase in speed has increased the loads transmitted by the axles by about 15 times compared to those at a speed of 31,5 km/h.

As already explained, the forces transmitted by a single axle are the same for all the axles of the train.

#### Structural response

In this analysis, the maximum amplitude obtained from the displacements of node 18133 is  $\pm 0,008$  mm (Figure 9-4). That is, a displacement about eight times greater than the previous one, however still too small to be truly influential on the tunnel.

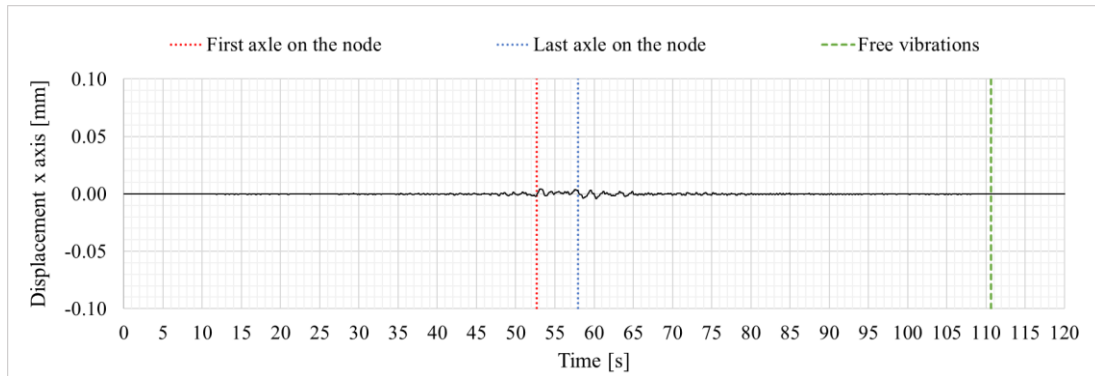


Figure 9-4: Transversal displacements node 18133 – TMV 160 km/h

For this case, since these are the maximum forces that can be exerted by this train, the variation of the axial forces in the stays is shown in the Table 9-3.



Table 9-3: Axial force on the anchorages – TMV 160 km/h

Anchor bar	Static axial force [kN]	Static stress [MPa]	Damping 6 %
			Load variation [kN]
Tube 2			
1	+10521	24,76	± 0,4
2	+13944	32,81	± 0,4
3	+12824	33,31	± 0,3
4	+12866	33,42	± 0,4
5	+13890	36,08	± 0,5
6	+14765	38,35	± 0,6
7	+13279	37,83	± 4,5
8	+13050	37,18	± 4,7
9	+13606	38,76	± 4,6
10	+14656	38,07	± 4,6
11	+13680	35,53	± 0,9
12	+12921	33,56	± 0,4
13	+13350	31,41	± 0,3
14	+10035	23,61	± 0,4
Tube 1			
15	+10521	24,76	± 2,5
16	+15232	39,56	± 0,6
17	+12824	33,31	± 1,4
18	+12837	33,34	± 1,6
19	+13890	36,08	± 1,1
20	+14078	40,11	± 0,9
21	+13279	37,83	± 4,5
22	+13132	37,41	± 4,7
23	+13606	38,76	± 4,6
24	+13978	39,82	± 4,6
25	+13680	35,53	± 1,1
26	+13049	33,89	± 1,1
27	+13350	31,41	± 1,5
28	+10035	23,61	± 1,6

The acting forces, considered the cross sections of the anchors, do not exceed the stress of 0,01 MPa.

It can therefore be assumed that the transverse actions induced by the motion of a TMV can be completely neglected for the tunnel at study.

## 9.2 High Speed Train - TAV

Also for this train, the results of the transverse interaction are shown for the critical speed of 45 km/h of hunting and for the maximum speed of 300 km/h, to evaluate the maximum forces and displacements.

### 9.2.1 TAV - 45 km/h

The total number of time steps used for the analysis is 2503, of which 65 steps to 10 s of free oscillations, and a time step of 0,16 s. The train takes a total of 390 s to travel through the tunnel, or 374,4 s for the first axle to cross the tunnel, plus 15,56 s of displacement between the first axle and the last. The total analysis is therefore 400 s, considering the 10 s of free oscillations. The solution took 4 hours with a high-performance computer. The data of the analysis are shown in Table 9-4.

Table 9-4: Analysis data TAV 45 km/h

Spatial step [m]	Time step [s]	N° steps	Train Speed [m/s]
2	0,16	2503	12,5

#### Train loads

Train contact force calculations are the same for passenger wagons and motor wagons. The final time history (containing hunting + irregularity) of the loads applied by each axle of the wagons is shown in Figure 9-5. The average value of the forces is zero.

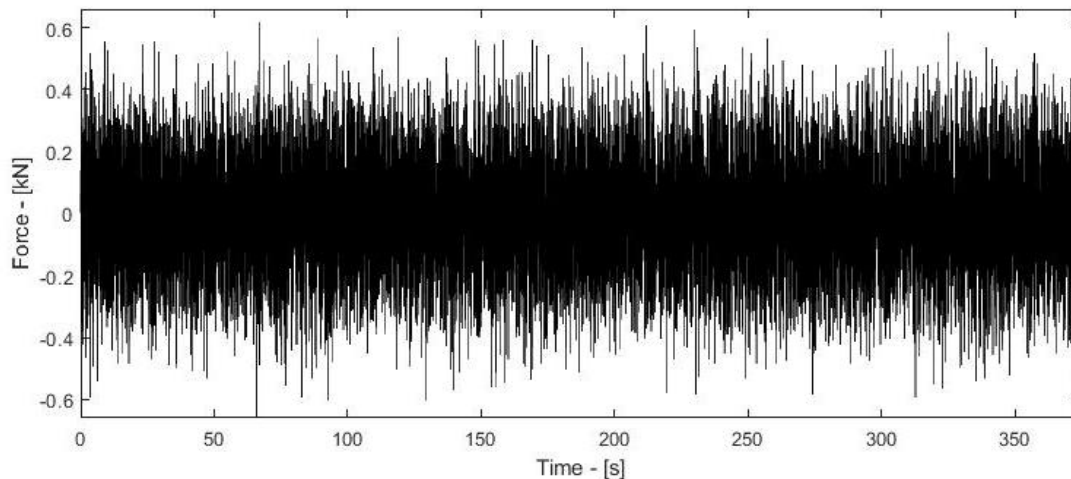


Figure 9-5: Contact force transmitted by an axle – TAV 45 km/h

The order of magnitude of the forces is close to that of the TMV at 31,5 km/h, being the speeds similar. Therefore, a variation of the tunnel displacements is not expected with respect to the first transverse interaction. The irregularities hide the undulatory motion of the hunting, which can however be observed in Figures 5-17 and 5-18.

### Structural response

The maximum amplitude obtained for the displacements of node 18133 (Figure 9-6) is  $\pm 0,0026$  mm, as expected larger than that of the TMV at 31,5 km/h, but once again negligible.

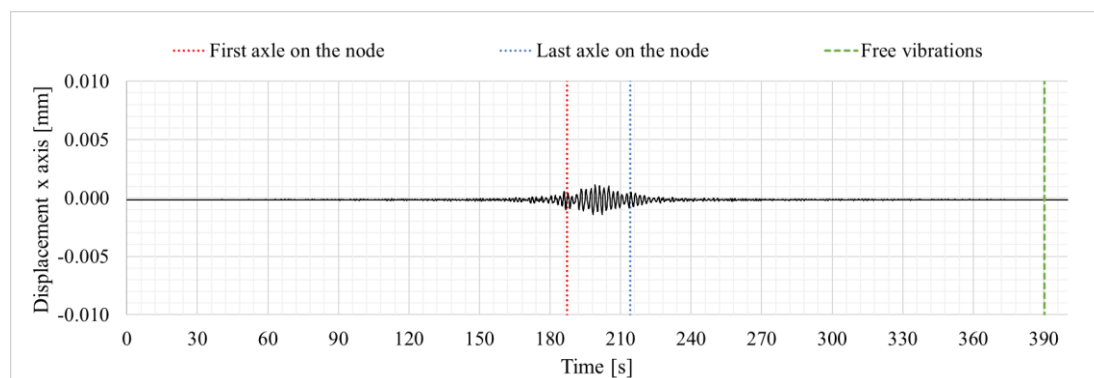


Figure 9-6: Transversal displacements node 18133 – TAV 45 km/h

The loads introduced in this interaction are not a problem for the tunnel. In fact, both the displacements of the nodes and the axial forces have variations too small to be effectively perceived by the system. The maximum displacement is of the order of a millesimal of a millimetre. It is therefore clear that for this train the critical speed given by hunting it is not significantly affecting the tunnel.

### 9.2.2 TAV - 300 km/h

In this analysis, the high-speed train runs at the maximum speed allowed by the Italian state railways.

The total number of time steps used for the analysis is 2857, of which 419 steps for 10 s of free oscillations, with a time step of 0,024 s. The train takes a total of 58,51 s to travel through the tunnel, or 56,18 s for the first axle to cross the tunnel, plus 2,33 s of displacement between the first axle and the last one. The total analysis time is therefore 68 s, considering the 10 s of free oscillations. The solution took 4 hours with a high-performance computer. The data of the analysis are shown in Table 9-5.

Table 9-5: Analysis data - TAV 300 km/h

Spatial step [m]	Time step [s]	N° steps	Train Speed [m/s]
2	0,024	2857	83,3333

### Train loads

The final time histories (hunting + irregularities) of the loads applied by each axle of the wagons are shown in Figure 9-7.

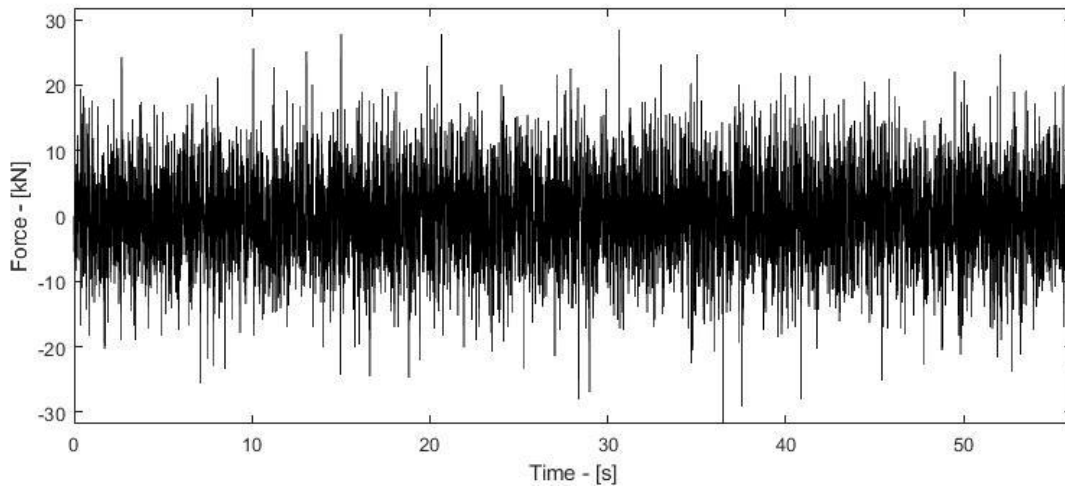


Figure 9-7: Contact force transmitted by an axle – TAV 300 km/h

The increase in speed has increased the loads transmitted by the axles by about 30 times compared to those at a speed of 45 km/h.

As already explained, the forces transmitted by the single axle are the same for all the axles of the train. More detail of these forces is found in Figure 5-19.

#### Structural response

In this analysis, the maximum amplitude obtained from the displacements of node 18133 is  $\pm 0,022$  mm (Figure 9-8). That is, a displacement about eight times greater than the previous one, and 3 times greater than that induced by a TMV at 160 km/h. However, the order of magnitude is still too small to be really relevant for the tunnel in exam.

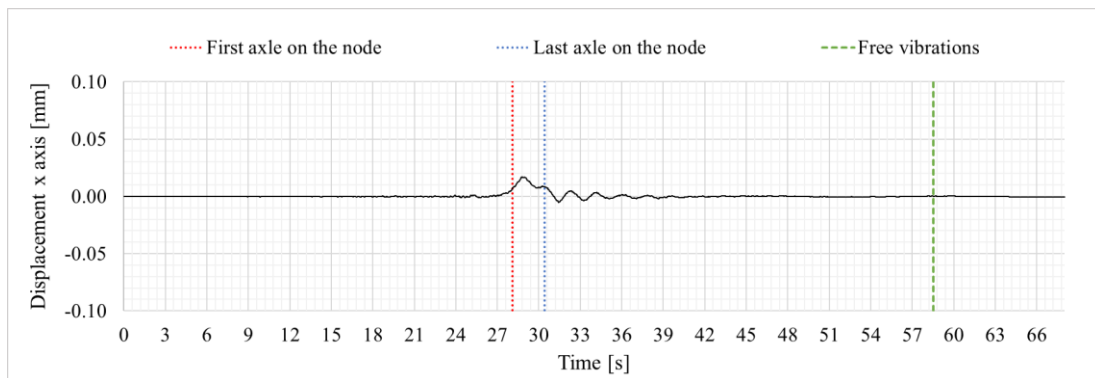


Figure 9-8: Transversal displacements node 18133 – TAV 300 km/h

Since this is the maximum speed that can be traveled, i.e. the forces computed are the maximum transversal forces that can be exerted by this train. The following Table 9-6 shows the variation of the maximum axial forces in the stays, to highlight that the transverse dynamics of a train is completely negligible for this tunnel.

Table 9-6: Axial force on the anchorages – TAV 300 km/h

Anchor bar	Static axial force [kN]	Static stress [MPa]	Damping 6 %
			Load variation [kN]
Tube 2			
1	+10521	24,76	± 0,3
2	+13944	32,81	± 0,5
3	+12824	33,31	± 0,4
4	+12866	33,42	± 0,4
5	+13890	36,08	± 0,8
6	+14765	38,35	± 0,5
7	+13279	37,83	± 4,5
8	+13050	37,18	± 4,7
9	+13606	38,76	± 4,7
10	+14656	38,07	± 4,6
11	+13680	35,53	± 1,2
12	+12921	33,56	± 0,4
13	+13350	31,41	± 0,4
14	+10035	23,61	± 0,4
Tube 1			
15	+10521	24,76	± 1,8
16	+15232	39,56	± 0,9
17	+12824	33,31	± 1,9
18	+12837	33,34	± 2,0
19	+13890	36,08	± 1,9
20	+14078	40,11	± 1,1
21	+13279	37,83	± 4,5
22	+13132	37,41	± 4,7
23	+13606	38,76	± 4,7
24	+13978	39,82	± 4,6
25	+13680	35,53	± 1,7
26	+13049	33,89	± 1,7
27	+13350	31,41	± 1,2
28	+10035	23,61	± 1,5

The forces acting on the stays have not undergone substantial increases compared to the case of a TMV at 160 km/h. Considering the cross sections of the anchors, the forces do not exceed the stress of 0,01 MPa.

It can be concluded that the transverse actions induced by the motion of a high speed train at any speed can be completely neglected for this SFT.

### **9.3 Summary of results**

It can be concluded that a more in-depth study of the transverse dynamics of the tunnel, coupled with that of a train, is not necessary. Also at this level of load definition it is apparent that the forces originating from the transverse motion of the train are not able to induce significant displacements on the tunnel. The forces on the stays are totally negligible in terms of stress, due to the large areas of the anchor bars.

In the initial hypotheses of the train model, for the study of transverse dynamics, the interaction of the train was neglected, assuming that the displacements of the tunnel were small enough to not interfere the motion of the train. This hypothesis was confirmed.

It can therefore be concluded that the actions induced by the transverse motion of a train on the Messina SFT can be neglected.

## TRAINS AND VEHICLES: STAYS' PERFORMANCE

In a previous thesis work, carried out by Palamà (2017), a study was conducted on the actions induced by the passage of vehicles on the prototype of the submerged floating tunnel of Messina. In that work, among the analyses carried out, the most demanding is that of 20 vehicles, 10 per tube, representative of the masses of a truck, which run in opposite directions at a speed of 70 km/h, spaced 150 meter from each other. The axial force losses in the 28 reference stays of Table 3-8, due to the passage of the vehicle, are reported in Table 10-1.

*Table 10-1: Axial force losses – [Palamà, 2017]*

Anchor bar	Static axial force [kN]	Static stress [MPa]	Damping 6 %
			Load variation [kN]
Tube 2			
<b>1</b>	+10521	24,76	– 49,41
<b>2</b>	+13944	32,81	– 13,37
<b>3</b>	+12824	33,31	– 8,97
<b>4</b>	+12866	33,42	– 7,48
<b>5</b>	+13890	36,08	– 4,91
<b>6</b>	+14765	38,35	– 3,82
<b>7</b>	+13279	37,83	– 2,55
<b>8</b>	+13050	37,18	– 2,84
<b>9</b>	+13606	38,76	– 2,94

<b>10</b>	+14656	38,07	- 2,74
<b>11</b>	+13680	35,53	- 2,84
<b>12</b>	+12921	33,56	- 4,83
<b>13</b>	+13350	31,41	- 13,14
<b>14</b>	+10035	23,61	- 46,36
<b>Tube 1</b>			
<b>15</b>	+10521	24,76	- 42,04
<b>16</b>	+15232	39,56	- 12,55
<b>17</b>	+12824	33,31	- 8,38
<b>18</b>	+12837	33,34	- 6,85
<b>19</b>	+13890	36,08	- 5,53
<b>20</b>	+14078	40,11	- 3,29
<b>21</b>	+13279	37,83	- 2,71
<b>22</b>	+13132	37,41	- 2,88
<b>23</b>	+13606	38,76	- 2,82
<b>24</b>	+13978	39,82	- 2,60
<b>25</b>	+13680	35,53	- 2,70
<b>26</b>	+13049	33,89	- 5,86
<b>27</b>	+13350	31,41	- 12,30
<b>28</b>	+10035	23,61	- 39,82

The total force induced on the stays, or rather the loss of tension, caused by the passage of vehicles and trains, at the same time, is given by the sum of the forces obtained in the previous analyses to the forces of Table 10-1.

The maximum loss caused by the trucks is approximately - 50 kN. The maximum loss caused by the trains is approximately - 680 kN, due to the TMV. The variation of the actions induced by the transverse dynamics is neglected.

It is apparent that trucks have a lower influence than trains, since these trucks are placed 150 m away from each other (safety travel distance). On the contrary, the wagons are one behind the other, creating a series of larger and closely spaced loads. In any case, the maximum total load that can be deduced from these analyses is - 730 kN. Let's suppose that this loss can reach - 1000 kN. Compared to the tension loads statically acting on the anchors this value corresponds to less than 1/10 for all the stays, equal to a maximum variation of the stress of about 3 MPa. This cyclic variation of the stresses on the stays is low, and it is not a problem even the loss of tension for the buoyancy of the tunnel.



## CONCLUSIONS

Floating tunnels are an innovative solution for today's transport, which requires increasing standards to ensure safe driving and high-speeds. The major advantage of these bridges is that they guarantee an almost zero environmental impact caused by infrastructures.

The main objective of this thesis was to study the dynamic response of a tunnel prototype to the transit of a train.

For the analysis of the vertical dynamics it was necessary to extend the INTER 6.0 research code, written for the dynamic analysis of vehicle-structure interaction, to the dynamic train-structure interaction, to the aim of analysing the capability of the Messina submerged floating tunnel prototype to resist the actions induced by a high-speed train. This numerical code, updated to version INTER 7.0, proved to be versatile for the addition of the wagon model.

For the analysis of the transverse dynamics, on the other hand, a Matlab program has been created, able to print the transversal forces induced by the axles of the wagon at each time instant, considering both hunting and rail irregularities. The approach for transverse dynamics is simplified compared to the approach for vertical dynamics. However, the results have shown that, for these actions, a study of coupled dynamics is not necessary.

The submerged tunnel was modelled in ANSYS APDL, starting from the PhD work of Shi Chunxia (2013), and adding the variable masses of the present study.

Starting from the Lagrange equations, it was possible to mathematically define the wagon-structure interaction problem with a system of ordinary differential equations that was previously derived to describe the coupled vehicle-structure behaviour. The two systems are coupled, but the solution is obtain with an uncoupled solution strategy. Since they could not be integrated separately, it was necessary to adopt a

step-by-step integration method with an iterative procedure. Of the two iterative procedures associated to the coupled formulation, in this work the so-called WTH is adopted. This procedure and derivation are the result of research works by Mulas et al. (2008 and 2010), who has developed the INTER code over the years, together with a number of graduate students. Among these, Maneo (2015) inserted the WTH procedure in the code, whereas Palamà (2017) gave to the code the ability to make vehicles interact with the submerged floating tunnel prototype, modelled externally in ANSYS. Starting from the work of Palamà, in this thesis, INTER has been further extended, introducing the wagon models, usable for analyses with any train and rail. The WTH (Whole Time History) procedure iterates along the entire time history. INTER computes the contact forces caused by the motion of the train, and plot them in a .txt file. The finite element model in ANSYS then is run by the code, and solved with a transient analysis, applying the forces plotted in the .txt file. The motion obtained by the tunnel is then used by INTER to compute the new forces generated by the train. This iteration is repeated until convergence is achieved.

The wagon model used for the vertical analysis is a plane model, with 10 DOFs. The DOFs represent four wheel vertical translations, two vertical translations and two pitch of the bogies, one vertical translation and one pitch of the carriage. The bodies are connected to each other with damped linear springs. To these DOFs, four contact points are added, also modelled with damped linear springs, which simulate the fastening system and rail pad of the rail. Once the model was set, the mass, stiffness and damping matrices were derived and defined inside INTER. Also the irregularities, applied to the model of the train, of both vertical profile and horizontal alignment, have been the object of a research work during this thesis.

Once INTER and MATLAB codes have been developed, numerical values for the simulation of trains and rails have been adopted. The study was conducted with a medium and a high speed passenger train. The two models of wagon represent a generic train and the high speed Frecciarossa 1000, respectively. The rails on which the trains run are of high class, that allow speeds up to 300 km/h.

One of the problems of the numerical analyses performed with INTER 7.0 concerns computational time. In fact, given the number of DOFs and the number of steps for the transient analysis, the resolution of the problem by ANSYS requires 4 hours of analysis, on a high performance computer, for each iteration.

The same times were needed with the transversal analyses, using the forces obtained from the Matlab code, developed in this thesis, since a constant spatial step was maintained.

In all the analyses conducted, the SFT reported very small displacements of the axis of the tubes, especially for the transversal analyses. This result is reasonable as the structure was designed to maintain the configuration and the functionality even under exceptional loads far exceeding those offered by trains, such as tsunamis or earthquakes. It is highlighted that the passage of a train creates a local effect vertically due to a static deformation caused by the weight of the train.

With regard to the performance of the stays, 28 of them were investigated along the two tubes, having different lengths and sections. The passage of the train creates a localized effect also for the stays. The anchor bar loses axial tension force in the

instant in which the train runs over the stay. However, these losses, combined with the maximum losses caused by the vehicles, have proved not to be critical for the buoyancy of the tunnel.

In all the analyses, no resonant behaviour of the structure was highlighted, either with damping at 1% or with damping at 6%. Furthermore, it was found that damping was not a critical parameter.

Given the results obtained, the question arises whether this bridge can withstand faster trains such as maglev or hyperloops. And vice versa, if the static deformations of the tunnel are low enough to ensure these trains run on it. It is reasonable to believe, that a further study based on magnetic levitation trains can give positive results, as they are lighter than the trains used in this study, and the deformations of the tunnel are sufficiently small.

A further relevant study on trains running on the SFT concerns the possibility that high-speed trains derail, or that vehicles have an accident with internal explosions causing a sudden and accidental impact on the tunnel shell. In this scenario, it would be necessary to evaluate the damage and consequences on the life of the elements that constitute the submerged tunnel.



## REFERENCES

- Biggs JM, Testa B, 1964. Introduction to structural dynamics. New York (NY): McGraw-Hill.
- Canetta D., 2017. Le prospettive della trazione ferroviaria per gli anni 2020-2030. ETR1000 Trenitalia, Bombardier. Padova.
- Chu KH, Dhar CL, Garg VK, 1979. Railway-Bridge impact: simplified train and bridge model. J Struct Div. 105:1823-1844.
- Chunxia S., (2013). Problems related to the seismic behavior of submerged floating tunnel. PhD Thesis. Politecnico di Milano, Italy.
- Claus H. & Schiehlen W., 1998. Modeling and simulation of railway bogie structural vibrations. Vehicle System Dynamics, 29:S1, 538-552.
- Deokhee W., Jihye S., Seungjun K., Woo-Sun P. 2019. Hydrodynamic behavior of submerged floating tunnels with suspension cables and towers under irregular waves. MDPI, Applied sciences. Korea.
- Diana G, Cheli F, 1989. Dynamic interaction of railway systems with large bridges. Veh Syst Dyn. 18:71-106.
- Fryba L, 1999. Vibration of solids and structures under moving loads. Springer Science & Business Media.
- Hamid A., Rasmussen K., Baluja M., Yang T-L. Dicembre 1983. Analytical description of track geometry variations - Volume I. U.S. Department of Transportation. Federal Railroad Administration (FRA).
- Koloušek V, McLean RF, Fleming JF, 1973. Dynamics in engineering structures. London: Butter-worths.
- Krylov AN, 1905. Mathematical collection of papers of the Academy of Sciences. Vol. 61. St. Petersburg. Russia.
- Ling L., Jiang P., Wang K., Zhai W., 2020. Dynamic interaction between rail vehicle and vibration-attenuating slab tracks. Construction and Building Materials. Elsevier.

- Mascella M. 2020. Global analysis of submerged floating tunnels under hydrodynamic loading. Tesi di Laurea Magistrale, Politecnico di Milano & Norwegian University of Science and Technology, Italia.
- Maneo A., 2015. Procedure di integrazione iterative nell'analisi dell'interazione veicolo-struttura. Tesi di Laurea Magistrale. Italia: Politecnico di Milano.
- Mulas M. G., Feriani A., & Candido L., 2010. Iterative procedures for the uncoupled analysis of vehicle-bridge dynamic interaction. International Conference on Noise and Vibration Engineering, including USD 2010. Proceedings of ISMA 2010.
- Mulas M. G., Feriani A., & Lucchini G., 2008. Vehicle-Bridges Interaction analysis: an uncoupled approach. Proceedings of ISMA 2008 International Conference on Noise and Vibration Engineering, 609-623.
- Mulas M.G., Martinelli L., Palamà G., 2018. "Dynamic interaction with travelling vehicles in a submerged floating tunnel", Proceedings of 9<sup>th</sup> International Conference on Bridge Maintenance, Safety and Management, labmas 2018, Melbourne 9-12 July 2018, Powers, Frangopol, Al-Mahaidi & Caprani (Eds), 2018 Taylor & Francis Group, London.
- Oregioni M., Triaca S. 2016. Analisi e progetto di tunnel flottanti sullo Stretto di Messina. Tesi di Laurea Magistrale. Italia: Politecnico di Milano.
- Palamà G., Dicembre 2017. Procedura iterativa nell'analisi dell'interazione dinamica veicoli struttura: applicazione al tunnel flottante sullo stretto di Messina. Tesi di Laurea Magistrale. Italia: Politecnico di Milano.
- Perotti F., Foti F., Martinelli L. & M. Tomasin, 2018. SFTs under dynamic loads: new design issues and numerical simulation. Powers, Frangopol, Al-Mahaidi & Caprani Eds, Maintenance, Safety, Risk, Management and Life-Cycle Performance of Bridges, London. Pages 885–892.
- Salcher P., Adam C., Kuisle A., 2019. A stochastic view of the effect of random rail irregularities on railway bridge vibrations. Taylor & Francis group Eds, Structure and infrastructure engineering. 15:12, 1649-1664.
- Stokes SGG, 1849. Discussion of a differential equation relating to the breaking of railway bridges. Printed at the Pitt Press by John W. Parker. 8:707-735.
- Timoshenko SP, 1922. On the forced vibrations of bridges. London Edinburgh Dublin Philos Mag J Sci. 43(43):1018-1019.
- Van Nguyen Dinh, Ki Du Kim, Pennung W., 2009. Dynamic analysis of three-dimensional-high-speed train interactions using a wheel-rail contact model.

- Wen RK, 1960. Dynamic response of beams traversed by two-axle loads. *J Eng Mech Div.* 86:91-112.
- Willis R, 1849. Preliminary essay to the Appendix B. Experiments for determining the effects produced by causing weights to travel over bars with different velocities. Report of the commissions appointed to inquire into the application of iron to railway structures, London W. Clowes and Sons.
- Zhai W., Zhaoling H., Chen Z., Ling L., Zhu S., 2019. Train-track-bridge dynamic interaction: a state-of-the-art review, *Vehicle System Dynamics*, 57:7, 984-1027.
- Zhu X. Q., Law S. S., 2002. Dynamic Load On Continuous Multi-Lane Bridge Deck From Moving Vehicles, *Journal of Sound and Vibration*, Vol. 251, No. 4, Academic Press, pp. 697-716.





# APPENDIX A

## 1- MATLAB CODE: IRREGULARITIES

The MATLAB code used for tracing and defining the various irregularities of the rails is reported.

### **Roughness.m**

```
clc
clear all
close all

for rouh=1:2

%% Data

l=4680; % [m] Length of the tunnel
m=500; % [m] Meters before and after the tunnel
L=l+m*2; % [m] Length of the profile
w=4; % Precision 1=every meter, 2=every 0.5 m, 4=every 0.25m
J=(l+m*2)*w; % Number of divisions
arm=2048;

omega_m= linspace(pi/50,4*pi,arm); % [rad/m] Frequencies windows

%% PSD

Q=(10^-7).*[7.51308, 5.9233]; % [m^2 rad/m] Profile and alignment
omega_r=0.0206; % [rad/m]
omega_c=0.8246; % [rad/m]

for k=1:size(Q,2)
    for i=1:size(omega_m,2)

Sn(k,i)=Q(k)/2*omega_c^2/((omega_m(i)^2+omega_r^2)*(omega_m(i)^2+omega_c^2)); % [m^3/rad]
    end
end

%% Typical irregularities
```

```

%%%%%% Profile

x=linspace(0,L,J); % [m] Length of the profile
DO=(max(omega_m)-min(omega_m))/arm;
Ir_old=zeros(1,J);

for j=1:arm
    fi=2*pi*rand;
    omega=omega_m(j);
    Aj=sqrt(Sn(1,j)*DO); % [m^3/rad * rad/m -> m]
    Ir=Ir_old+(Aj.*cos(omega.*x+fi));
    Ir_old=Ir;
end
Ir=sqrt(2/pi).*Ir_old;

IR(1,:)=Ir;

%%%%%% Alignment

x=linspace(0,L,J); % [m] Length of the profile
DO=(max(omega_m)-min(omega_m))/arm;
Ir_old=zeros(1,J);
for j=1:arm
    fi=2*pi*rand;
    omega=omega_m(j);
    Aj=sqrt(Sn(2,j)*DO); % [m]
    Ir=Ir_old+(Aj.*cos(omega.*x+fi));
    Ir_old=Ir;
end
Ir=sqrt(2/pi).*Ir_old;

IR(2,:)=Ir;

X=linspace(0,L,J);

%% Final irregularities/roughness

for i=1:J
    for j=1:2
        RR(j,i)=IR(j,i);
    end
end

% RR and X are the final irregularities and length of the profile

%% Plot irregularities for Vertical interaction

if rouh==1
    roughness1(1,1)=size(X,2)-2;
    roughness1(2,1)=0;
    roughness1(3,1)=-m;
    roughness1(4,1)=X(4)-X(3);

```

```

        for j=5:(size(X,2)+2)
            roughness1(j,1)=X(j-3)-m;
            roughness1(j,2)=RR(1,j-3);
        end
    writematrix(roughness1,'roughness 1.dat')
elseif rouh==2
    roughness2(1,1)=size(X,2)-2;
    roughness2(2,1)=40;
    roughness2(3,1)=-m;
    roughness2(4,1)=X(4)-X(3);
        for j=5:(size(X,2)+2)
            roughness2(j,1)=X(j-3)-m;
            roughness2(j,2)=RR(1,j-3);
        end
    writematrix(roughness2,'roughness 2.dat')
end
end

```



## 2- MATLAB CODE: TRANSVERSAL FORCES

The MATLAB code used for the calculation of the transverse forces due to hunting, and the extrapolation into files readable by ANSYS APDL is shown below. The first command recalls a part of the previous MATLAB code so as to have the irregularity values defined each time in a random way.

### Hunting.m

```
%% Alignments data input

Roughness_alignment;

%% DATA ENTRY

%Define the velocity of the train in km/h
%Train 1 travels between 0 and 160 km/h
%Train 2 travels between 0 and 300/400 km/h
v=300 %[km/h] DATA ENTRY
v=v/3.6 %[m/s]

%Define the train for which to calculate the forces:
% 1 = Medium-low speeds
% 2 = High speeds
Treno = 2 % DATA ENTRY

%% Trains properties definition

if Treno==1
    mwT=1.776; %[ton]

    massT=(mwT)*1000; %[kg]

    mwP=1.776; %[ton]

    massP=(mwP)*1000; %[kg]

elseif Treno==2
    mwT=1.873; %[ton]

    massT=(mwT)*1000; %[kg]

    mwP=1.873; %[ton]
```

```

    massP=(mwP)*1000; %[kg]
end

%% Trains geometries

if Treno==1
    nvT=2; %Number of motor wagons
    nvP=8; % Number of passengers wagons
    ppT=[1,10]; %Positions passengers wagons
        q=ones(1,nvT+nvP);
            for i=1:size(ppT,2)
                q(ppT(i))=0;
            end
    lvT=20.2; %[m]Length motor wagons
    lvP=25; %[m]Length passenger wagons
    daT=2.5; %[m]Distance axles motor
    daP=2.5; %[m] Distance axles passeggers
    da2T=14; %[m]Distance boogies motor
    da2P=17.5; %[m]Distance boogies passengers
    ddt=0; %[m]Distance between two wagons
    rw=0.455; %[m] Wheels radius
    con=1/20; %Wheels conicity
    A=0.005; %[m]Hunting amplitude

elseif Treno==2
    nvT=2; %Numero di vagoni traino
    nvP=6; %Numero di vagoni passeggeri
    ppT=[1,10]; %Posizione dei vagoni di traino
        q=ones(1,nvT+nvP);
            for i=1:size(ppT,2)
                q(ppT(i))=0;
            end
    lvT=26.30; %[m]Lunghezza del treno di traino.
    lvP=24.9; %[m]Lunghezza del treno Passeggeri.
    daT=2.85; %[m]Distanza assali traino.
    daP=2.85; %[m]Distanza assali passeggeri.
    da2T=17.4; %[m]Distanza carrelli traino.
    da2P=17.4; %[m]Distanza carrelli passeggeri.
    ddt=0; %[m]Distanza tra un vagone e l'altro.
    rw=0.460; %[m] raggio delle ruote
    con=1/40; %Conicità della ruota
    A=0.002; %[m]Hunting amplitude
end

s=1.5; %[m]Wheel distance/Axle length

%% Serpeggiamento - Hunting

HL=2*pi*sqrt(rw*s/(2*con)) %[m] Lunghezza d'onda

if v*3.6>=200
    fs=100; %Seconds fraction
else
    fs = 50;
end

```

```

end

x=0:v/fs:L;
t=(x./v);

Hs=A.*sin(2.*v.*t.*pi./HL); %[m]Displacements
Hv=A*2*pi*v/HL.*cos(2.*v.*t.*pi./HL); %[m/s]Velocities
Ha=-A*pi^2*4*v^2/HL^2.*sin(2.*v.*t.*pi./HL); %[m/s^2]Accelerations

HFT=(Ha.*massT)./(1000*2); %[kN]
HFP=(Ha.*massP)./(1000*2); %[kN]

%% Irregolarità - Irregularities

Ir;
tt=(xx./v);

dt=diff(tt);
di=diff(Ir);

%Velocity
vv=di./dt;
dv=diff(vv);

%Acceleration
aa=dv./dt(2:end);

%% Final irregularities accelerations
IRa=zeros(1,size(J,2));
for i=3:J
    IRa(1,i)=aa(1,i-2);
end

% IRa, xx and tt are the final irregularities accelerations, length
of the profile, and times.

% Inertial force due to boogie displacement, divided by two axles
IrFT=(IRa.*massT)./(1000); %[kN]
IrFP=(IRa.*massP)./(1000); %[kN]

%% Final forces

%Interpolation of the forces every v/fs s as for the hunting

FFT=HFT;
for i=1:(size(HFT,2))
    FFT(i)=HFT(i)+interp1(tt,IrFT,t(i)); %[kN]
end

FFP=HFP;
for i=1:(size(HFP,2))
    FFP(i)=HFP(i)+interp1(tt,IrFP,t(i)); %[kN]

```

```

end

%% Distribution of the forces in the axles of the convoy

%Each wagon has 4 rwheels. Forces are applied in each axle, hence
delayed of a time dist/velocity.

L_train=(lvP+ddtt)*nvP+(lvT+ddtt)*nvT-ddtt %[m]

    if q(1)==0
        lv_1=lvT;
        da2_1=da2T;
        da_1=daT;
    else
        lv_1=lvP;
        da2_1=da2P;
        da_1=daP;
    end
    if q(end)==0
        lv_2=lvT;
        da2_2=da2T;
        da_2=daT;
    else
        lv_2=lvP;
        da2_2=da2P;
        da_2=daP;
    end

Leff=L_train-(lv_1-da2_1-da_1)/2-(lv_2-da2_2-da_2)/2; %[m] Is the
distance between the first wheel and the last one

tempo_totale=0:1/fs:(Leff+L)/v; %[s] Total time
tempo_totale=tempo_totale(end)

for k=1:(nvT+nvP)
    if q(k)==0
        Forze=FFT;
        lv=lvT;
        da2=da2T;
        da=daT;
    else
        Forze=FFP;
        lv=lvP;
        da2=da2P;
        da=daP;
    end
    lv_old=lv;
    da2_old=da2;
    da_old=da;

    for j=1:4
        if j==1
            if k==1
                shift=0;

```



```

        else
            shift=shift_old+((lv-da2-da)/2+ddtt+(lv_old-da2_old-
da_old)/2)/v;
        end
        elseif j==2
            shift=shift_old+da/v;
        elseif j==3
            shift=shift_old+(da2-da)/v;
        elseif j==4
            shift=shift_old+da/v;
        end
        F_train(k*4-4+j,:)=Forze;
        t_train(k*4-4+j,:)=shift+t;
        shift_old=shift;
end
end

%% Sampling and transformation of the forces

n_ist=round(1+4680/(2)+Leff/(2)) % Total number of time instant

ist_t=(2)/v %[s]time step to use in ANSYS
% 2 is the spatial step
temp=0;
l_trave=18;
k=0;
for i=1:n_ist
    time(i,1)=temp;
    n_assali=0;
    p_NAN=1000;
    for j=1:size(F_train,1)
        F(j,1)=interp1(t_train(j,:),F_train(j,:),temp);
        if isnan(F(j,1))
            else
                if j<p_NAN
                    p_NAN=j;
                end
                n_assali=n_assali+1;
            end
        end
    end
    time(i,2)=n_assali*2;

    for j=p_NAN:(n_assali+p_NAN-1)
        pos=v*(temp-t_train(j,1));
        n_travi=floor(pos/l_trave);
        l_travel=pos-(n_travi*l_trave);
        l_trave2=l_trave-l_travel;

        FA=-(F(j,1)*l_trave2^2/l_trave^3)*(3*l_trave-2*l_trave2);
        MA=-(F(j,1)*l_travel*l_trave2^2)/l_trave^2;
        FB=-(F(j,1)*l_travel^2/l_trave^3)*(3*l_trave-2*l_travel);
        MB=+(F(j,1)*l_travel^2*l_trave2)/l_trave^2;

        if n_travi==0

```

```

        n_nodoA=18001;
        n_nodoB=18003;
    elseif n_travi==1
        n_nodoA=18003;
        n_nodoB=18005;
    elseif n_travi>=2 && n_travi<=257
        n_nodoA=18005+(n_travi-2);
        n_nodoB=18005+-(n_travi-1);
    elseif n_travi==258
        n_nodoA=18261;
        n_nodoB=18263;
    elseif n_travi==259
        n_nodoA=18263;
        n_nodoB=18265;
    end

    k=k+1;
    carichi_treno(k,1)=n_nodoA;
    carichi_treno(k,2)=FA*1000; % [N]
    carichi_treno(k,3)=MA*1000; % [Nm]
    k=k+1;
    carichi_treno(k,1)=n_nodoB;
    carichi_treno(k,2)=FB*1000; % [N]
    carichi_treno(k,3)=MB*1000; % [Nm]
end

temp=temp+ist_t;
end

fl=10; %secondi
nist_fl=round(fl/ist_t);

for i=size(time,1):(size(time,1)+nist_fl)
    time(i+1,1)=time(i,1)+ist_t;
    time(i+1,2)=0;
end

writematrix(time,'time.csv')
writematrix(carichi_treno,'carichi_treno.csv')

```

Whenever there is the desire to run two different trains in the tunnel, the previous MATLAB code must be started by the following code, identical to the previous one, but with the additional modifications reported.

### **Hunting\_Twotrains.m**

```

Hunting;
F_train1=F_train;
t_train1=t_train;

```

```

Roughness_alignment;
%% DATA ENTRY

.

.

.

.

.

%% Sampling and transformation of the forces

n_ist=round(1+4680/(2)+Leff/(2))

ist_t=(2)/v %[s]
temp=0;
l_trave=18;
k=0;
for i=1:n_ist
    time(i,1)=temp;
    n_assali1=0;
    n_assali2=0;
    p_NAN1=1000;
    p_NAN2=1000;
    for j=1:size(F_train1,1)
        F1(j,1)=interp1(t_train1(j,:),F_train1(j,:),temp);
        if isnan(F1(j,1))
            else
                if j<p_NAN1
                    p_NAN1=j;
                end
            n_assali1=n_assali1+1;
        end
    end
    for j=1:size(F_train2,1)
        F2(j,1)=interp1(t_train2(j,:),F_train2(j,:),temp);
        if isnan(F2(j,1))
            else
                if j<p_NAN2
                    p_NAN2=j;
                end
            n_assali2=n_assali2+1;
        end
    end
end
time(i,2)=n_assali1*2+n_assali2*2;

for j=p_NAN1:(n_assali1+p_NAN1-1)
    pos=v*(temp-t_train1(j,1));
    n_travi=floor(pos/l_trave);
    l_travel=pos-n_travi*l_trave;
    l_trave2=l_trave-l_travel;

```

```

FA=- (F1(j,1)*l_trave2^2/l_trave^3)*(3*l_trave-2*l_trave2);
MA=- (F1(j,1)*l_travel*l_trave2^2)/l_trave^2;
FB=- (F1(j,1)*l_travel^2/l_trave^3)*(3*l_trave-2*l_travel);
MB+= (F1(j,1)*l_travel^2*l_trave2)/l_trave^2;

if n_travi==0
    n_nodoA=18001;
    n_nodoB=18003;
elseif n_travi==1
    n_nodoA=18003;
    n_nodoB=18005;
elseif n_travi>=2 && n_travi<=257
    n_nodoA=18005+(n_travi-2);
    n_nodoB=18005+(n_travi-1);
elseif n_travi==258
    n_nodoA=18261;
    n_nodoB=18263;
elseif n_travi==259
    n_nodoA=18263;
    n_nodoB=18265;
end

k=k+1;
carichi_treno(k,1)=n_nodoA;
carichi_treno(k,2)=FA*1000; %[N]
carichi_treno(k,3)=MA*1000; %[Nm]
k=k+1;
carichi_treno(k,1)=n_nodoB;
carichi_treno(k,2)=FB*1000; %[N]
carichi_treno(k,3)=MB*1000; %[Nm]
end

for j=p_NAN2:(n_assali2+p_NAN2-1)
    pos=v*(temp-t_train2(j,1));
    n_travi=floor(pos/l_trave);
    l_travel=pos-n_travi*l_trave;
    l_trave2=l_trave-l_travel;

    FA=- (F2(j,1)*l_trave2^2/l_trave^3)*(3*l_trave-2*l_trave2);
    MA+= (F2(j,1)*l_travel*l_trave2^2)/l_trave^2;
    FB=- (F2(j,1)*l_travel^2/l_trave^3)*(3*l_trave-2*l_travel);
    MB=- (F2(j,1)*l_travel^2*l_trave2)/l_trave^2;

    if n_travi==0
        n_nodoA=118265;
        n_nodoB=118263;
    elseif n_travi==1
        n_nodoA=118263;
        n_nodoB=118261;
    elseif n_travi>=2 && n_travi<=257

```

```

        n_nodoA=118261-(n_travi-2);
        n_nodoB=118261-(n_travi-1);
elseif n_travi==258
    n_nodoA=118005;
    n_nodoB=118003;
elseif n_travi==259
    n_nodoA=118003;
    n_nodoB=118001;
end

k=k+1;
carichi_treno(k,1)=n_nodoA;
carichi_treno(k,2)=FA*1000; % [N]
carichi_treno(k,3)=MA*1000; % [Nm]
k=k+1;
carichi_treno(k,1)=n_nodoB;
carichi_treno(k,2)=FB*1000; % [N]
carichi_treno(k,3)=MB*1000; % [Nm]
end

temp=temp+ist_t;
end

fl=10; %secondi
nist_fl=round(fl/ist_t);

for i=size(time,1):(size(time,1)+nist_fl)
    time(i+1,1)=time(i,1)+ist_t;
    time(i+1,2)=0;
end

writematrix(time,'time.csv')
writematrix(carichi_treno,'carichi_treno.csv')

```

## APPENDIX B

### STRUCTURAL MATRICES FOR THE TRAIN MODELS

*Mass matrix*

$$\underline{\underline{M}}_j = \left[ \begin{array}{cccc|cccccccccccc} 0 & 0 & 0 & 0 & 0 & 0 & 0 & 0 & 0 & 0 & 0 & 0 & 0 & 0 & 0 \\ 0 & 0 & 0 & 0 & 0 & 0 & 0 & 0 & 0 & 0 & 0 & 0 & 0 & 0 & 0 \\ 0 & 0 & 0 & 0 & 0 & 0 & 0 & 0 & 0 & 0 & 0 & 0 & 0 & 0 & 0 \\ 0 & 0 & 0 & 0 & 0 & 0 & 0 & 0 & 0 & 0 & 0 & 0 & 0 & 0 & 0 \\ - & - & - & - & + & - & - & - & - & - & - & - & - & - & - \\ 0 & 0 & 0 & 0 & m_w & 0 & 0 & 0 & 0 & 0 & 0 & 0 & 0 & 0 & 0 \\ 0 & 0 & 0 & 0 & 0 & m_w & 0 & 0 & 0 & 0 & 0 & 0 & 0 & 0 & 0 \\ 0 & 0 & 0 & 0 & 0 & 0 & m_w & 0 & 0 & 0 & 0 & 0 & 0 & 0 & 0 \\ 0 & 0 & 0 & 0 & 0 & 0 & 0 & m_w & 0 & 0 & 0 & 0 & 0 & 0 & 0 \\ 0 & 0 & 0 & 0 & 0 & 0 & 0 & 0 & m_1 & 0 & 0 & 0 & 0 & 0 & 0 \\ 0 & 0 & 0 & 0 & 0 & 0 & 0 & 0 & 0 & m_2 & 0 & 0 & 0 & 0 & 0 \\ 0 & 0 & 0 & 0 & 0 & 0 & 0 & 0 & 0 & 0 & M & 0 & 0 & 0 & 0 \\ 0 & 0 & 0 & 0 & 0 & 0 & 0 & 0 & 0 & 0 & 0 & I_1 & 0 & 0 & 0 \\ 0 & 0 & 0 & 0 & 0 & 0 & 0 & 0 & 0 & 0 & 0 & 0 & I_2 & 0 & 0 \\ 0 & 0 & 0 & 0 & 0 & 0 & 0 & 0 & 0 & 0 & 0 & 0 & 0 & I_\theta & 0 \end{array} \right]$$











50000,50000,50000,50000	!Ct1,Ct2,Ct3,Ct4 kg/s o Ns/m
8.75,8.75,1.25,1.25	!geom m
Vagone 3	
41750,3934,3934,2080000	!M,I1,I2,Iteta(beccheggio) kgm2
265000,265000,590000,590000,590000,590000	!Ks1,Ks2,Kp1,Kp2,Kp3,Kp4 N/m
45120,45120,19620,19620,19620,19620	!Cs1,Cs2,Cp1,Cp2,Cp3,Cp4 kg/s o Ns/m
1776,1776,1776,1776,3040,3040	!m1,m2,m3,m4,Mu1,Mu2 kg
12000000,12000000,12000000,12000000	!Kt1,Kt2,Kt3,Kt4 N/m
50000,50000,50000,50000	!Ct1,Ct2,Ct3,Ct4 kg/s o Ns/m
8.75,8.75,1.25,1.25	!geom m
Vagone 4	
41750,3934,3934,2080000	!M,I1,I2,Iteta(beccheggio) kgm2
265000,265000,590000,590000,590000,590000	!Ks1,Ks2,Kp1,Kp2,Kp3,Kp4 N/m
45120,45120,19620,19620,19620,19620	!Cs1,Cs2,Cp1,Cp2,Cp3,Cp4 kg/s o Ns/m
1776,1776,1776,1776,3040,3040	!m1,m2,m3,m4,Mu1,Mu2 kg
12000000,12000000,12000000,12000000	!Kt1,Kt2,Kt3,Kt4 N/m
50000,50000,50000,50000	!Ct1,Ct2,Ct3,Ct4 kg/s o Ns/m
8.75,8.75,1.25,1.25	!geom m
Vagone 5	
41750,3934,3934,2080000	!M,I1,I2,Iteta(beccheggio) kgm2
265000,265000,590000,590000,590000,590000	!Ks1,Ks2,Kp1,Kp2,Kp3,Kp4 N/m
45120,45120,19620,19620,19620,19620	!Cs1,Cs2,Cp1,Cp2,Cp3,Cp4 kg/s o Ns/m
1776,1776,1776,1776,3040,3040	!m1,m2,m3,m4,Mu1,Mu2 kg
12000000,12000000,12000000,12000000	!Kt1,Kt2,Kt3,Kt4 N/m
50000,50000,50000,50000	!Ct1,Ct2,Ct3,Ct4 kg/s o Ns/m
8.75,8.75,1.25,1.25	!geom m
Vagone 6	
41750,3934,3934,2080000	!M,I1,I2,Iteta(beccheggio) kgm2
265000,265000,590000,590000,590000,590000	!Ks1,Ks2,Kp1,Kp2,Kp3,Kp4 N/m
45120,45120,19620,19620,19620,19620	!Cs1,Cs2,Cp1,Cp2,Cp3,Cp4 kg/s o Ns/m
1776,1776,1776,1776,3040,3040	!m1,m2,m3,m4,Mu1,Mu2 kg
12000000,12000000,12000000,12000000	!Kt1,Kt2,Kt3,Kt4 N/m
50000,50000,50000,50000	!Ct1,Ct2,Ct3,Ct4 kg/s o Ns/m
8.75,8.75,1.25,1.25	!geom m
Vagone 7	
41750,3934,3934,2080000	!M,I1,I2,Iteta(beccheggio) kgm2
265000,265000,590000,590000,590000,590000	!Ks1,Ks2,Kp1,Kp2,Kp3,Kp4 N/m
45120,45120,19620,19620,19620,19620	!Cs1,Cs2,Cp1,Cp2,Cp3,Cp4 kg/s o Ns/m
1776,1776,1776,1776,3040,3040	!m1,m2,m3,m4,Mu1,Mu2 kg
12000000,12000000,12000000,12000000	!Kt1,Kt2,Kt3,Kt4 N/m
50000,50000,50000,50000	!Ct1,Ct2,Ct3,Ct4 kg/s o Ns/m
8.75,8.75,1.25,1.25	!geom m
Vagone 8	
41750,3934,3934,2080000	!M,I1,I2,Iteta(beccheggio) kgm2
265000,265000,590000,590000,590000,590000	!Ks1,Ks2,Kp1,Kp2,Kp3,Kp4 N/m
45120,45120,19620,19620,19620,19620	!Cs1,Cs2,Cp1,Cp2,Cp3,Cp4 kg/s o Ns/m
1776,1776,1776,1776,3040,3040	!m1,m2,m3,m4,Mu1,Mu2 kg
12000000,12000000,12000000,12000000	!Kt1,Kt2,Kt3,Kt4 N/m
50000,50000,50000,50000	!Ct1,Ct2,Ct3,Ct4 kg/s o Ns/m
8.75,8.75,1.25,1.25	!geom m
Vagone 9	
41750,3934,3934,2080000	!M,I1,I2,Iteta(beccheggio) kgm2
265000,265000,590000,590000,590000,590000	!Ks1,Ks2,Kp1,Kp2,Kp3,Kp4 N/m
45120,45120,19620,19620,19620,19620	!Cs1,Cs2,Cp1,Cp2,Cp3,Cp4 kg/s o Ns/m
1776,1776,1776,1776,3040,3040	!m1,m2,m3,m4,Mu1,Mu2 kg
12000000,12000000,12000000,12000000	!Kt1,Kt2,Kt3,Kt4 N/m
50000,50000,50000,50000	!Ct1,Ct2,Ct3,Ct4 kg/s o Ns/m



8.7,8.7,1.425,1.425	lgeom m
Vagone 4	
36498,1664,1664,1710000	!M,I1,I2,lteta(beccheggio) kgm2
682000,682000,3880000,3880000,3880000,3880000	!Ks1,Ks2,Kp1,Kp2,Kp3,Kp4 N/m
60000,60000,32000,32000,32000,32000	!Cs1,Cs2,Cp1,Cp2,Cp3,Cp4 kg/s o Ns/m
1873,1873,1873,1873,2775,2775	!m1,m2,m3,m4,Mu1,Mu2 kg
12000000,12000000,12000000,12000000	!Kt1,Kt2,Kt3,Kt4 N/m
50000,50000,50000,50000	!Ct1,Ct2,Ct3,Ct4 kg/s o Ns/m
8.7,8.7,1.425,1.425	lgeom m
Vagone 5	
36498,1664,1664,1710000	!M,I1,I2,lteta(beccheggio) kgm2
682000,682000,3880000,3880000,3880000,3880000	!Ks1,Ks2,Kp1,Kp2,Kp3,Kp4 N/m
60000,60000,32000,32000,32000,32000	!Cs1,Cs2,Cp1,Cp2,Cp3,Cp4 kg/s o Ns/m
1873,1873,1873,1873,2775,2775	!m1,m2,m3,m4,Mu1,Mu2 kg
12000000,12000000,12000000,12000000	!Kt1,Kt2,Kt3,Kt4 N/m
50000,50000,50000,50000	!Ct1,Ct2,Ct3,Ct4 kg/s o Ns/m
8.7,8.7,1.425,1.425	lgeom m
Vagone 6	
36498,1664,1664,1710000	!M,I1,I2,lteta(beccheggio) kgm2
682000,682000,3880000,3880000,3880000,3880000	!Ks1,Ks2,Kp1,Kp2,Kp3,Kp4 N/m
60000,60000,32000,32000,32000,32000	!Cs1,Cs2,Cp1,Cp2,Cp3,Cp4 kg/s o Ns/m
1873,1873,1873,1873,2775,2775	!m1,m2,m3,m4,Mu1,Mu2 kg
12000000,12000000,12000000,12000000	!Kt1,Kt2,Kt3,Kt4 N/m
50000,50000,50000,50000	!Ct1,Ct2,Ct3,Ct4 kg/s o Ns/m
8.7,8.7,1.425,1.425	lgeom m
Vagone 7	
36498,1664,1664,1710000	!M,I1,I2,lteta(beccheggio) kgm2
682000,682000,3880000,3880000,3880000,3880000	!Ks1,Ks2,Kp1,Kp2,Kp3,Kp4 N/m
60000,60000,32000,32000,32000,32000	!Cs1,Cs2,Cp1,Cp2,Cp3,Cp4 kg/s o Ns/m
1873,1873,1873,1873,2775,2775	!m1,m2,m3,m4,Mu1,Mu2 kg
12000000,12000000,12000000,12000000	!Kt1,Kt2,Kt3,Kt4 N/m
50000,50000,50000,50000	!Ct1,Ct2,Ct3,Ct4 kg/s o Ns/m
8.7,8.7,1.425,1.425	lgeom m
Vagone 8	
36498,1664,1664,1710000	!M,I1,I2,lteta(beccheggio) kgm2
682000,682000,3880000,3880000,3880000,3880000	!Ks1,Ks2,Kp1,Kp2,Kp3,Kp4 N/m
60000,60000,32000,32000,32000,32000	!Cs1,Cs2,Cp1,Cp2,Cp3,Cp4 kg/s o Ns/m
1873,1873,1873,1873,2775,2775	!m1,m2,m3,m4,Mu1,Mu2 kg
12000000,12000000,12000000,12000000	!Kt1,Kt2,Kt3,Kt4 N/m
50000,50000,50000,50000	!Ct1,Ct2,Ct3,Ct4 kg/s o Ns/m
8.7,8.7,1.425,1.425	lgeom m
0.25,0.5,0.024	!beta,gamma,deltat